Reliability Analysis of Overhead Transmission Line Multilayered Stranded Conductor/Clamp Assemblies for Fretting Fatigue Failure

By

Oluwafemi Olumide Thomas

Department of Civil Engineering

McGill University

Montreal, Canada

A thesis submitted to McGill University in partial fulfilment of

the requirements for the degree of

Doctor of Philosophy

ACKNOWLEDGEMENTS

I wish to express my sincere gratitude to my advisers, Prof. Luc Chouinard and Prof. Sébastien Langlois for their constant support, invaluable patience and insightful ideas and guidance over the years.

I would like to acknowledge the financial support of the Natural Science and Engineering Research Council of Canada (NSERC), the Funding program InnovÉÉ, of Fonds de Recherche du Québec-Nature et Technologies (FRQNT) through Centre d'etudes interuniversitaire des structures sous charges extrêmes, Hydro-Québec and Réseau de Transport d'Électricite (RTE).

I am grateful to members of the Hydro-Québec and Réseau de Transport d'Electricité committee formed by the research group on the mechanical and structural aspects of transmission lines. Their constructive criticism of my work during the progress of this research has led to the results presented in this thesis.
Special thanks to my colleagues Amine Omrani and Pedro Henrique Rocha at the Université de Sherbrooke, and Sasan Sttarpanah Karganroudi for their friendship and many discussions that have helped in shaping this thesis.

Finally, and most importantly, I would like to thank my parents and siblings for their love, encouragement and support.

ABSTRACT

Failure of transmission line overhead conductors due to fretting fatigue has led to an increased research effort in understanding the mechanical behavior of these multi-body structures from an experimental perspective and more recently from a computational perspective. However, research devoted to understanding the structural reliability of overhead conductors undergoing deterioration due to fretting fatigue is limited. The current approach to estimate the reliability of these structures has depended on the performance of expensive experiments on conductor – clamp systems that are then grouped into classes on the basis of the idealized stress method. Reliability estimates are then usually defined for the first wire failure of a conductor or some percentage of wire failures in terms of the number of cycles to failure for a specified idealized stress level. A limitation of this approach is that it is not based on the distribution of stresses at the local contact points responsible for initiating and propagating fretting fatigue cracks. The use of this approach results in large uncertainties on the prediction of conductor fatigue life since it does not account for the characteristics of different conductor/clamp configurations.

In this thesis, the sources of variability in overhead conductor fatigue life prediction are first identified. A framework for assessing the reliability of overhead conductors under fretting fatigue conditions is then developed. The framework uses finite elements analyses of single contacts and of the conductor/clamp assembly to determine the state of stress at each wire-wire and wire-clamp/keeper contact. The state of stress at contacts is used to evaluate the fretting fatigue potential and to evaluate the probability of fatigue failure at each contact using single wire plain fatigue data. The Poisson binomial distribution is used to estimate the probability of failure for single and multiple wire failures considering all the contact within the conductor/clamp assembly and to develop fragility curves. The model is validated through comparisons with experimental data. Stress-number of cycle curves for one or more wire

failures are presented for overhead conductors. Distribution of the number of wire failures in a conductor are also presented. Unlike the current approach, the framework presented in this thesis does not rely on performing expensive tests on the conductor and provides a means for generating specific conductor-clamp SN curves and safe limits for overhead conductor fatigue assessment and management.

RÉSUMÉ

La défaillance des conducteurs aériens des lignes de transport électriques due à la fatigue par frottement est le sujet de plusieurs projets de recherche expérimentaux et de modélisation numérique. Par contre, peu de projets de recherche se sont penchés sur l’évaluation de la fiabilité mécanique des conducteurs aériens assujettis à la fatigue par frottement. L'approche actuelle pour estimer la fiabilité des conducteurs se base sur la réalisation d'expériences coûteuses sur différents assemblages conducteur-pince et le regroupement des résultats sur la base de la méthode des contraintes idéalisées. Les estimations de fiabilité sont alors généralement définies pour la première défaillance d’un fil du conducteur ou un certain pourcentage de fils brisés en fonction du nombre de cycles pour un niveau de contrainte idéalisé spécifié. Une limitation de cette approche est qu'elle n'est pas basée sur la distribution des contraintes aux points de contact locaux responsables de l'initiation et de la propagation des fissures de fatigue par frottement. L'utilisation de cette approche engendre plusieurs incertitudes sur la prédiction de la durée de vie du conducteur car elle ne tient pas compte des caractéristiques des différentes configurations de conducteur/pince.

Dans cette thèse, les sources de variabilité dans la prédiction de la durée de vie en fatigue des conducteurs aériens sont d'abord identifiées. Une procédure pour l’évaluation de la fiabilité des conducteurs aériens dans des conditions de fatigue par frottement est ensuite développée. La procédure se base sur des analyses par éléments finis du contact entre deux fils ainsi que des contacts multiples pour un assemblage conducteur/pince. L'état de contrainte aux contacts est utilisé pour évaluer le potentiel de fatigue par frottement et pour évaluer la probabilité de rupture par fatigue à chaque contact à l'aide de données de fatigue sur un fil. La distribution binomiale de Poisson est utilisée pour estimer la probabilité de défaillance pour un ou plusieurs fils en tenant compte de tous les contacts dans l'assemblage conducteur/pince et pour

développer des courbes de fragilité. Le modèle est validé par des comparaisons avec des données expérimentales. Des relations contrainte-nombre de cycles pour une ou plusieurs défaillances de fil sont également dérivées à partir du modèle. Contrairement à l'approche actuelle, la procédure présentés dans cette thèse ne dépend pas de la réalisation de tests coûteux sur le conducteur et fournit un moyen de générer des courbes SN spécifiques pour un assemblage particulier ainsi que des limites de sécurité pour l'évaluation et la gestion de la fatigue des conducteurs aériens.

TABLE OF CONTENTS

Symbols and Notations

μ	friction coefficient
∇	partial derivatives
$\Gamma_{(.)}$	Surface region
$\Omega_{(.)}$	Volume region
$\mathcal{L}_{(.)}$	Line region
$[H(.)]$	Heaviside step function
$[Sgn(.)]$	Sign function
u	Displacement
$\dot{()}$	time derivative
E	Modulus of elasticity
G	Shear modulus
E^*	Composite modulus
$\hat{E}$	Composite modulus
W	Work done
$\lambda_{()}$	Lagrange multiplier
$\varepsilon_{(.)}$	Penalty parameter
$g_{(.)}$	Gap function
$u_{(T)}$	Tangential sliding distance
$u_{(N)}$	Normal penetration distance
$\sim$	Distributed according to
$\mathbb{P}(x)$	Probability of the event *x*
$\mathbb{E}(x)$	Expectation of *x*.
$\mathbb{V}\mathrm{ar}(x)$	Variance of *x*
$(a\|b)$	Conditional variable *a* given *b*
$(a \cup b)$	*a* union *b*
$(a \cap b)$	*a* intersection *b*

$f_x(.)$	Probability density function of the random variable X
$F_X(.)$	Cumulative distribution function of the random variable X
$Q-Q$	Quantile-Quantile
$P-P$	Probability-Probability
CDF	Cumulative distribution function
ECDF	Empirical cumulative distribution function
PDF	Probability Density Function
EPDF	Empirical Probability Distribution Function
TBT	Timoshenko Beam Theory
NTN	Node-to-Node
BTB	Beam-to-Beam
STS	Surface-to-Surface
NTS	Node-to-Surface
S	Slave
M	Master
C	Contact or Contactor
T	Target
f	Vibration frequency
RCFM	Running Condition Fretting Maps
MRFM	Material Response Fretting Maps
MC	Million Cycle
CIGRE	Conseil International des Grands Reseaux Electriques
CSBL	Cigré Safe Boarder Line
EPRI	Electric Power Research Institute
OPGW	Overhead Ground Wires with Optical Fibers
$ACSR$	Aluminum Conductor Steel Reinforced
LPC	Last Point of Contact
KE	Keeper Edge

CSC	Center of Suspension Clamp
P-S	Poffenberger-Swart
Y_b	Bending amplitude at 89mm from the last point of contact
σ_a / ε_a	Idealized stress resulting from bending amplitude
F_c	Clamping force
T	Conductor tension
T_0	Initial tension
$\mathfrak{B}$	Number of failed wires
β	Bending angle
β_p	Bending angle at passive end of conductor
β_0	Bending angle at the active end of conductor
EI	bending stiffness of conductor
E_a	Elastic modulus of aluminum wire
E_i	Elastic modulus of wire *i*
E	Energy dissipated at a contact
I_i	Moment of inertia of wire *i*
d_c	Diameter of conductor
d_i	Diameter of wire *i*
d_j	Axial position of wire center line *j*
θ	Angular position of wire center line
N	Number of cycles
SN	Stress-number of cycles
$\boldsymbol{v}$	Poisson ratio
n_i	Number of wires in layer i
r_c	Radius of slave beam element
r_t	Radius of master beam element
$\Delta\sigma$	Stress range
$Q(t)$	Tangential force of slave node at time *t*
u(t)	Sliding distance of slave node at time *t*

SWT	Smith-Watson-Topper fatigue criteria
$SWT_L \mid Y_b = y$	SWT value obtained from finite element model at a given bending amplitude
$SWT_R \mid N = N_i$	SWT value obtained from plain fatigue model of aluminum wires at a given number of cycles
$f(SWT_R \mid N = N_i)$	probability density function of plain fatigue model of aluminum wires
$\mu(SWT_R)$	mean of the distribution of plain fatigue model of aluminum wires
$\sigma(SWT_R)$	standard deviation of plain fatigue model of aluminum wires
$SWT_{L_m} \mid y_b$	SWT of wire segment *m*
σ_1	Maximum principal stress
$G(E)$	Indicator function for fretting regimes
$G(E_{m,\mathcal{F}})$	Indicator function for fretting regimes for wire segment *m* with contact at the top and bottom
$\mathfrak{B}$	*Number of wire failures*
$k(\sigma_d, \sigma_\theta)$	Two-dimension gaussian kernel with parameters σ_d, σ_θ
$\overbrace{SWT_L \mid y_b(d_j, \theta_j)}^{smoothened}$	SWT value for a given bending amplitude at wire axial and angular position obtained from finite element model and averaged with gaussian kernel $k(\sigma_d, \sigma_\theta)$
LPC_{model}	Last point of contact observed in finite element model
LPC_{exp}	Last point of contact observed in experiment

Originality and Contributions

To the best of the author's knowledge, this dissertation includes the following original contributions:

1. Establishment of equivalence conditions for the fatigue analysis of contacts using beam elements versus solid elements
    a. Development of a mixed dimensional finite element model for a single wire to clamp contact.
    b. Application of sub-modelling technique to the computational solution of a single wire to clamp contact
    c. The application of a multiaxial fatigue procedure for fatigue analysis using beam elements
2. Development of a framework for determining the probabilistic fatigue endurance capability of stranded overhead conductor-clamp system using the finite element method and fatigue properties of the aluminum wires of the conductor
    a. Criteria for selecting conductor contacts for fatigue assessment
    b. Development of fragility curves for overhead conductor fatigue as a function of bending amplitude and number of wires failed.
    c. Model capable of predicting multiple wire failures in overhead conductors
    d. Probability density function of the number of wires failed after a given number of cycles
    e. Fatigue SN curves of overhead conductors for multiple wire failures generated from the numerical procedure.

Contribution of Authors

This thesis has been prepared following a manuscript format per the Office of Graduate and Postdoctoral studies. Three article publications presented in this thesis are all the candidate's original work. Chapter 3 contains the first manuscript, which has been published in Lecture Notes in Mechanical Engineering Series. Data collection and statistical analysis were performed by the candidate in Mathematica® program. Prof. Chouinard and Prof. Langlois supervised the work. Chapter 4 contains the second manuscript, which is planned for submission to the Journal of Fatigue and Fracture of Engineering Materials and Structures. The Computational finite element model was developed by the candidate in ANSYS® finite element system. Analysis of the finite element element model results were performed by the candidate in Mathematica® programming language. Amine Omrani provided experimental data used to validate the finite element model. Prof. Chouinard and Prof. Langlois supervised the work. Chapter 5 contains the third manuscript, which has been published in the journal, Frontiers in Computational Methods in Structural Engineering. Computational Analysis using the ANSYS® finite element system was performed by the candidate. Probabilistic analysis were perfomed by the candidate in Mathematica® and C++. Prof. Chouinard and Prof. Langlois supervised the work.

1 INTRODUCTION

1.1 OVERVIEW

Failure of overhead transmission line conductors resulting from wind-induced vibrations has been known since the 1920's (Varney, 1926)[1]. Since then research on different fronts have been initiated. This includes the development of analytical mathematical models that allows relating the bending amplitude of the conductor to a global measure of stress (Poffenberger and Swart, 1965). Experimental developments also followed with the construction of specialized conductor fatigue test benches (Cardou and Cloutier, 1990; McGill and Ramey, 1986; Rawlins, 1979; Varney, 1928) that allowed the use of a conductor global stress measure to be related to the number of cycles to failure of wires in the conductor. The analysis of these experiments were used to evaluate the effect of the bending amplitude on fatigue, the type of contact damage occurring between wires in the same layer, in adjacent layers and between wires and the suspension clamp and keeper (Zhou et al., 1994a; Zhou et al. 1994b; Zhou et al., 1996). These experimental tests also revealed that the micro slip state of contact between wires and wire/supports in the sticking and mixed fretting regime are responsible for failure from fretting fatigue.

Figure 1-1(a) shows a typical transmission line and its components. Figure 1-1(b) details the connection between the conductor and the suspension clamp. In this region, the conductor is retained to the suspension clamp by a clamping force F_c applied to the keeper through U-bolts. Under the self-weight of the conductor, the conductor is initially at an angle β_0 relative to the

[1] This document appears to be the one of the first document to describe aeolian vibrations on a transmission line, although this name as it is known now was not used in that document.

horizontal (Figure 1-1(b)). Under the action of wind-induced motions, the conductor oscillates

a.

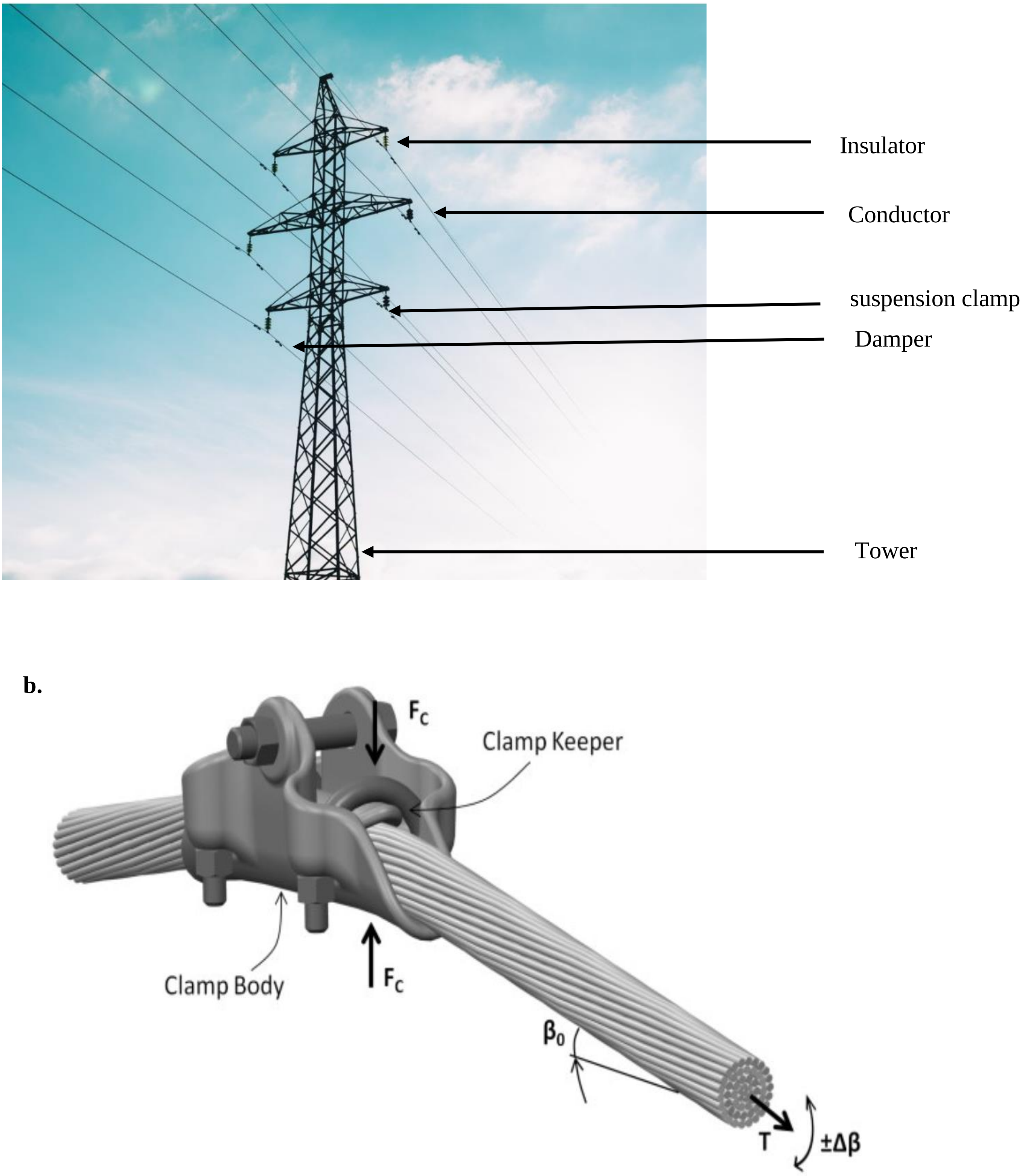

Figure 1-1:(a) Typical transmission line showing its components (Source: Mechatrofice (2020). (b). Detail of the connection between the conductor and suspension clamp (Source: Lalonde et al. (2018)).

through the angle $\pm\Delta\beta$ around β_0, which produces alternating bending stresses in the region of the suspension clamp. The alternating bending stresses can lead to fretting fatigue failures

a. **b.**

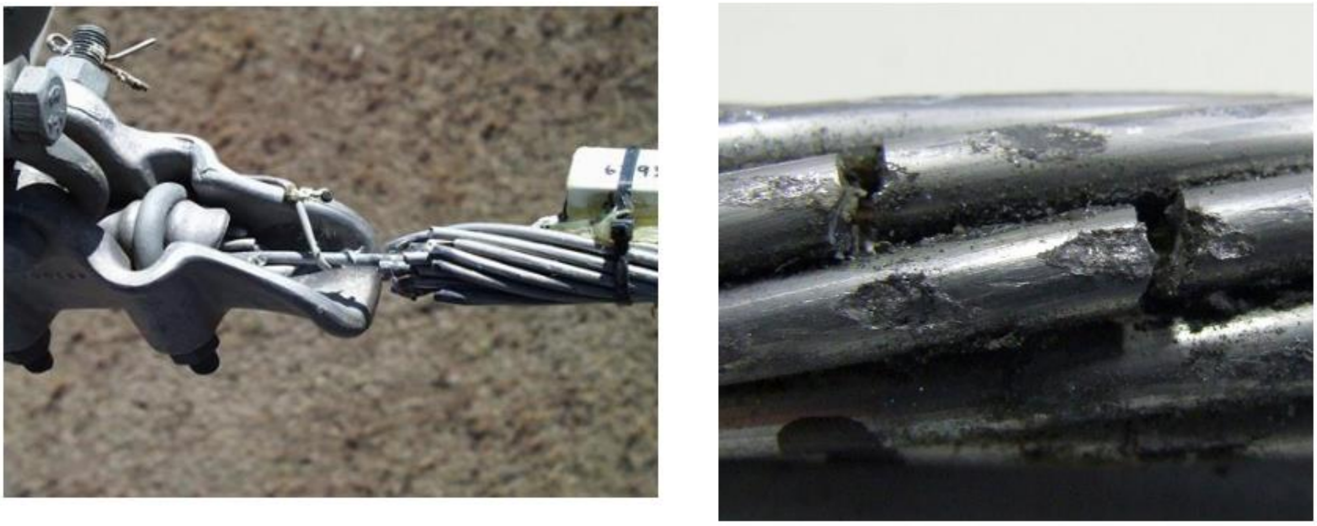

Figure 1-2: (a) Fatigue failure of a conductor at a suspension clamp (b). Typical wire breakage in fretting fatigue in overhead conductors at suspension clamps. (Source: CIGRÉ WG B2.47 (2017))

of the conductor as shown in Figure 1-2.

Given the multibody contact nature of stranded conductor-clamp systems, the determination of the internal forces and moments in the wires is required to determine which contacts are most likely to fail due to fretting fatigue. Analytical models (Cardou and Jolicoeur, 1997; Costello, 1997; Feyrer, 2015; McConnel and Zemke, 1982; Papailiou, 1997) were developed to study the behavior of stranded cables without the clamp. Lévesque et al. (2011) and Lévesque and Legeron (2012) developed numerical models based on the finite element method for a single wire to clamp contact and a wire to wire contact respectively. For these local computational models, the contact loads were determined by inverse analysis from strain gauge results. It was not until recently that a complete model of a conductor-clamp system (global model) was completed using a computational approach (Gang, 2013; Lalonde et al., 2018). With the global computational approach, it was possible for the first time to obtain the distribution of internal forces and moments in a conductor-clamp system.

It has become evident that the global models do not provide a sufficient degree of resolution to the localized contact stresses that are responsible for fretting fatigue failure in overhead conductors due to restrictions of computation resources ; they must be coupled with local models to obtain detailed distribution of stresses. Said et al. (2020) have proposed an approach for coupling a computational global model to a computational local model. Their approach corresponds to selecting force quantities that are believed to influence conductor fatigue from the global model and applying them on a local model as boundary conditions.

The end-product of all computational models developed for overhead conductor-clamp assemblies is to predict the fatigue life of the constituent wires of the conductor. However, there has been no study that has attempted to study from a computational perspective the fatigue strength of conductors by using information on the fatigue of its constituent wires in the context of multiple wire failures. Rather, the predictions are mostly experimental, are restricted to first wire failure (Cloutier et al., 2006; Hardy and Leblond, 2001; Omrani et al., (2021)) or some percentage of the wires of a conductor (CIGRÉ, 1979) within a deterministic framework. These conductor fatigue strength models are based on performing expensive experimental tests on the conductor-clamp system whose fatigue resistance is sought. This is an expensive and time-consuming procedure. This limits the ability of transmission system operators (TSO) to perform robust reliability analyses of their overhead lines experiencing aeolian vibrations and to put in place measures for the inspection, maintenance and replacement of transmission line assets.

According to the American Society of Civil Engineers (ASCE) 2021 infrastructure report card on energy (ASCE, 2021), transmission and distribution (T&D) systems suffer from reliability issues. The cost of power outages in the USA ranges from $28 to 169 annually per households and $8,851 per minute for critical sectors such as data centers. To offset the incurred costs due to power outages, the industry increasesd spending on transmission line assets from 15.6 billion USD in 2012 to 21.9 billion USD in 2017.

In order to improve the reliability of T&D assets and optimize operational costs, reliability-based methods are best suited for implementing optimal maintenance and replacement plans.

1.2 Problem Description

The analysis of the failure of overhead conductors due to fretting fatigue has been mostly based on deterministic multiaxial fatigue models, and deterministic/probabilistic experimentally derived stress–life (SN) curves (Hardy and Leblond, 2001). Hathout (2016) and Hathout et al. (2015) have on the other hand used fuzzy logic to predict the conductor fatigue life resulting from fretting fatigue. Both the SN and fuzzy logic models are based on a global response of the conductor and do not consider the localized contact physics that is responsible for conductor fatigue.

There is a need for the development of physics-based probabilistic fatigue models for conductor–clamp systems. Such a development is needed for the assessment and performance prediction of existing conductor-clamp systems and the development of new conductor-clamp systems. However, this development has been challenging due to the highly nonlinear nature of the problem. In addition, the presence of multibody contact interactions greatly complicates the analysis and solution of the problem. The question which is answered herein is:

"How can the fretting fatigue reliability of overhead conductors be estimated using fatigue properties of aluminum wires."

The problem studied in this thesis provides a framework to overcome these challenges and to develop a probabilistic model to assess the fatigue resistance of conductor-clamp systems for single or multiple wire failures. This encompasses the development of computational strategies for the analysis of multibody contacts in overhead conductors and the development of structural reliability strategies for the assessment of the fatigue resistance of conductor–clamp systems.

1.3 Research Scope and Objectives

The research reported herein is on the probabilistic analysis of fretting fatigue resistance of multi-layered stranded cables supported at suspension clamps. The scope being the development of a framework that yields the probabilistic fatigue resistance of any conductor–clamp configuration in terms of fragility curves and SN curves. This scope is accomplished through the following objectives of the research:

a. Development of FE models for single wire to clamp contact using beam theory and full 3D elasticity theory; demonstration of the equivalence between fatigue conditions in beam theory and the 3D elasticity theory.
b. Develop fragility curves for the fatigue resistance of overhead conductor–clamp systems under multiple wire failures scenario.
c. Development of a method for determining the distribution of the number of wire failures in a conductor–clamp systems as a function of the number of cycles.
d. Provide stress–number of cycles (SN) curves for conductor–clamp systems using the numerical framework for single and multiple wire failures

1.4 Research Methodology

The development of fatigue resistance models for overhead conductor-clamp assemblies has always required the performance of fatigue tests. The exception to this is the work of Gang (2013). However, this study does not present the fatigue resistance in terms of SN curves or fragility curves. To date, most of the fatigue data compiled by these tests are for the first wire failure and there exists no systematic method in the literature to predict multiple wire failures.

Most of the current approaches for defining the fatigue resistance of conductor-clamp assemblies such as the EPRI endurance limit method proposed in Cloutier et al. (2006), the CIGRÉ safe boarder line method (CIGRÉ, 1979) and the safe limit proposed by Hardy and Leblond (2001) are based on experimental compiled data in (Cloutier et al. 2006; Rawlins, 1979; CIGRÉ 1979).

This research is aimed at developing a framework for defining the fatigue resistance of conductor-clamp assemblies in terms of fragility curves, fatigue curves and distribution of the number of failed wires in a conductor-clamp assembly using a combination of the finite element method and information on plain fatigue of aluminum wires. The method followed herein involves the following:

1) Calibration of experimental fatigue curves to be used for validation of computational fatigue curves.
2) Identification of a method for the analysis of conductor-clamp assemblies that provides the best computational cost in terms of time and solution variables.
3) A comparison of the 3D Timoshenko beam finite element modeling approach against the 3D solid finite element modeling approach to discover the merits and demerits of the Timoshenko beam theory in modeling contacts in conductor-clamp assemblies.
4) Determination of information required to know if a contact in a conductor-clamp assembly will fail or not (i.e. contact failure probability).
5) Identification of the method that can combine the individual contact failure probabilities to yield the probability of failure of the conductor-clamp assembly in terms of multiple wire failures (i.e. fragility curves).
6) Define an approach to determine fatigue curve (i.e. SN curve) for the conductor-clamp assembly for single or multiple wire failures.

7) Determine the distribution of the number of wire failures as a function of the number of fatigue cycles for the conductor-clamp assembly.

1.5 Research Publications

a) **Thomas, O.O**., Chouinard, L.E., and Langlois, S. (2020). A Probabilistic Stress-Life Model for Fretting Fatigue of Aluminum Conductor Steel Reinforced Cable-Clamp Systems. In: Liyanage J., Amadi-Echendu J., Mathew J. (eds) Engineering Assets and Public Infrastructures in the Age of Digitalization. Lecture Notes in Mechanical Engineering. Springer, Cham. https://doi.org/10.1007/978-3-030-48021-9_78
b) **Thomas, O.O**., Chouinard, L., and Langlois, S. (2022) Probabilistic Fatigue Fragility Curves for Overhead Transmission Line Conductor-Clamp Assemblies, Accepted for publication in Frontiers in Built Environment: Computational Methods in Structural Engineering.
c) **Thomas, O.O**., Chouinard, L., Langlois, S., and Omrani, Study of the Fatigue of Wire to Clamp Contacts Using Solid and Beam Elements. To be Submitted to the Journal of Fatigue and Fracture of Engineering Materials and Structures.

1.6 Manuscript Layout

This thesis consists of six chapters. Chapter 1 briefly introduces the problem of fatigue failure in overhead conductors caused by wind induced vibration. This followed by a summary of the description of the problem addressed in this thesis. Subsequently, the scope and objectives, methodology and the layout of the manuscript is presented.

Chapter 2 reviews the existing literature on fatigue of conductor-clamp assemblies. The methods for stress analysis of contacts in conductor-clamp assemblies are reviewed. Subsequently, fatigue resistance of conductor-clamp systems is reviewed from a structural reliability point of view.

Chapter 3 derives fatigue curves for conductor-clamp assemblies with tight confidence intervals from experimental data available in Cloutier et al. (2006). These fatigue curves will be used as validation for the fatigue curves to be derived from a computational approach in subsequent chapters.

In Chapter 4, a comparison of the 3D Timoshenko beam finite element approach and the 3D solid finite approach is carried out in other to examine the limitations and strength of the Timoshenko beam theory in fatigue life predictions of conductor-clamp contacts. The comparison entailed reproducing a single wire fatigue test bench using both 3D Timoshenko beam theory and 3D elasticity theory. From this work, it was concluded that while the Timoshenko beam theory allowed for rapid fatigue life assessment, its life estimates are biased and an approach to remedy this bias is required.

Chapter 5 presents a framework for generating fragility curves and SN curves for the fatigue resistance of overhead conductor-clamp assemblies. In this chapter, the 3D Timoshenko beam model is used with a maximum likelihood approach to correct the bias of the Timoshenko beam theory. The 3D Timoshenko beam finite element, the plain fatigue data of aluminum wires and the Poisson binomial distribution are combined to produce fragility curves, fatigue curves and distribution of number of wires failures for a Bersfort conductor-clamp assembly. Subsequently, the results of the analysis are validated and discussed.

Finally, Chapter 6 presents the summary and conclusions of the research study, along with future research recommendations.

1.7 REFERENCES

ASCE (2021). A Comprehensive Assessment of America's Infrastructure: 2021 Report Card for America's Infrastructure.

Cardou, A., and Cloutier, L. (1990). Fatigue Strength Characterization of ACSR Electrical Conductors at Suspension Clamps *Electric Power Systems Research, 19*, 61-71.

Cardou, A., and Jolicoeur, C. (1997). *Mechanical Models of Helical Strands* (Vol. 50).

Cloutier, L., Goudrea, S., and Cardou, A. (2006). Fatigue of Overhead Conductors. In J. K. Chan, D. G. Havard, C. B. Rawlins, & J. Weisel (Eds.), *EPRI Transmission Line Reference Book: Wind-induced Conductor Motion* (2nd ed.). Palo Alto, CA: EPRI.

CIGRÉ (1979). *Recommendations for the Evaluation of the Lifetime of Transmission Line Conductors* (Electra n 63).

CIGRÉ WG B 2.47(2017). *Guide on Repair of Conductors and Conductor-Fittings.*

Costello, G. A. (1997). *Theory of Wire Ropes* (2nd ed.). New York Springer Science + Business

Feyrer, K. (2015). *Wire Ropes (Tension, Endurance, Reliability)* (2nd ed.): Springer

Gang, Qi. (2013). *Computational Modeling for Stress Analysis of Overhead Transmission Line Stranded Conductors Under Design and Fretting Fatigue Conditions* (PhD), McGill University Montreal, Quebec

Hathout, I. (2016). *Fuzzy probabilistic expert system for overhead conductor assessment and replacement* Paper presented at the Best practices for EHV line design and asset management San Diego, USA.

Hathout, I., Callery-Broomfield, K., and Tang, T. T. T. (2015). *Fuzzy probabilistic expert system for overhead conductor assessment and replacement.* Paper presented at the IEEE Power and Energy Society General Meeting.

Hardy, C., and Leblond, A. (2001). *Statistical Analysis of Stranded Conductor fatigue Endurance Data* Paper presented at the Proceeding of the Fouth International Symposium on Cable Dynamics, Montreal, Canada

Lalonde, S., Guilbault, R., and Langlois, S. (2018). Numerical Analysis of ACSR Conductor–Clamp Systems Undergoing Wind-Induced Cyclic Loads. *IEEE Transactions on Power Delivery, 33*(4), 1518-1526. doi:10.1109/TPWRD.2017.2704934

Lévesque, F., and Legeron, F. (2012). *Effect of mean tension on interwire contacts in overhead conductors*

Lévesque, F., Goudrea, S., and Cloutier, L. (2011). Elastic-Plastic Microcontact Model for Elliptical Contact Areas and Its Application to a Treillis Point in Overhead Electric Conductors *ASME Journal of Tribology, 133*.

McGill, P. B., and Ramey, G. E. (1986). EFFECT OF SUSPENSION CLAMP GEOMETRY ON TRANSMISSION-LINE FATIGUE. *Journal of Energy Engineering-Asce, 112*(3), 168-184.

McConnel, K. G., and Zemke, W. P. (1982). A Model to Predict the Coupled Axial Torsion Properties of ACSR Electrical Conductors *Experimental Mechanics, 22*(7), 237-244.

Mechatrofice (2020, May, 03). Overhead vs Underground Lines-Advantages and Disadvantages. Mechatrofice.com. https://mechatrofice.com/electrical/overhead-vs-underground

Omrani, A., Langlois, S., Van Dyke, P., Lalonde, S., Karganroudi, S. S., and Dieng, L. (2021). Fretting fatigue life assessment of overhead conductors using a clamp/conductor numerical model and biaxial fretting fatigue tests on individual wires. *Fatigue & Fracture of Engineering Materials & Structures, 44*(6), 1498-1514. doi:10.1111/ffe.13444

Papailiou, K. O. (1997). On the bending stiffness of transmission line conductors. *IEEE Transactions on Power Delivery, 12*(4), 1576-1583. doi:10.1109/61.634178

Poffenberger, J. C., and Swart, R. L. (1965). Differential Displacement and Dynamic Conductor Strain. *IEEE Transactions on Power Apparatus and Systems, 84*(4), 281-289. doi:10.1109/TPAS.1965.4766192

Rawlins, C. B. (1979). Fatigue of overhead conductors. In *EPRI Transmission Line Reference Book: Wind-induced Conductor Motion*. Palo Alto, CA: EPRI.

Said, J., Garcin, S., Fouvry, S., Cailletaud, G., Yang, C., and Hafid, F. (2020). A multi-scale strategy to predict fretting-fatigue endurance of overhead conductors. *Tribology International, 143*, 106053. doi:https://doi.org/10.1016/j.triboint.2019.106053

Varney, T. (1926). Notes on the Vibration of Transmission-Line Conductors. *Transactions of the American Institute of Electrical Engineers, XLV*, 791-795. doi:10.1109/T-AIEE.1926.5061272

Varney, T. (1928). The Vibration of Transmission-Line Conductors. *Transactions of the American Institute of Electrical Engineers, 47*(3), 799-807. doi:10.1109/T-AIEE.1928.5055059

Zhou, Z. R., Cardou, A., Fiset, M., and Goudreau, S. (1994a). Fretting fatigue in electrical transmission lines. *Wear, 173*(1), 179-188. doi:http://dx.doi.org/10.1016/0043-1648(94)90271-2

Zhou, Z. R., Cardou, A., Goudreau, S., and Fiset, M. (1994b). FRETTING PATTERNS IN A CONDUCTOR–CLAMP CONTACT ZONE. *17*(6), 661-669. doi:10.1111/j.1460-2695.1994.tb00264.x

Zhou, Z. R., Cardou, A., Goudreau, S., and Fiset, M. (1996). Fundamental investigations of electrical conductor fretting fatigue. *Tribology International, 29*(3), 221-232. doi:http://dx.doi.org/10.1016/0301-679X(95)00074-E

2 LITERATURE REVIEW

This chapter presents a comprehensive review of the literature on the aspects that are relevant to this work. This includes fretting fatigue, analytical and computational contact mechanics, and fatigue life assessment. The approach taken herein is to provide a historical perspective of each aforementioned areas that applies to fretting fatigue problems of overhead conductors. Shortcomings of the current methodologies are highlighted and discussed.

2.1 FRETTING FATIGUE

Failure of engineering materials from fretting fatigue is a well-documented phenomenon (see e.g. Hills and Nowell, (1994)) and the topic of multiple ongoing research projects in industry and academia. Fretting is defined as a small amplitude oscillatory motion that occurs between surfaces of bodies in contact (Waterhouse, 1992). When contacting surfaces are subjected to this oscillatory motion, fretting can lead to the formation of oxide debris; this phenomenon is termed fretting wear and

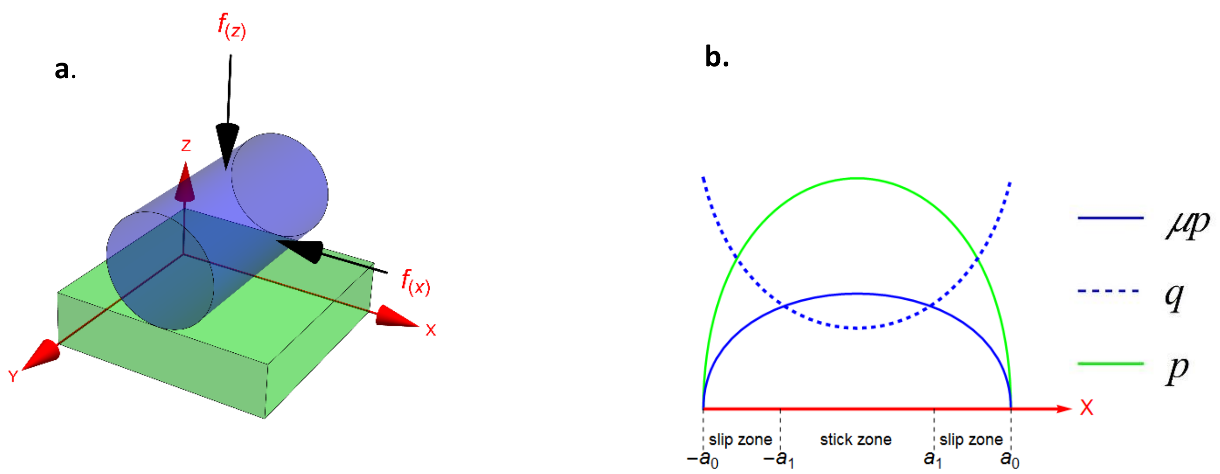

Figure 2-1: (a) cylinder on flat contact ; (b) Cattaneo – Midlin representation of the interface stresses in the XZ plane (reproduced from (Waterhouse, 1992))

in the case of the formation and propagation of fatigue cracks, it is termed fretting fatigue (Waterhouse, 1992). In fretting fatigue, It has been established that Cattaneo–Mindlin condition (also called stick-slip condition)[2,] as shown in figure 2-1 (b), must be present for fretting cracks to initiate (Waterhouse, 1992). This condition require a stick and a slip zone

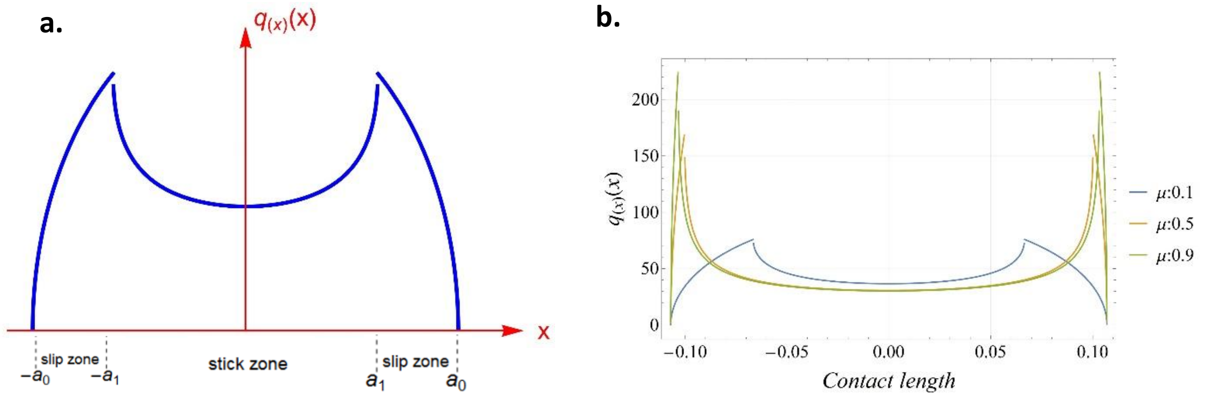

Figure 2-2: (a) Tangential stress distribution of cylinder in contact with a plane (b). Effect of friction coefficient on the tangential stress distribution for cylinder to plane contact

within the contact region which can be defined from the shear traction $\boldsymbol{q}_{(x)}(x,y)$,. If the contact is not frictionless in the *x-direction*, the coefficient of friction μ leads to the development of shear traction $\boldsymbol{q}_{(x)}(x,y)$, which is unbounded at the contact edges (Barber, 2018; Waterhouse, 1992) as shown in Figure 2-1(b) and related to the force $\boldsymbol{f}_{(x)}$. This behavior of the contact is obtained when it is assumed that the contact region is in full stick mode (i.e. $(-a_0\ to\ +a_0\ )$). A corrective solution to the tangential stress is thus the requirement that rather than having a full stick contact, regions of micro–slip must develop at the edges of the contact region (i.e. $(\pm a_0\ to \pm a_1\ )$) and a region of stick (i.e. $(-a_1\ to + a_1\ )$) in the central portion of the contact (Barber, 2010). Thus, in the slip region, the admissible shear traction is $\mu\boldsymbol{p}_{(z)}(x,y)$, while in the stick zone, the admissible shear traction must be less than $\mu\boldsymbol{p}_{(z)}(x,y)$ as shown in figure 2-2(a) (Barber, 2018). The equation of the tangential stress distribution is given as (Barber, 2010):

[2] This was referred to as sticking regime (Zhou and Vincent, 1995) while it is referred to as partial slip regime in (Jeong and Lee, 2006).

$$\boldsymbol{q}_{(x)}(x) = \frac{2\mu \boldsymbol{f}_{(z)}}{\pi a^2}\left(\sqrt{a_0^2 - x^2} - [H(a_1^2 - x^2)]\sqrt{a_1^2 - x^2}\right) \tag{2.1}$$

From Figure 2.2 (a) one notes that the maximum values of the tangential stress occurs at the stick-slip boundary, which corresponds to the position of failures of wires observed in ACSR conductors (Zhou et al., 1996).

The slope to the tangential stress distribution given by Equation (2.1) is not defined at the stick-slip boundary. The tangential stress at the spatial stick-slip boundary[3] is defined by analytic continuation (Gray et al., 2006; Knopp, 1945). Also, since $\nabla\left(\boldsymbol{q}_{(x)}(x)\right)$ increases with the friction coefficient, as shown in Figure 2-2 (b), the order of the polynomial to approximate $\boldsymbol{q}_{(x)}(x)$ is dependent on the friction coefficient[4]

A condition similar to the Cattaneo–Mindlin condition (CMC) has been presented by Zhou and Vincent (1995), which is termed the mixed fretting regime (MFR). Differences between fretting fatigue resulting from MFR as compared to the Cattaneo–Mindlin condition are the morphology of the contact damage, the sensitivity to bulk stress, the tangential force–displacement relationship, and the number of cycles at which fretting fatigue failure is observed. Zhou and Vincent (1995) reported that while particle detachment is limited to the regions of micro-slip in the CMC as seen in Figure 2-3 and 2-5 (a), in the MFR, the particle detachment is often limited to the initial elastic contact zone as seen in Figure 2-4 and 2-5 (c). The tangential force–displacement relationship for the CMC shows a quasi–linear relation in the stabilized state while those of the MFR shows a closed elliptical loop in the stabilized state

[3] Such a requirement is not necessary for the maximum value of the normal contact pressure.
[4] This has the important implication that a single discretization (e.g. in finite elements) cannot approximate properly the tangential stress and thus the size of the discretization should be dependent on the friction coefficient if the value of the tangential stress at the stick-slip boundary is important.

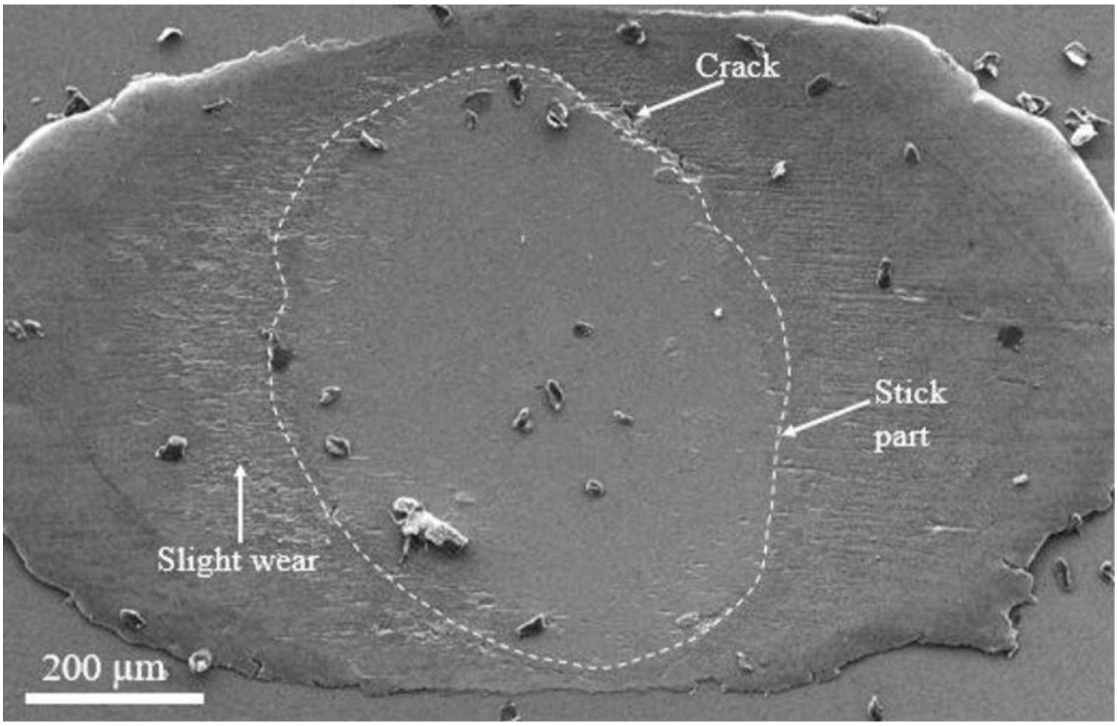

Figure 2-3: Contact experiencing the CMC condition with a central stick region. Source: (Foggi, 2020)

as shown in Figure 2.6 (a) and (b) respectively. In comparison, gross slip (Figure 2.6 (c)) presents the largest energy dissipation with a parallelepiped-closed loop. In terms of the number of cycles observed before failure is reached, the difference between MFR and CMC is about a factor of 10 with contacts in MFR experiencing lower number of cycles before failure (Zhou and Vincent, 1995). The coefficient of friction has also been reported to be higher in mixed fretting regime when compared to the Cattaneo–Mindlin condition and the gross slip regime (Zhou and Vincent, 1995). Unlike gross–slip, where the contact degradation and size increases due to the relatively large movement of the contact interface and wear (Cloutier et al., 2006; Zhou and Vincent, 1995), in MFR the displacement is just large enough to cause scarring of the contact area but only a slight increase in the contact size is observed with increasing number of cycles (Zhou and Vincent, 1995).

More recently, Jang and Barber (2011) have discovered a phenomenon from a numerical perspective, which appears to be a special case of the MFR phenomenon. In their work, they

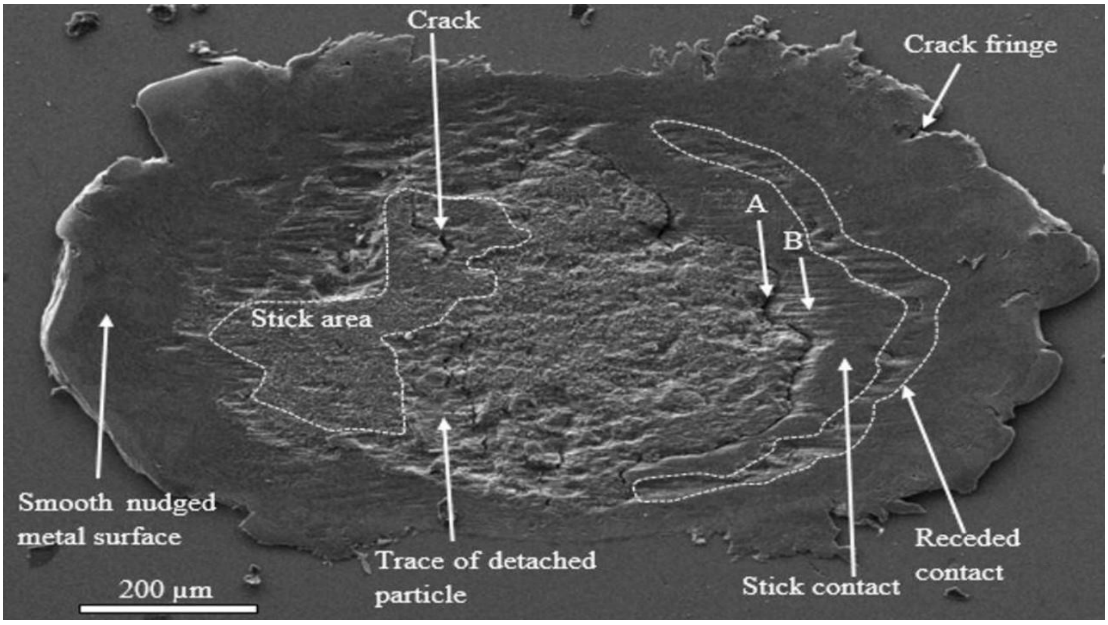

Figure 2-4: Contact experiencing mixed fretting regime conditions. Source: (Foggi, 2020)

point out the importance of phase shift between the normal force and the tangential force. It was shown that in the case where the amplitude of the normal force exceeds the mean normal force and a phase shift exists between the normal and tangential force, a higher amount of energy dissipation is observed when compared against a case where the normal and tangential forces are in phase. This is in line with the observation of Barber et al. (2011) and Zhou and Vincent (1995) where higher energy dissipation is associated with increased tendency of fretting fatigue failure. It also aligns with the observation of Lalonde (2017) where a phase shift was observed between the axial force and bending moment in wires between the keeper edge (KE) and last point of contact (LPC) of a conductor.

Barber et al. (2011) have also reported the occurrence of separation[5], which can occur as much as 50% of the time during cycling. This phenomenon of possible contact separation between wire of the external layer and the clamp has been conjectured by Cardou et al. (1993) and they provide experimental evidence for its occurrence in a 42/7 Bersimis conductor-clamp system.

[5] Part of the contact interface will be in contact and another part separate in space or the whole contact separates and comes back in contact in time.

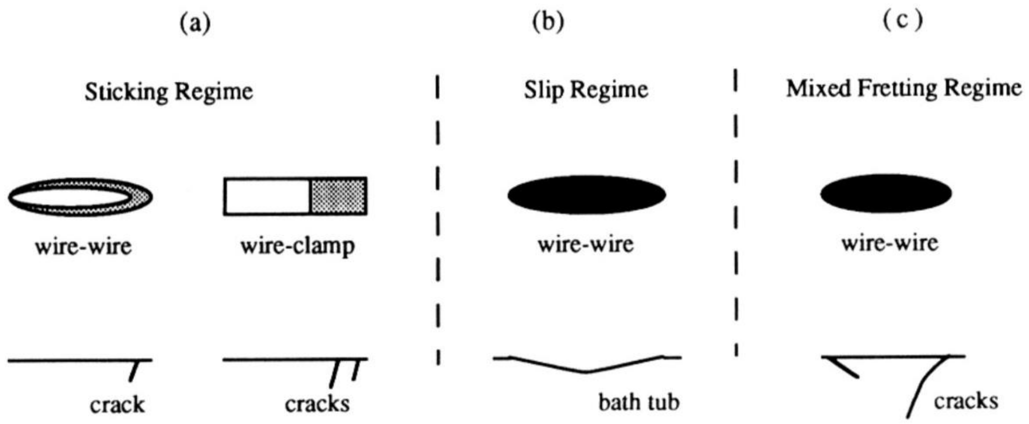

Figure 2-5: Contact damage morphology for (a) Sticking regime; (b) Slip (gross slip) regime; (c) Mixed fretting regime. Source: (Zhou et al., 1996)

However, no discussion on the occurrence of this phenomenon has appeared since their work in 1993.

In conductor fatigue, all three fretting regimes (i.e. stick-slip, mixed fretting regime and gross slip) have been observed (Azevedo et al., 2009; Zhou and Vincent, 1995) with contacts in the stick-slip regime being geometrically close to those in the mixed fretting regime (Zhou and Vincent, 1995).

Three distinct damage morphologies corresponding to the three fretting regimes have been reported by Zhou et al. (1996) in ACSR conductors (Figure 2.5). In this figure, wire to wire contacts in the sticking (stick–slip) regime within the clamp experience damage with an asymmetry in the slip region being restricted to regions where the wire enters the clamp. The reduced size of the slip zone (or the lack of it) in the region where the wire enters the clamp has been attributed to the compressive effect of the clamping force (Zhou and Vincent, 1995). The cracking initiation location as indicated for contacts in the partial slip regime is not restricted to wire–wire contacts only but cracks can also be initiated at the contacts between the wires of the conductor and the clamp. The wearing damage illustrative of the gross–slip regime is seen in Figure 2.5 (b) while the damage over the entire elliptical region of the contact in the mixed fretting regime and the corresponding larger crack length is seen in Figure 2.5 (c).

In conclusion, three different fretting regimes have been identified as occurring in conductor fatigue (Zhou et al., 1996): the sticking regime, the mixed fretting regime and the gross slip

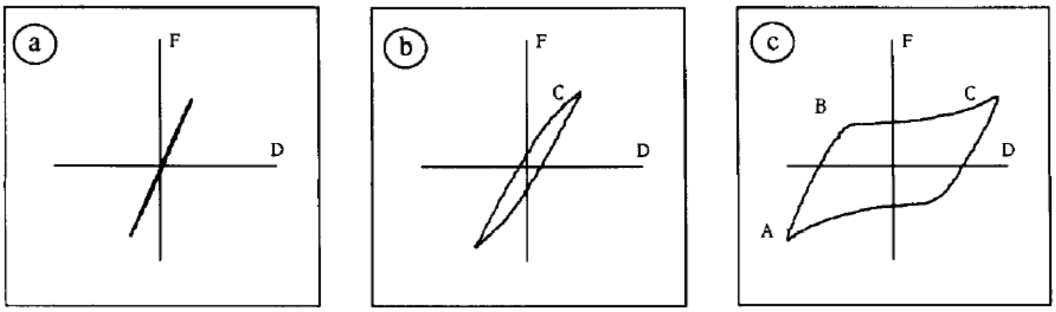

Fig. 1. Variations of the tangential force as a function of the displacement: (a) closed cycle; (b) elliptical cycle; (c) parallelepipedic cycle.

Figure 2-6: (a) Tangential force - displacement relation for stick -slip at stabilized state. (b) Tangential forced-displacement relation for mixed fretting regime at the stabilized state. (c). Tangential force-displacement for gross-slip regime in the stabilized state

regime. The sticking regime is based on the occurrence of the CMC conditions in the contact and displays a quasi-linear tangential force displacement relationship. The MFR in comparison with contacts in the sticking regime displays a closed elliptical tangential force displacement relation. These are the two fretting states that lead to fretting fatigue failure. This shows that the energy dissipation of contacts is an important parameter in the quantification of fretting failures and should be included in modelling.

2.2 METHODOLOGIES TO ASSESS FRETTING INDUCED STRESSES

In order to estimate fretting fatigue induced stresses, the mathematical tools of contact mechanics are required to determine the stresses at the contact and at the interior of the bodies in contact. Thus, contact mechanics models are reviewed in this section. A global overview of the equilibrium equations for contact problems are discussed, followed by a review of analytical solutions and the assumptions on which they are based. Finally, studies using the finite element method (FEM) for the solution of conductor contact mechanics are reviewed. This section closes with shortcomings of the analytical and finite element studies and highlights areas for improvements.

2.2.1 Equilibrium Equations for Bodies in Contact

To review the methods available for the solution of contact problems, consider the diagram shown in Figure 2.7 for three bodies in contact (Omrani, 2021)[6], with the orthogonal cartesian coordinate system defining the origin located at some point in space as shown. With $\boldsymbol{p}$, $\boldsymbol{t}$, $\boldsymbol{u}$ and $\boldsymbol{u}_{C_B}$ representing force boundary condition on the clamp, wire and displacement boundary condition on the wire and clamp bottom respectively. Equilibrium equations for this three-body contact can be written using the principle of virtual work following the approach presented in (Konyukhuv and Izi, 2015; Konyukhuv and Schweizerhof, 2012; Washizu, 1975)[7]:

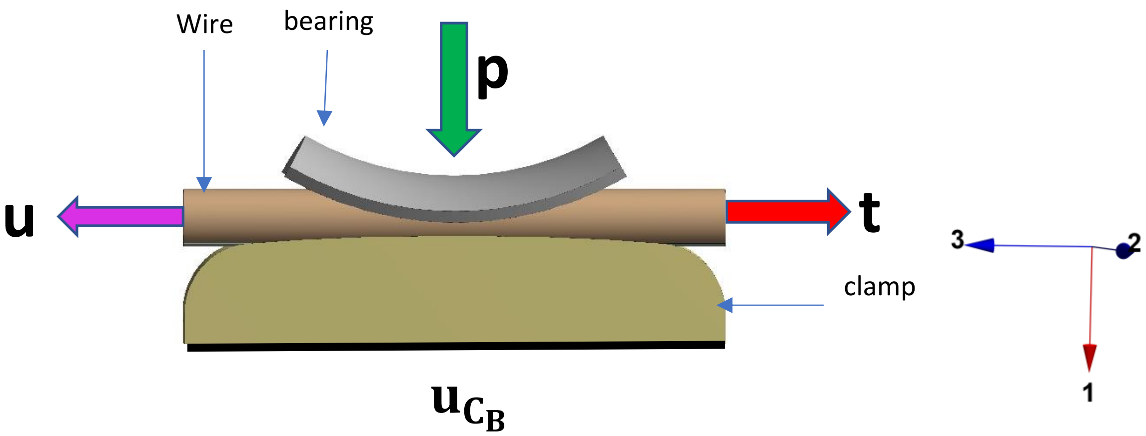

Figure 2-7: Three-body system with two unilateral contacts

$$\sum_{B\cup W\cup C} \int (\nabla_i \dot{\sigma}^{ij}) \delta \dot{u}_j \, d\Omega + \sum_{B\cup W\cup C} \int \dot{t}^j_{(n)} \, \delta \dot{u}_j \, d\Gamma + \sum_{(B\cap W)\cup(w\cap C)} \int \dot{\sigma}^j_{(n)} \delta \dot{u}_j \, d\Gamma = \mathbf{0} \quad (2.1)^8$$

[6] This problem has been analyzed experimentally by Omrani (2021) and it thus provides a good case study for analyzing the fretting behavior of a simple fretting contact.
[7] The displacements attached to the contact terms should be considered as those at the contact points.
[8] Note that the Einstein summation convention applies as $\nabla_i \dot{\sigma}^{ij} = \sum_{i=1}^{3} \nabla_i \dot{\sigma}^{ij} = \nabla_1 \dot{\sigma}^{1j} + \nabla_2 \dot{\sigma}^{2j} + \nabla_3 \dot{\sigma}^{3j}$

Where $\mathrm{i,j} = 1,2,3$, $\nabla_i(.) = \frac{\partial(.)}{\partial x^i}$, $\nabla_i \dot{\sigma}^{ij}$ represents the gradient of the internal stress rates evaluated over the respective volume domains Ω_B, Ω_W, and Ω_C which represent the volume of the bearing, wire and clamp respectively. $\delta \dot{u}_{j,(.)}$ represents the variation in velocity of the corresponding body, $\dot{\sigma}^j_{(\boldsymbol{n})}$ represents the projection of an arbitrarily oriented stress rate vector to the three orthogonal directions of the respective surfaces $\Gamma_{(.)}$: bearing bottom (B_B), wire top (W_T), wire bottom (W_B) and clamp top (C_T). It is thus observable from (2.1) that $\dot{\sigma}^j_{(\boldsymbol{n})} \stackrel{\text{def}}{=} \{\dot{\sigma}^1_{(n)}, \dot{\sigma}^2_{(n)}, \dot{\sigma}^3_{(n)}\}$ are simply the contact stress rates. $\dot{t}^j_{(\boldsymbol{n})}$ and $\dot{p}^j_{(\boldsymbol{n})}$ are the projections of the applied boundary conditions $\dot{\boldsymbol{t}}$ and $\dot{\boldsymbol{p}}$ along the unit normal $\boldsymbol{n} \stackrel{\text{def}}{=} \frac{\boldsymbol{\nabla} \Gamma_{(.)}}{\|\boldsymbol{\nabla} \Gamma_{(.)}\|}$ to $\Gamma_{(W_R)}$ and $\Gamma_{(B_B)}$.

For each of the contact interface shown in Figure. 2-7, equilibrium of the components of stress acting on each point (or contact interface point) must hold as follows (Konyukhuv and Izi, 2015):

$$\dot{\sigma}^j_{(n)} d\Gamma_{B_B} + \dot{\sigma}^j_{(n)} d\Gamma_{W_T} = 0 \tag{2.2}$$

$$\dot{\sigma}^j_{(n)} d\Gamma_{W_B} + \dot{\sigma}^j_{(n)} d\Gamma_{C_T} = 0 \tag{2.3}$$

By making the contact vectors on the wire surface (top and bottom) the subject in (2.2) and (2.3) and substituting into (2.1), the following is obtained:

$$\sum_{B \cup W \cup C} \int (\nabla_i \dot{\sigma}^{ij}) \delta \dot{u}_j \, d\Omega \; + \sum_{B \cup W \cup C} \int \dot{t}^j_{(n)} \, \delta \dot{u}_j \, d\Gamma + \sum_{(B \cap W) \cup (w \cap C)} \int \dot{\sigma}^j_{(n)} \delta\big(\dot{u}_{j,M} - \dot{u}_{j,S}\big) \, d\Gamma \; = \mathbf{0} \tag{2.4}$$

where M and S are the master and slave surfaces. Equation (2.4) is subject to the boundary

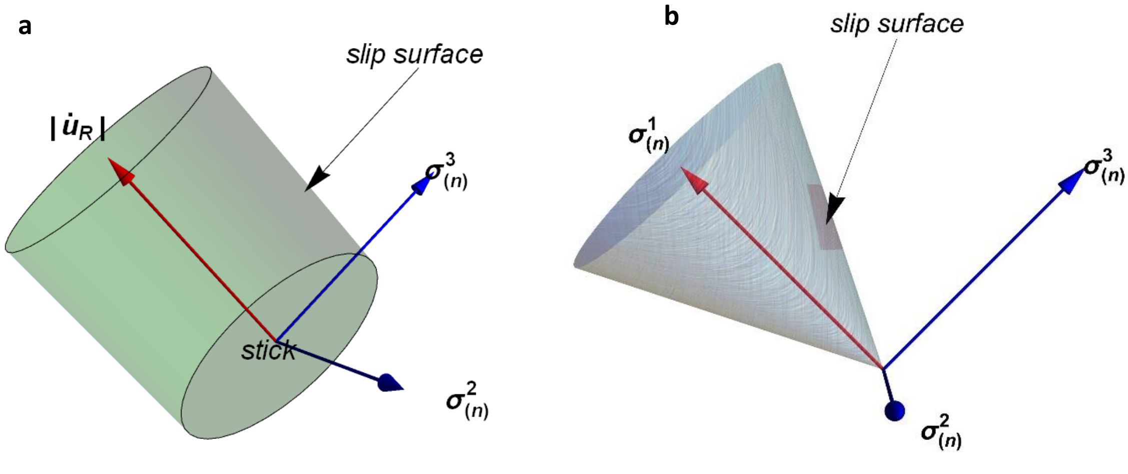

Figure 2-9: (a) Relationship between tangential stress vector components and the resultant slip velocity in 3D stress-velocity space. (b) Friction cone illustrating the Coulomb friction relation between the contact pressure and the tangential stress vector in 3D stress space (Reproduced from Yastrebov, 2013).

conditions shown in Figure 2.7, the Hertz-Signori-Moreau conditions in normal (Konyukhuv

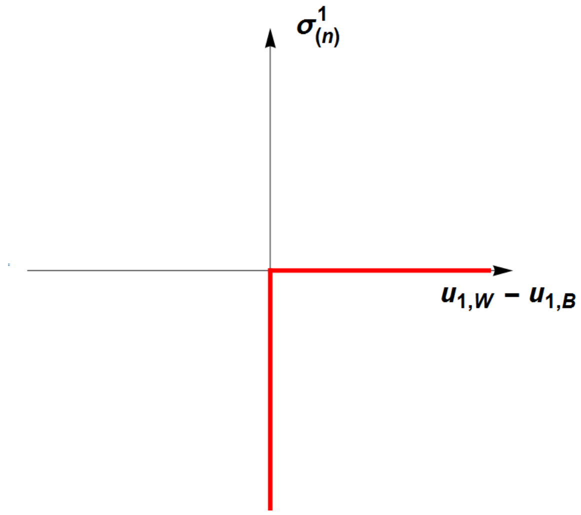

Figure 2-8: Relationship between the contact pressure and the penetration/non-penetration condition (Reproduced from Yastrebov, 2013).

and Izi, 2015; Konyukhuv and Schweizerhof, 2012) and tangential directions (Hills et al., 1993; Konyukhuv and Izi, 2015; Konyukhuv and Schweizerhof, 2012; Yastrebov, 2013) in Figures 2-8 and 2-9 respectively. Further details on Equation (2.4) are provided in Appendix B.

The equilibrium equations for the simple contact system given by Equations (2.4) can be extended to a conductor-clamp system as:

$$\sum_{k=1}^{n+2}\left(\int \underbrace{\left(\nabla_i \delta \dot{u}_{j,k}\right)\dot{\sigma}^{ij}}_{internal\ energy\ terms} \, d\Omega_k\right)+\sum_{k=1}^{2n+2} \underbrace{bc_k}_{boundary\ \ terms} + \underbrace{\sum_{k=1}^{n_{contact}}\left(\int \dot{\sigma}^{j}_{(n)} \underbrace{\left(\delta \dot{u}_{j,k}-\delta \dot{u}_{j,k+1}\right)}_{contact\ terms} \, d\Gamma_k\right)}_{cross-contacts}$$

$$+\underbrace{\sum_{k=1}^{n}\left(\int \dot{\sigma}^{j}_{(n)} \underbrace{\left(\delta \dot{u}_{j,k}-\delta \dot{u}_{j,k+1}\right)}_{contact\ terms} \, d\Gamma_k\right)}_{line\ contacts}+\underbrace{\sum_{k=1}^{n_{keeper/camp}}\left(\int \dot{\sigma}^{j}_{(n)} \underbrace{\left(\delta \dot{u}_{j,k}-\delta \dot{u}_{j,k+1}\right)}_{contact\ terms} \, d\Gamma_k\right)}_{keeper\ and\ clamp\ contacts} = \mathbf{0}; \qquad (2.5)$$

This relation (2.5) is also subject to the same constraints shown in Figures 2-8 and 2-9 for each contact pair. The internal energy terms are those of the wire, keeper and clamp and bc_k correspond to the set of the boundary conditions of aforementioned entities, n is the number of wires , $n_{keeper/camp}$ is the number of contacts between the keeper/clamp and the external layer and $n_{contact}$ is the number of contact points between all two adjacent layers. Compared to the simple system in Figure 2-7, the number of terms increases significantly with the number of wires in the conductor. Further details on Equation (2.5) are provided in Appendix B.

The equations (2.1) through (2.5) show properties of a contact important for solving conductor fretting fatigue problems. These properties are highlighted in Table 2-1.

Table 2-1: Properties of a Contact System

No.	Property	Comment	Reference
1	Path dependent solution	The presence of friction, which is path dependent, has led to the introduction of a time variable in the equilibrium equations even though the problem is static	Hills et al.(1993)
2	Coupling of contact integrals on opposing surfaces	The contact integrals are coupled through the displacement $u_{j,W}$. Thus, in general, conditions on an interface affect those on its sister interface. E.g. the distribution of $\sigma^{j}_{(\boldsymbol{n})}$ on $\Gamma_{W_B} \cap \Gamma_{C_T}$ will be affected by geometry	Lévesque et al. (2011)

		of interface $\Gamma_{W_T} \cap \Gamma_{B_B}$ (Geometric asymmetry)	
3	Coupling of the normal and tangential stresses	Normal and tangential stresses are coupled through the Coulombs friction. In general, normal loadings will produce tangential tractions.	Johnson (1985) Timoshenko (1941)
4	Coupling of contact integrals to boundary conditions	Asymmetry in the boundary conditions will lead to asymmetry in the tractions on Γ (Loading asymmetry). The contact tractions depend on the way the loading is applied, and the body supported (Saint-Venant principle).	Johnson (1985) Barber (2018)
5	Discontinuous nature	Both the contact pressure and tangential stress contain discontinuous functions in time and space	Barber (2018)
6	Phase difference	Depending on the BC, the normal pressure and tangential stress can be out of phase. This leads to non-proportional loading of a contact.	Barber et al.(2011)
7	Bifurcation phenomenon	Three deformation modes can occur between the LPC and the point where the wire exits the bearing (BE). This affects the type of contact established on $\Gamma_{W_B} \cap \Gamma_{C_T}$. In other words, it is possible to have some part of an interface be in contact (i.e. fulfils 2.7) and another part of the same interface be separated at a given time *t* It is also possible that at a time t_1 an interface is in contact and a time t_2 it is separated. The occurrence of a precise deformation mode is dependent on the bending moment, the applied normal contact force and boundary conditions	Cardou et al.(1993)
8	Stick-Sliding phenomenon	Like point 7 above, it is possible to have some part of an interface be in stick and (i.e. fulfils 2.9) and another is sliding (i.e. fulfils 2.10). This is the partial-slip condition. It is also possible that at a time t_1 an interface is in sticking and a time t_2 it is sliding.	Jang and Barber (2011)
10	The reliability of the	Since the number of wires control the number of contacts points for fretting, it also	

	conductor should depend on the number of contact points	controls the fatigue reliability of a conductor. An increase in the number of fatigue contacts points increases the chances of finding failure points. In other words, increases the probability of failure of the conductor	

To solve fretting problems, we must thus attend to the nature of contact equations (2.1) through (2.5) and pay attention to the properties of the contact such as those given in Table 2-1 as they determine the methodology to solve a contact problem and predicting fretting failures.

The solution methods in the discussions to follow make various assumptions or use alternative means in order to satisfy or justify neglecting the properties in Table 2-1. A collection of the various methods for solving contact problems are collected in Appendix A. Amongst these methods, only four of them are reviewed herein for the purpose of this thesis. For details of the other methodologies, Appendix A provides references for further information.

2.2.2 Analytical Methods

In developing analytical solutions for contact problems, different approaches have been proposed in the literature. The discussion herein does not intend to cover all methods available in the literature. Rather, the emphasis is on analytical methods that provide solutions for contacts typical to ACSR conductors such as elliptical contacts between crossing wires in a conductor and line contacts between wires and the clamp/keeper. Studies on conductors are reviewed to highlight their assumptions, limitations and advantages. Methods using structural elements (such as beams) are also reviewed given that some numerical studies on conductors (Baumann and Novak, 2017; Lalonde, 2017) are based on contacts between structural elements.

The analytical solutions are categorized as : (1) Stress and Displacement Functions, (2) The Method of Dimensionality Reduction, (3) Structural Elements in Conductor Contact Mechanics.

2.2.2.1 Stress and Displacement Functions:

This is commonest approach to construct analytical solutions to the equilibrium equations (2.5) where a stress function or a displacement function that satisfies the equilibrium equation of the individual bodies and the contact conditions is required. In two dimensional problems and problems satisfying the half-plane assumption[9], the Flamant solution for the normal loading and tangential of a half–plane at the origin as shown in Figure 2-10 can be combined to give the Airy stress function for a two–dimensional surface subjected to a normal load and a

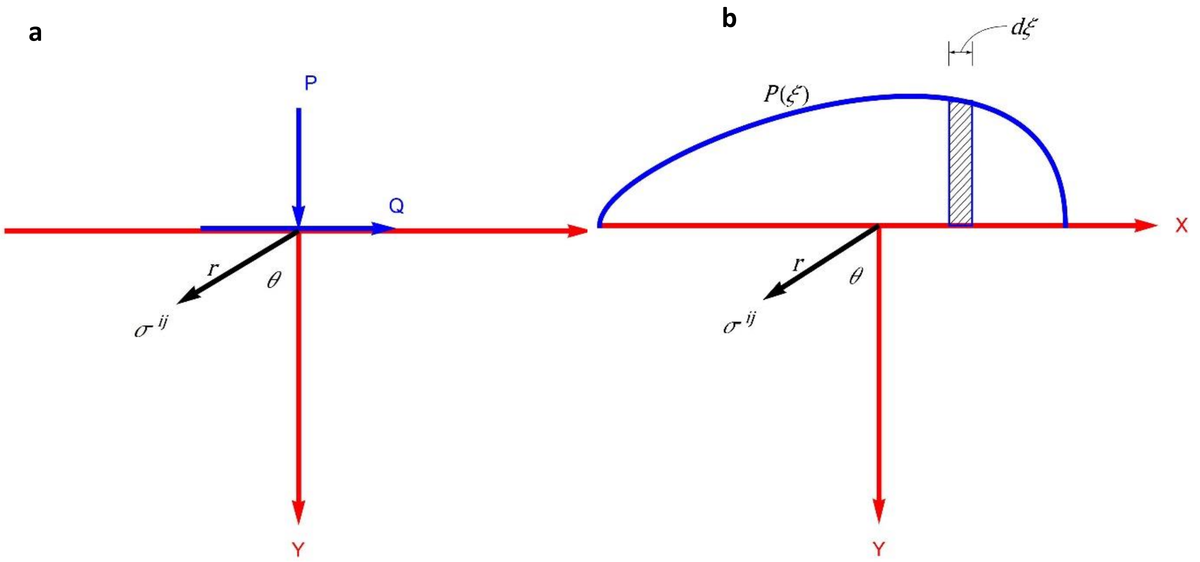

Figure 2-10: (a) Point force P and Shear force Q acting on the Surface of a Half-Plane and the resulting stresses in the Half – Plane (b). Pressure distribution acting over the surface of a Half – Plane. Note that the distribution of Q(ξ) lies on the x axis for each dξ (Reproduced from (Hills et al. 1993))

shearing force Q across the surface (Hills et al., 1993):

$$\emptyset = -\frac{r\theta}{\pi}(P\sin\theta + Q\cos\theta) \tag{2.6}$$

[9] With this assumption, the contact patch dimensions are small compared to the dimensions of the bodies and thus we can treat the contact integrals in equation (2.4) independently.

Equation (2.6) is the Airy stress function for the half–plane subject to a point load P and shearing force Q where the definitions of r and θ are shown in Figure 2-10 (a). The individual stress components are obtained from the relation between the stress components and the stress function (Hills et al., 1993). From the set of equations for the point force solutions, the solutions for other forms of loading on the half-plane such as that presented in Figure 2-10(b) can be obtained by discretizing the distribution of the load over the half–plane and integrating the resulting point force solutions of each discretization over the contact length as described in Barber (2018). In this case, the solutions are given in Hills et al. (1993) and Johnson (1985). In three-dimensional space, Boussinesq stress functions can be used to obtain the stresses (Barber 2010) and displacement functions of Papkovich-Neuber as described in Barber (2010). The complex variable representation of Muskhelishvili (1954) have also been used to construct solutions of the stress fields.

Lévesque et al. (2011) have used this approach to obtain the stress fields in the contact between a wire compressed between two identical clamps which led to a conclusion that the influence of the opposing contact interface cannot be ignored. This conclusion is also in line with those of Timoshenko and Goodier (1951) and (Johnson, 1985) who have shown that the way the body is supported is important. The observation of Lévesque et al. (2011) is so because for a wire to clamp contact, it is difficult that both the contact length and width respect the half-space assumption and as such, the stress field at the top and bottom contacts interact thereby violating the half-space assumption.

A limitation of this approach is that it requires the distribution of the normal pressure, shear stresses on the interface, or dimensions of the contact patch. When this is not known, the slope formulation[10] (Barber, 2018; Hills et al., 1993) of the contact gap functions are obtained in terms of the stress functions for the point force solution. This approach leads to Cauchy integrals for the contact pressure and shear tractions subject to only the conditions that they satisfy the equilibrium conditions of the contact tractions. For the case of a wire-to-clamp contact with the assumption that both wire and clamp are deformable, is a line contact and the half-space assumption holds, the Cauchy integrals can be written as (Barber, 2018) :

$$\frac{du_x}{dx} = \frac{-2\beta p(x)}{E^*} - \frac{2}{\pi E^*}\int_b^a \frac{q_x(\xi)d\xi}{(x-\xi)} \tag{2.7}$$

$$\frac{du_z}{dx} = \frac{-2\beta p(x)}{E^*} - \frac{2}{\pi E^*}\int_b^a \frac{p(\xi)d\xi}{(x-\xi)} + \frac{2\beta q_x(\xi)}{E^*} \tag{2.8}$$

$$\frac{du_y}{dx} = -\frac{2}{\pi E'}\int_b^a \frac{q_y(\xi)}{(x-\xi)} \tag{2.9}$$

Where $u_x, u_y \ and \ u_z$ are the relative surface displacement between the wire and clamp in the x, y and z direction as shown in Figure 2-11 (b), β represents the degree of coupling between the tangential traction $q_x(\xi)d\xi$ and the normal pressure $p(\xi)d$, E^* and E'represents the composite modulus of both contact materials defined as:

$$\frac{1}{E'} = \frac{1+v_{wire}}{E_{wire}} + \frac{1+v_{clamp}}{E_{clamp}} \tag{2.10}$$

$$\frac{1}{E^*} = \frac{1-{v_{wire}}^2}{E_{wire}} + \frac{1-{v_{clamp}}^2}{E_{clamp}} \tag{2.11}$$

[10] This is called the Integral equation formulation sec. 6.2 of Barber (2018) because it leads to an Integral equation. However, this integral is obtained from the derivative of the gap function in Equation 6.6 of the same document and thus the name.

This approach has been used by Andresen et al. (2019) for the solution of a compound punch indenting a half-plane with normal force, tangential force and bending moment. Ciavarella et al. (1998) have also analyzed a flat punch with rounded edges subjected to normal force and tangential force.

The flat punch with rounded edges solution of Ciavarella et al.(1998) represents the solution

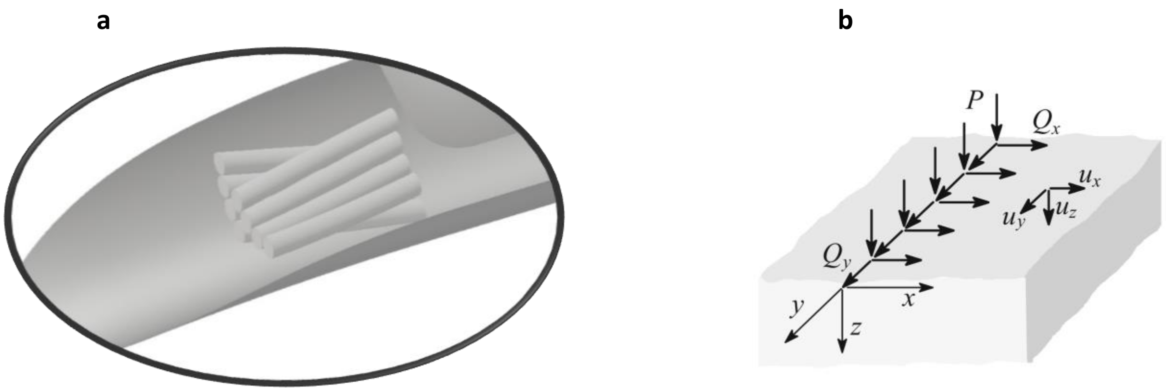

Figure 2-11: (a) Diagram of the various types of contacts in a conductor. (b) Corresponding half space representation of the wire to clamp contact (Image b reporduced from (Barber, 2018))

of the symmetric wire to clamp experimental set-up presented in Lalonde (2017) and shown in Figure 2-12 in the longitudinal direction subject to the restriction that the coupling between the clamp and wire be ignored since their modulus of elasticity are similar and the half space assumption is satisfied. It is important to mention that the contact analyzed by Lalonde (2017) is a three-dimensional contact given that the surface profiles of both bodies are quadratic and the gap functions along the R_{c1} and R_{c2} (see Figure 2-12(a)) both vary; hence, the plain strain solution of Ciavarella et al.(1998) is only applicable over a thin strip at the center of the contact and its applicability decreases in the R_{c2} direction due to the decrease in the contact pressure. The observations of Lévesque et al. (2011) also hold for the fretting set-up of Lalonde (2017) if the contact length is greater than the diameter of the wire.

The fretting fatigue test set-up of Omrani (2021) (Figure 2-7) is similar to that of Lalonde (2017) (Figure 2-12a) except that it does not preserve the geometric symmetry of Figure 2-12a. If the contact normal load is small such that the contact satisfies the half-space assumption, then the wire to clamp contact can be treated as a half-space and the functional form of the contact normal pressure of the contact between the wire and clamp will be the same as that of Lalonde (2017). However, if the half-space assumption is violated, then in accordance with the observation of Lévesque et al. (2011) the contact pressure at the wire-to-bearing contact may affect the contact pressure at the wire-to-clamp contact.

For the wire to wire contact, the normal contact solution for such problems are due to Hertz

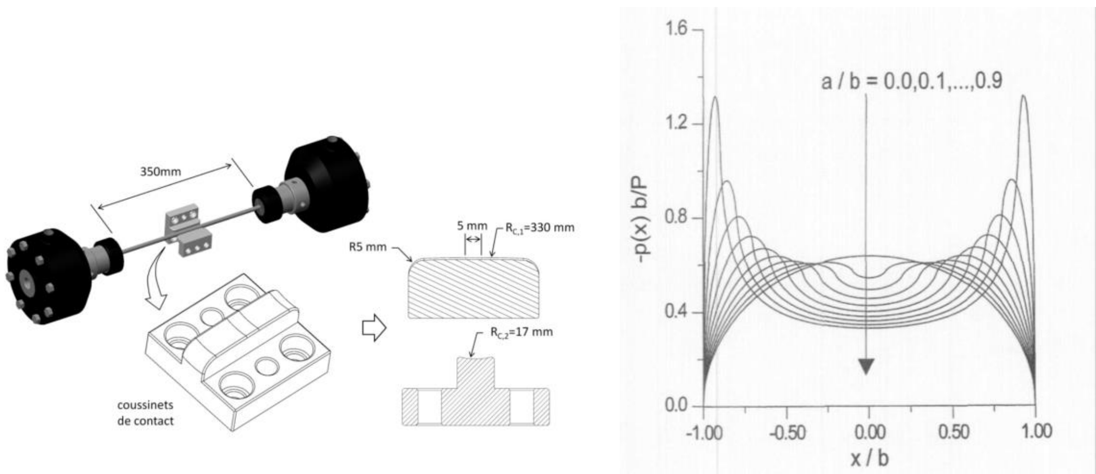

Figure 2-12: (a) Symmetric Wire to Pad Configuration (Source: Lalonde, 2017a). (b) Contact pressure distribution along longitudinal contact region (Source: Ciavarella et al. 1998)

(Barber, 2018; Johnson, 1985) for the elliptical contact case. However, this solution also has the limitation that the half-space assumption must be satisfied (Barber, 2018; Johnson, 1985). Tangential stresses for the three-dimensional elliptical contact in sliding condition can be obtained by methods presented by (Barber, 2018; Hills et al., 1993; Johnson, 1985).

When friction exists between the interfaces in contact, the contact is in partial slip; two portions exist at the contact interface. A portion of full stick where $q(x,y) < \mu\, p(x,y)$ and a region of slip $q(x,y) = \mu\, p(x,y)$ with μ being the friction coefficient. The method to construct partial slip solutions to contact problems are summarized by Hills et al. (2018). Barber (2018) discusses the cases for the partial slip solutions of elliptical contacts for monotonically increasing shear force, cyclic shear force and cyclic normal force. A similar technique (for the cyclic shear case) has been applied by Lévesque and Legeron (2010) for an elastic-perfectly plastic contact of wire to clamp contact. However, cases of cyclic normal and cyclic shear loads are yet to be analyzed for the wire-to-clamp and wire-to-wire contact using these methods.

2.2.2.2 The Method of Dimensionality Reduction

The method of dimensionality reduction (MDR) (Popov and Heb, 2015) is another method for the analysis of three-dimensional contacts. Although not yet applied to conductor contact

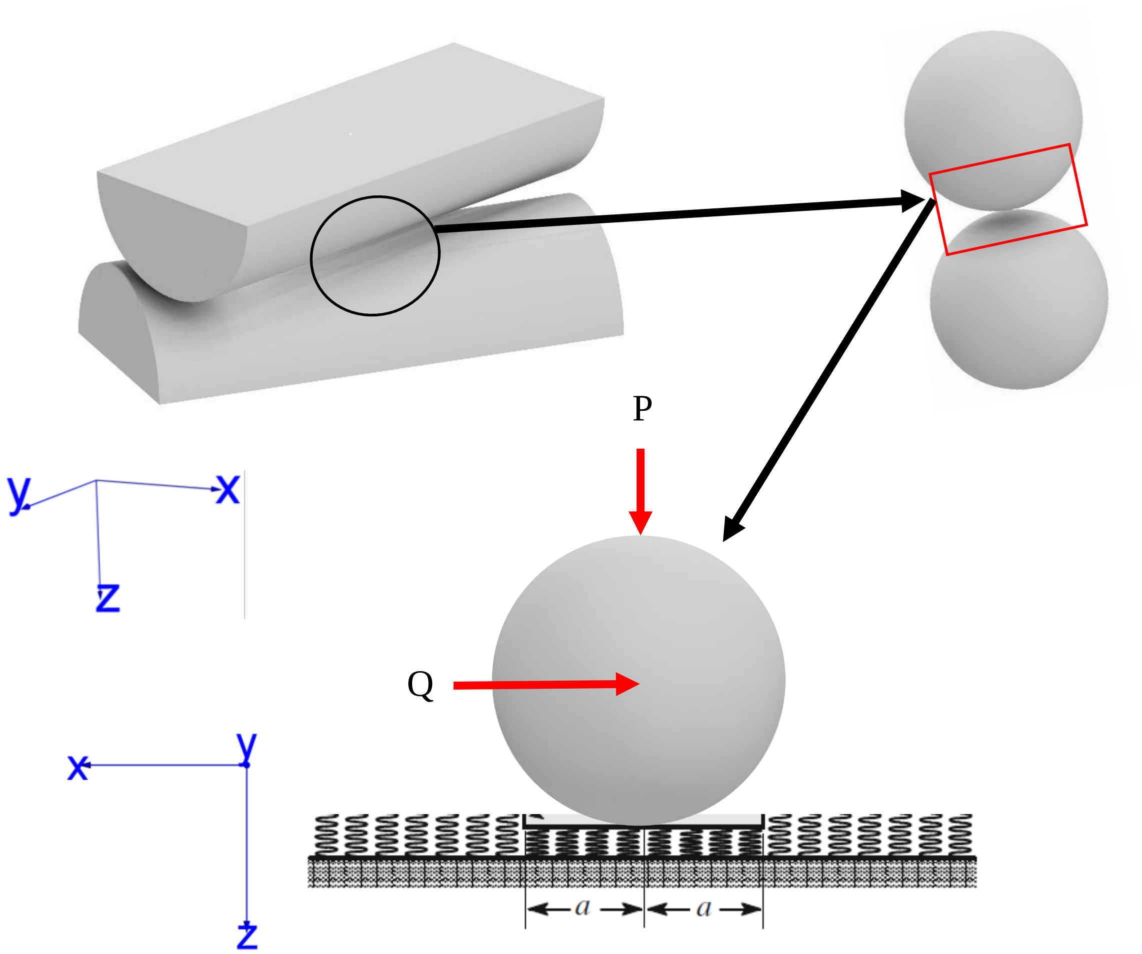

Figure 2-13:(a) Point contact in a conductor. (b). Equivalent spheres embedded in the half-space representing wires. (c). Equivalent Winkler foundation model indented by a sphere equal to the wire of the radius. (Image (c) is modified from (Barber, 2018)).

problems, the MDR requires that the contact be of an axisymmetric nature and involves mapping of the three–dimensional problem into an equivalence one–dimensional problem of the indenter indenting a series of independent springs (wrinkle foundation). Figure 2-13 shows the application of the MDR to the point contact of a conductor.

When the contact patch is small, spheres of radius equal to the wire radius can be embedded in the respective half-space representing the conductor wires. In this case, it can also be assumed that the deformations produced by the contact tractions (both normal and tangential) are the same as those that would be produced in an equivalent body (sphere in this case) in contact with a plane surface (Barber, 2018). With this simplification, normal gap functions of the contacting spheres can be described by the equivalent sphere of radius R in contact with a plane:

$$\frac{1}{R} = \frac{1}{R_1} + \frac{1}{R_2} \tag{2.12}$$

Where R_1 and R_2 represent the radius of the wires that compose the contact. The resulting contact equations are provided by (Popov and Heb, 2015) and given below for the case of normal contact:

$$\Delta k_z = E^* \Delta x \tag{2.13}$$

Where Equation (2.13) represents the stiffness of an individual spring of the contact that supports the sphere over a small distance Δx and E^* is the composite modulus defined in Equation (2.11). The vertical displacement in the contact zone is given by (Popov and Heb, 2015):

$$u_z(x) = d - \frac{x^2}{2R_{wink}} \tag{2.14}$$

Where d represents the depth of the elastic foundation after the application of the load P *and* $\frac{x^2}{2R_{wink}}$ represents the normal gap function of the equivalent Winkler foundation -sphere model before loading. By using the Popov rule of $R_{wink} = R/2$, the half contact length is obtained from (2.14) by setting $u_z(a)$ = 0 (Popov and Heb, 2015):

$$a = \sqrt{Rd} \tag{2.15}$$

The normal force-displacement relation of the foundation and the sphere is obtained by integrating the spring relation over the contact length:

$$P = \int_{-a}^{+a} E^* u_z(x) = \int_{-\sqrt{Rd}}^{+\sqrt{Rd}} E^* \left(d - \frac{x^2}{R}\right) dx = \frac{4}{3} E^* d\sqrt{dR} \tag{2.16}$$

Equations (2.15) and (2.16) are the exact solutions for the case of a contact between two spheres. By using d from (2.15) in (2.16), we obtain the half contact length a as (Lévesque, 2009; Popov and Heb, 2015):

$$a = \left(\frac{3\ P\ R}{4\ E^*}\right)^{1/3} \tag{2.17}$$

The normal contact pressure can be obtained from the following integral (Popov and Heb, 2015):

$$\sigma_{zz}(r) = \frac{1}{\pi} \int_{r}^{\infty} \frac{d/dx\left(p_x(x)\right)}{\sqrt{x^2 - r^2}}\ dx \tag{2.18}$$

where $p_x(x)$ is the linear force density defined as:

$$p_z(x) = \frac{f_N(x)}{\Delta x} \tag{2.19}$$

and $f_N(x) := \Delta k_z\, u_z(x)$.

For the case of two wires in contact as shown in Figure 2-13(a), Equation (2.18) gives the contact pressure as (Popov and Heb, 2015):

$$\sigma_{zz}(r) = -\frac{2}{\pi} E^* \left(\frac{d}{R}\right)^{1/2} \sqrt{1 - \left(\frac{r}{a}\right)^2} \tag{2.20}$$

Following the same approach as for the normal contact force P, the tangential stiffness per unit length Δk_x is defined as:

$$\Delta k_x = G^* \Delta x \tag{2.21}$$

where $G^*$is defined as:

$$\frac{1}{G^*} = \frac{2 - v_1}{4G_1} + \frac{2 - v_2}{4G_2} \tag{2.22}$$

and G_1 and G_2 are the shear modulus of the first and second wires respectively and G^* is the composite shear modulus of the contact.

In tangential contact, a spring may be sticking or sliding when the contact is in partial slip. For the case of sticking, let $x = \pm c$ represent the boundary that separates the stick region from the slip region and noting that at this boundary $q_x(c) = \mu f_N(c)$, where q_x and $f_N$represents the tangential force and normal force on an individual spring on the stick–slip boundary, the sticking force on a spring on this boundary using this Coulomb condition is then :

$$G^* \Delta x\, u_x(c) = \mu \left(d - \frac{c^2}{R}\right) E^* \Delta x \tag{2.23}$$

Which gives the tangential displacement of a spring at the stick-slip boundary as

$$u_x(c) = \mu \frac{E^*}{G^*}\left(d - \frac{c^2}{R}\right) \tag{2.24}$$

For the contacts in the slip–zone, the same Coulomb law holds with the boundary now being between *c to a*. Using this, the total tangential force in the contact zone is:

$$Q = \underbrace{2\int_0^c G^*\, u_x\, dx}_{contribution\ from\ stick\ region} + \underbrace{2\int_c^a \mu\left(d - \frac{x^2}{R}\right)E^*}_{contribution\ from\ sliding\ region} = \mu P\left(1 - \left(\frac{c}{a}\right)^3\right) \tag{2.25}$$

$$\frac{c}{a} = \left(1 - \frac{Q}{\mu P}\right)^{1/3} \tag{2.26}$$

The stresses induced in the contact is given by Abel integrals of the form (Popov and Heb, 2015) :

$$\tau_{zr}(r) = \frac{1}{\pi}\frac{1}{r}\frac{d}{dr}\int_r^a \frac{d/d\left(q_x(x)\right)}{\sqrt{x^2 - r^2}}dx - \frac{1}{\pi}\frac{q_x(a)}{\sqrt{a^2 - r^2}} \tag{2.27}$$

where $q_x(x) := \frac{\Delta k_x u_x}{\Delta x}$. The tangential stress for the two-wire contact illustrated in Figure 2-13 is then:

$$\tau_{zr}(r) = -\frac{2\mu E^*}{R\pi}\left\{\sqrt{a^2 - r^2}\ \ [H\left(1 - \frac{r}{a}\right)] - \sqrt{c^2 - r^2}\ \ H\left(1 - \frac{r}{c}\right)\right\} \tag{2.28}$$

$$where\ [H(.)]\ is\ the\ heaviside\ step\ function$$

The MDR converts the three dimensional contact into two one-dimensional problems – one in the normal direction and the other in the tangential direction. The MDR provides the exact solutions for the axially symmetric contact problem of two spheres either in tangential or normal contact. Thus, if the contact between two wires can be approximated by a circular area[11] and fulfil the half–space assumption, the MDR also provides methodologies easier to implement than the full elliptical solution resulting from stress and displacement stress functions. One of its advantages is for non–monotonic variation of the tangential force as the incremental equations are easier to solve numerically than those using the stress and displacement functions since the problem becomes one-dimensional.

Not all conductor contacts can be idealized as half-space thereby limiting the applicability of the method of dimensionality reduction. Furthermore, its applicability reduces with increasing eccentricity of a contact ellipse[12]. In this regard, the experimental work of Omrani (2021) has shown that under the action of bending moment, the eccentricity of contact can become large for wire to clamp contacts making the MDR inapplicable to such contacts.

2.2.2.3 Structural Elements in Conductor Contact Mechanics

In 2018, it was shown by Lalonde et al.(2018) that a variation in bending moment governs the conductor fatigue phenomenon between the keeper edge (KE) and the last point of contact (LPC). More recently, Omrani et al. (2021) have also shown that bending moment creates elliptical contacts with large semi major axis. If this is the case, then the method of dimensionality reduction and using stress and displacement functions with the half-space assumption cannot be used.

One of the approaches to overcome the restriction of the half-space assumption is to treat the wires of the conductors as a beam where the effect of the bending moment can be included. It has been remarked by Timoshenko and Goodier (1951) and Johnson (1985) that if the beam depth is large in comparison with the length of the contact, then the stress field in the contact

[11] Such an approximation has been used by Lévesque and Legeron (2010)
[12] The contact marks often found in conductors are of elliptic geometry.

region can be regarded as a superposition of the usual Hertzian contact stresses and those from simple bending theory. However, when the contact length becomes comparable to the depth of the beam, the stresses are bending dominated.

The analytical solution of contact problems using elements such as beams, plates and shells is an area that has been less studied. However, beam and shell structures are increasingly used for solution of conductor problems (Baumann and Novak, 2017; Lalonde et al., 2018) due to the reduced number of degrees of freedom. However since structural elements reduce the three-dimensional details of contacts, it is important to determine what information is lost for contact

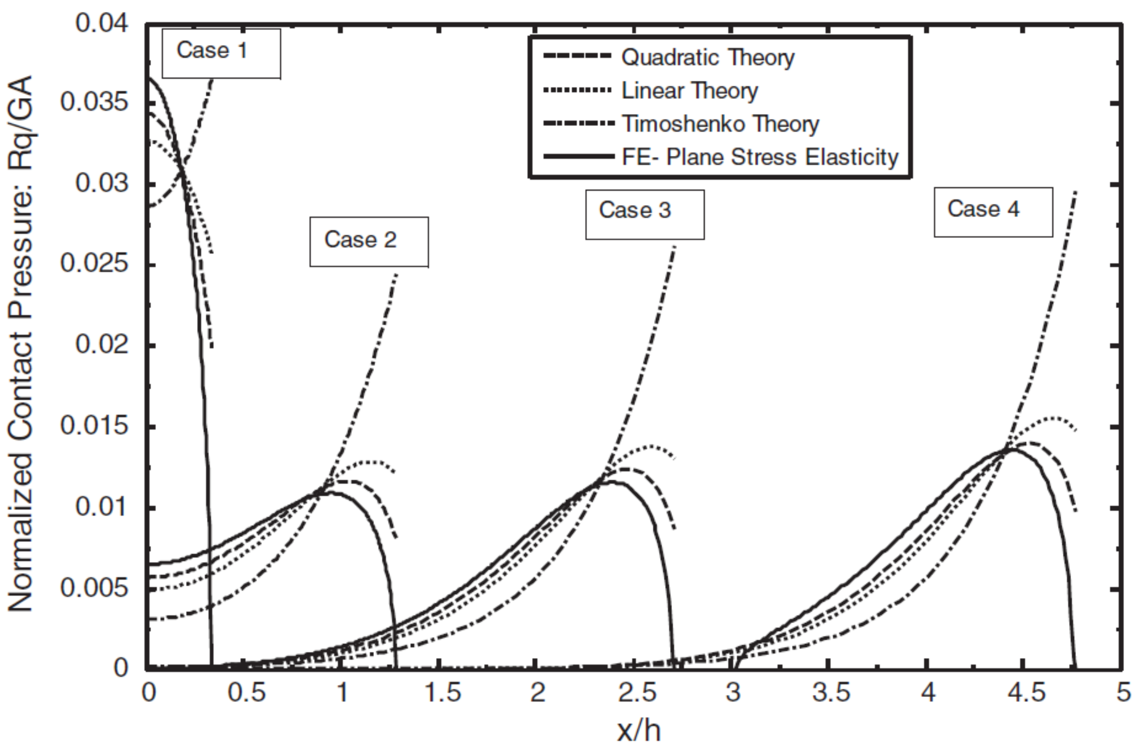

Figure 2-14: Contact pressure between a 2D beam and a circular surface (Gasmi, Joseph, Rhyne, & Cron, 2012).

analysis. In addition, in beam theory, the distribution of stresses is a function of the order of the interpolating polynomial.

Consider a beam under indentation by a force (P_{app}) that is in contact with a cylindrical surface , it reacts with a normal line contact pressure q at the contact line, the distribution of the line pressure follows the Hertz contact pressure (Gasmi et al., 2012; Castillo and Barber, 1997; Kim et al., 2014) as shown in Figure 2-14 (case 1) but for P_{app} greater than some value P_0, the contact line bifurcates into two contact regions at the ends of the contact region with a separation region at the center of the contact as shown by Kim et al. (2014). This behavior also

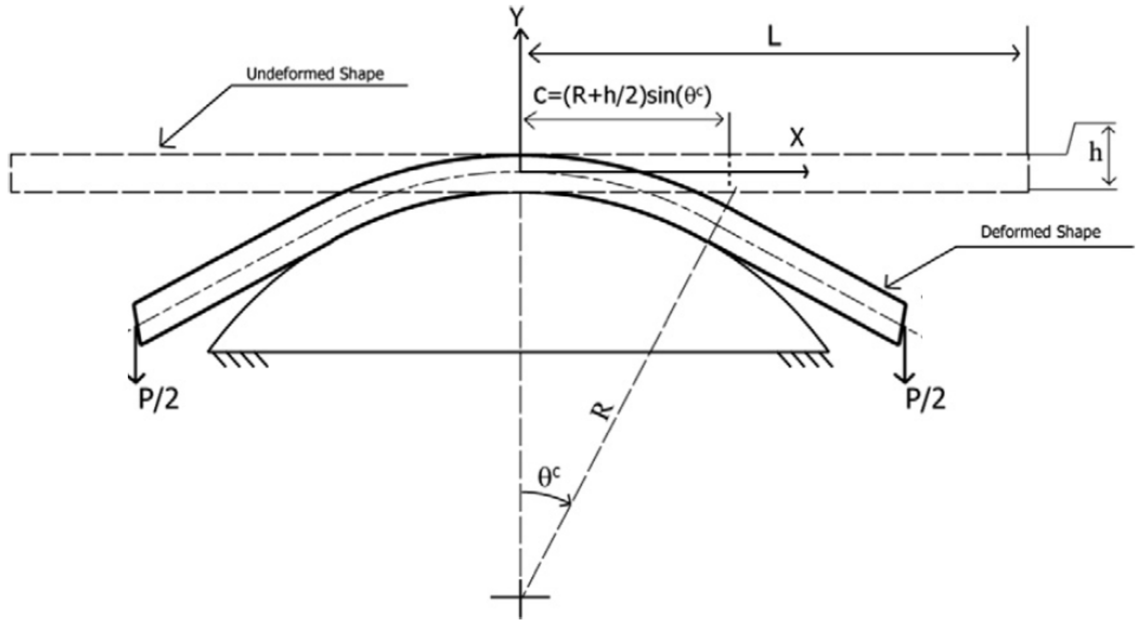

Figure 2-15: Frictionless beam to cylindrical surface contact with symmetric end shear and moment loading (Adapted from: Gasmi et al., 2012)

holds true if instead of applying the contact force we apply end moments (Essenburg, 1975; Naghdi and Rubin, 1989) or apply vertical forces to the ends of the beam (Gasmi et al., 2012) as shown in Figure 2-15. This bifurcated contact pressure distribution is different from that observed in the normal Hertz contact problem for the half–plane and this has been attributed to the localized bending of the beam in the contact region (Barber, 2018; Essenburg, 1975)[13].

Figure 2-14 shows the normalized line contact pressure between a plane beam and a cylindrical surface obtained from a 2D FE analysis and from three different beam theories developed by

[13] Page 264 of Barber (2018) for further discussion on this phenomenon.

Gasmi et al. (2012). A diagrammatic representation of the beam and cylindrical surface is shown in Figure 2-15.

In this analysis, the beam lays symmetrically on the surface and is subjected to symmetrical shear forces at it ends. When the half contact length (*x–coordinate)* is less than the depth of the beam h, (Figure 2-14 (case 1)), the contact pressure approximates a 2D Hertzian contact distribution as predicted by the plane stress finite element model. For the same contact length, the Timoshenko beam theory (TBT) predicts a different distribution and predicts that the maximum contact pressure is at the edge of the contact region rather than at the center. As the contact half–length increases beyond the depth of the beam, two different types of contact pressure distributions different from the Hertz type emerge. The first one (case 2) has a lower contact pressure at the center of the contact and peaks towards the end for $x=1.2h$ (Figure 2-14 (case 2)); the TBT captures the trend of the contact line pressure distribution but peaks at the contact edge. For the last two contact pressure distributions (Figure 2-14, case 3 and 4) where the half contact length $x > 2.5h$, there is no contact at the center. The TBT is able to capture the separation but again peaks at the edge, which is incorrect. In fact, the TBT overestimates the contact force per unit length in all cases. This is because the TBT is stiffer than the higher-order beam theories. Nonetheless, the resultant contact force and displacement are the same for all the beam theories investigated by Gasmi et al. (2012) and they all match those of the plane elasticity FE solution.

It was remarked by Gasmi et al. (2012) that depending on the beam displacement kinematics, the contact length at which separation begins varies. It was observed that for separation to occur in the TBT, the half contact length needed to be greater than ten times the beam depth (i.e. $x > 10h$). This differs from higher beam theories and the elasticity solution presented in (Gasmi et al., 2012). This observation implies that if the TBT is used to model the contact between a

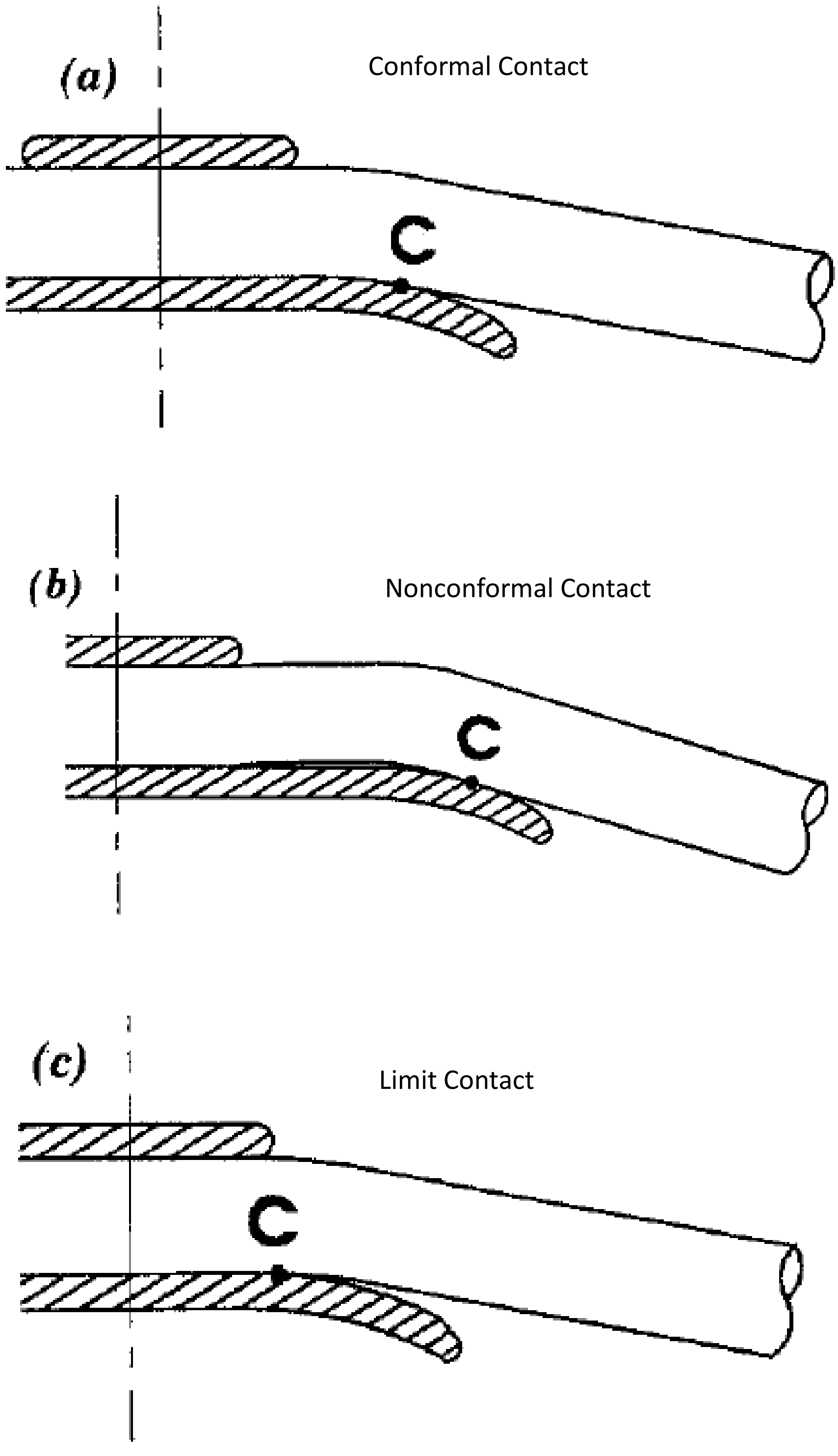

Figure 2-16: Three types of contact modes between a conductor and a clamp (Alain Cardou, Leblond, & Cloutier, 1993)

beam and a surface, when separation is supposed to occur due to bending, it may predict a contact condition. This conclusion has also been explicitly observed by Naghdi and Rubin (1989).

The condition of separation has been observed in an ACSR Bersimis conductor's axial plane of symmetry (Cardou et al., 1993) as shown in Figure 2-16 (b). In their work, these authors used strain gauges attached to the bottom face of the clamp to reproduce the contact line

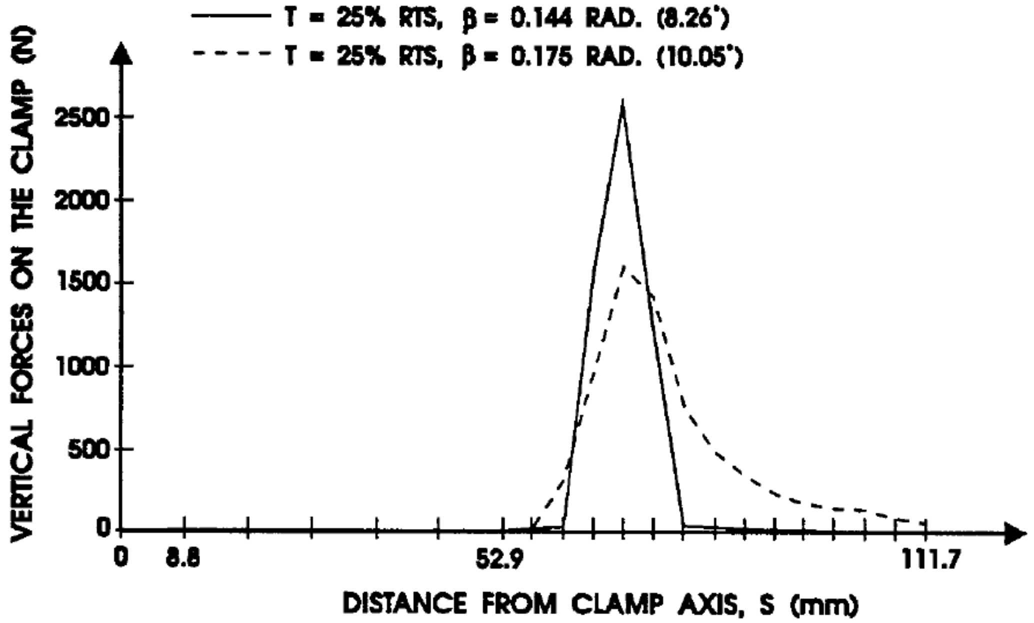

Figure 2-17: Contact line force prediction for contact between Bersimis conductor and a generic clamp (Source: Cardou et al. (1993))

pressure on the wire to clamp contact. This contact line pressure is as shown in Figure 2-17. This crude approximation reproduced from strain gauge measurements gives an approximation to the distributions shown in Figure 2-14 case 1 and 2.

The observation of the unique contact pressure distribution shown in Figures 2-14 and 2-17, which has been attributed to bending, has been often neglected in the modeling of single contacts between a wire and the clamp (Redford et al., 2018;) and in single wire to clamp experiments (Zhou et al., 1995). It is only recently that Omrani et al. (2021) has been able to conceive a single wire to clamp experiment that considers the effect of bending.

Essenburg (1975), Naghdi and Rubin (1989), and Gasmi et al. (2012) have shown that to approximate the line pressure properly using the TBT, the Timoshenko beam theory must include higher order terms, especially for the transverse normal stress. For example, for the 2D Timoshenko beam theory, the kinematics for small strain-small displacement are given as (Gasmi et al., 2012):

$$U_x(x,y) = U(x) + y\theta(x) \tag{2.30}$$

$$U_y(x,y) = w(x) \tag{2.31}$$

Where $U_x(x,y)$ represents the axial deformation of the beam, $U_y(x,y)$ represents the deformation of the beam in the direction perpendicular to the axial direction, y represents the thickness coordinate of the beam, $w(x)$ is the displacement of the beam centerline and $\theta(x)$ the rotation of the beam centerline. The strains obtained by the Timoshenko beam kinematics Equations (2.31) imply that the strain in the thickness direction $\varepsilon_{yy} = \frac{\partial U_y(x,y)}{\partial y} = 0$ and thus the beam cannot carry any normal strain in the normal direction. This is one of the anomalies responsible for the behavior of this beam theory shown on Figure 2-14. Hence, for the TBT the contact line pressure is balanced by shear and bending only.

Another anomaly arising from the Timoshenko beam theory when used for contact problems is its inability to model bending moments induced by the contact loads. Since the loads are applied at the elastic line representing the beam, these moments are lost. This can be observed from the equilibrium equations for a 2D Timoshenko beam in contact with a cylindrical surface at the top and bottom(Gasmi et al., 2012)[14]:

$$\frac{dN(x)}{dx} = -(q_x^+ + q_x^-) \tag{2.32}$$

[14] This reference did not denote the contact tractions as $q_x^{(+)}$ and $q_x^{(-)}$ but used a single term q_x. This is correct since only the centerline of the beam can be loaded. However, $q_x^{(+)}$ and $q_x^{(-)}$ are used here to indicate that the beam could be loaded at the top and bottom

$$V(x) - \frac{dM(x)}{dx} = 0 \tag{2.33}$$

$$\frac{dV(x)}{dx} = -\left(q_y^+ + \ q_y^-\right) \tag{2.34}$$

subject to the appropriate mechanical and geometric boundary conditions.

where $N(x)$, $V(x)$ and $M(x)$ represent the axial force, shear force, bending moment along the beam center line coordinate *x*. $q_x^+ + q_x^-$ represents the tangential tractions at the top and bottom of the beam and $q_y^+ + \ q_y^-$ represents the normal traction at the top and bottom of the beam. Since $U_y(x, y)$ is independent of *y*, the contact tractions are at the beam centerline and not at the beam surface (top or bottom).

To correct for the loss of moment and to include the influence of the transverse normal strain, (Gasmi et al., 2012) used the following beam kinematics:

$$U_x(x, y) = U(x) + y\theta(x) \tag{2.35}$$

$$U_y(x, y) = w(x) + y\psi(x) + y^2\beta(x) \tag{2.36}$$

the kinematics now include a quadratic dependence of $U_y(x, y)$ as a function of *y*, and the normal strain $\varepsilon_{yy} = \psi(x) + \ 2y\beta(x)$ is not zero, unlike the Timoshenko beam. Thus, this beam theory is closer to reality. The equilibrium equations for the 2D beam with kinematics given by Equations *(2.35 and 2.36)* are provided in (Gasmi et al., 2012) as:

$$\frac{dN(x)}{dx} = -(q_x^+ + q_x^-) \tag{2.37}$$

$$V(x) - \frac{dM(x)}{dx} = \frac{h}{2}(q_x^+ - q_x^-) \tag{2.38}$$

$$\frac{dV(x)}{dx} = -\left(q_y^+ + q_y^-\right) \quad (2.39)$$

$$H(x) - \frac{dJ(x)}{dx} = \frac{h}{2}\left(q_y^+ - q_y^-\right) \quad (2.40)$$

$$2S(x) - \frac{dT(x)}{dx} = \frac{h^2}{4}\left(q_y^+ + q_y^-\right) \quad (2.41)$$

subject to the appropriate mechanical and geometric boundary conditions.

where $H(x) = \int \sigma_{yy}\, dA,\ J = \int y\, \tau_{xy}\ dA,\ S = \int y\, \sigma_{yy}\ dA,\ T = \int y^2 \tau_{xy}\ dA\ \mathit{and}$ A is the cross-sectional area of the beam. Immediately from Equations (2.38) and (2.39), the quantities $\frac{h}{2}(q_x^+ - q_x^-)$ and $\frac{h}{2}\left(q_y^+ - q_y^-\right)$ are identified as the moment[15] terms missing from the Timoshenko formulation, which, if the difference between contact tractions is small do not matter.

This beam formulation[16] given by Equations (2.37) through (2.41) now accounts for the normal strain and moments couples due to contact, the number of equations has increased. However, the beam theory like the TBT still has a contact pressure distribution that is discontinuous at the contact edge.

Given the observation that for small difference in the contact tractions, the contact moment terms do not matter, the increasing complexity of beam theories and the complexity of conductor-clamp contact analysis, the Timoshenko beam theory is a good compromise between complexity and accuracy for the reliability analysis of conductor-clamp assemblies. The limitations such as prediction of sticking instead of separation (Gasmi et al., 2012) and large

[15] In a 3D case, a moment term resulting from torsion is also present. See (konyukhuv & Schweizerhof, 2012) so that in total there are three couples not accounted for by the Timoshenko beam theory

[16] This beam formulation is the same one shown in Figure 2-14 called quadratic beam theory

contact pressure concentration at the contact edge as shown in Figure 2-14 for the TBT will lead to predicting probabilities of failure than are higher than they should be. Thus, before the TBT can be used for reliability analysis of overhead conductor-clamp assemblies, it is necessary to develop ad hoc strategies that would counteract the effect of the deficiencies of the TBT on fatigue life predictions.

2.2.3 The Finite Element Method

In the numerical solution of contact problems in conductors, the finite element method is the most used procedure (Gang, 2013; Baumann and Novak 2017, Lalonde et al., 2018; Said et al., 2020). Herein, only the literature on modelling full conductor/clamp assemblies are reviewed.

Gang (2013) presented the first finite element (FE) model of a conductor-clamp system with all contacts reproduced in a 3D solid FE framework. This work explored the behavior of a 2-layer Drake conductor under tension and bending reproducing experimental observations of Zhou et al.(1994b) that the critical regions for fretting fatigue are between the keeper edge (KE) and the last point of contact (LPC) between the conductor and the clamp. The disadvantage of this model is the small model length considered. The meshing scheme of this work is shown in Figure 2-18c. Only a length of 184mm was studied; even with this small length, a fretting cycle was reported to take 3.5 days (Gang, 2013) Also, symmetry conditions were used at the suspension clamp center (SCC). It has however been shown by Baumann and Novak (2017) to produce consistent bending stiffness for the Drake conductor, the model length must be at least 500mm. Thus, it is not practical to use such a modeling approach for the purpose of structural reliability computations where multiple runs of the same model are required.

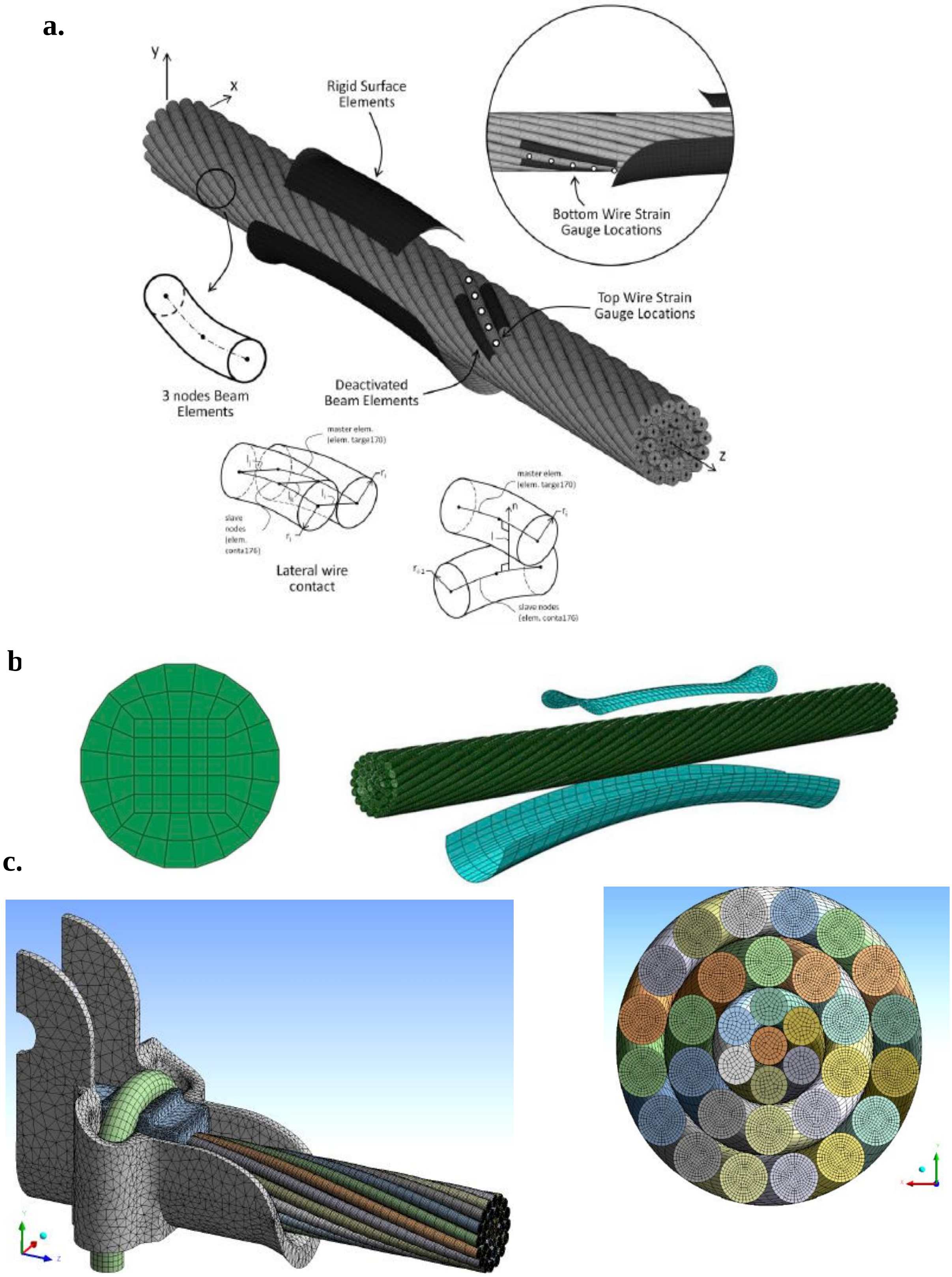

Figure 2-18:Finite Element Models of Overhead Conductors Using (a). Timoshenko beam to beam and beam to surface contact (b). Hexahedron solid elements with quadrilateral surface to surface contact (c). Hexahedron solid elements with quadrilateral surface to surface contact (Sources: Lanlonde at al. (2018); Said et al. (2020); Gang (2013))

Lalonde et al. (2018) produced the FE model of a conductor-clamp system using 3D

Timoshenko beam finite elements with beam-to-beam (BTB) contacts and beam-to-surface (BTS) contacts as shown in Figure 2-18 a. This approach overcomes the limitation of the model of Gang (2013) allowing for large model lengths and efficiency in computation time. For a Bersfort conductor-clamp assembly, a computation time of 18 hours was reported. Hence, the approach of Lalonde et al. (2018) is a more efficient alternative for studying the reliability of overhead conductors.

The limitation of the 3D Timoshenko beam approach of Lalonde et al. (2018) is the same as those discussed in section 2.3.2 for the Timoshenko beam theory. In addition to these, the 3D Timoshenko beam approach is unable to account for stress gradient observed in fretting fatigue in overhead conductors.

To account for the rapidly varying stress along the depth and surface of the wires of the conductor, Said et al. (2020) have used a multiscale approach where the global conductor model is first solved (Figure 2-18 (b)) and the forces from this global model are applied to a local model of a single wire-wire contact. In this work, the variation of the normal force as a function of time has been neglected in the local model. However, as observed by Lalonde et al. (2018) the contact conditions can go from contact to separation in a load cycle for the contacts between the last layer of a conductor and the bottom of the suspension clamp. In other words, the normal force varies considerably and is null where separation occurs. It is also known that bending can introduce contact normal tractions that are quite different from those produced by a static normal force (Kim et al., 2014) with the contact normal pressure distribution tending to be larger in size (Omrani et al. 2021). Thus, the modeling approach of Said et al. (2020) does not apply to the wire to clamp contacts which have mostly a varying normal force component due to bending. These set of contacts have also been shown to be critical for fretting fatigue in a Bersfort conductor by Omrani et al. (2021).

2.2.4 Summary

The equations of equilibrium for a three-body contact problem exemplifying the contact between a conductor wire and the clamp were discussed. It was extended to a conductor-clamp assembly. Three methods that are available to solve a contact problem were reviewed from the literature. The simplifying assumptions and limitations of each of the method were discussed. For the analytical models that rely on the half-space assumption, it has been discussed that this assumption is not valid for the conductor wire to clamp contact as discussed by (Lévesque et al., 2011) and observed experimentally in the work of Omrani et al. (2021). For the models that make use of beam theory, it has been discussed that normal stress to the beam axis are important variables that limit the applicability of the beam theories constrained against normal deformation to describe properly the separation kinematics between the KE and LPC. Nevertheless, the beam theories produce the correct stress resultants and resultant displacements (Gasmi et al., 2012) and thus can be used as ad hoc approach for fretting fatigue analysis of overhead conductors if what is required is the fatigue life of the conductor and the exact contact stress distribution is not needed.

The finite element method was reviewed, it was concluded that the FE method with beam discretization provides the most efficient means for computational structural reliability analysis of overhead conductors. Thus, this approach is adopted and used in this thesis.

2.3 STRUCTURAL RELIABILITY OF OVERHEAD CONDUCTOR-CLAMP SYSTEMS

In the previous sections, the behavior of contacts in conductors was derived under the assumption that the factors controlling the response of the conductor are known and that the mathematical models are exact. However, as evidenced by the scatter from fatigue experiments of aluminum wires (4.28$\times 10^6$- 5.29$\times 10^8$ cycles around the endurance limit of 50 MPa) (Kaufman, 2008) and three layer conductor fatigue tests (2.5$\times 10^6$- 5$\times 10^8$ cycles around the endurance limit of 8.5 MPa) (Cloutier et al., 2006), the modeling of this phenomenon should include uncertainty quantification.

2.3.1 Fatigue Resistance of Overhead Conductor-Clamp Systems

Conductor-clamp assemblies are multi-component systems and a fundamental question that arises here is how to relate the failure of wires to the overall failure of the conductor, which can be defined as a function of the total number of aluminum wires that fail, e.g. 1st wire failure, 2nd wire failure, 3rd, 4th, or *n*th wire failure.

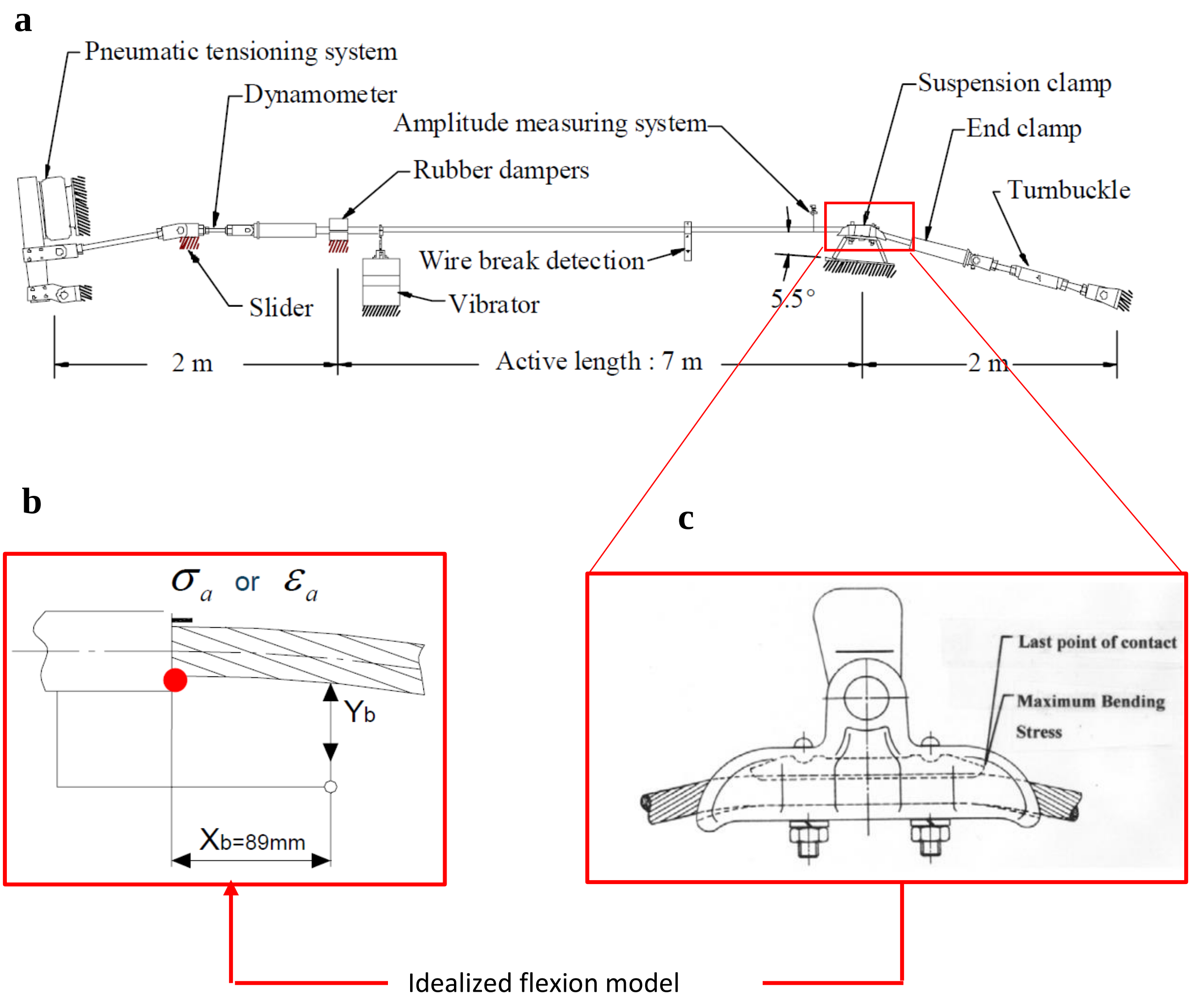

Figure 2-19: Fatigue testing bench for conductor clamp systems (Adapted from (CIGRE-WG-B2.30, 2010)

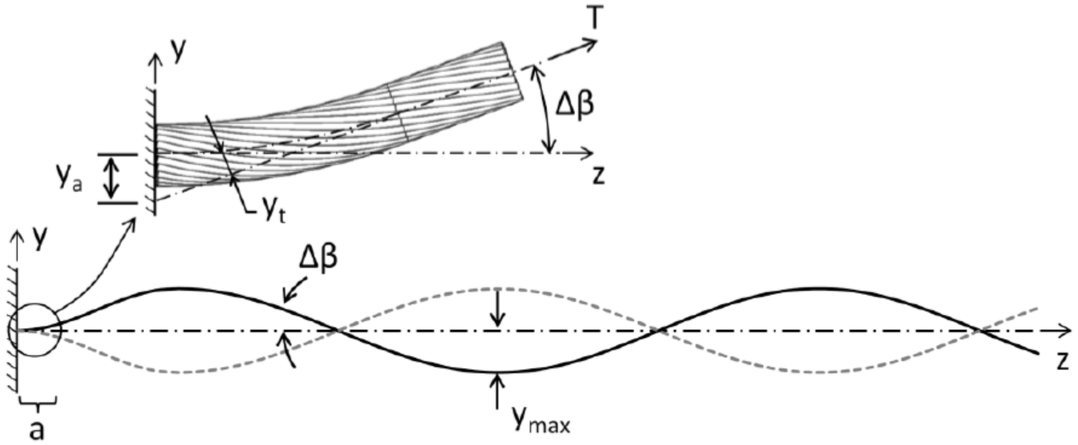

Figure 2-20: Vibration of a conductor in a conductor conductor fatigue test bench (Adapted from Lalonde et al. (2017))

To characterize the fatigue resistance of conductor-clamp assemblies, the conductor-clamp assembly is tested in a specialized testing system shown in Figure 2-19 (a). The conductor is subjected to standing wave vibration as shown in Figure 2-20. Close to the clamp, the conductor is assumed rigidly fixed as shown in Figure 2-19 (c) and the conductor deflection near the fixed end is shown in Figure 2-20. The bending moment *M* induced in the conductor due to the tension *T* near the fixed end are related by (Cloutier et al., 2006; Lalonde 2017):

$$\frac{d^2 y_t}{dz^2} = \frac{M}{E\,I} = \frac{T}{E\,I} y_t \tag{2.42}$$

Where $E\,I$ is the bending stiffness of the conductor. With boundary conditions $z \to \infty, y_t \to 0$ and $z = 0, \frac{dy_t}{dz} = \Delta\beta$, and small displacement assumption, the curvature at the fixed end is given as (Cloutier et al. 2006; Lalonde et al. 2017):

$$\left(\frac{d^2 y_t}{dz^2}\right)_{z=0} = \frac{T}{E\,I} A \tag{2.43}$$

where $A = y(z) / \left(e^{-\sqrt{T/EI}\,z} - 1 + \sqrt{T/EI}\;z\right)$ and $y(z) = -y_a + \Delta\beta\, z + y_t$.

By assuming that the wires of the conductor bending independently, the bending stiffness of the conductor becomes:

$$EI = \sum_{i=1}^{number\ of\ wires} E_i\, I_i \tag{2.44}$$

where E_i and I_i are the Young modulus and moment of inertia of the *i*th wire. With Equation (2.43), it is possible to define an idealized stress σ_a or strain $\varepsilon_a$which relates the amplitude of vibration $y(z)$ at some distance *z* from the fixed end. The industry standard for the distance z is 89mm (Cloutier et al., 2006; IEEE, 2006) as shown in Figure 2-19 (c). Thus, the idealzed stress and strain are (Poffenberger and Swart, 1965; Cloutier et al., 2006; IEEE, 2006; Lalonde et al. 2017):

$$\sigma_a = \frac{d\, E_a\, \left(\frac{T}{4\, EI}\right)}{\left(e^{-\sqrt{T/EI}\ z} - 1 + \sqrt{T/EI}\ \ z\right)} Y_b \tag{2.45}$$

$$\varepsilon_a = \frac{d\ \left(\frac{T}{4\, EI}\right)}{\left(e^{-\sqrt{T/EI}\ z} - 1 + \sqrt{T/EI}\ \ z\right)} Y_b \tag{2.46}$$

where $Y_b = 2\, y(z = 89)$. The Equations (2.45) and (2.46) are called the Poffenberger-Swart Formula. Note that the Poffenberger-Swart equation does not refer to the contact conditions in a conductor.

With the Poffenberger-Swart equation, it is possible to relate the number of cycles at which a conductor wire fails $N := \{N_1, N_2, \cdots\cdots, N_k \mid k \, is \, number \, of \, aluminum \, wires\}$ to the idealized stress or idealized strain.

Using the specialized fatigue test bench (Figure 2-19 (a)) and the Poffenberger-Swart Formula, the set of idealized stress and number of cycles to failure is collected as:

$$\sigma_a N = \{(\sigma_{a,1}, N_{k,2}), (\sigma_{a,1}, N_{k,2}), \cdots\cdots, (\sigma_{a,i}, N_{k,i}) \mid i \, is \, the \, number \, of \, fatigue \, test\} \quad (2.47)$$

A plot of $\sigma_{a,i}$ against $N_{n,i}$ on a linear-log scale characterizes the fatigue resistance of the conductor as the number of cycles the conductor-clamp assembly can undergo at a given idealized stress amplitude before N_k wire failure is observed $N_k|\sigma_a$. This plot is called an SN curve or Wohler curve (Castillo and Fernandez-Canteli, 2009).

Using the set of the Poffenberger-Swart stress and the observed number of cycles to failure, different approaches have been proposed to describe the fatigue resistance of overhead conductor-clamp assemblies.

2.3.1.1 CIGRÉ's Safe Border Line Method

One of the first approaches proposed to define overhead conductor-clamp assemblies' fatigue resistance is the CIGRÉ (Conseil International des Grands Réseaux Electriques) safe border line. The CIGRÉ safe border line is a curve defined as $\sigma_a = A\, N_1^b$ fitted to the dataset of the Poffenberger-Swart stress σ_a and observed number of cycles to first wire failure N_1 (CIGRÉ, 1979), where A and b are regression coefficients.

CIGRÉ (1979) defines the fatigue resistance of multilayer and single layer conductors in typical clamps as:

$$\underbrace{\sigma_a = \begin{array}{ll} 450N^{-0.20}, & N \leq 1.56 \times 10^7 cycles \\ 263N^{-0.17}, & N > 1.56 \times 10^7 cycles \end{array}}_{multilayer\ conductor} \tag{2.48}$$

$$\underbrace{\sigma_a = \begin{array}{ll} 730N^{-0.20}, & N \leq 2.0 \times 10^7 cycles \\ 430N^{-0.17}, & N > 2.0 \times 10^7 cycles \end{array}}_{single\ layer\ conductor} \tag{2.49}$$

These curves provides a conservative limit above which a conductor is deemed unsafe and endangered to fail due to fretting fatigue.

These safe limits do not provide a probability distribution function of the conductor fatigue resistance; rather they represent a lower bound on the idealized stress level below which the conductor is considered safe for a given number of cycles. It has however been pointed out by Hardy and Leblond (2001) that the CIGRÉ safe border line is not safe when considering multilayer (i.e. two and three layer conductors) and is over conservative for single layer ACSR conductors. The CIGRÉ safe border line is also limited to the first wire failure of the conductor.

2.3.1.2 Hardy and Leblond (2001) Safe Limit

Hardy and Leblond (2001), use the experimental test results on fatigue from EPRI (1979) for first wire failure, and estimate a probability distribution function for the fatigue resistance of conductor-clamp assemblies, $f_{lnN_1|\sigma_a}(n)$ by assuming that the logarithm of the number of cycles to first wire failure for a given stress level follows a student *t* distribution. Using their results, they show that the CIGRÉ safe borderline for multilayer conductors lies next to the median curve of their distribution. In the case of single layer ACSR, their results illustrate that the CIGRÉ safe borderline gives a conservative value of fatigue resistance in comparison to their result. Like the CIGRÉ safe borderline method, this method is also limited to the first wire failure of the conductor, cannot account for multiple wire failure, depends on the simplification of the Poffenberger-Swart equation and depends on performing multiple tests on conductor-clamp assemblies.

2.3.1.3 EPRI's Endurance Limit Method

In Cloutier et al. (2006) the Electric Power Research Institute (EPRI) presents datasets of fatigue results on conductors of single, double and 3-layer ACSR. Using this data, it was determined that a good fatigue resistance for single and multilayer conductors at 500 million cycles is 22.5 MPa and 8.5 MPa respectively in terms of Poffenberger-Swart stress. Using this limit, the allowable bending amplitude (Y_b) for a conductor -clamp assembly can be obtained from Equation (2.45) as:

$$Y_b = \frac{\left(e^{-\sqrt{T/EI}\ z} - 1 + \sqrt{T/EI}\ \ z\right)}{d\ E_a\ \left(\frac{T}{4\ EI}\right)} \sigma_a \tag{2.50}$$

This EPRI approach does not utilize the distribution of $f_{N_1|\sigma_a}(n)$. Rather it states that a conductor-clamp assembly can withstand 500 million cycles of Poffenberger-Swart stress if its bending amplitude is below that predicted by Equation (2.50).

The EPRI approach cannot account for multiple wire failures as it is limited to the first wire failure, assumes that effects such as the contact conditions are implicit in the Poffenberger-Swart stress.

2.3.1.4 Neural Network Approaches

In Kalombo et al. (2020), Câmara et al. (2021) and Câmara et al. (2022), neural networks were used to determine the median of $f_{N_1|\sigma_a}(n)$ but do not provide a distribution for it. Like the previous methods, this method is dependent on testing the conductors in specialized fatigue test bench such as Figure 2-19 (a). This method also does not make any refernce to contact conditions, the clamp/keper radius, clamping torque in the conductor and assumes that they are implicit in the Poffenberger-Swart stress. It is also only limited to the first wire failure in the conductor-clamp assembly and unable to account for multiple wire failures.

2.3.1.5 Lalonde et al. (2017) Approach

Lalonde et al. (2017) used the finite element model of a conductor without the clamp to determine the fatigue resistance of Drake and Crow ACSR conductors supported at suspension clamps. The wires of the conductor are modeled using 3D Timoshenko beam finite elements and the contact between the wires are modeled as beam-to-beam contacts. In this approach, the contact interaction between the wires are considered and the assumption of minimum bending stiffness of the Poffenberger-Swart relation is discarded. However, the conductor is still

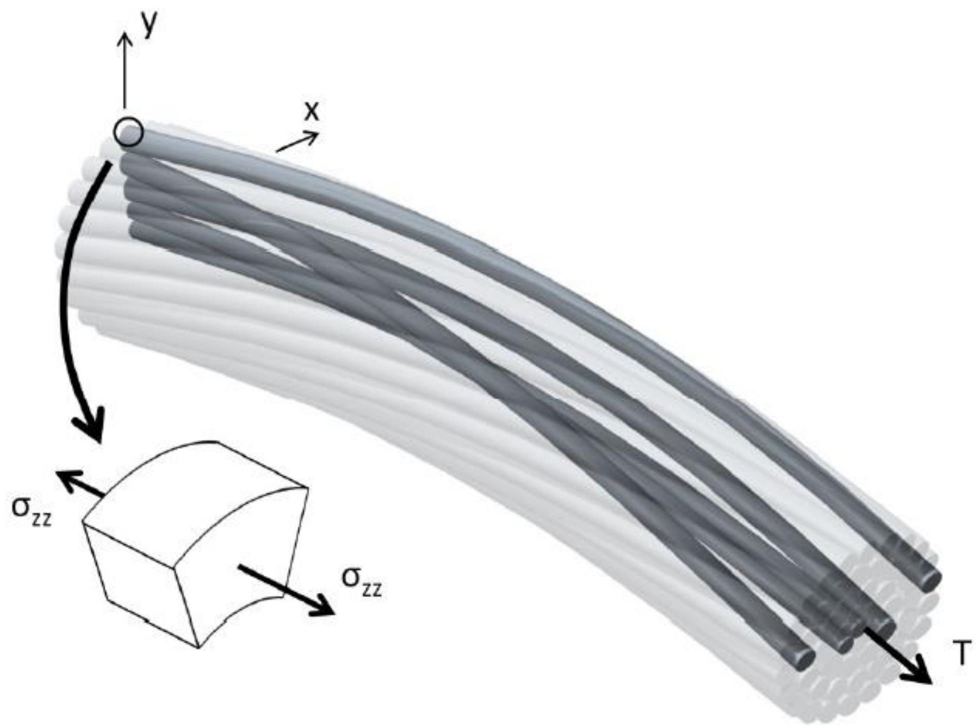

Figure 2-21: Diagrammatic representation of the model of Lalonde et al. (2017) (Reproduced from Lalonde et al. 2017)

modelled as a set of wires with contact and a fixed end as shown in Figure 2-21.

Due to the use of the FE model, the maximum stress at the fixed end (Figure 2-21) in each layer of the conductor can be computed. Using the stress and strain values together with the fatigue properties of the aluminum wires that compose the conductor, Lalonde et al. (2017) were able to predict the median fatigue resistance of conductor-clamp assemblies without resorting to special fatigue testing.

The approach of Lalonde et al. (2017) is limited as it does not account for the effect of the suspension clamp, does not account for multiple wire failure as it is limited to first wire failure, it does not account for the possibility of fatigue failures on the same layer of a conductor and does not provide the distribution of $f_{N_k|\sigma_a}(n)$.

2.3.1.6 Gang (2013) Approach

The work of Gang (2013) utilized a 3D FE analysis of a conductor-clamp assembly where the wire and suspension clamp are discretized with 8 node Hexagons. Like the method of Lalonde et al. (2017), it does not depend on the assumption Poffenberger and Swart (1965). It is also devoid of the fixed end assumption of Lalonde et al. (2017). In this method, the Contact between the wires and wire to clamp are implemented with surface-to-surface contact elements. From the stress analysis performed, the stress amplitude and mean stress values are used together with modified Goodman relation (Stephens et al. 2001) to give predictions of the endurance limit of the conductor at 500 million cycles.

The approach of Gang (2013) although accounts for all contacts in the conductor, it does not account for the fact that not all contacts will lead to failure. The approach is also limited to first wire failure only and cannot predict multiple wire failures. This method unfortunately does not give any information about $f_{N_1|\sigma_a}(n)$ but requires that the estimated endurance limit be used together with the fatigue data available in EPRI (2006). Thus, making this method depend on experimental data generated by special fatigue test bench for conductor-clamp assemblies.

2.3.1.7 Numerical-Experimental Approach of Omrani et al. (2022)

In the work of Omrani et al. (2021), a 3D FE approach similar to that of Lalonde et al. (2017) was used. However, in this case the clamp and keeper of the conductor are modeled and their contact specified with beam-to-surface contact.

Using the combined bending and tensile stress to locate the most solicited contact in the conductor-clamp assembly. With this information, a special wire to pad fatigue test bench was designed to reproduce this contact. The experimental results from the wire to pad fatigue test can be used to construct $f_{N_1|\sigma_a}(n)$. It was observed by these authors however that the median of their fatigue life distribution for a given idealized stress is higher than that observed experimentally in the conductor-clamp assembly (Lévesque, 2005). In addition, the standard deviation of the experimental result on the conductor clamp assembly were higher than those produced by the experimental wire to pad experiment.

The reasons for the discrepancy between the approach of Omrani et al. (2021) and observations on the actual conductor-clamp assembly (Lévesque, 2005) may be attributed to the inability of the approach to account for the increased probability of failure due to the presence of multiple contacts in the conductor.

2.3.2 Limitations of the Current Approach in Determining Conductor Fatigue Resistance

The main disadvantage of the experimental methods described above is that they necessitate multiple expensive conductor fatigue tests. The test methodology relies on the idealized flexion model (i.e. Poffenberger-Swart idealization of the conductor-clamp assembly) to group results from conductors with different types of wires, clamp radius and number of wires into classes based on the number of wire layers. This grouping increases the scatter in results in addition to the scatter from aleatory uncertainties on material properties. For example, considering the clamp radius, a wire is in contact along the circular portion of the clamp, the bending moment and contact pressure in the wire following the Timoshenko beam hypothesis and assuming frictionless condition is (Gasmi et al., 2012) [17]:

$$\frac{E\,I}{R} + \left(m_o - \,c\,\frac{P}{2} + \,L\,\frac{P}{2} - \frac{E\,I}{R}\right)\cosh\left(\frac{\sqrt{G\,A}\,(c\, -\, x)}{\sqrt{EI}}\right) + \frac{1}{2}\frac{\sqrt{E\,I}\,\,P\,\,\sinh\left(\frac{\sqrt{G\,A}\,(c\, -\, x)}{\sqrt{EI}}\right)}{\sqrt{G\,A}} \quad (2.51)$$

where *E I* is the bending stiffness, *R* is the clamp radius, *L* is the length of the wire, *P/2* is the loads applied at the ends of the wire, m_o is the bending moment applied at the end of the wire, *c* is the contact length and *x* is the coordinate along the wire length. The effect of the clamp radius is thus evident from Equation (2.51). In the classical approach of using conductor *S-N* curves, this effect is a source variability given that the idealized flexion model is used to represent the EPRI fatigue data (Cloutier et al. 2006), which increases the uncertainty on the estimate of fatigue life. The different sources of uncertainty in conductor fatigue as summarized in Figure 2-22 and are implicitly included in the idealized flexion approach.

Another important issue with the aggregation of conductor fatigue data is that coupled contact systems[18] are sensitive to initial conditions. Barber (2011, 2012) has conjectured that for coupled contact problems a slight change in the initial conditions leads to different energy dissipation characteristics. In practice, it implies that if conductors are not positioned in the test bench in the same manner, it results into different local contact conditions, which may explain some of the differences in results obtained with different experimental test benches.

The methods that have made use of FE method such as those of Omrani et a. (2021), Lalonde et al. (2018) and Gang (2013) have not been able to account for the increase in probability of

[17] This solution is based on the 2D Timoshenko beam assumption with the beam subjected to end shear forces and end moments. Only the solution for the contact region is given. It is based on small displacement assumption

[18] By coupled, it is meant that a change in the tangential tractions causes a change in the normal traction and vice versa. Bending moment can induce such behavior.

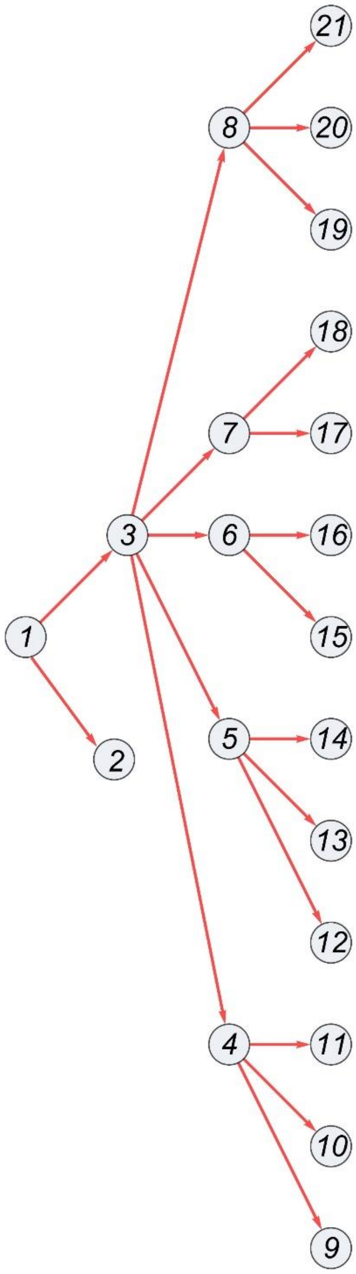

1. Conductor fatigue resistance
2. Material fatigue resistance
3. Conductor parameters
4. Geometry
5. Loading conditions
6. Conductor size effect
7. Testing system
8. Modelling
9. Wire geometry
10. Clamp radius
11. Keeper radius
12. Clamping torque
13. Amplitude
14. Conductor tension
15. Wire size
16. Number of wires per layer
17. Difference in testing systems
18. Human error in measurement
19. Exact location of contact
20. Friction coefficient
21. Modeling simplifications

Figure 2-22: Tree diagram of sources of uncertainty in conductor fatigue

failure of the conductor due to the presence of multiple contacts in the conductor. They have also not been able to take into account the various fretting regimes in determining the fatigue life of conductor-clamp assemblies.

Given the advancement in numerical models that can replicate experimental test bench results (Lalonde et al., 2018), it is possible to propagate uncertainties in the analysis of the conductor fatigue phenomenon by eliminating factors that are well controlled and can be considered deterministic. This approach is used in the next sections to estimate the uncertainty on the state of stress at contact points and reduce the uncertainty on fatigue life prediction in comparison to those derived from the idealized bending model. The effect of the presence of various fretting regimes in the conductor-clamp assembly are considered. The increase in the probability of failure of the conductor-clamp assembly due to presence of multiple contacts is also shown. A framework to derive the probability density function $f_{N_k|\sigma_a}(n)$ for any number k of wire failure is developed.

2.4 Summary and Outlook

Various methods for assessing the internal stresses and contact stresses in overhead conductors have been reviewed; from which it was concluded that the finite element approach using 3D beams with beam-to-beam and beam-to-surface contact represents the best compromise between solution time and solution variables necessary for reliability analysis of overhead conductor-clamp assemblies.

The general reliability problem has been briefly discussed. Various approaches for representing the resistance of overhead conductors available in the literature have been discussed. As pointed out, these methods rely on expensive experiments to determine the fatigue resistance of a conductor-clamp configuration. To overcome this, in the next chapters of the thesis, a numerical approach is presented that can determine the fatigue resistance of overhead conductors in terms of SN curves and fragility curves. This approach also overcomes the limitations of the previous methods that only predict first wire failure. To achieve this, chapter 3 entails an analysis of the current EPRI results (Cloutier et al. 2006) on conductor fatigue results. The outcome of chapter 3 shall be used as a validation for the model to be developed. In chapter 4, equivalence between fatigue resistance computations using beam models or solid models is established. This chapter shows that although the Timoshenko beam presents some paradoxes in modeling contact, it has the capability to be used for fatigue resistance computations. In chapter 5, a framework to predict the distribution of fatigue resistance of overhead conductors is proposed. This framework is validated with experimental results available in the literature (Lévesque, 2005) and model established in chapter 3.

2.5 References

Andresen, H., Hills, D. A., and Vázquez, J. (2019). Closed-form solutions for tilted three-part piecewise-quadratic half-plane contacts. *International Journal of Mechanical Sciences, 150*, 127-134. doi:https://doi.org/10.1016/j.ijmecsci.2018.09.024

Azevedo, C. R. F., Henriques, A. M. D., and Pulino filho, A. R. (2009). Fretting fatigue in overhead conductors: Rig design and failure analysis of a Grosbeak aluminum cable steel reinforced conductor *Engineering Failure Analysis, 16*, 136-151.

Barber, J. R. (2018). *Contact Mechanics* (Vol. 250): Springer.

Barber, J. R. (2010). *Elasticity* (3rd ed. Vol. 172): Springer.

Barber, J. R. (2011). Frictional systems subjected to oscillating loads. *Annals of Solid and Structural Mechanics, 2*(2), 45-55. doi:10.1007/s12356-011-0017-5

Barber, J. R. (2012). Frictional systems under periodic loads — History-dependence, non-uniqueness and energy dissipation. *Journal of Physics: Conference Series, 382*, 012002. doi:10.1088/1742-6596/382/1/012002

Barber, J. R., Davies, M., and Hills, D. A. (2011). Frictional elastic contact with periodic loading. *International Journal of Solids and Structures, 48*(13), 2041-2047. doi:https://doi.org/10.1016/j.ijsolstr.2011.03.008

Baumann, R., and Novak, P. (2017). Efficient Computation and Experimental validation of ACSR Overhead Line Conductors Under Tension and Bending *CIGRE Science and Engineering, 9*, 5-16.

Cãmara, E. C. s. B., Kalombo, R. B., Ferreira, J. L. A., Araújo, J. A., and Freire Júnior, R. C. S. (2021). Estimating fatigue behavior of a family of aluminum overhead conductors using ANNs. *Fatigue & Fracture of Engineering Materials & Structures, 44*(4), 983-996. doi:10.1111/ffe.13408

Câmara, E. C. B., Kalombo, R. B., Ferreira, J. L. A., Araújo, J. A., and Freire Júnior, R. C. S. (2022). Estimating the fatigue behavior of a family of aluminum conductor cables using ANNs applying the Poffenberger-Swart formula. *International Journal of Fatigue, 159*. doi:10.1016/j.ijfatigue.2022.106766

Cardou, A., Leblond, A., and Cloutier, L. (1993). Suspension Clamp and ACSR Electrical Conductor Contact Conditions. *Journal of Energy Engineering, 119*(1), 19-31. doi:10.1061/(ASCE)0733-9402(1993)119:1(19)

Castillo, J., and Barber, J. R. (1997). Lateral contact of slender prismatic bodies. *Proceedings of the Royal Society of London. Series A: Mathematical, Physical and Engineering Sciences, 453*(1966), 2397-2412. doi:10.1098/rspa.1997.012

Ciavarella, M., Hills, D. A., and Monno, G. (1998). The influence of rounded edges on indentation by a flat punch. *212*(4), 319-327. doi:10.1243/0954406981521259

CIGRÉ (1979). *Recommendations for the Evaluation of the Lifetime of Transmission Line Conductors* (Electra n 63).

Cloutier, L., Goudrea, S., and Cardou, A. (2006). Fatigue of Overhead Conductors. In J. K. Chan, D. G. Havard, C. B. Rawlins, & J. Weisel (Eds.), *EPRI Transmission Line Reference Book: Wind-induced Conductor Motion* (2nd ed.). Palo Alto, CA: EPRI.

Essenburg, F. (1975). On the Significance of the Inclusion of the Effect of Transverse Normal Strain in Problems Involving Beams With Surface Constraints. *Journal of Applied Mechanics, 42*(1), 127-132. doi:10.1115/1.3423502 %J Journal of Applied Mechanics

EPRI. (1979). *Transmission Line Reference Book*. Retrieved from Palo Alto, CA.

Gasmi, A., Joseph, P. F., Rhyne, T. B., and Cron, S. M. (2012). The effect of transverse normal strain in contact of an orthotropic beam pressed against a circular surface. *International Journal of Solids and Structures, 49*(18), 2604-2616.

Gang, Qi. (2013). *Computational Modeling for Stress Analysis of Overhead Transmission Line Stranded Conductors Under Design and Fretting Fatigue Conditions* (PhD), McGill University Montreal, Quebec

Gray, A., Abbena, E., and Salamon, S. (2006). *Modern Differential Geometry of Curves and Surfaces with Mathematica*: Chapman & Hall/CRC.

Hardy, C., and Leblond, A. (2001). *Statistical Analysis of Stranded Conductor fatigue Endurance Data* Paper presented at the Proceeding of the Fouth International Symposium on Cable Dynamics, Montreal, Canada

Hills, D. A., and Nowell, D. (1994). *Mechanics of Fretting Fatigue* Springer-Science.

Hills, D. A., Ramesh, R., Barber, J. R., and Moore, M. R. (2018). Methods to solve half-plane partial slip contact problems. *International Journal of Solids and Structures, 155*, 155-159. doi:https://doi.org/10.1016/j.ijsolstr.2018.07.019

Hills, D. A., Nowell, D., and Sackfield, A. (1993). *Mechanics of Elastic Contacts* Butterworth Heinemann.

IEEE (2006). IEEE Guide for Aeolian Vibration Field Measurements of Overhead Conductors In. New York, USA: IEEE.

Jang, Y. H., and Barber, J. R. (2011). Effect of phase on the frictional dissipation in systems subjected to harmonically varying loads. *European Journal of Mechanics - A/Solids, 30*(3), 269-274. doi:https://doi.org/10.1016/j.euromechsol.2011.01.008

Johnson, K. L. (1985). *Contact Mechanics*. Cambridge, UK: Cambridge University Press.

Jeong, S. H., and Lee, Y. Z. (2006). *Determination of the Fretting Regimes Under Stick-Slip Condition Using the Phase Difference Between Friction and Relative Displacement*. Paper presented at the ASME 2006 International Joint Tribology Conference, San Antonio, USA.

Kalombo, R. B., Martínez, J. M. G., Ferreira, J. L. A., da Silva, C. R. M., and Araújo, J. A. (2015). Comparative Fatigue Resistance of Overhead Conductors Made of Aluminium and Aluminium Alloy: Tests and Analysis. *Procedia Engineering, 133*(Supplement C), 223-232. doi:https://doi.org/10.1016/j.proeng.2015.12.662

Kaufman, J. G. (2008). *Properties of Aluminum Alloys: Fatigue Data and Effects of Temperature, Product Form, and Processing* Retrieved from Ohio, USA.

Kim, J. H., Ahn, Y. J., Jang, Y. H., and Barber, J. R. (2014). Contact problems involving beams. *International Journal of Solids and Structures, 51*(25), 4435-4439. doi:https://doi.org/10.1016/j.ijsolstr.2014.09.013

Knopp, K. (1945). *Theory of Functions (Elements of the General Theory of Analytic Functions)*: Dover

Konyukhuv, A., and Izi, R. (2015). *Introduction to Computational Contact Mechanics (A Geometrical Approach)* (1st ed.): Wiley.

Konyukhuv, A., and Schweizerhof, K. (2012). *Computational Contact Mechanics (Geometrically Exact Theory for Arbitrary Shaped Bodies)* (Vol. 67): Springer.

Lalonde, S. (2017). *Strategie de Modelisation 3D Des Solides Toronnes Appliquee a L'etude de La Fatigue Des Conducteurs de Lignes de Transport D'Energie Electrique* (Ph.D), Universite de Sherbrooke Serbrooke.

Lalonde, S., Guilbault, R., and Langlois, S. (2017). Modeling multilayered wire strands, a strategy based on 3D finite element beam-to-beam contacts - Part II: Application to wind-induced vibration and fatigue analysis of overhead conductors. *International Journal of Mechanical Sciences, 126*, 297-307. doi:http://dx.doi.org/10.1016/j.ijmecsci.2016.12.015

Lalonde, S., Guilbault, R., and Langlois, S. (2018). Numerical Analysis of ACSR Conductor–Clamp Systems Undergoing Wind-Induced Cyclic Loads. *IEEE Transactions on Power Delivery, 33*(4), 1518-1526. doi:10.1109/TPWRD.2017.2704934

Lévesque, F. (2005). *Etude de l'applicabilite de la regle de Palmgren-Miner aux conducteurs electriques sous chargements de flexion cyclique par blocs.* (MSc), Universite Laval.

Lévesque, F., and Legron, F. (2010). *Contact mechanics based fatigue indicators for overhead conductors*

Lévesque, F., Goudreau, S., Cloutier, L., and Cardou, A. (2011). Finite element model of the contact between a vibrating conductor and a suspension clamp. *Tribology International, 44*(9), 1014-1023. doi:https://doi.org/10.1016/j.triboint.2011.04.006

Muskhelishvili, N. I. (1954). *Some Basic Problems of the Mathematical Theory of Elasticity* (J. R. M. Radok, Trans.): Springer.

Naghdi, P. M., and Rubin, M. B. (1989). On the significance of normal cross-sectional extension in beam theory with application to contact problems. *International Journal of Solids and Structures, 25*(3), 249-265. doi:https://doi.org/10.1016/0020-7683(89)90047-4

Omrani, A. (2021). *Evaluation De La Resistance En fatigue Des Conducteurs Aeriens Par Le Couplage D'Une Approache Numerique Et Experimentale.* (Ph.D), Universite de Sherbrooke Quebec.

Popov, V. L., and Heb, M. (2015). *Method of Dimensionality Reduction in Contact Mechanics and Friction* (J. A. T. Gray, Trans.): Springer.

Redford, J. A., Gueguin, M., Nguyen, M. C., Lieurade, H. P., Yang, C., Hafid, F., and Ghidaglia, J. M. (2019). Calibration of a numerical prediction methodology for fretting-fatigue crack initiation in overhead power lines. *International Journal of Fatigue, 124*, 400-410. doi:https://doi.org/10.1016/j.ijfatigue.2019.03.009

Said, J., Garcin, S., Fouvry, S., Cailletaud, G., Yang, C., and Hafid, F. (2020). A multi-scale strategy to predict fretting-fatigue endurance of overhead conductors. *Tribology International, 143*, 106053. doi:https://doi.org/10.1016/j.triboint.2019.106053

Stephens, R. I., Fatemi, A., Stephens, R. R., and Fuchs, H. O. (2001). *Metal fatigue in engineering.* Wiley-Interscience

Timoshenko, S. (1941). *Strength of Materails II: Advanced Theory and Problems* (2nd ed.): D. Van Nostrand Company

Timoshenko, S., and Goodier, J. N. (1951). *Theory of Elasticity* (2nd ed.). New York McGraw-Hill.

Washizu, K. (1975). *Variational Methods in Elasticity and Plasticity* (2nd ed.): Pergamon press.

Waterhouse, R. B. (1992). Fretting fatigue. *International Materials Reviews, 37*(1), 77-98. doi:10.1179/imr.1992.37.1.77

Yastrebov, V. (2013). *Numerical Methods in Contact Mechanics*. Great Britain: ISTE Wiley.

Zhou, Z. R., Cardou, A., Goudreau, S., and Fiset, M. (1996). Fundamental investigations of electrical conductor fretting fatigue. *Tribology International*, *29*(3), 221-232. doi:http://dx.doi.org/10.1016/0301-679X(95)00074-E

Zhou, Z. R., and Vincent, L. (1995). Mixed fretting regime. *Wear, 181-183*, 531-536. doi:https://doi.org/10.1016/0043-1648(95)90168-X

3 A PROBABILISTIC STRESS – LIFE MODEL FOR FRETTING FATIGUE OF ALUMINUM CONDUCTOR STEEL REINFORCED CABLE – CLAMP SYSTEMS[19]

3.1 INTRODUCTION

Conductors of transmission lines are subjected to a variety of cross – flow induced vibrations such as aeolian vibration, sub-conductor oscillation and galloping (Cloutier et al., 2006). Of these, the phenomenon of fatigue due to aeolian vibrations is discussed in this paper. The fatigue of materials is often treated from two approaches – *a total life approach* which includes the *stress – life (S – N) approach* and *strain – life approach; a damage tolerant approach* based on fracture mechanics (Suresh, 1998). The S – N approach is often used in representing fatigue test data on conductors (Cloutier et al., 2006), where the fatigue data are generated using a test bench. The fatigue stress levels are quantified using Poffenberger and Swart (P – S) relationship (Poffenberger and Swart, 1965) or the maximum antinode amplitude (Cloutier et al., 2006) while the number of cycles is quantified as the first wire failure in (Cloutier et al., 2006) or 10% of the total number of aluminum wires by (CIGRÉ, 1979). The data set and criteria set in (Cloutier et al., 2006) are used herein.

There have been previous statistical analysis on conductor fatigue lifetime data (Hardy and Leblond, 2001; Thi-lien, 2015). These models present the S – N regression curve in terms of the conditional cumulative distribution function for the lifetime given a stress level $F\left(N_1|\sigma_{yb} = \sigma_{yb,i}\right)$, where N_1 is lifetime of the first wire of the conductor and $\sigma_{yb,i}$ is the *i*th

[19] Thomas, O.O., Chouinard, L.E., and Langlois, S. (2020). A Probabilistic Stress-Life Model for Fretting Fatigue of Aluminum Conductor Steel Reinforced Cable-Clamp Systems. In: Liyanage J., Amadi-Echendu J., Mathew J. (eds) Engineering Assets and Public Infrastructures in the Age of Digitalization. Lecture Notes in Mechanical Engineering. Springer, Cham. https://doi.org/10.1007/978-3-030-48021-9_78

stress level at 89mm from the last point of contact between the conductor and the clamp. Confidence intervals about the 50th percentile curve are then produced based on an assumed lognormal distribution of the lifetime. However, $F\left(N_1|\sigma_{yb} = \sigma_{yb,i}\right)$ cannot be constructed from data because the amount of conductor fatigue data at each stress level is too small and non-constant variance of each $F\left(N_1|\sigma_{yb} = \sigma_{yb,i}\right)$. The solution usually adopted is to ignore the variation of variance with stress level or treat it as a function of the stress level (Hardy and Leblond, 2001; Thi-lien, 2015). Because of these, the fit of the model to data cannot be checked using simple statistical means such as probability plots or the theoretical probability density function (PDF) checked against that of the data. Rather the validity of the model is checked by minimizing the empirical risk, use of the coefficient of correlation (Hardy and Leblond, 2001) or plot of the residuals. Strictly speaking minimizing the empirical risk (EMR) doesn't guarantee good prediction ability of the model (Vapnik, 1998). The EMR of the model presented herein will still be compared with the one of the model previously proposed by (Hardy and Leblond, 2001) for the same class of conductor

The previous works (CIGRÉ, 1979; Hardy and Leblond, 2001; Thi-lien, 2015) have not assessed also the tail behaviour of their fatigue distributions. Hence there is no information on how the run – out data influence the model prediction and generalization ability. The model presented herein allows studying how the run – outs can influence the tail distribution. The region of validity of these previous models are also not known. Is it valid in the region of the mean? Is it valid at the extremes? When making predictions, an engineer would like to know the region of validity and limitations of his model.

The general objective of this paper is to present an S – N model that allows to evaluate the conductor lifetime, evaluate the accuracy of such prediction and show the effect of ignoring run – out fatigue data on conductor S – N regression models. Due to the limited amount of data in conductor fatigue testing, the model presented herein uses a normalization variable that allows data pooling from various stress levels allowing a larger amount of data to be used in generating the CDF and PDF and checking the theoretical distribution against the empirical probability density function (EPDF) and empirical cumulative distribution function (ECDF).

In the sections to follow, considerations and assumptions used to select the required distribution function are presented. This is followed by a presentation of the methodology used to determine the model parameters. Results of goodness of fit test are presented; finally, validation dataset excluded from the model training are used to check the prediction ability of the model.

3.2 Determination of Distribution Functions

To determine the fatigue characteristics of stranded conductors, a fatigue test is usually carried out on a test bench. The fatigue stresses are characterized by two stress indicators : P – S relationship or the maximum antinode. These relationships are presented in (Cloutier et al., 2006). The stress indicators are obtained as a function of the bending amplitude at 89mm from the last point of contact of the conductor with the clamp or as a function of the maximum antinode amplitude in the test span. A plot of these stresses against the natural logarithm of number of cycles to failure gives S – N plots which are different for both stress indicators.

The lognormal distribution is usually assumed for the CDF $F\left(N_1|\sigma_{yb} = \sigma_{yb,i}\right)$ in conductor fatigue data analysis (CIGRÉ, 1979; Hardy and Leblond, 2001; Thi-lien, 2015). However, it is assumed that $F\left(N_1|\sigma_{yb} = \sigma_{yb,i}\right)$ can also take an extreme value distribution. Consider a conductor with *n* number of wires subject to stress at $\sigma_{yb,i}$:

$$N_1|\sigma_{yb,i} = Min\left(N_1, N_2, \ldots\ldots, N_n|\sigma_{yb} = \sigma_{yb,i}\right) \tag{3.1}$$

It is seen that the if the lifetime of the first wire of the conductor is used as a criterion to stop the conductor fatigue test, then the conductor lifetime can be considered from the point of view of extreme value statistics of the minimum. The condition of independence between the N_i is not necessary for admissibility of an extreme value distribution to $F(N_1|\sigma_{yb} = \sigma_{yb,i})$ (Castillo, 1988). The first wire to fail is considered as the weak wire in the whole conductor, thus the Weibull distribution for the minimum is selected to model $F(N_1|\sigma_{yb} = \sigma_{yb,i})$.

The distribution of stress level given a number of cycle to first wire failure $F(\sigma_{yb}|N_1 = N_{1,i})$ is unknown. The normal, lognormal and Weibull distributions have been adopted in the literature to model stress distributions in fatigue (Hanaki et al. 2010). A Weibull distribution is selected to model this distribution. This selection is influenced by some statistical consideration as follows: given any other distribution of $F(\sigma_{yb}|N_1 = N_{1,i})$, such distributions could be transformed to a Weibull distribution (Castillo and Galambos, 1987). A physical consideration that also influences the selection over the normal or lognormal is that under field conditions, the aeolian peak stresses have been defined to follow Rayleigh distribution et (Noiseux et al., 1986) which is a special case of the Weibull distribution (Marshall and Olkin, 2007).

It is accepted that a marginal and conditional density are required to construct $F(\sigma_{yb,}, N_1)$, the joint distribution of the stress level and first wire lifetime. However, it has also been accepted that joint distributions can be specified by their conditionals only (Arnold et al., 1999; Besag, 1974; Bhattacharyya, 1943; Castillo and Galambos, 1987). In this light, it is possible to specify the form of $F(\sigma_{yb,}, N_1)$ given that both conditionals have been identified. A bivariate function when both conditionals are Weibull distributions is given in (Castillo and Fernandez-Canteli, 2009; Castillo and Galambos, 1987) :

$$F(N_1, \sigma_a) = 1 - \exp\left[-\left(\frac{(h(N_1)-\zeta)(g(\sigma_{yb})-\xi)-\lambda}{\delta}\right)^{\beta}\right]; N_1, \sigma_a \in \mathbb{R}_{++} \quad (3.2)$$

$$where\ V = (h(N_1) - \zeta)\left(g(\sigma_{yb}) - \xi\right); h\ and\ g\ are \log\ functions$$

$$\zeta, \xi, \lambda, \beta\ and\ \delta\ are\ model\ parameters$$

3.3 FITTING THE MODEL TO DATA

To fit the model to data, the parameters ζ and ξ are first estimated using a least square approach. Once the values of the parameters ζ and ξ have been determined, the location parameter λ, scale δ and shape parameter β of $F(N_1, \sigma_{yb})$ can be determined by standard methods of parameter estimation; see e.g. (Castillo and Fernandez-Canteli, 2009; Kotz and Nadarajah, 2000) The maximum likelihood (ML) method has been used to estimate λ, δ, β respectively as (Cousineau, 2009; Crowder et a., 1991; Kotz and Nadarajah, 2000):

$$maximize\left\{\prod_{i \epsilon U} j(V_i; \beta, \delta, \lambda)\right\}\left\{\prod_{i \epsilon C} S(V_i; \beta, \delta, \lambda)\right\} \quad (3.3)$$

Subject to the constraint that the Jacobian matrix is stationary. Where j is the Weibull density function and S the survival function, U is a set of failure data and C is a set of run-out data. The

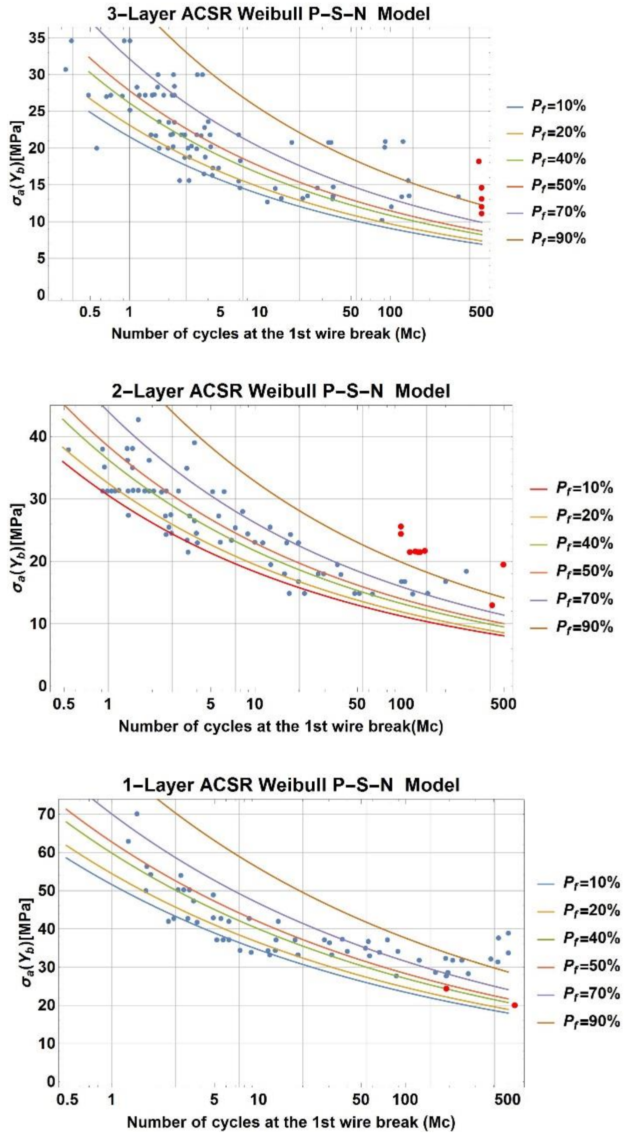

Figure 3-1: S - N Curves in terms of Bending Amplitude

analysis done herein has not considered the effect of run-out on the model parameters hence the survival function in (3) was not utilized in obtaining the likelihood function. All data were treated as failure data. Because run-outs are not usually considered in the statistical treatment of conductor fatigue data, see e.g. (Hardy and Leblond, 2001), this approach has been followed to show the effect of not considering run – out on the S – N curve.

The stress – lifetime pair dataset available in (Cloutier et al., 2006) were collected for single, double and 3-layer ACSR class of conductors in terms of bending amplitude. The fitted stress – first wire lifetime models with bending amplitude stress indicator are shown in Figure 3.1. The run-out points are indicated in red on these plots.

3.4 EVALUATING THE GOODNESS OF FIT OF THE MODEL

There are various ways to test if a selected distribution function model is a good fit for the underlying distribution that generates the data. The simplest being the comparison of the EPDF and ECDF to that of the selected theoretical distribution. If there is a resemblance between the EPDF and the theoretical PDF, it is acceptable to conclude that the selected distribution is a probable function that generated the sample data. If the ECDF also converges well to the theoretical CDF, then it is expected that the frequency of fatigue failure events converges to their probability of occurrence.

In Figure 3.2a, the theoretical CDF of the parameter V is compared against its ECDF for the single layer, two layer and three layer ACSR group of conductors. Figure 2b also presents the theoretical PDF of the parameter V against its EPDF for the same class of conductors. It is observable that the theoretical PDF and CDF are a good fit to the EPDF and ECDF respectively for all three classes of conductors. The PDF's of the two layer and single layer conductor is more right skewed than the three layer ACSR conductors confirming the already available knowledge of a decreasing fatigue lifetime with increasing number of layers of the conductor.

A problem that occurs with judging visually the closeness of the theoretical CDF to the ECDF is due to the curvature of the theoretical CDF. It is difficult to observe differences in the upper tail where the curve begins to flatten out. To remedy this, probability plots can be used to check the distribution assumption. These plots are also better in determining the appropriate distribution for small finite sample size than comparing the EPDF and theoretical PDF

(Montgomery and Runger, 2003). Therefore, probability paper plots are also presented to corroborate the comparison of the ECDF, EPDF and their theoretical equivalent of the model. Approximate linearity on the probability plots allows to determine if the selected model is a plausible representation of the underlying distribution. Two types of probability paper plots namely the quantile – quantile (QQ) plot and the probability plot (PP) are used to check the model fit. The plotting coordinates of each of these probability paper plots are given respectively as follows (Crowder et al. 1991):

$$\left[\left(LogN_{1,i} - \zeta\right)\left(Log\sigma_{yb,i} \; - \xi\right)\right]_j, F^{-1}\left(p_j\right) \tag{3.4}$$

$$p_j, F\left(\left[\left(LogN_{1,i} - \zeta\right)\left(Log\sigma_{yb,i} \; - \xi\right)\right]_j ; \; \hat{\alpha}\right) \tag{3.5}$$

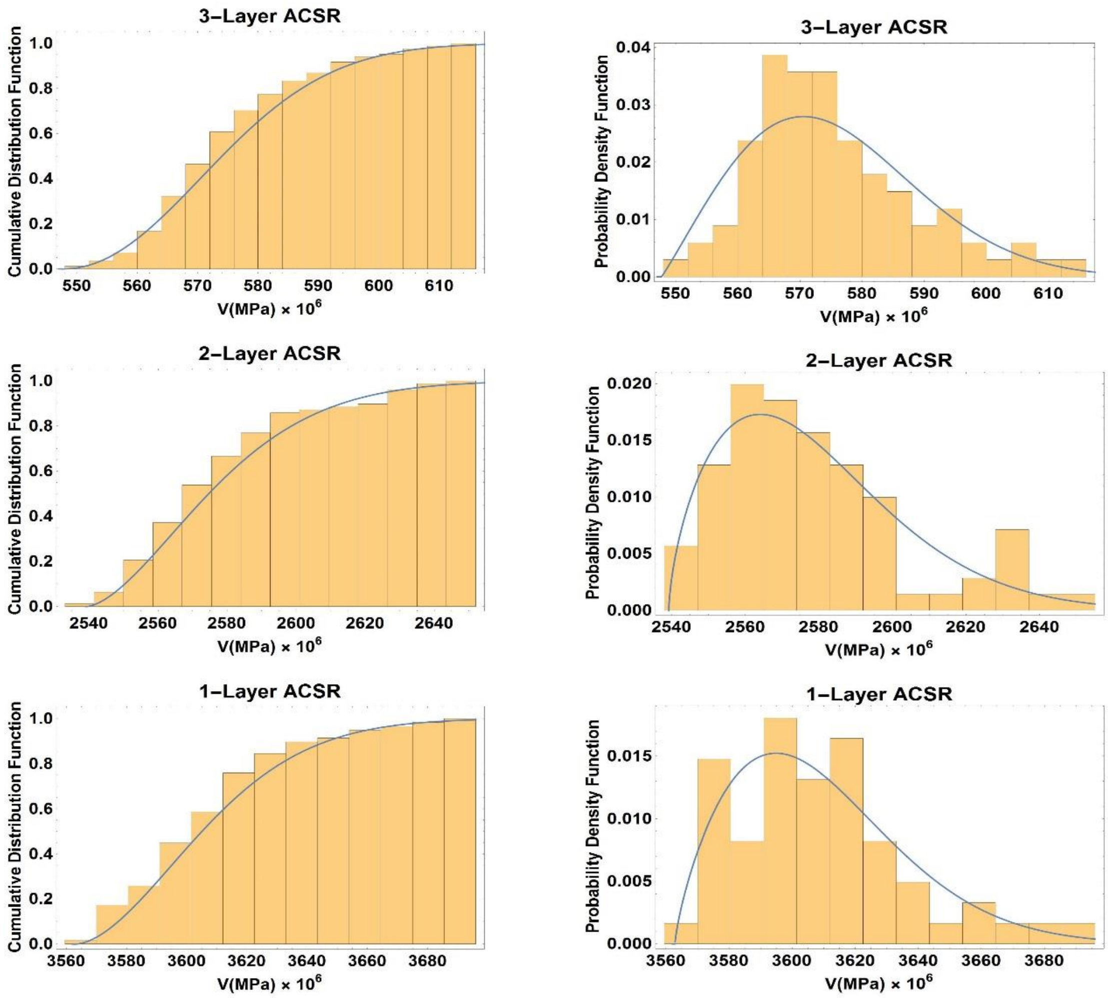

Figure 3-2(a) Comparison of CDF to ECDF *(b) Comparison of PDF to EPDF*

Where F is the selected CDF, j represents the ordering of the random sample and $\hat{\boldsymbol{\alpha}}$ the estimate of the model parameters. The point estimates of the model parameters from the ML method are used. The difference between the PP and QQ plots is in the region with highest variability (Crowder et al. 1991). In the PP plots, the points at the tails of the distribution have the lowest variability (Crowder et al. 1991). The opposite is true for the QQ plot. From an engineering point of view, the PP plot can thus be used to judge the fit of the model around the central region of the distribution while the extreme points can be judged by the QQ plot because in fatigue, the upper points are usually those with the greatest variability. The PP plots for the three classes of conductors is presented in Figure 3.3a and the QQ plots in Figure 3.3b. Linearity of the PP plot for all three class of conductors shows that the distribution assumption is valid. The QQ plots however show instability at the tails. Factors that could contribute to this include: the model not accounting for the effect of run - out, lesser amount of data points at the extremes, the distribution is not valid at the upper tail (D'Agostino and Stephens, 1986) and the higher variability assigned to extreme points by the QQ plots (Crowder et al. 1991). Interestingly, the QQ plot for the three layer class of conductors shows a trend at the upper tail suggesting a Weibull distribution with different parameters; that is the points show a linear trend parallel to the line.

Previous models (CIGRÉ, 1979; Hardy and Leblond, 2001) have not provided any information on the region of validity of their model hence it is impossible to know where prediction can be made with the model with a high degree of accuracy. The model presented herein gives a

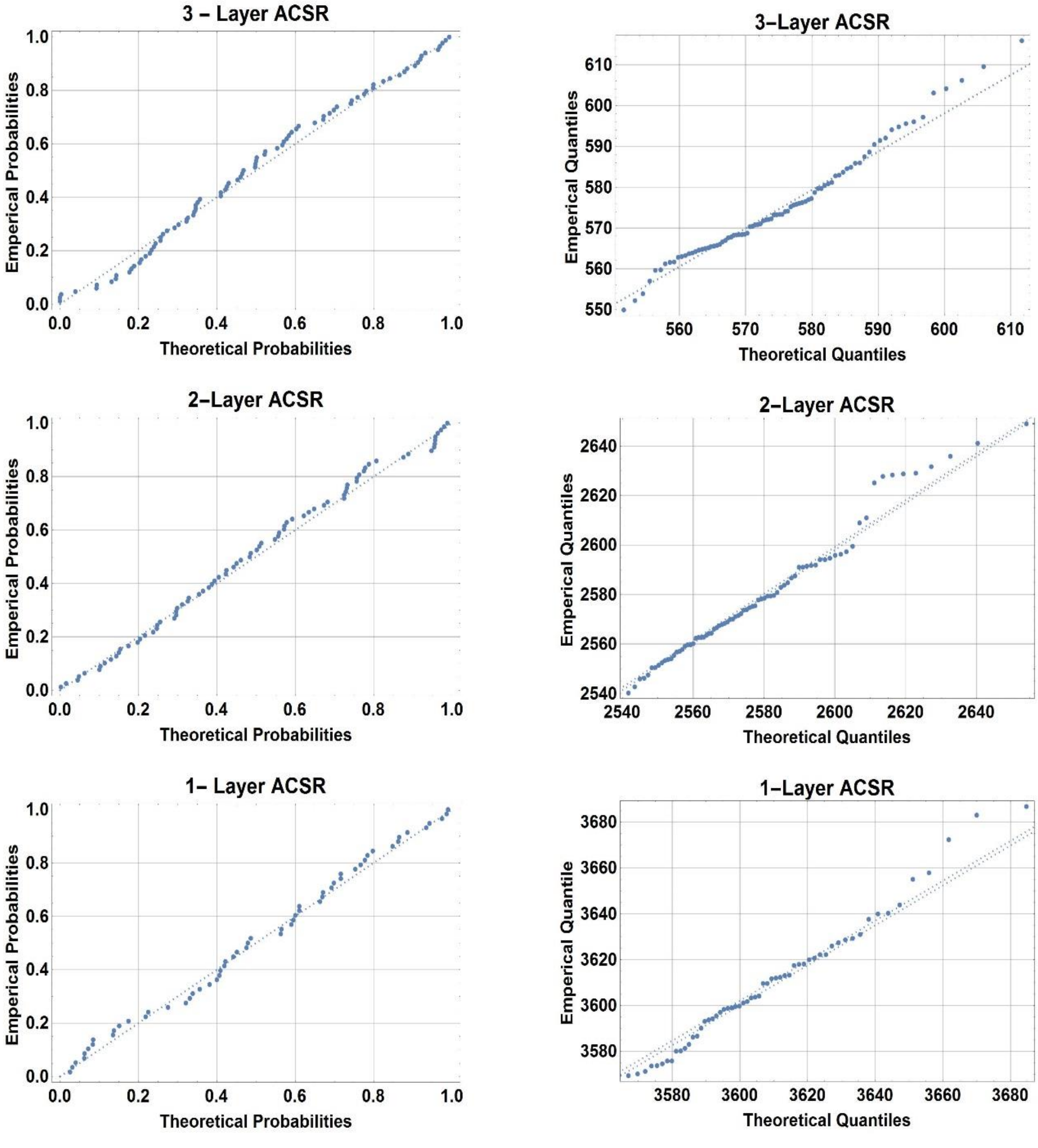

Figure 3-3(a): Probability - probability plot for all three classes of ASCR conductors; (b) Quantile - Quantile plots for three classes of ACSR conductors

quantitative measure of its region of validity, which can be determined from the PP and QQ plots.

3.5 Model Validation

To test the predictive ability of the model, validation dataset which were excluded from the training process are used. Table 3.1 gives the data source, the type of conductor, the stress level, data type (run out or failure), the actual number of cycles to failure recorded when the test was terminated and the probability of failure.

It is usual in the conductor fatigue literature to select a curve for failure analysis that is based on a certain probability of failure (CIGRÉ, 1979; Hardy and Leblond, 2001) and suggested as a lower bound curve. Such a selection is not made herein. However, for the sake of validation, the 50^{th} percentile curve has been selected to predict the lifetime of the first wire failure. The model predictions are presented in Table 3.1. The computed probabilities of failure are computed using the actual number of cycles to failure and the stress level.

The model doesn't perform well on the run – out data. This is as expected as run – outs weren't accounted for in the model. Very good agreement is obtained between the model predicted number of cycles to failure and all data from (Fade et al. 2012) for the Ibis 26/7 conductor. The mean number of cycles to first wire failure are approximately equivalent to that predicted by the model in table 1 as seen in columns 5 and 6. The reason for this accuracy is that if one looks at the S-N for the class of conductors which this Ibis 26/7 belongs to (2 – layer), it is observed that those stress levels are at the extreme lower tail of the distribution. A concurrent look at the QQ and PP plots for this class of conductors shows that that the variability at the lower tail is properly captured by the model. For the Tern 45/7 conductor, the model underestimates the lifetime. To explain this, observe from the S-N for its class of conductors (3-layer) that the P – S stress level of 29.65 MPa is in the lower tail of the distribution. A concurrent look at the PP and QQ plots for the three layer class of conductors shows that the model probability of failure and quantiles are both underestimated by the model respectively. For the Bersfort conductor submitted to a P – S stress level of 11.58 MPa, the model overestimates the lifetime at the 50th percentile curve. Again, to explain this, it is observed in the S-N curve for its class of conductors (3-layer) that this stress level is in the upper tail of the distribution. A concurrent look at the QQ plots of this class of conductor shows that the model overestimates the distribution quantiles at the upper tail. This overestimation at the upper tails shows the influence of not accounting for run out on the distribution or excluding them from the analysis.

A point of caution in interpreting these results is to recall the meaning of probability from a frequentist point of view. It is expected that the frequency converges to the probability with increasing sample size (Vapnik, 1998) thus it is not surprising that where the average value of a number of lifetimes is presented in table 1, it is closer to the prediction of the model. Thus, not all the overestimation or underestimation by the model discussed above is due to tail distribution error but accounting for run-outs should decrease tail prediction error.

To further show the validity of the model, the methodology of (Hardy and Leblond, 2001) is compared with the model presented herein. The statistical analysis in (Hardy and Leblond, 2001) has been repeated with the 84 data points used for the model presented for 3 – layer class of conductors. Given the large amount of data now available, a lognormal distribution as postulated by (Hardy and Leblond, 2001) is used and the Strohmeyer model (Strohmeyer, 1914) used to represent the 50th percentile curve as done by (Hardy and Leblond, 2001). To compare the performance of both models, the empirical risk of both models is computed. The model that has the minimal empirical risk is considered the better model (Vapnik, 1998). The empirical risk is computed as (Vapnik, 1998):

$$R_{(emp)}(\hat{\alpha}) = \frac{1}{l}\sum_{i=1}^{l}\left(Log\ N_{1,i} - I\left(N_{1,i},\hat{\alpha}\right)\right)^2 \qquad (6)$$

Table 3-1: Validation dataset for conductor vibration using bending amplitude stress indicator

Data Source	***Conductor Type***	$(\sigma_{a(Yb)})$ ***(MPa)***	***Data Type***	***Actual Number of Cycles to Failure*** $(*\,10^6)$	***Predicted Number of Cycles to Failure*** $(*\,10^6)$	***Probability of Failure***
(Cloutier et al., 2006)	Rail 45/7	10.53	Run out	318.07	163.93	0.66
	Crow 54/7	16.96	Run out	24.78	11.92	0.69
(Goudreau, Lévesque, et al., 2010)	Bersfort 48/7	11.58	Failure	71.74	102	0.40
	Tern 45/7	29.65	Failure	1.11	1.00	0.61
		29.65	Failure	1.87	1.00	0.74
		29.65	Failure	2.74	1.00	0.82
(Fadel et al., 2012)	Ibis 26/7	25.08	Failure	5.50	6.67	0.42
		25.08	Failure	2.98	6.67	0.18
		28.22	Failure	3.00	3.92	0.39
		28.22	Failure	1.90	3.92	0.21
		31.35	Failure	2.47 (mean)	2.45	0.5
		34.49	Failure	1.13 (mean)	1.61	0.36
		39.82	Failure	1.00 (mean)	0.86	0.56
		43.31	Failure	0.53 (mean)	0.59	0.45

Where the function I is the 50th percentile curve and l is the length of the dataset. The obtained empirical risks are presented in Table 3.2. On this basis, the model presented herein outperforms the previous model on the 3-layer ACSR class of conductors and is a better model in predicting the time to failure of the first wire of the 3-layer class of conductor.

Table 3-2: Comparison of Empirical Risk

Model	$R_{(emp)}(\alpha)$
Present Model	1.62
(Hardy & Leblond, 2001)	2.29

Because the empirical risk is also a measure of the model error, the model presented herein has lower prediction error and produces tighter confidence interval about the 50th percentile curve than the type of model presented in (Hardy and Leblond, 2001).

3.6 Conclusion and Subsequent Research

A statistical analysis on the ACSR conductor fatigue data has been conducted. Non-constant variance of the conditional density of lifetime given stress level has been considered by the model. The region of validity of the model has been shown using quantile – quantile probability paper plots and probability – probability paper plots. The Normalization variable used by the model allows to construct the empirical probability density and cumulative distribution functions. It is shown that the theoretical CDF and PDF for all classes of conductors examined agree with the ECDF and EPDF respectively. The model prediction capability is demonstrated by comparing predictions of the model with a validation dataset. Good agreement is obtained in the region of the mean. It is shown that the effect of run – out on the conductor must be accounted for in conductor fatigue statistical analysis to improve the tail behaviour. Comparison of the present model and a previous model showed that the present model provide a lower prediction error and tighter confidence intervals. However, a lacuna of the present model is that one of the marginal densities doesn't exist. Nonetheless, the emphasis is on predicting as closely as possible the time to first wire failure and the model has demonstrated its capability for this. Further analysis is required to refine the model and to ensure that it provides the minimum possible risk in prediction, which will guarantee minimum error in residual life estimation of transmission line conductors subjected to aeolian vibrations.

3.7 References

Arnold, B. C., Castillo, E., and Sarabia, J. M. (1999). *Conditional Specification of Statistical Models* (1st ed.): Springer

Besag, J. (1974). Spatial Interaction and the Statistical Analysis of Lattice Systems. *Journal of the Royal Statistical Society. Series B (Methodological), 36*(2), 192-236.

Bhattacharyya, A. (1943). On Some Sets of Sufficient Conditions Leading to the Normal Bivariate Distribution. *Sankhyā: The Indian Journal of Statistics (1933-1960), 6*(4), 399-406.

Castillo, E. (1988). *Extreme value Theory in Engineering* Carlifornia, USA. : Academic Press Inc. .

Castillo, E. and Fernandez-Canteli, A. (2009). *A Unified Statistical Methodology for Modeling Fatigue Damage*: Springer.

Castillo, E. and Galambos, J. (1987). LIFETIME REGRESSION MODELS BASED ON A FUNCTIONAL EQUATION OF PHYSICAL NATURE. *Journal of Applied Probability, 24*(1), 160-169.

CIGRÉ (1979). *Recommendation for the Evaluation of the Lifetime of Transmission Line Conductors* (Electra n 63).

Cloutier, L., Goudrea, S., and Cardou, A. (2006). Fatigue of Overhead Conductors. In J. K. Chan, D. G. Havard, C. B. Rawlins, & J. Weisel (Eds.), *EPRI Transmission Line Reference Book: Wind-induced Conductor Motion* (2nd ed.). Palo Alto, CA: EPRI.

Cousineau, D. (2009). Fitting the three-parameter weibull distribution: review and evaluation of existing and new methods. *IEEE Transactions on Dielectrics and Electrical Insulation, 16*(1), 281-288. doi:10.1109/TDEI.2009.4784578

Crowder, M. J., kimber, A. C., Smith, R. L., and Sweeting, T. J. (1991). *Statistical Analysis of Reliability Data* Springer Science + Business Median, B.V.

D'Agostino, R. B., and Stephens, M. A. (1986). *Goodnss of Fit Techniques* New York Marcel Dekker, Inc.

Fadel, A. A., Rosa, D., Murça, L. B., Fereira, J. L. A., and Araújo, J. A. (2012). Effect of high mean tensile stress on the fretting fatigue life of an Ibis steel reinforced aluminium conductor. *International Journal of Fatigue, 42*, 24-34. doi:https://doi.org/10.1016/j.ijfatigue.2011.03.007

Goudreau, S., Lévesque, F., Cardou, A., and Cloutier, L. (2010). Strain measurements on ACSR conductors during fatigue tests II - Stress fatigue indicators. *IEEE Transactions on Power Delivery, 25*(4), 2997-3006. doi:10.1109/TPWRD.2010.2042083

Hanaki, S., Yamashita, M., Uchida, H., and Zako, M. (2010). On stochastic evaluation of S–N data based on fatigue strength distribution. *International Journal of Fatigue, 32*(3), 605-609. doi:https://doi.org/10.1016/j.ijfatigue.2009.06.001

Hardy, C., and Leblond, A. (2001). *Statistical Analysis of Stranded Conductor fatigue Endurance Data* Paper presented at the Proceeding of the Fouth International Symposium on Cable Dynamics, Montreal, Canada

Kotz, S., and Nadarajah, S. (2000). *Extreme Value Distributions: Theory and Applications* London, UK: Imperial Collge Press.

Marshall, A. W., and Olkin, I. (2007). *Life Distributions*. New York: Springer

Montgomery, D. C., and Runger, G. C. (2003). *Applied Statistics and Probability for Engineers* (3rd ed.). New York, USA: John Wiley & Sons, Inc.

Noiseux, D. U., Hardy, C., and Houle, S. (1986). Statistical Methods Applied to Aeolian Vibrations of Overhead Conductors. *Journal of Sound and Vibrations, 113*(2), 245-255.

Poffenberger, J. C., and Swart, R. L. (1965). Differential Displacement and Dynamic Conductor Strain. *IEEE Transactions on Power Apparatus and Systems, 84*(4), 281-289. doi:10.1109/TPAS.1965.4766192

Strohmeyer, C. E. (1914). *The determination of fatigue limits under alternating stress conditions* Paper presented at the Proceedings of the Royal Society of London

Suresh, S. (1998). *Fatigue of Materials* (2nd ed.). Cambridge, UK: Cambridge University Press

Thi-lien, D. (2015). *Analyse des essais a amplitudes variables realises sur le conducteur Aster 570* Retrieved from France

Vapnik, V. N. (1998). *Statistical Learning Theory* New York: John Wiley & Sons, Inc

3.8 Summary and Outlook

Chapter 3 has presented the probabilistic SN curves for conductor-clamp assemblies using experimental data on conductors of different classes. The developed SN curves will be used to compare the probabilistic SN curves to be derived in chapter 5 from a numerical perspective. The method presented in chapter 3 relies on experimentally testing of conductor-clamp assemblies which is expensive and time-consuming. To reduce the requirement of testing every conductor-clamp assembly to determine it's fatigue resistance, chapter 4 presents a numerical study of the contact between a wire and a clamp. The purpose of this numerical study is to observe the ability or inability of the Timoshenko beam to predict the fatigue life of a typical wire-to-clamp contact that is found in overhead conductor-clamp assemblies.

4 STUDY OF THE FATIGUE OF WIRE TO CLAMP CONTACTS IN OVERHEAD CONDUCTOR USING SOLID AND BEAM ELEMENTS[20]

4.1 INTRODUCTION

The failure of stranded cables used as overhead conductors due to fretting fatigue has been the subject of extensive research in the transmission line community (CIGRE-WG-B2.30, 2010; Cloutier et al., 2006). These works have led to an understanding of the mechanisms of fretting fatigue in overhead conductors at the conductor level (global level). Fatigue failure is associated to small amplitude relative motions at the contacts between wires of adjacent layers or at contacts between wires and the suspension clamp and spacer clamps (Cloutier et al., 2006; McGill and Ramey, 1986).

The understanding of conductor fretting fatigue in the past four decades has gone through various phases, which include the development of conductor test benches (Azevedo et al., 2009; Fadel et al., 2012; Lévesque, et al., 2010; Kalombo et al.,2015; McGill and Ramey, 1986; Zhou et al., 1994; Zhou et al., 1996) which have led to an understanding of the failure mechanisms, the effect of the clamp geometry and the development of empirical stress–life relationships for various classes of conductors using the bending amplitude (Y_b) or maximum antinode amplitude (Y_{max}) to characterize vibration amplitudes. However, these tests did not provide much insight on the distribution of internal forces and moments through wire-wire and wire-clamp contacts. The next phase of research consists of the development of mathematical models to replicate the full conductor clamp system with all contacts (Gang, 2013; Lalonde et al., 2018; Said et al. 2020a). The latter have shown that bending stresses induced in the wires

[20] Thomas, O.O., Chouinard, L., Langlois, S., and Omran (2022) Study of the Fatigue of Wire to Clamp Contacts Using Solid and Beam Elements. To be Submitted to the Journal of Fatigue and Fracture of Engineering Materials and Structures.

between the keeper edge (KE) and the last point of contact (LPC) are important factors to consider in conductor fretting fatigue (Lalonde et al., 2018).

More recently, attention has evolved to the development of experimental set-ups that reproduce local wire to wire contacts or wire to clamp contacts (Omrani et al., 2021; Rocha et al., 2019; Said et al., 2020a; Zhou et al., 1995). This was been done in conjunction with the development of numerical models of single contacts with loads obtained from conductor level models (Said, 2020a; J. Said et al., 2020b). The single contact models have improved the understanding of effects such as the clamp compressive stresses on fretting fatigue (Said et al., 2020b) and provide stress distributions required for multiaxial fatigue models and predicting the number of cycles to failure.

The local level models are mostly based on the finite element method (FEM) (see e.g. (Lévesque and Legeron, 2012; Redford et al., 2019; Rocha et al., 2019; Said et al., 2020a; Said et al., 2020b). However, most of these models have been developed for contacts that satisfy the half space assumption (Lévesque and Legeron, 2012; Pereira et al. 2020; Rocha et al., 2019) or are symmetric (Lévesque et al., 2011; Redford et al., 2019; Said et al., 2020a) with respect to contact interfaces. However, (Zhou et al., 1994) have reported contact lengths that invalidate the half-space assumption. For example, contact lengths up to 90% of the wire diameter has been reported between the keeper edge (KE) and the last point of contact (LPC) (Zhou et al., 1994). In such cases, the stresses in the region of contact are dependent on the shape of wires, which cannot be ignored. Similarly, the geometry of the penultimate wires cannot be neglected in the analysis of the interface between the clamp and the wire (Figure 4-1). Also, the ultimate layer wires to clamp contact and the penultimate wire form a geometrically asymmetric system

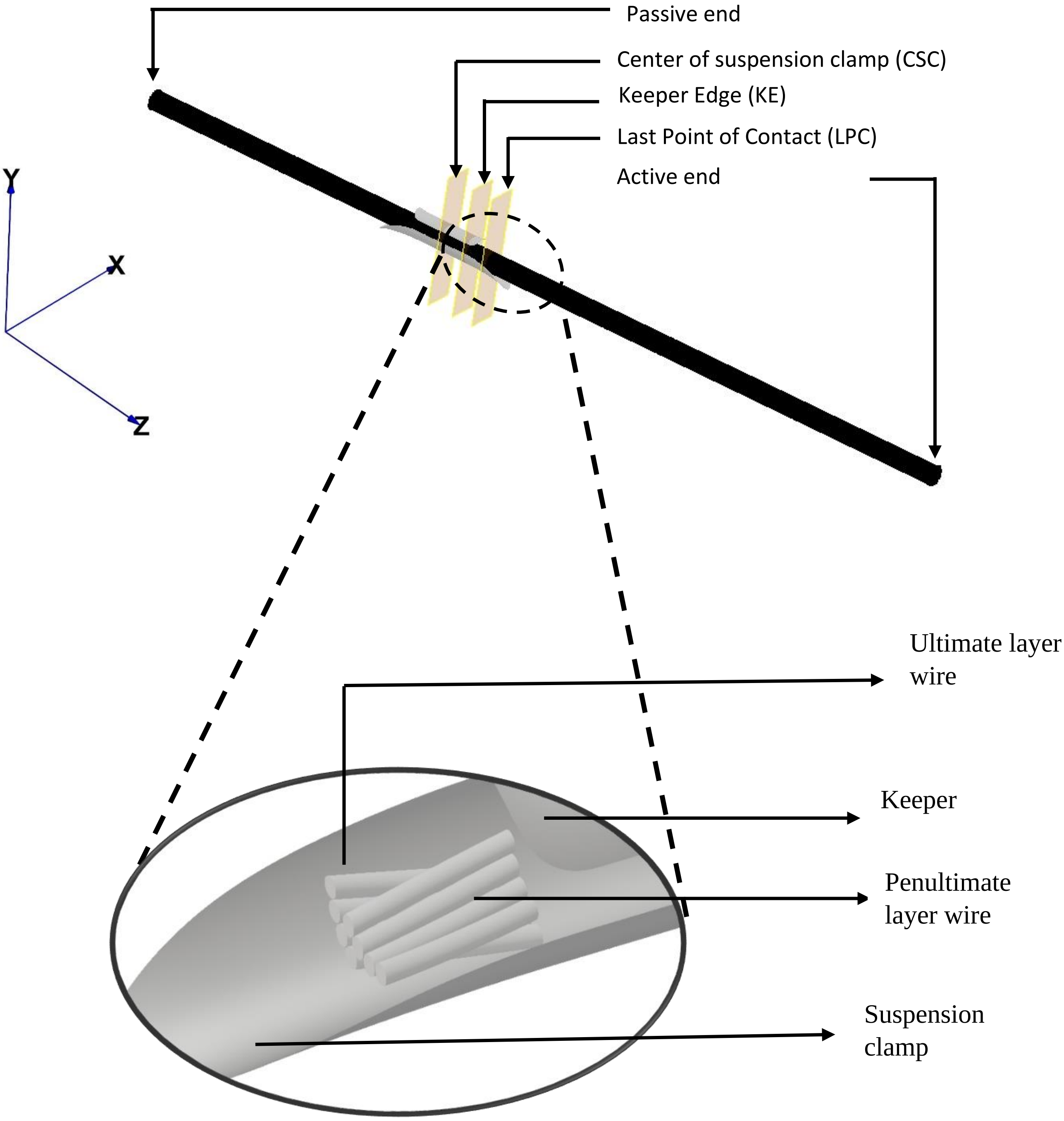

***Figure 4-1**: Geometric representation of a Bersfort conductor-clamp system illustrating the geometric asymmetry of the wire to clamp contact.*

which induces bending in the ultimate layer wire. These peculiarities of the wire-to-clamp contact system have not been studied.

In this work, we thus develop local level FE models for an asymmetric wire to clamp contact with contact length that exceeds the diameter of the wire that are found in transmission line conductor-clamp systems. A three-dimensional finite element model of the wire and a clamp is developed using a submodelling technique. For the purpose of understanding the limitations of beam theory in fretting fatigue life prediction, a 3D FE Timoshenko beam to surface representation of the wire to clamp contact is simultaneously developed. The effect of contact parameters, mesh refinement, friction coefficient and asymmetry of the geometry and loading on the response of the contact system is studied. Multiaxial fatigue criteria are applied to the 3D solid and 3D beam solutions for fatigue life predictions. The life prediction from the numerical models are compared with those obtained from experimental observations of the same contact system.

4.2 METHODOLOGY

4.2.1 Finite Element Meshing Scheme

The contact system studied in this work is an asymmetric contact system shown in Figure 4-2. This contact configuration is taken from a Bersfort conductor shown in Figure 4-1. However, for simplicity the angle between the clamp and the wire is neglected. Rather than supposing that the wire is compressed between two similar clamps, it is assumed that it is in contact with the clamp on the bottom interface with radius as depicted in Figure 4-2 and a steel bearing on the top interface with radius 23mm in the XZ plane and 15mm in the XY plane. The wire length is 350mm with diameter of 4.24mm. Other dimensions of the geometry are shown in Figure 4-2.

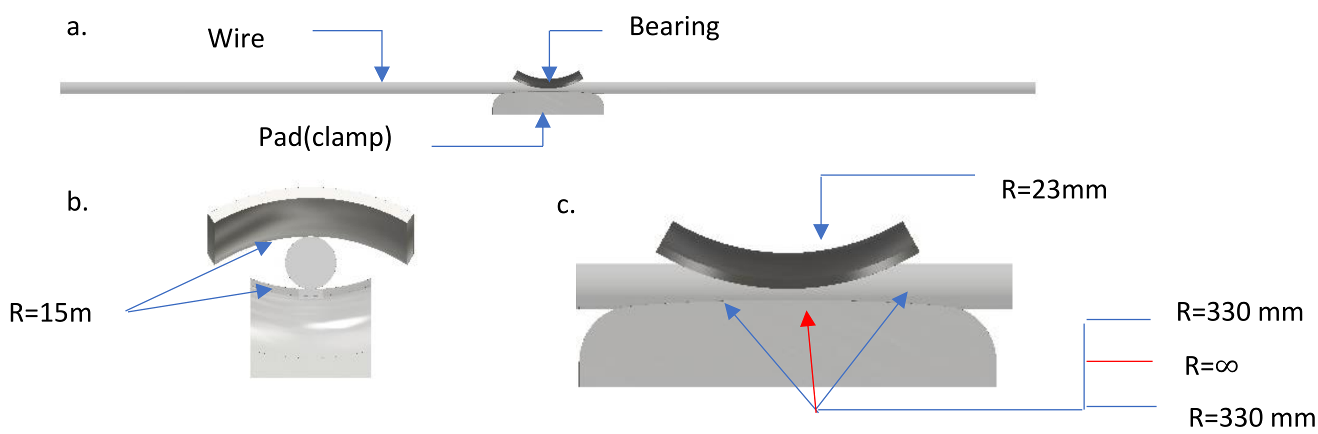

***Figure 4-2**: Geometry of the contact system. (a) Full geometry of the contact system. (b). Front view of the contact system. (c). Close-up of side view of the contact system.*

The properties of the contact system components used in the numerical models are given in Table 1. All numerical analyses assume linear elastic behavior for both the aluminum Al 1350 – H19 wire and the A350 – T6 pad.

Table 4-1: Properties of components of the contact system

Component	Material	*Elastic Modulus (E) (GPa)*	*Poisson ratio (ν)*	Material behaviour
Bearing	Steel	rigid	-	Rigid
Wire	AA 1350 – H19	69	0.33	Linear elastic
Clamp (Pad)	A 350 – T6	73	0.33	Linear elastic

The 3D solid finite element mesh of the contact system is shown in Figure 4-3 and Figure 4-4 for the global model and submodels respectively. Only a 60-degree arc segment of the steel bearing as indicated in Figure 4-2 has been included in the computations. The meshing scheme details are presented in Table 4-2 for the boundary layer regions of all meshes. The boundary layer regions have dimensions of $40mm \times 2mm \times 0.8mm$ and $33.37mm \times 2mm \times 0.8mm$ for the wire and pad respectively in the global meshes as shown in Figure 4-3. For the submodel meshes, the boundary layer has dimensions $10mm \times 0.6mm \times 0.2mm$ and $10mm \times 0.6mm \times 0.07mm$ for the wire and pad respectively as shown in Figure 4-4. All meshes in the boundary layer are made of linear hexahedrons. The pad is meshed with quadratic tetrahedrons in the global model and linear hexahedrons in the submodel. The bearing is meshed with

Table 4-2: Mesh sizing for the boundary layer region of the Solid finite element models

Component	Global Meshes (μm)			Submodel Meshes (μm)			
	Coarse	Medium	Fine	Coarse	Medium	Fine	Ultra fine
Bearing	100	100	100	-	-	-	-
Wire and pad	400	200	100	100	50	20	10

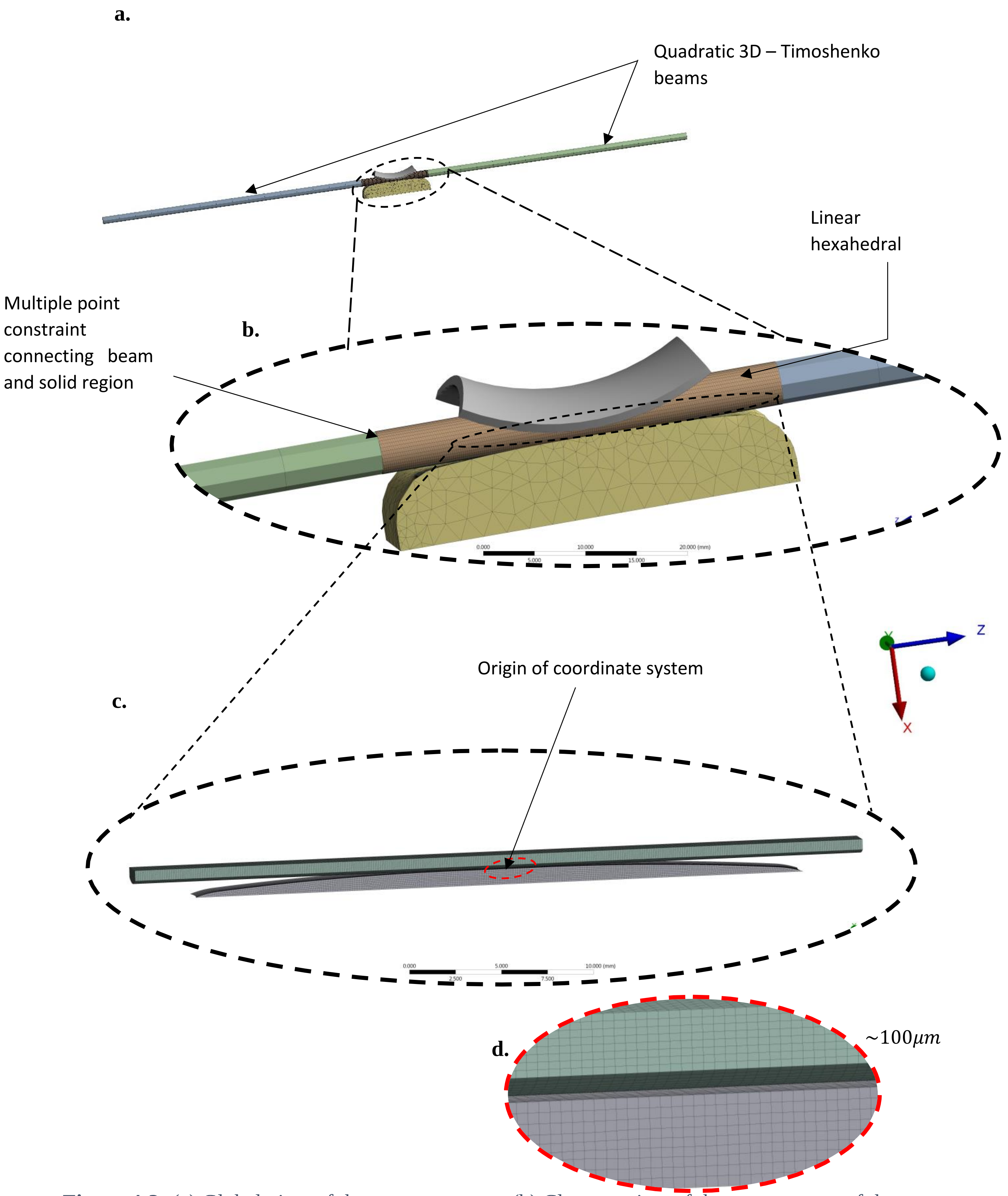

Figure 4-3: (a) Global view of the contact system. (b) Close up view of the contact zone of the global fine mesh. (c). Boundary layer region of the fine global mesh. (d). Close up view of the boundary layer mesh sizing in the fine global mesh

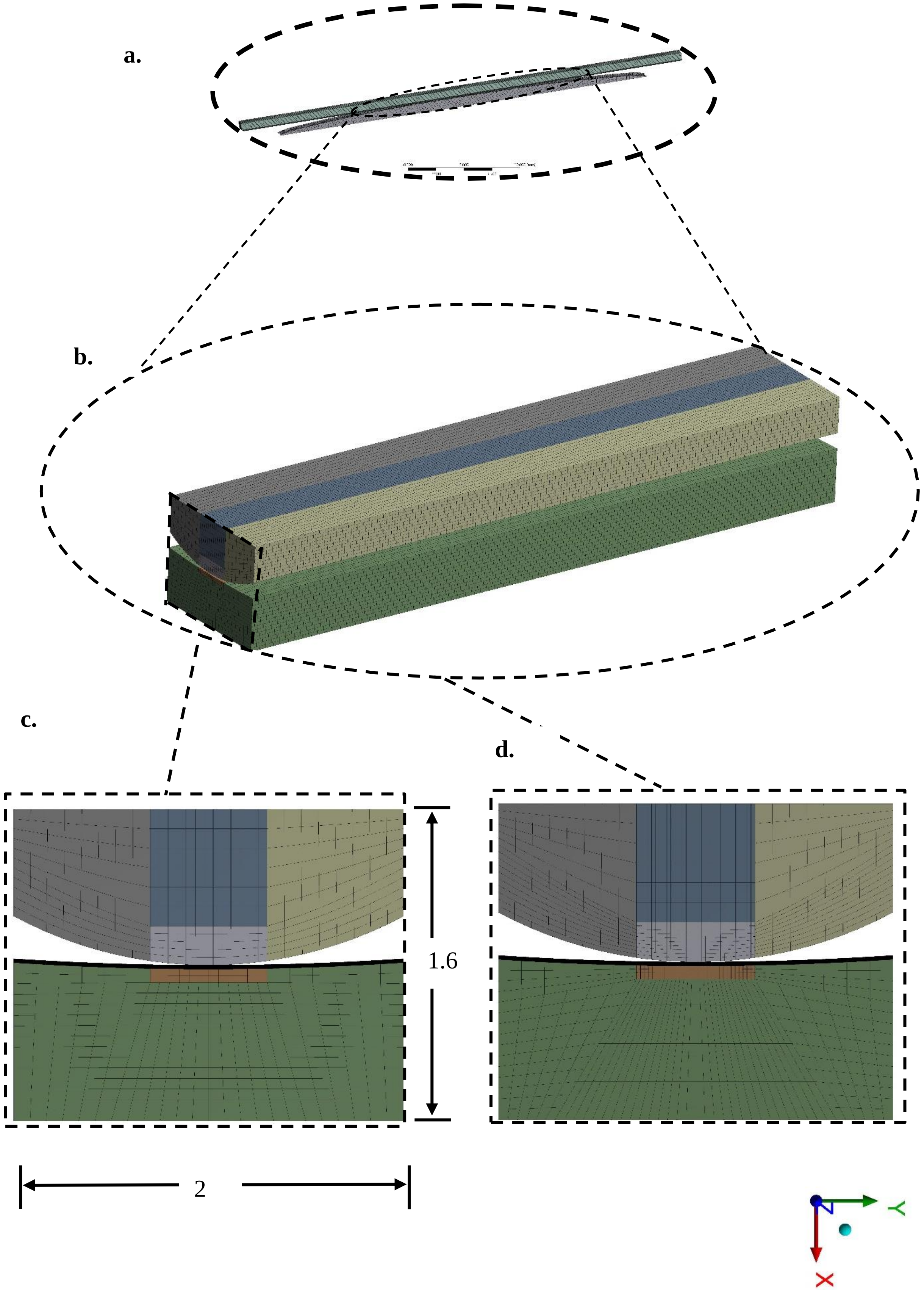

Figure 4-4: (a)). Boundary layer region of the fine global mesh. (b)3D view of the resulting submodel region. (c). Cross section of submodel medium (d). Cross section of submodel fine. Dimensions indicated in mm.

four noded rigid shell elements. For the regions of the wire not within clamp, the 3D Timoshenko beam with quadratic displacement interpolation function and 10mm in length is used as shown in Figure 4-3 (a). The node of the 3D beam is coupled to the nodes of the 3D hexahedral elements at the point of intersection as shown in Figure 4-3 (b) using multiple point constraints. In implementing the submodelling procedure of Cormier et al. (1999), the displacement from the cut boundary between the boundary layer region in the global fine mesh is transferred to the coarse, medium, fine and ultra fine mesh (Table 4-2) of the submodel.

For the 3D Timsohenko beam and shell representation of the contact system, the meshing scheme is shown in Figure 4-5. The length of the 3D Timoshenko beam element is 0.25mm and the length and width of the shell elements used to discretized the bearing and pad are 0.25mm. A node to surface representation is used to represent contact between the beam and the clamp/bearing. The normal and tangential interactions are modelled with the augmented Lagrange method. The element sizes were chosen as 0.25mm for the beam and shells.

All computations are performed using the commercial finite element code Ansys®. For the 3D solid representation (Figures) 4-3 and 4-4. the contact between the wire and the pad is discretized with frictional surface-to-surface contact algorithm with wire and pad defined as the slave and master surfaces respectively. For the bearing to wire contact, the wire and bearing are set as the slave and master respectively and is frictionless. To model the normal and tangential contact interaction, the normal Lagrange and the augmented Lagrange method (ANSYS, 2018b) were used for the wire to bearing and wire to pad respectively. For the 3D Timoshenko beam and shell representation (Figure 4-5), the node-to-surface algorithm was used to enforce contact between the wire to pad and wire to bearing contact. In both cases, the wire is defined as the slave.

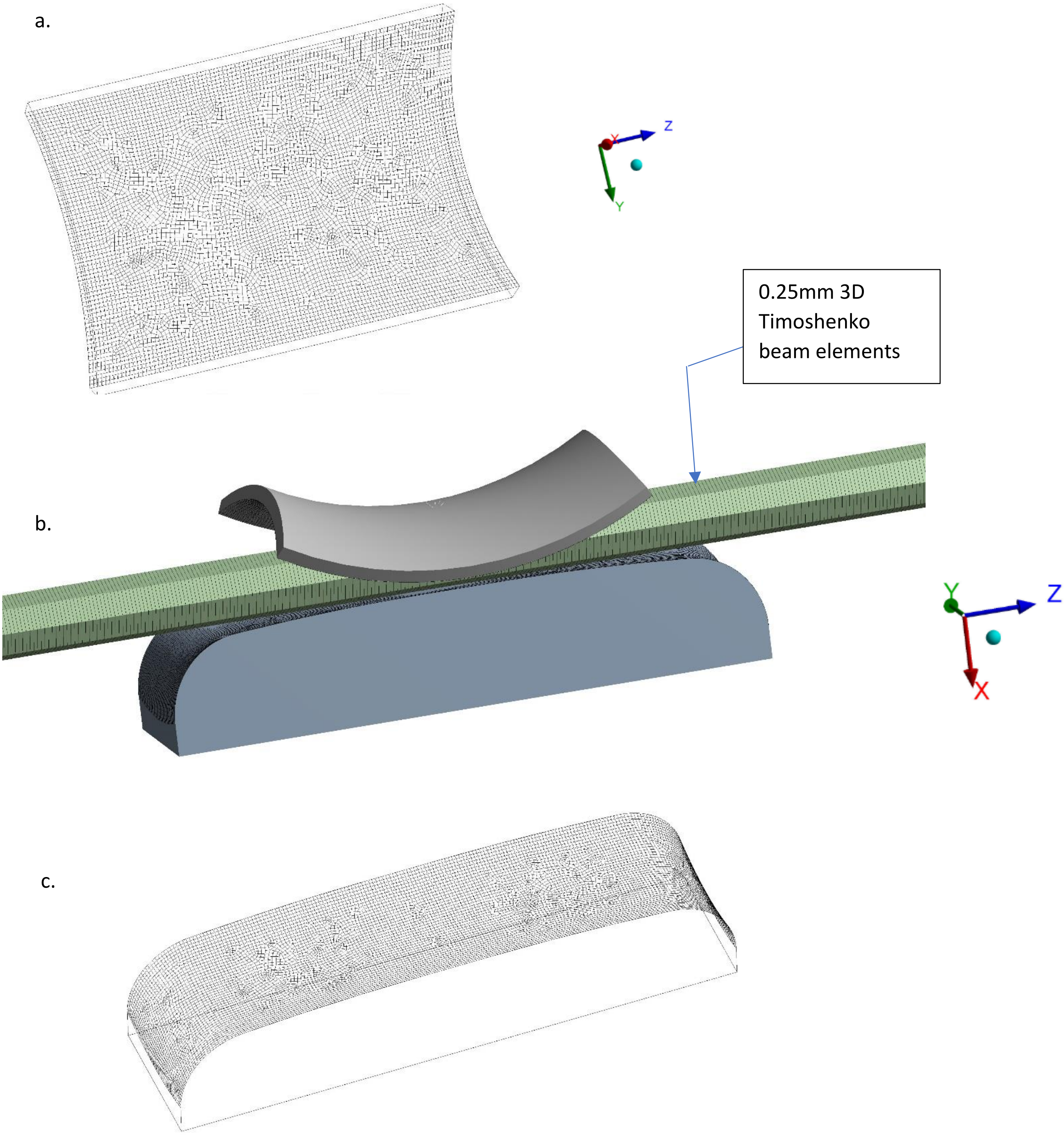

Figure 4-5: Beam to Shell Representation of contact system. (a). Discretization of bearing with 0.25mm shell elements. (b)Contact system with wire discretized with 0.25mm 3D Timoshenko beam elements. (c). Pad discretized with 0.25mm shell elements

4.2.2 Loading Scheme

The loading protocol for the global 3D solid (Figure 4-3) and 3D beam (Figure 4-5) FE model is presented in Figure 4-6 (a) and the application scheme of the loads are shown in Figure 4-6 (b). The base of the pad is fixed in all directions preventing any motion. For the bearing, the shell nodes are all coupled to a master node located at the centroid of the bearing. At the

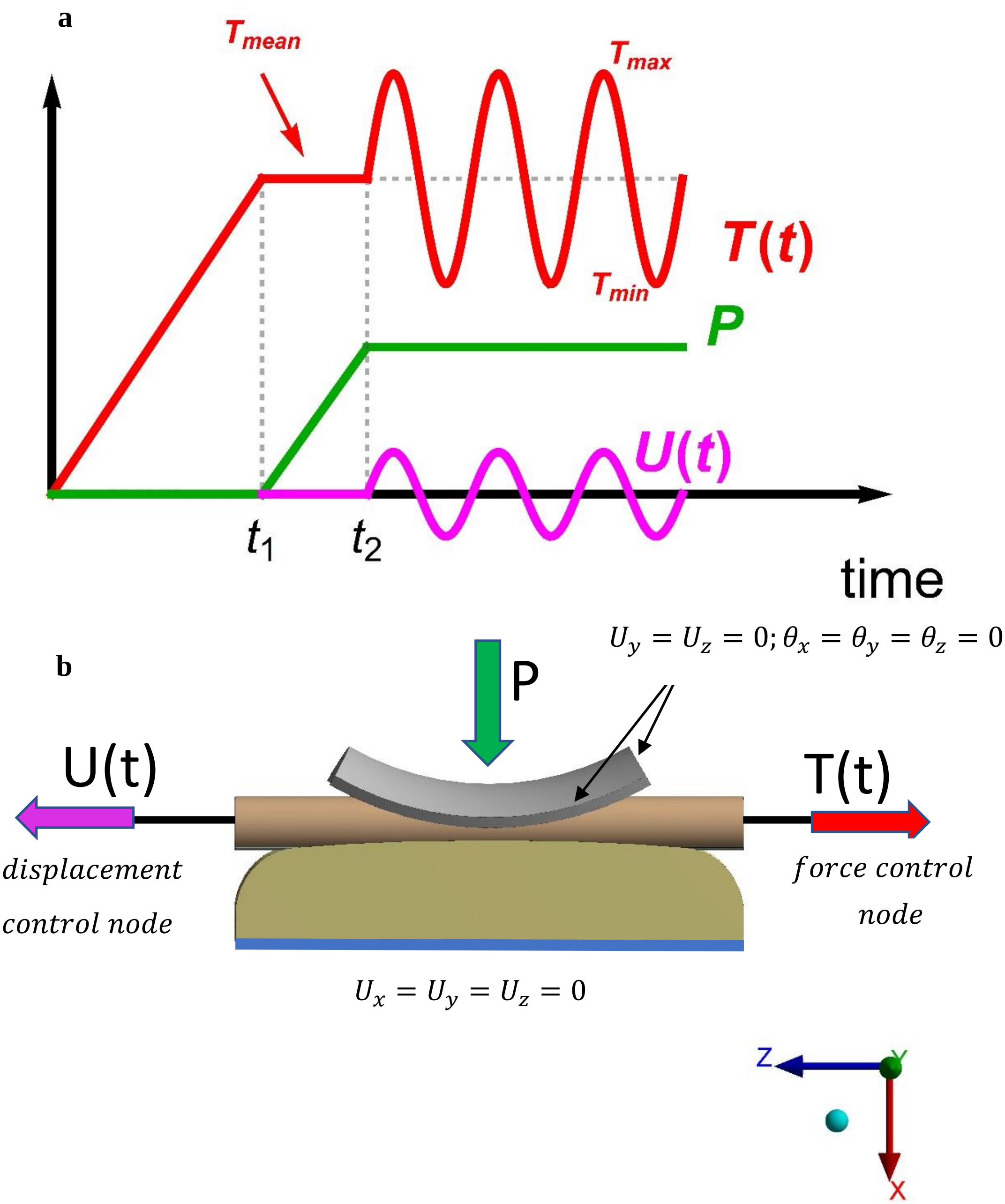

***Figure 4-6**: (a) Loading protocol for the global FE models. (b). Load application and boundary conditions*

beginning of the loading scenario, the displacement node (see Figure 4-6 (b)) is fixed in all displacement and rotation degrees of freedom and the mean tension T_{mean} is applied to the force control node. With T_{mean} held in place, the contact force P is applied to the master node of the bearing. At the end of the contact force application phase, t_2, the tension force T(t) and the displacement U(t) are applied to the force and displacement control nodes respectively.

The loading scheme presented in Figure 4-5 (a) is performed for five different values of the displacement boundary condition U(t) and the force boundary condition T(t). These five numerical simulation scenarios are presented in Table 4-3, where the signs represent the directions of the displacement or force with respect to the coordinate system shown in Figure 4-6 (b) with origin at the center of the wire to clamp contact.

Once the solution of the fine global model is obtained, its displacements are applied to the submodel meshes.

Table 4-3: Values of the force and displacement boundary conditions for five considered loading scenarios

No.	$T_{\max}(N)$	$T_{min}(N)$	$T_{mean}\ (N)$	$U_{min}(mm)$	$U_{max}(mm)$	$U_{mean}(mm)$	$P(N)$
1	-912	-545	729	-0.127	0.127	0	500
2	-1153	-305		-0.03	0.03		
3	-1228	-239		-0.033	0.033		
4	-1298	-170		-0.0188	0.033		
5	-1364	-93		-0.009	0.009		

4.3 Results and Discussion

One of the problems of submodelling using displacements in fretting problems is that the contact parameters such as the normal contact stiffness (ε_N), tangential contact stiffness (ε_T), the normal gap (u_N) and tangential gap(u_T) can affect the solutions (Elke and Sracic, 2019; Rajasekaran and Nowell, 2005). Another problem is the location of the boundaries of the submodel when they are too close to the contact region, inaccuracies in the predicted contact

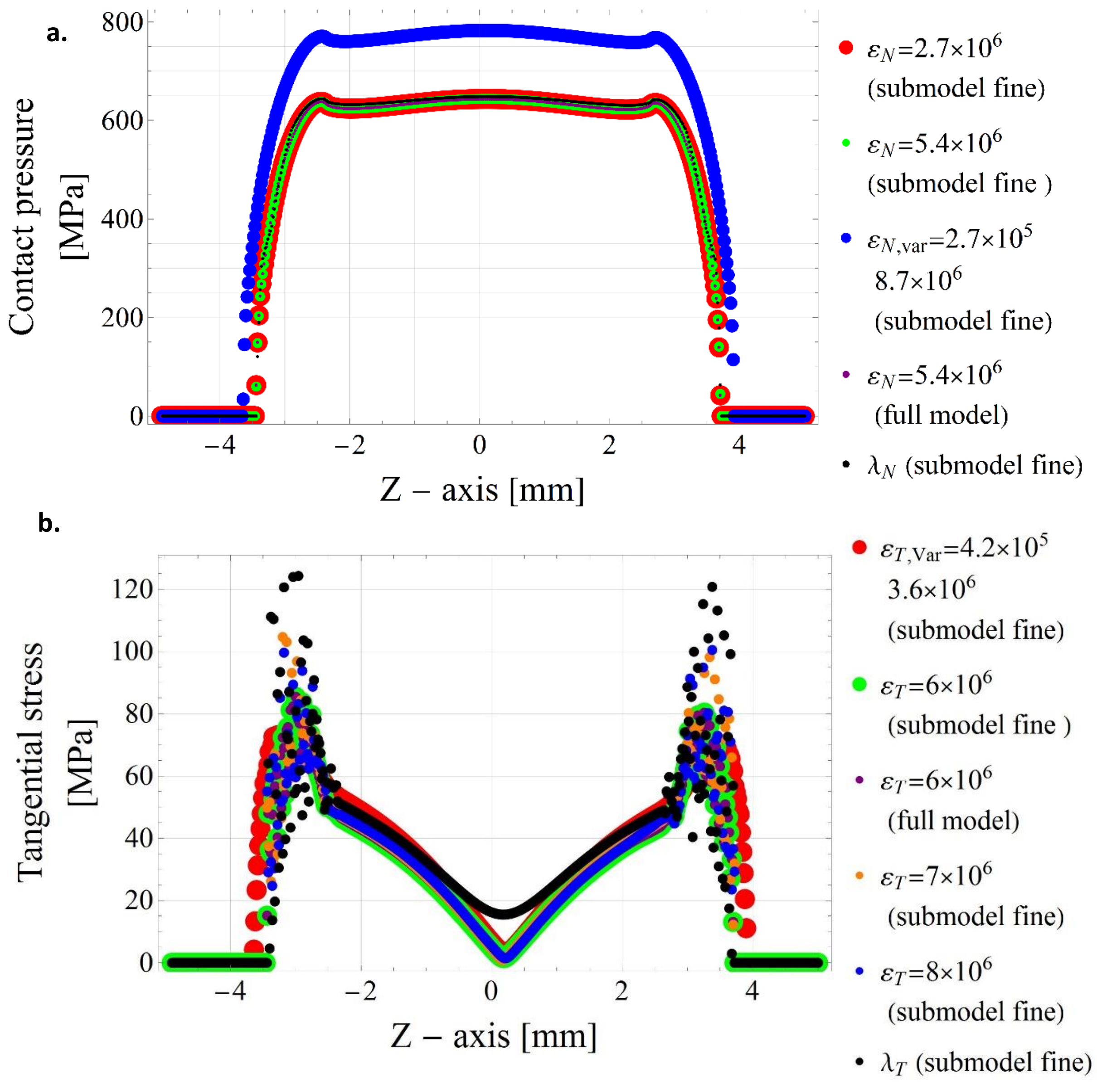

Figure 4-7: (a). Effect of normal contact stiffness on contact pressure distribution. (b). Effect of tangential contact stiffness on tangential stress

tractions can occur (Elke and Sracic, 2019). To guard against these problems, numerical experiments were performed to determine a value for the contact stiffnesses that was stable across both the global model and submodels. This is presented in Figure 4-7 (a) and 4-7 (b) for the normal pressure and tangential stress respectively at the time t_2 (see Figure 4-6 (a)) for the solid model. All results in the Figure 4- 7 are obtained with $20\mu m$ mesh submodel except for the full model which has a $20\mu m$ mesh in the boundary layer and is a full geometry of figure 4-3(a). In addition, a full model that allows for checking the adequacy of the parameters and boundary effect is included in both figures. In these results, u_N and u_T are fixed at the default value 0.1 and 0.01 the element dimension in the contact zone (ANSYS, 2018a). Also included in Figure 4-7 are results in which ε_N and ε_T are determined automatically by the ANSYS system and allowed to vary during the solution and between scales at the wire to pad interface and denoted $\varepsilon_{N,Var}$ and $\varepsilon_{T,Var}$. The minimum and maximum value of $\varepsilon_{N,Var}$ and $\varepsilon_{T,Var}$ are what is shown in Figure 4-7.

Figure 4-7 (a) indicates that if the normal constant stiffness can vary between the scales, an overestimation of the contact pressure can occur while in the case of the tangential stress, it can lead to an underestimation when compared to the Lagrange multiplier method (λ_N and λ_T). The contact pressure is overestimated by 25.6%. This high error is due to an underestimation of the contact stiffness in the global scale, which led to error in the contact interface displacement.

It is also seen from these Figures that the boundary location of the submodel is adequate as it gives similar results in contact tractions to the full model and there is no need to enlarge the submodel region. Hence the contact stiffness parameters are set at 5.4×10^6 and $7 \times 10^6\ N/mm^3$ for the normal and tangential direction respectively for the rest of all solutions in this work for the 3D solid model.

To validate the predictions of the solid model, the contact length determined experimentally by Omrani et al. (2021) for the stick zone is 6.2mm while the stick zone shown for the solid model in Figure 4-7 is 6.7mm representing an error of about 8%.

An interesting feature of this contact system is that although the central region of the clamp is flat along the Z-axis, the central region of the contact pressure displays the characteristics of a contact imprinted by a compound punch (Vázquez et al., 2010) with finite radius in its center and rounded at its edges. This shows that the profile of the indenter (bearing in this case) for such a large contact has an effect on the wire-clamp pressure profile. This has consequences for the analysis of contacts in a conductor-clamp system such as between the ultimate layer and the keeper or clamp. The indenting geometry of the penultimate wire cannot be neglected from the analysis for such a geometrically asymmetric system.

4.4 Mesh Convergence and Friction Coefficient Effect

The effect of the friction coefficient on the convergence rate of fretting fatigue problems has been reported by (Pereira et al., 2016) for two dimensional fretting problems. Here, we verify the convergence in the resultant tangential shear traction at the leading edge (Q_{max}) and trailing edge (Q_{min}) of contact during the cyclic motion as shown in Figure 4-8 for all meshes and loading scenarios. The contact pressure values at the specified locations are also checked for convergence since they are coupled to the tangential tractions. The maximum principal stress in a cycle are also checked since these are found to be good indicators of failure tendency in fretting fatigue at stress concentrations (Taylor, 2007) and are presented in Table 4. The range of friction coefficient studied is from 0.7 to 1.1 for the wire to pad contact. This is the range of friction coefficient covers the range reported in Omrani et al. (2022) for the wire to clamp contact.

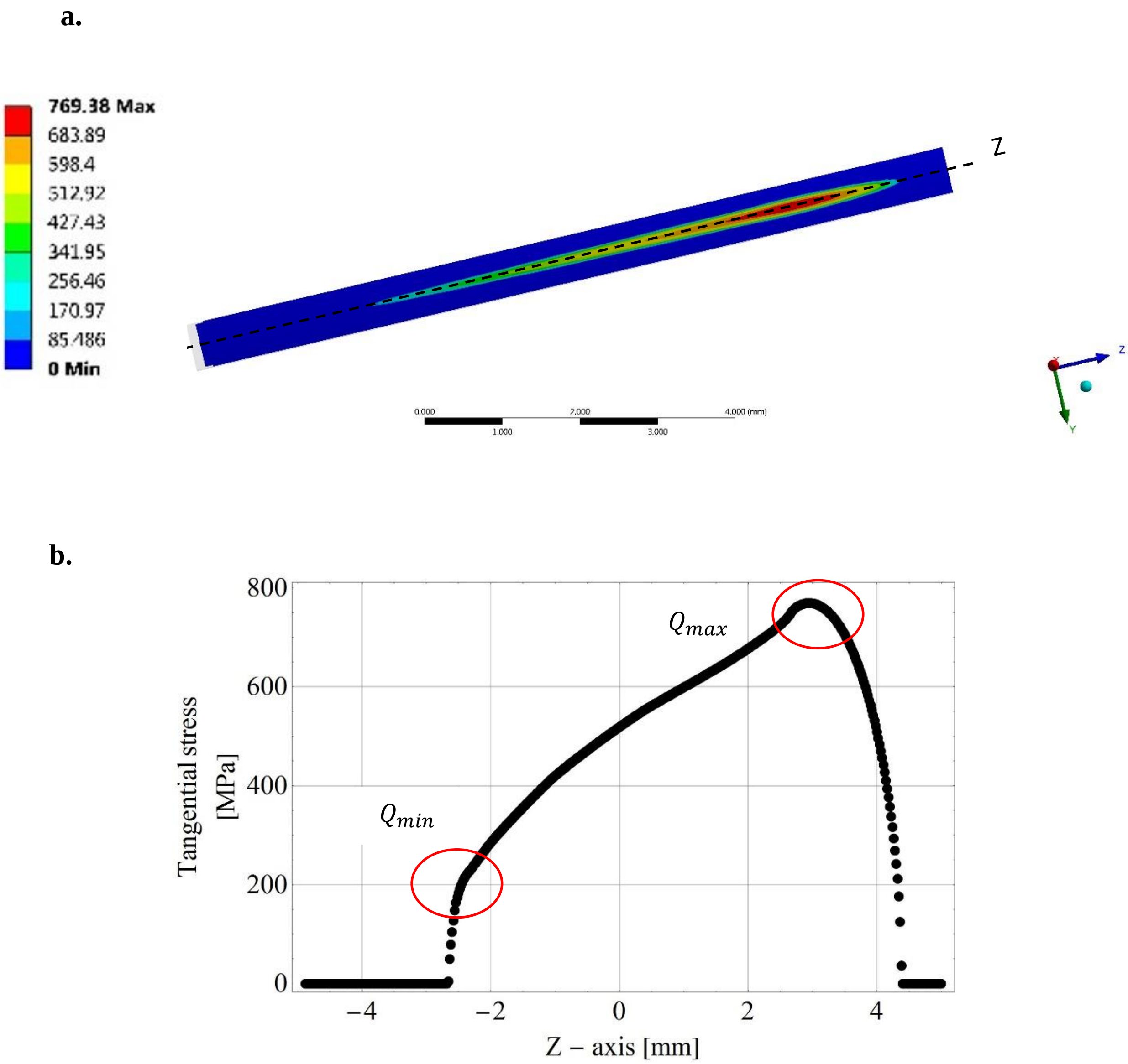

Figure 4-8*: (a)Three-dimensional view of typical resultant tangential shear traction. (b). Typical resultant contact shear traction along the line Z-Z on the surface of the wire to clamp contact indicating the tangential stress.*$(\Delta T =, 30MPa, \mu = 0.9)$

It is observed from Figure 4-9 that the increase in the friction coefficient increases the tangential stress distribution peaks Q_{max} and Q_{min}. But more importantly, the peak Q_{min} becomes steeper with increasing friction coefficient as seen on the finest meshes. Thus, the friction coefficient increases the tangential stress gradient along the longitudinal axis of the

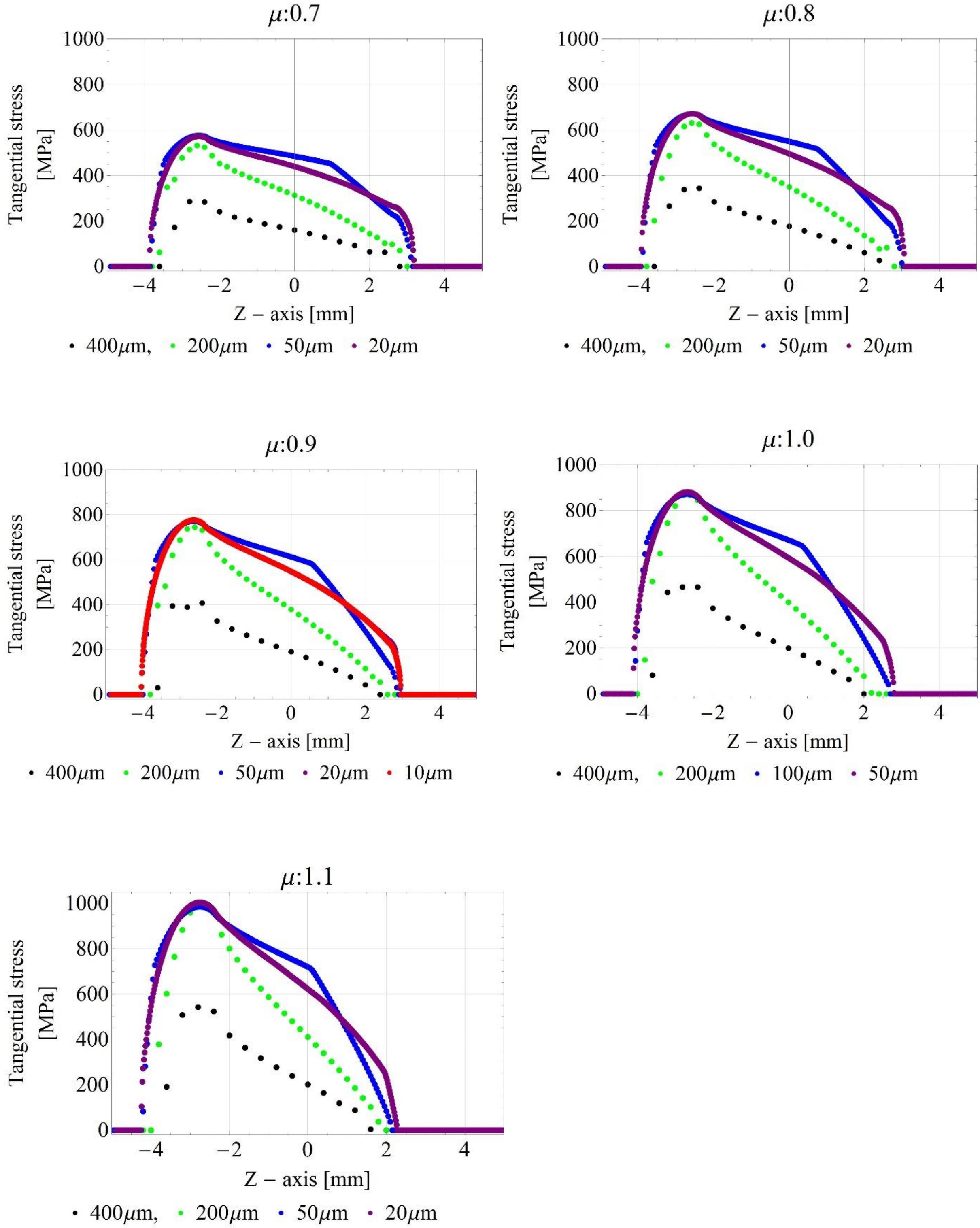

Figure 4-10: Effect of friction coefficient on tangential stress distribution with mesh refinement for the loading scenario 4

contact for which a smaller mesh grid will be required.

Table 4-4: Convergence of contact stress quantities with mesh refinement for the loading scenario 4

ΔT	μ	Mesh size	Tangential stress Q_{min} [MPa]	Tangential stress Q_{max} [MPa]	Maximum principal stress [MPa]	Contact pressure $p_{min}\ [MPa]$	Contact pressure $p_{max}\ [MPa]$
565	0.7	400	0	285.95	197.19	0	408.52
		200	0	530.57	275.03	0	759.25
		100	200.31	919	323.83	288.99	1316.49
		50	226.67	575.79	349.34	309.69	822.56
		20	265.35	572.03	424.15	377.31	817.19
	0.8	400	0	344.86	231.15	0	429.38
		200	0	639.84	291.72	0	793.81
		100	141.69	1088.65	362.22	174.63	1369.31
		50	178.52	671.49	399.09	215.07	839.36
		20	258.94	671.89	500.11	327.04	839.86
	0.9	400	0	400.96	271.54	0	451.79
		200	0	747.57	341.45	0	828.63
		100	0	1283.60	415.06	97.93	1427.95
		50	119.89	766.14	465.02	127.47	856.84
		20	230.14	780.67	578.27	260.20	862.21
		10	222.17	775.75	650.24	250.67	861.95
	1.0	400	0	465.43	295.30	0	463.96
		200	0	867.51	385.53	0	868.55
		100	0	1449.82	488.49	0	1449.82
		50	0	871.53	536.78	0	871.53
		20	227.16	881.04	667.48	227.16	881.04
	1.1	400	0	544.69	320.22	0	495.48
		200	0	1000.57	437.29	0	905.37
		100	0	1617.26	538.32	0	1467.77

		50	0	984.87	616.37	0	895.34
		20	254.58	1003.5	765.21	227.68	912.31

In Table 4, the maximum principal stress in a cycle is seen to have not converged at any mesh level even at the submodel mesh with a $10\mu m$ mesh or the smallest friction coefficient. However, as mentioned by (Taylor, 2007) a mesh size smaller than the critical distance is sufficient for fatigue life estimation. Also, following the work of Omrani et al. (2022), that shows that the mean friction coefficient of the wire to pad contact is 0.9, this friction coefficient will be used for the rest of this study. For this particular friction coefficient, as seen in Table 4 and Figure 4-9, the normal contact pressure and tangential stress have completely converged at a mesh size of 20 μm. Thus this mesh size will be used for fatigue life assessment of the wire to clamp interface using the 3D solids.

4.5 FATIGUE DAMAGE PARAMETERS AND LIFE ESTIMATION

4.5.1 3D FE Solid Model Fatigue Life Estimation

The submodelling procedure for the 3D solid and the 3D beam approach presented in section 2 is applied to estimate the lifetime of the AA 1350 – H19 wire in the contact system. This is achieved using the point method (PM) of the theory of critical distances (TCD) (Taylor, 2007) together with Smith – Watson – Topper (SWT) criteria (Rocha et al., 2019) for the solid elements. The fatigue criteria is evaluated for all loading scenarios as follows:

$$SWT(\frac{L}{2}, t) = \sqrt{\sigma_{n,a}(t)\ \sigma_{n,max}(t)} \tag{4.1}$$

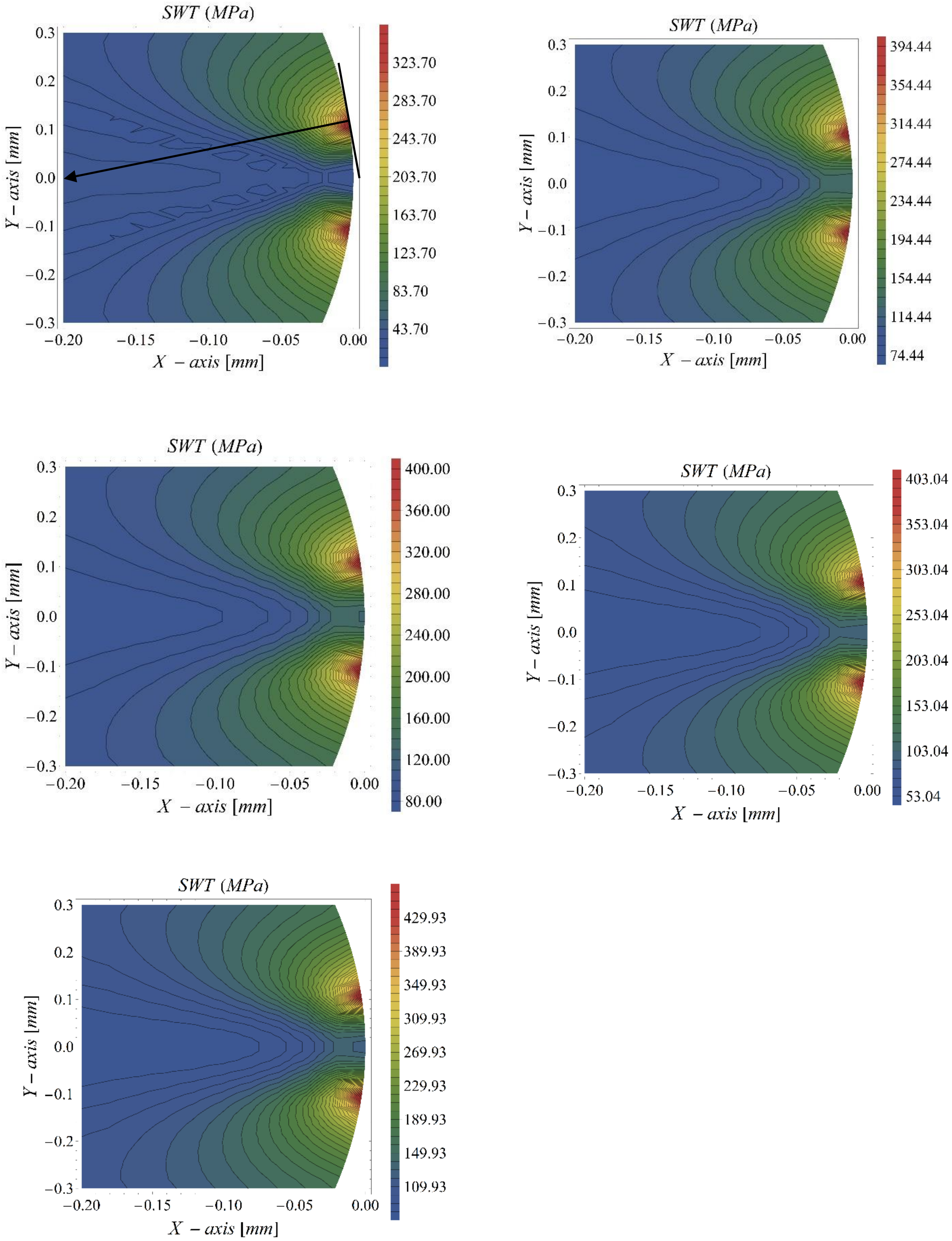

Figure 4-11: SWT Values for all five loading scenarios computed at $\mu = 0.9$. (a) through (e) represents SWT values for loading scenario 1 through 5

where L represents the critical length and t represents time. $\sigma_{n,a}(t)$ is the stress amplitude on the failure plane and $\sigma_{n,max}(t)$ is the maximum normal stress on the failure plane. In using the point method in three dimensions, we identify the failure plane using (1). The focus path on this plane is chosen as shown in Figure 4-10 (a) where the tangent to the maximum stress is drawn and a line orthogonal to it is the focus path.

4.5.2 3D Timoshenko Beam Fatigue Life estimation

For the beam model, the stress computations for the five loading scenarios are shown in Table 5. Each beam solution takes on average 30 minutes as compared to the solid solutions that took

Table 4-5: 3D Timoshenko beam results for fatigue life assessment

Axial stress amplitude σ_a (MPa)	Bending stress amplitude σ_b (MPa)	Minimum Axial stress $\sigma_{a,min}$ (MPa)	Maximum Axial stress $\sigma_{a,max}$ (MPa)	Axial mean stress $\sigma_{a,mean}$ (MPa)	Bending mean stress $\sigma_{b,mean}$ (MPa)	Alternating shearing stress σ_v (MPa)	Mean shear stress $\sigma_{v,mean}$ (MPa)	Combined mean stress $\sigma_{a+b,mean}$ (MPa)	Maximum combined stress $\sigma_{a+b,max}$ (MPa)	SWT σ_{SWT} (MPa)	SWT/C_{ld} (MPa)
45	0	6.6	96	51.63	46.11	0	15.90	97.74	142.74	80	94.12
40	0	11.52	91.61	51.63	46.125	0	15.96	97.76	138	74.3	87.41
35	0	15.82	86.72	51.63	46.04	0	15.98	97.67	133.12	68.69	80.81
30	<2	21.60	81.68	51.68	31.08	0	16.53	82.71	112.75	58.20	68.47
25	<3	38.60	64.61	51.63	25.12	0	10.08	76.75	89.76	34.17	40.2

on average 20 hours. An interesting observation from the results of the beam model stress results given in Table 4-5 is that a mean bending stress, alternating bending stress and mean shear stress exist even when no bending moment is applied. This bending moment and shear force is a result of the contact normal force and tangential force as the Timoshenko beam resist a normal contact force by shear and bending. Thus, it is seen that this bending moment and shear increases mean stress in the wire. However, the increase is bending dominated rather than shear dominated especially at high amplitudes. Thus, in the Timoshenko beam theory the purpose of the contact is to act as a stress concentrator that increases the mean bending stress and mean shear stress in the contact region. This is in agreement with the work of (Lalonde et al., 2018) that showed that the contact between a wire and a clamp in a Bersfort conductor is governed by a bending amplitude. Although the presence of mean bending stress was not assessed in that study, from our observation in this work, there is the possibility of increased mean bending and shear stress in the wires. Thus, this is an observation that should be further studied.

For the purpose of life prediction, the plain fatigue data of Kaufman (2008) is used to calibrate the stress-number of cycles curve for prediction. The fatigue data of Kaufman (2008) used to calibrate the prediction model (SN curve) were obtained from rotating bending test. However, the test of set-up modelled herein is loaded mainly in tension. Thus, in accordance with literature evidence (Bannantine et al.1989; Milella, 2013) that the fatigue limit of a material in axial loading is less compared to rotation bending, the calculated SWT values in the 3D Timoshenko beam model in Table 4-5 are modified as (Bannantine et al.1989; Milella, 2013):

$$C_{ld} = \frac{SWT_{axial}}{SWT_{bending}} = (2m + 2)^{-1/m} \qquad (2)$$

Where m is the Weibull exponent. A Weibull exponent of 25 (Milella, 2013) was chosen giving a load factor C_{ld} of 0.8. The factored SWT values are given in the last column of Table 4-5. A comparison of the predicted and experimental fatigue lives is given in Figure 4-11. It is seen that despite the crudeness of the beam and shell modeling approach, they can predict the fatigue lives of the wire to clamp contact. This is not surprising given that the Timoshenko beam satisfies the contact equations of equilibrium in the global sense. However, one observes that the predictions of the solid model are closer to the experimental values than those of the beam model. This can be explained by the fact that the solid model accounts for deformation modes such as normal deformation in the normal force direction whereas the Timoshenko beam is not

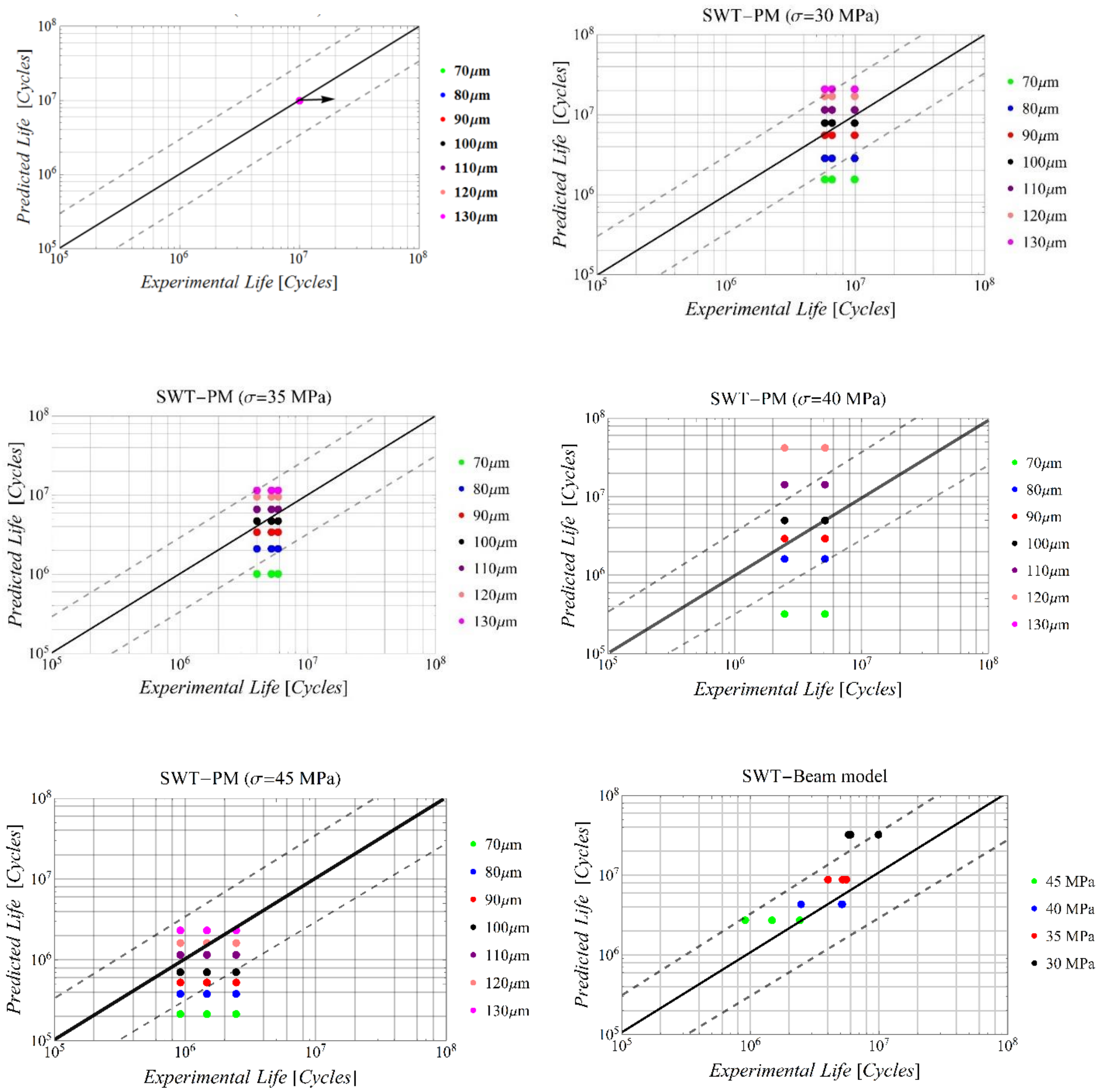

Figure 4-12: Comparison of the experimental life against the predicted life time for loading scenario 1 through 5 from top left to bottom left.

able to deform in such a manner and must instead generate shear and bending stresses.

4.6 PREDICTION OF FAILURE LOCATION AND DISTRIBUTION OF STRESS

Although it has been demonstrated herein that Timoshenko beam theory is capable of being used for fretting fatigue life predictions, there are downsides to using this beam theory. One of the first problem with the Timoshenko beam theory is in the prediction of the location of failure.

In Figure 4-12 below, the distribution of the SWT for the solid model and beam model are shown for the axial stress amplitude of 45 MPa. In this Figure, the failure point of the solid model and the beam model are identified. While the solid model identifies a failure location of 3mm from the center of the contact, the beam model identifies 4.25mm from the center of the contact. This behavior of the Timoshenko beam is not surprising since it does not contain the displacement polynomials to approximate the stress field exactly but only does so in an average sense over the depth of the beam.

However, the beam approach can predict a contact length that is comparable to both the solid approach and the experimental observation. Figure 4-13 shows the contact length for the beam, solid and experimental observation for an axial stress amplitude of 45 MPa. Since the shear force and bending moment resist the normal contact force in the beam model, either can be checked to detect the length of the contact. For the solid model, the contact pressure when the actuator F pulls (in black), and pushes (in blue) are plotted. A comparison of the contact lengths

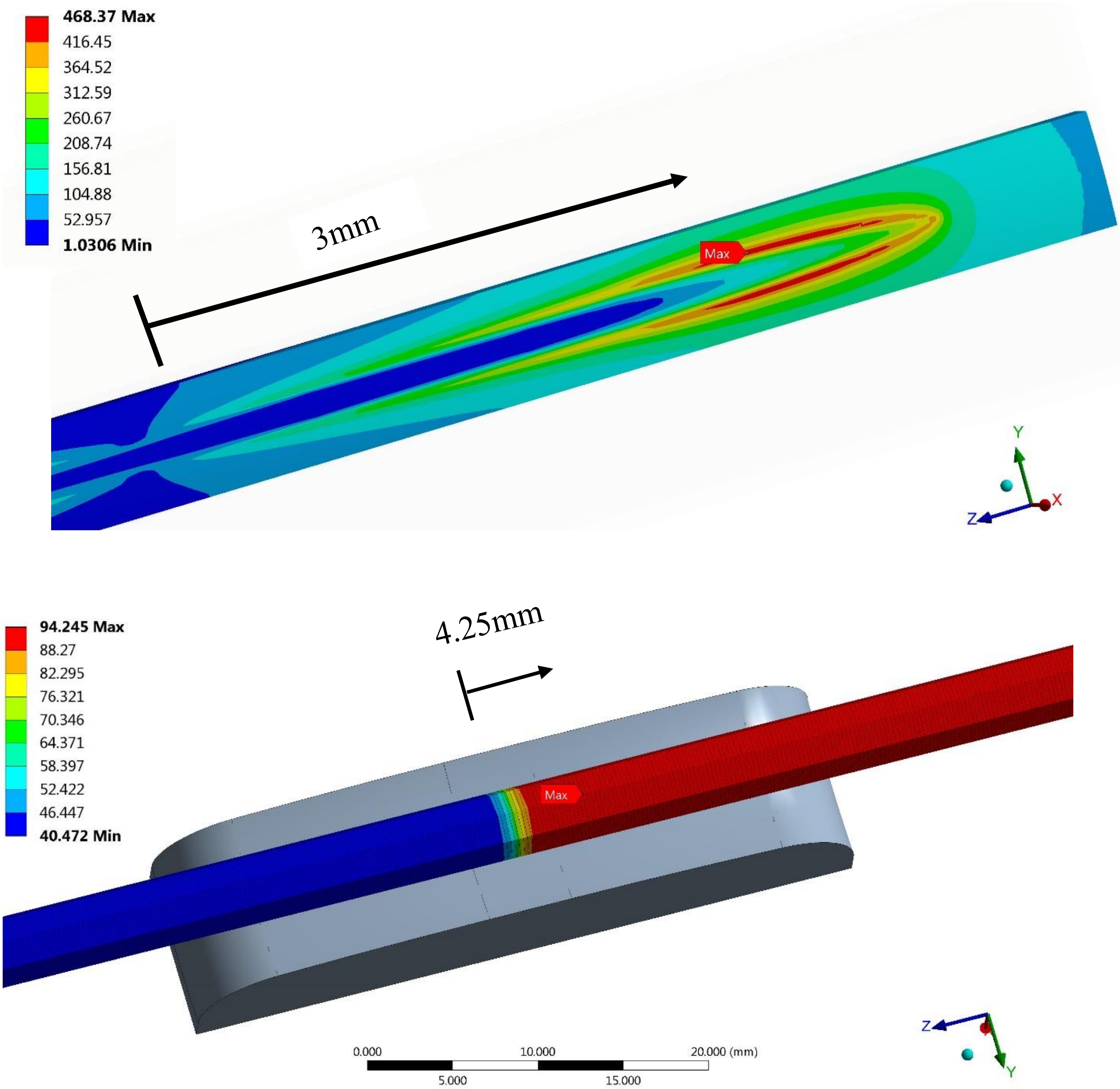

Figure 4-13: Comparison of prediction of location of failure using SWT between solid and beam model for axial stress amplitude of 45 MPa: (a). Solid model (b). Beam model

that the beam model predicts a contact length of 8mm, the solid model a contact length of 8.1mm and the experimental value reported by Omrani et al. (2021) is 8.8mm. However, one notices that the contact pressure for the solid model experiences a contact and no contact phase at the edge between -3 to -4mm and 3 to 4mm. This corresponds to the slip region observed in

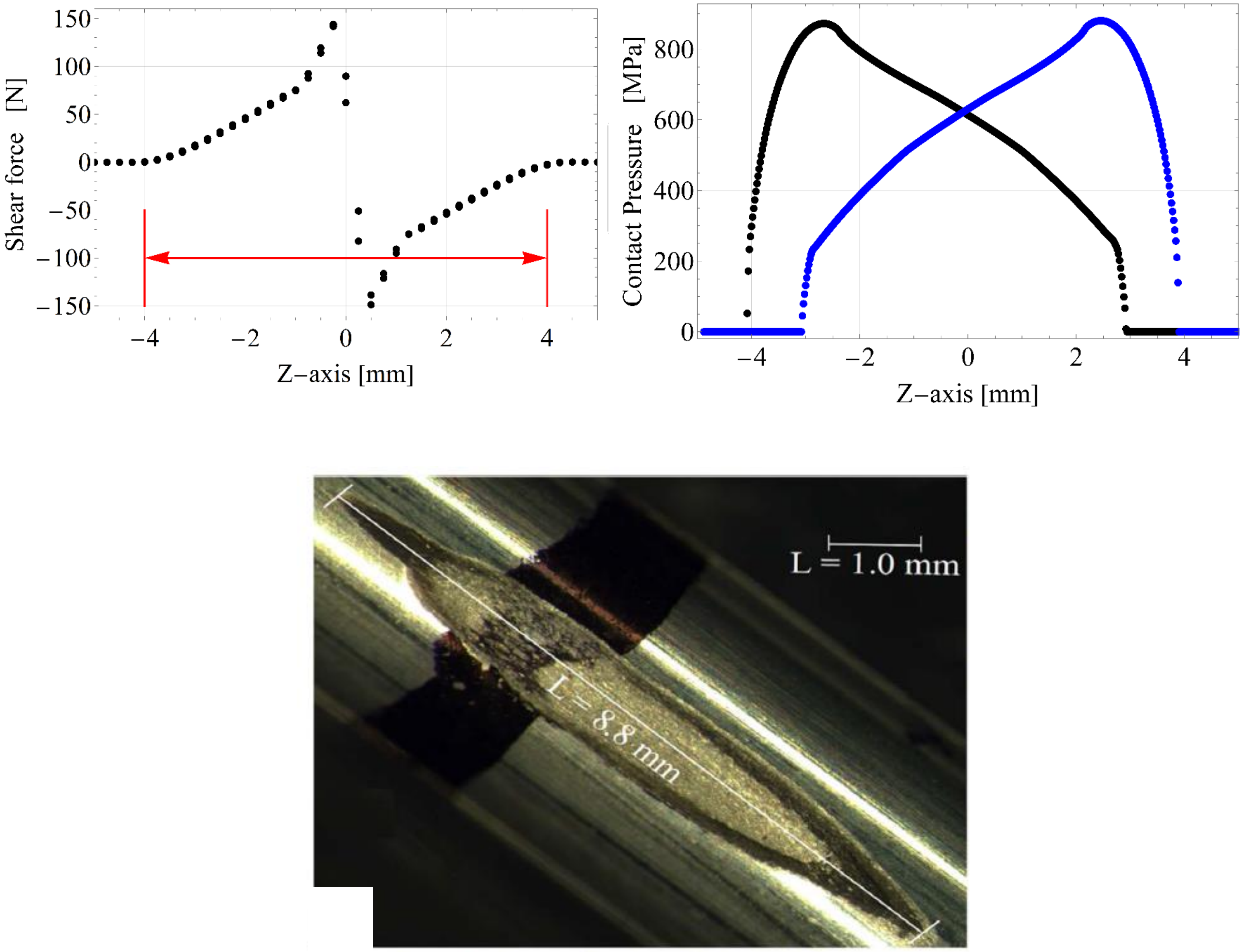

Figure 4-14: Comparison of the contact length prediction of (a) Beam model (b). Solid model (c). Experimental Observation

(Omrani et al. 2021) as shown in Figure 4-20 (c) and is about 1.37mm in length in the experimental observation. The beam model cannot show this since it is only required to satisfy the force equilibrium conditions in an average sense over the depth of the beam. However, for the case of the solid elements, equilibrium is satisfied locally allowing for local features to be detected. It is also observed that the contact pressure changes as the actuator F pulls or pushes, but the shear force remains constant. In other words, Timoshenko beam, since it is only required to satisfy force equilibrium, cannot detect this coupling of the normal and tangential stress that causes the normal contact pressure to oscillate.

4.7 CONCLUSIONS

A numerical strategy to assess the fatigue life of a single wire to clamp contact was developed using the solid and beam finite element method and the multiaxial Smith-Wastson-Topper relationship. The following conclusions are drawn from this work:

1. For submodels to satisfy force equilibrium, the contact stiffnesses should be kept the same across all scales when penalty-based methods are used.
2. For wire to clamp contacts in a overhead conductor not satisfying the half space assumption, the geometry of the indenting wire (i.e. the penultimate wire) cannot be neglected as this affects the stress distribution at the wire to pad contact due to asymmetry in the geometric configuration and should be considered in life estimation.
3. For adequate prediction of fatigue life in fretting fatigue of a wire to clamp contact, it is not necessary that all members of the stress tensor be converged but if the contact normal pressure and tangential stress which represent the stress concentration due to contact are converged on a given mesh, then it is possible to make reliable predictions using this mesh.
4. The Timoshenko beam model can be reliable for fretting fatigue life estimation if local features such as location of contact failure, tangential stress and contact pressure distributions are of secondary importance to the analyst.
5. It was observed that effect of a normal force for the 3D Timsohenko contact was to introduce a mean bending stress and mean shear stress in the contact.

6. The normal based stress criterion (SWT) has shown to provide reliable fatigue life predictions for wire to clamp contacts in both solid and beam models and should be explored further for use in a full conductor clamp system.
7. The results of the solid model are less biased in comparison to the beam model.
8. The solid model SWT values are not sensitive to the type of fatigue data used to calibrate the prediction model as compared to the beam model.

4.8 REFERENCES

ANSYS. (2018a). ANSYS Mechanical APDL Contact Technology Guide (Version R19.0). Canonsburg, USA: ANSYS

ANSYS. (2018b). ANSYS Mechanical APDL Element Reference (Version R19.0). Canonsburg, USA: ANSYS

Azevedo, C. R. F., Henriques, A. M. D., and Pulino filho, A. R. (2009). Fretting fatigue in overhead conductors: Rig design and failure analysis of a Grosbeak aluminum cable steel reinforced conductor *Engineering Failure Analysis, 16*, 136-151.

Beisheim, J. R., & Sinclair, G. B. (2008). Three-Dimensional Finite Element Analysis of Dovetail Attachments With and Without Crowning. *Journal of Turbomachinery, 130*(2). doi:10.1115/1.2751486

CIGRE-WG-B2.30. (2010). *Engineering Guidelines Relating To Fatigue Endurance Capability of Conductor/Clamp Systems*

Cloutier, L., Goudrea, S., and Cardou, A. (2006). Fatigue of Overhead Conductors. In J. K. Chan, D. G. Havard, C. B. Rawlins, & J. Weisel (Eds.), *EPRI Transmission Line Reference Book: Wind-induced Conductor Motion* (2nd ed.). Palo Alto, CA: EPRI.

Elke, W. J., III, and Sracic, M. W. (2019). *Effects of Cut Boundary Location on Finite Element Submodels With Contacts.* Paper presented at the ASME 2019 International Design Engineering Technical Conferences and Computers and Information in Engineering Conference.

Fadel, A. A., Rosa, D., Murça, L. B., Fereira, J. L. A., and Araújo, J. A. (2012). Effect of high mean tensile stress on the fretting fatigue life of an Ibis steel reinforced aluminium conductor. *International Journal of Fatigue, 42*, 24-34. doi:https://doi.org/10.1016/j.ijfatigue.2011.03.007

Gang, Q. (2013). *Computational Modeling for Stress Analysis of Overhead Transmission Line Stranded Conductors Under Design and Fretting Fatigue Conditions* (PhD), McGill University Montreal, Quebec

Goudreau, S., Lévesque, F., Cardou, A., and Cloutier, L. (2010). Strain measurements on ACSR conductors during fatigue tests II - Stress fatigue indicators. *IEEE Transactions on Power Delivery, 25*(4), 2997-3006. doi:10.1109/TPWRD.2010.2042083

Johnson, K. L. (1985). *Contact Mechanics*. Cambridge, UK: Cambridge University Press.

Kalombo, R. B., Martínez, J. M. G., Ferreira, J. L. A., da Silva, C. R. M., & Araújo, J. A. (2015). Comparative Fatigue Resistance of Overhead Conductors Made of Aluminium and Aluminium Alloy: Tests and Analysis. *Procedia Engineering, 133*(Supplement C), 223-232. doi:https://doi.org/10.1016/j.proeng.2015.12.662

kardak, A. A. (2015). *On an effective submodelling procedure for stresses determined with finite element analysis* (PhD), Louisiana State University Louisiana.

Lalonde, S., Guilbault, R., & Langlois, S. (2018). Numerical Analysis of ACSR Conductor–Clamp Systems Undergoing Wind-Induced Cyclic Loads. *IEEE Transactions on Power Delivery, 33*(4), 1518-1526. doi:10.1109/TPWRD.2017.2704934

Levesque, F., and Legeron, F. (2012). *Effect of mean tension on interwire contacts in overhead conductors*

Levesque, F., and Legron, F. (2010). *Contact mechanics based fatigue indicators for overhead conductors*

McGill, P. B., & Ramey, G. E. (1986). EFFECT OF SUSPENSION CLAMP GEOMETRY ON TRANSMISSION-LINE FATIGUE. *Journal of Energy Engineering-Asce, 112*(3), 168-184.

Omrani, A., langlois, S., Van Dyke, P., Karganroudi, S. S., and lalonde, S. (2019). *Fatigue Strength Evaluation for Individual strands of Overhead Conductors using a boaxial fretting fatigue test bench* Paper presented at the ICMFF12.

Pereira, K., Bordas, S., Tomar, S., Trobec, R., Depolli, M., Kosec, G., . . . Mancusi, G. (2016). On the Convergence of Stresses in Fretting Fatigue. *Materials, 9*(8). doi:10.3390/ma9080639

Rajasekaran, R., and Nowell, D. (2005). On the finite element analysis of contacting bodies using submodelling. *The Journal of Strain Analysis for Engineering Design, 40*(2), 95-106.

Redford, J. A., Gueguin, M., Nguyen, M. C., Lieurade, H. P., Yang, C., Hafid, F., and Ghidaglia, J. M. (2019). Calibration of a numerical prediction methodology for fretting-fatigue crack initiation in overhead power lines. *International Journal of Fatigue, 124*, 400-410. doi:https://doi.org/10.1016/j.ijfatigue.2019.03.009

Rocha, P. H. C., Díaz, J. I. M., Silva, C. R. M., Araújo, J. A., and Castro, F. C. (2019). Fatigue of two contacting wires of the ACSR Ibis 397.5 MCM conductor: Experiments and life prediction. *International Journal of Fatigue*, *127*, 25-35. doi:https://doi.org/10.1016/j.ijfatigue.2019.05.033

Sackfield, A., Hills, D., Vázquez, J., and Domínguez, J. (2010). The mechanical behaviour of a symmetrical punch with compound curvature. *The Journal of Strain Analysis for Engineering Design, 45*(4), 209-222. doi:10.1243/03093247JSA633

Said, J., Fouvry, S., Cailletaud, G., Yang, C., and Hafid, F. (2020). Shear driven crack arrest investigation under compressive state: Prediction of fretting fatigue failure of aluminium strands. *International Journal of Fatigue*, *136*, 105589. doi:https://doi.org/10.1016/j.ijfatigue.2020.105589

Said, J., Garcin, S., Fouvry, S., Cailletaud, G., Yang, C., and Hafid, F. (2020). A multi-scale strategy to predict fretting-fatigue endurance of overhead conductors. *Tribology International, 143*, 106053. doi:https://doi.org/10.1016/j.triboint.2019.106053

Taylor, D. (2007). *The Theory of Critical Distances : A New Perspective in Fracture Mechanics* Oxford, UK: Elsevier

Zhou, Z. R., Cardou, A., Fiset, M., and Goudreau, S. (1994). Fretting fatigue in electrical transmission lines. *Wear*, *173*(1), 179-188. doi:http://dx.doi.org/10.1016/0043-1648(94)90271-2

Zhou, Z. R., Cardou, A., Goudreau, S., and Fiset, M. (1996). Fundamental investigations of electrical conductor fretting fatigue. *Tribology International, 29*(3), 221-232. doi:http://dx.doi.org/10.1016/0301-679X(95)00074-E

Zhou, Z. R., Goudreau, S., Fiset, M., and Cardou, A. (1995). Single wire fretting fatigue tests for electrical conductor bending fatigue evaluation. *Wear, 181-183*, 537-543. doi:https://doi.org/10.1016/0043-1648(95)90169-8

4.9 Summary and Outlook

This work has shown that the 3D Timoshenko beam theory can be used for fatigue life estimation in wire to clamp contacts observed in overhead conductor. However, a bias in the fatigue life estimation is observed in comparison to that made using solid 3D solid finite elements. Hence, a methodology is required to correct this bias so that this method is applicable to the prediction of fatigue life of overhead-conductor clamp assemblies. In chapter 5, we develop an ad-hoc method based on a maximum likelihood estimator that corrects the bias observed in the use of the 3D Timoshenko beam theory for fatigue life estimation. Using this approach, a framework is developed that considers all contacts in the conductor to predict multiple wire failure of conductor-clamp assemblies.

5 PROBABILISTIC FATIGUE FRAGILITY CURVES FOR OVERHEAD TRANSMISSON LINE CONDUCTOR-CLAMP ASSEMBLIES[21]

5.1 INTRODUCTION

Aging of infrastructure coupled with a projected increased reliance on electric energy has been an issue of concern for electrical utilities worldwide. Overhead conductors are the major components of a transmission line network and there has been an increased interest in estimating the residual life of the overhead conductors for improving asset management planning (Hathout, 2016; Pouliot et al., 2020). The dominant mechanisms associated with the degradation of overhead transmission line conductors is atmospheric corrosion and fretting fatigue. Amongst these two phenomena, fretting fatigue has received the most attention.

For conductor-clamp assemblies, field observation has shown that fretting fatigue is caused by aeolian vibrations that induce cyclic bending of the conductor and that fatigue damage is confined to the clamp/keeper where the conductor is supported (CIGRÉ 2010; Cloutier et al., 2006; Rawlins, 1979) (Figure 5.1). The cyclic motion of the conductor causes relative motions at wire-to-wire, wire-to-clamp and wire-to-keeper contacts (Cloutier et al., 2006). The relative motion at contacts leads to the phenomenon of fretting, which is a surface degradation process that leads to the formation of surface cracks (Hills and Nowell, 1994). In the presence of tension (Hills and Nowell, 1994) and bending moment (Lalonde at al., 2018) in the wires, the surfaces cracks propagate through the wire leading to fretting fatigue failure.

[21] Thomas, O.O., Chouinard, L., and Langlois, S. (2022) Probabilistic Fatigue Fragility Curves for Overhead Transmission Line Conductor-Clamp Assemblies, Accepted for publication in Frontiers in Built Environment: Computational Methods in Structural Engineering.

Simplified analytical models have been developed to relate the bending amplitude (Y_b) of vibration of the conductor at a specified distance from the last point of contact (LPC) with the clamp, to an idealized stress measure σ_a at the topmost fiber of the conductor at the LPC

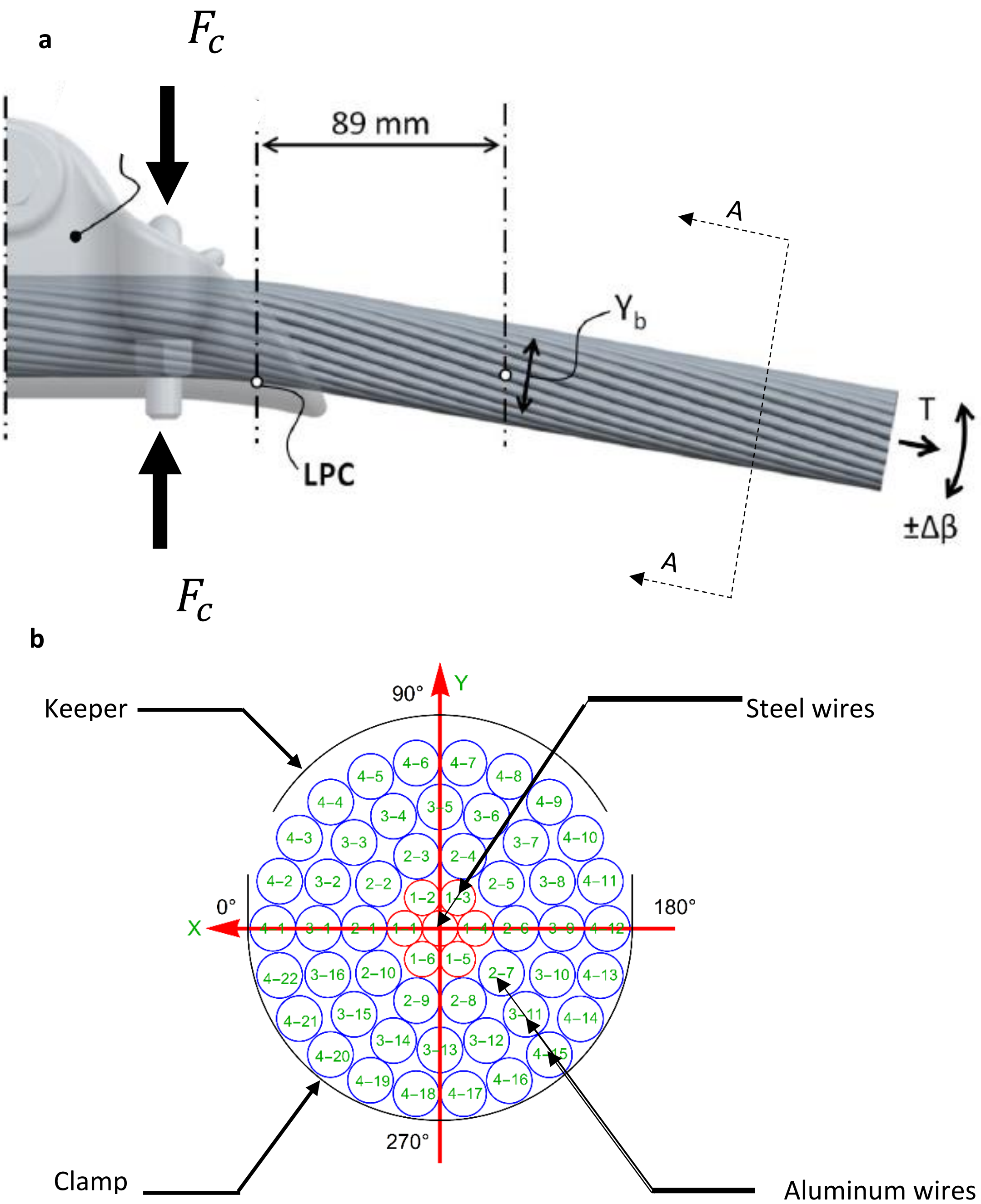

Figure 5: (a). Typical conductor-clamp assembly with applied conductor tension T, Clamping force F_c, change in alternating bending angle ($\Delta\beta$) and bending amplitude (Yb) (Adapted from Lalonde et al (2018)) (b). Cross section A-A of a typical conductor-clamp assembly showing the steel wires, aluminum wires, keeper and clamp configuration and the wire numbering system.

(Figure 5.1 (a) and Figure 5.2) (Poffenberger and Swart, 1965). The idealized bending stress is defined in Lalonde et al. (2017) as:

$$\sigma_a = \frac{d_c\, E_a \left(\frac{T}{4\, EI}\right)}{e^{-\sqrt{T/EI}\, z} - 1 + \sqrt{T/EI}\;z} Y_b \tag{5.1}$$

where d_c is the diameter of the conductor, E_a is the modulus of elasticity of aluminum, T is the tension applied to the conductor, Y_b is the bending amplitude at 89mm from the last point

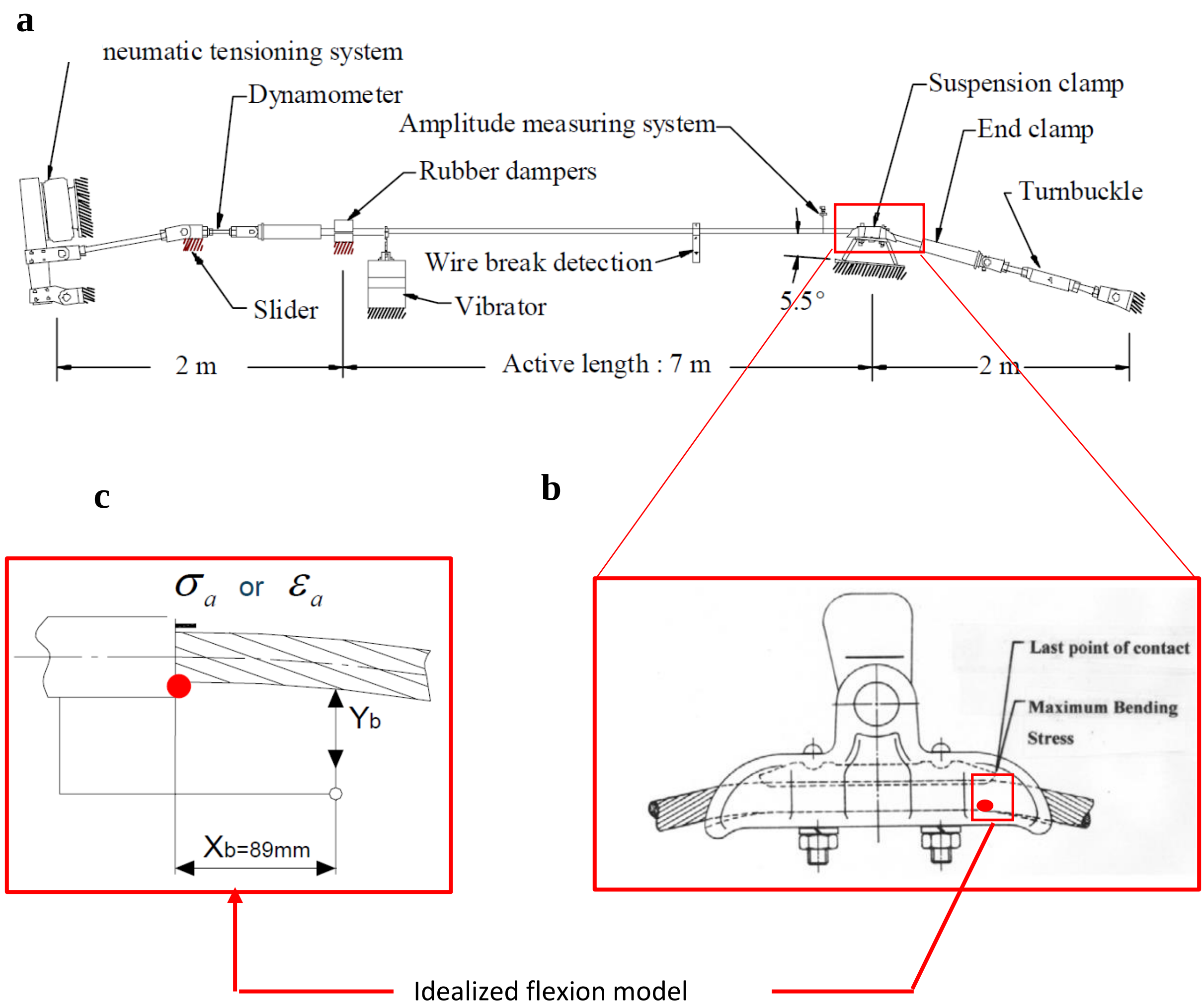

Figure 2: (a). Fatigue testing bench for conductor clamp systems (Adapted from (CIGRE, 2010). (b). Conductor-clamp assembly showing region of maximum bending stress . (c). Simplified representation of the conductor-clamp assembly and the idealized stress or strain induced by bending amplitude Y_b

of contact as shown in Figure 1a, and EI is the bending stiffness of the conductor defined in Cloutier et al. (2006) as:

$$EI = \sum_{i=1}^{number\ of\ wires} E_i\ I_i \tag{5.2}$$

where E_i and I_i are the Young modulus and moment of inertia of the i^{th} wire. The idealized stress obtained from Equation (5.1) is derived under the assumption that the conductor wires act independently in the region where the conductor enters the clamp, and is modeled as a Euler-Bernoulli beam with a fixed end (Figure 5.2 (c)) (Cloutier et al., 2006).

Based on the idealized stress model, experimental fatigue test benches, such as that shown in Figure 5.2 (a), are used to obtain experimental stress-number of cycles data $\{\sigma_a\ , Number\ of\ cycles\}$ data for given conductor-clamp assemblies (Cardou and Cloutier, 1990; CIGRE, 1979; Cloutier et al., 2006). Compilations of these experimental datasets have been used to derive empirical Stress-Number of cycles (SN) curves to predict first wire failures in conductors (Cloutier et al., 2006; Rawlins, 1979; CIGRE, 1979; Hardy and Leblond, 2001; and Thomas et al., 2020). However, SN models derived from experimental test benches that rely on the idealized bending model have limited applicability due to the reliance on the idealized stress, which neglects effects associated with the clamping force and clamp/keeper. Another limitation from compiled databases is the lack of uniform testing protocols between laboratories. Finally, the tests are very expensive and time consuming to perform, and the resulting SN curves are usually valid only for the first wire failure in the conductor.

In order to derive SN curves for multiple wire failures, Lalonde et al. (2017) modeled a conductor using 3D beam elements. However, this work did not model the clamp/keeper of conductor/clamp assembly but only the conductor was modelled, and it was assumed that the clamp/keeper can be replaced by fixed end boundary conditions. The stresses developed at the fixed end are then used to determine the number of cycles to failure from plain wire fatigue data from which first wire failure SN curves were developed. The limitation of this work is the simplification of the clamp/keeper as a fixed end boundary condition and its inability to account for the possibility of failure at multiple locations within a conductor-clamp assembly.

Models have also been proposed that focus on a single critical location for wire failure and do not account for the possibility of failure at multiple locations within the conductor-clamp assembly (Said et al., 2020; Omrani et al., 2021). In Omrani et al. (2021), a numerical model of the conductor-clamp assembly is used to identify the wire and contact with the largest contact stresses, which is assumed to be the location for the first wire failure. The state of stress obtained from the numerical model for different amplitudes of vibration is used to specify loads to be applied in single wire fretting fatigue experiments and to develop a (first-wire failure) SN curve for the conductor-clamp assembly. However, results from these single contact experiments overestimate the number of cycles at which first wire failure are observed experimentally for conductor-clamp assemblies with multiple wire-wire and wire-clamps contacts.

Considering the limitations of current models, the objective of this work is to propose a framework that combines the physically based numerical model of Lalonde et al. (2018), single wire plain fatigue data, and probabilistic models to estimate fragility and SN curves that can account for multiple contacts and multiple wire failures within conductor-clamp assemblies. To achieve this, the finite element model of Lalonde et al. (2018) for a Bersfort conductor is used to assess the fretting regimes and internal stresses at each contact. A fatigue criterion is proposed that considers the fretting regimes, internal stresses and the plain fatigue strength of the constituent wires of the conductor. The fatigue criterion is used to rank contacts for fatigue failure and to estimate the probability of failure from plain fatigue data for a given amplitude and number of cycles. Surfaces representing the probabilities of failure of each layer in the Bersfort conductor are generated for varying number of cycles and bending amplitude. The Poisson Binomial distribution is then used to generate fragility curves that considers different probabilities of failure at each contact point and wire-to-wire variability in fatigue resistance, which gives fatigue life predictions for one or multiple wire failures (up to 3 in this application). The fragility curves are compared to empirical cumulative distribution functions derived from experimental data for the same conductor-clamp configuration (Levesque, 2005). The probability distribution for the number of failed wires as a function of the number of cycles is also obtained. SN curves generated from the new approach for 1st wire failures are also presented for the specimen conductor-clamp configuration and compared against the current available SN curves.

5.2 The Finite Element Modeling Methodology

A finite element model is used to reproduce the conditions of the experimental fatigue test bench used by Levesque (2005) (Figure 5.2). The model follows the procedure of Lalonde et al. (2018), which uses quadratic 3D Timoshenko beam elements (10mm in length) for the wires, and quadratic rigid shell elements (2.5mm in length and width) for the clamp and keeper. The wire-wire, and wire-clamp/keeper contacts are modeled using line-to-line and line-to-surface contact elements in the ANSYS® system. Lalonde et al.(2018) has demonstrated that the beam model can accurately reproduce the strains measured experimentally in the wires of the Bersfort conductor-clamp assembly.

In this work, the conductor-clamp assembly modeled is a Bersfort conductor-clamp as shown in Figure 5.3. A cross-section of the conductor is shown in Figure 5.1 (b) and the length of the conductor is 1600 mm. Additional geometric details on the conductor-clamp assembly can be

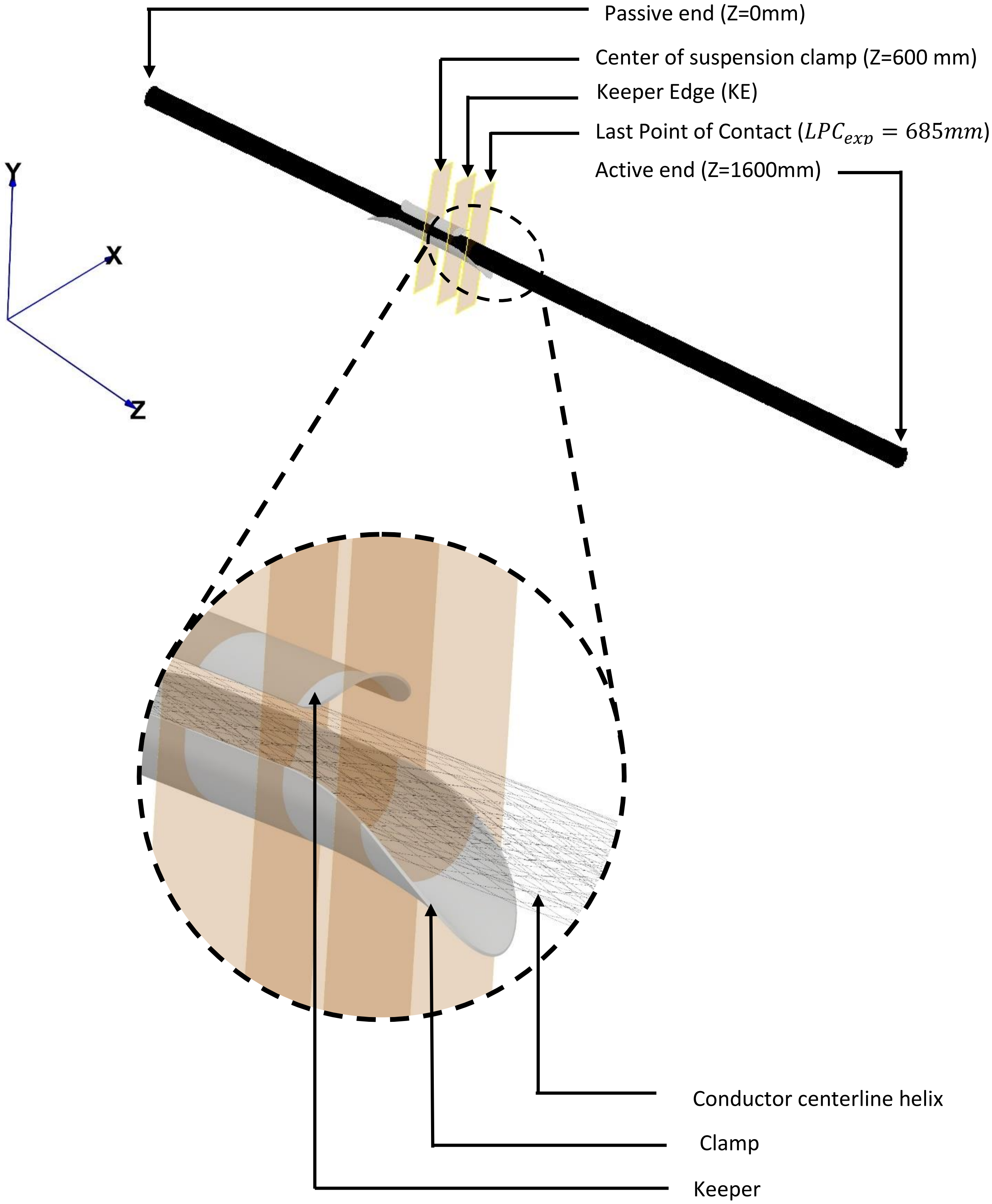

Figure 3: Geometric representation of the Bersfort conductor-clamp system

found in Lalonde et al. (2018) and Goudreau et al. (2010). The finite element mesh of the conductor-clamp assembly and contact elements are shown in Figure 5.4.

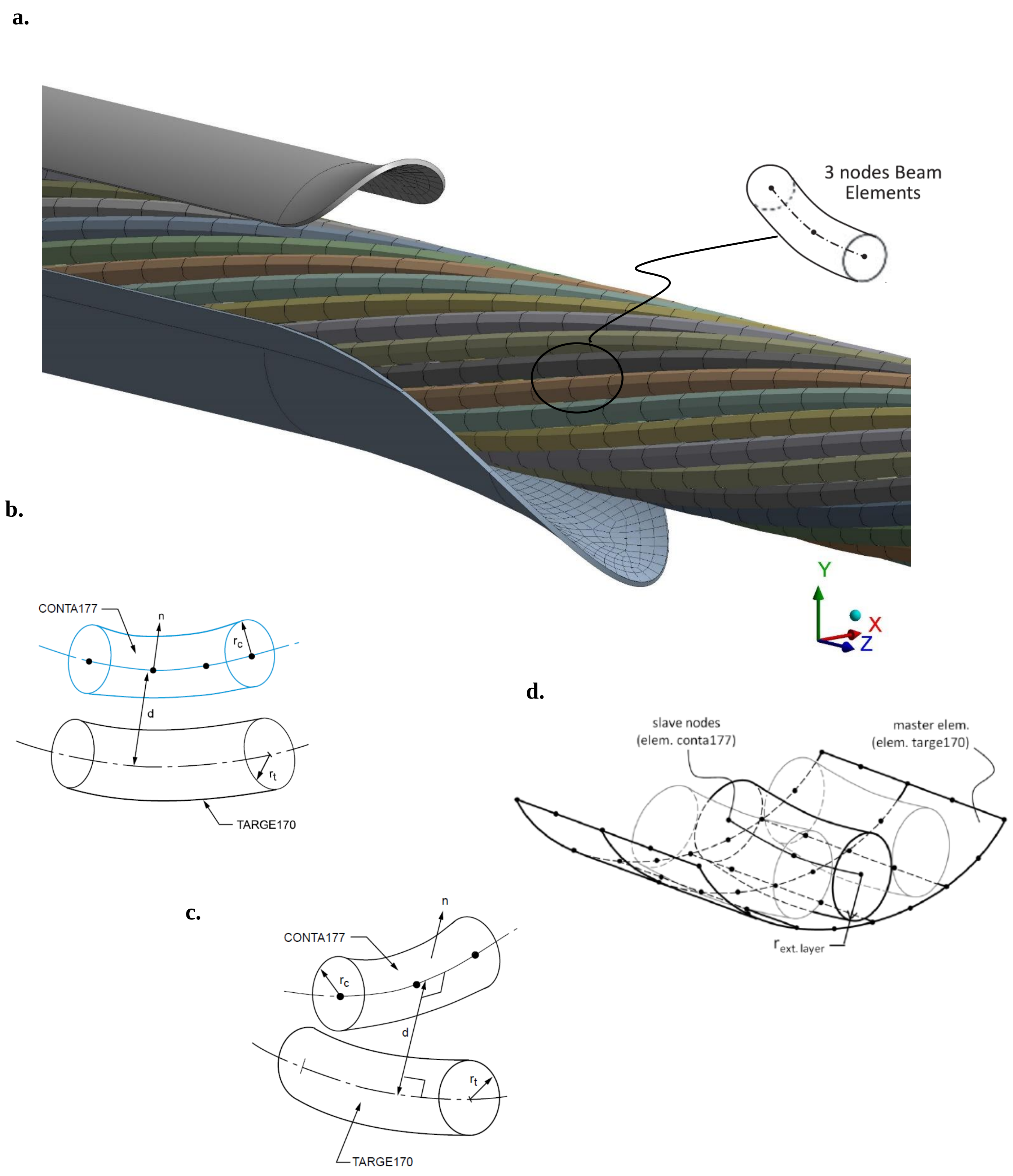

Figure 4: (a) Finite element mesh of the Bersfort conductor-clamp assembly showing the beam and rigid shell elements. (b). Line-to-line contact between the conductor wires of the same layers modeled with slave element CONTA177 and master element TARGE170. (c). Line-to-line contact between the conductor wires of different layer modeled with slave element CONTA177 and master element TARGE170. (d). Line-to-surface contact between the Layer 4 wires and the keeper/clamp

The material properties of the conductor wires are listed in Table 1. The core is a steel wire in the center of the conductor (Figure 5.1 (b)). The layer numbering and wire numbering is also shown in Figure 1b. The coefficient of friction is 0.3 for steel-to-steel contacts and 0.9 for aluminum-to-aluminum and aluminum-to-steel contacts (Lalonde et al., 2018; Omrani et al., 2021).

The beams are modeled as linear elastic elements with large displacement and rotation capabilities. The linear elastic assumption has been shown to provide fretting fatigue life predictions for aluminum wires that are in agreement with experimental fatigue life observations (Rocha et al.2019; Said et al., 2020).

Table 5.1: Characteristics of the Bersfort Conductor

Layer	n_i	d_i (mm)	E_i (GPa)	v
Core	1	3.32	207	0.3
1	6	3.32	207	0.3
2	10	4.27	69	0.33
3	16	4.27	69	0.33
4	22	4.27	69	0.33

n_i: *number of wires in layer i ;*
d_i: *diameter of wires in layer i ;*
E_i: *elastic modulus of wires in layer i;;*
v: *Poisson ratio ;*

5.3 Load Application and Sequencing Scheme

The loading sequence of the Bersfort conductor finite element model follows the experimental procedure established in Levesque (2005) who tested Bersfort conductors with the fatigue test bench shown in Figure 5.2, and is similar to the sequence used by Lalonde et al. (2018) in their numerical model. For the load application to the model, the nodes of the beams at the passive end of the conductor are coupled to a master node located at the center of the conductor using

Multiple Point Constraints (MPC) (Figure 5.5). The nodes of beams at the active end (Figure 5.5) are similarly coupled to a master node at the center of the conductor. For the clamp/keeper, all the nodes are coupled using rigid MPC. For the clamp, all nodal degrees of freedom (DOF) are fixed for displacements and rotations. For the keeper all rotation and displacement are fixed

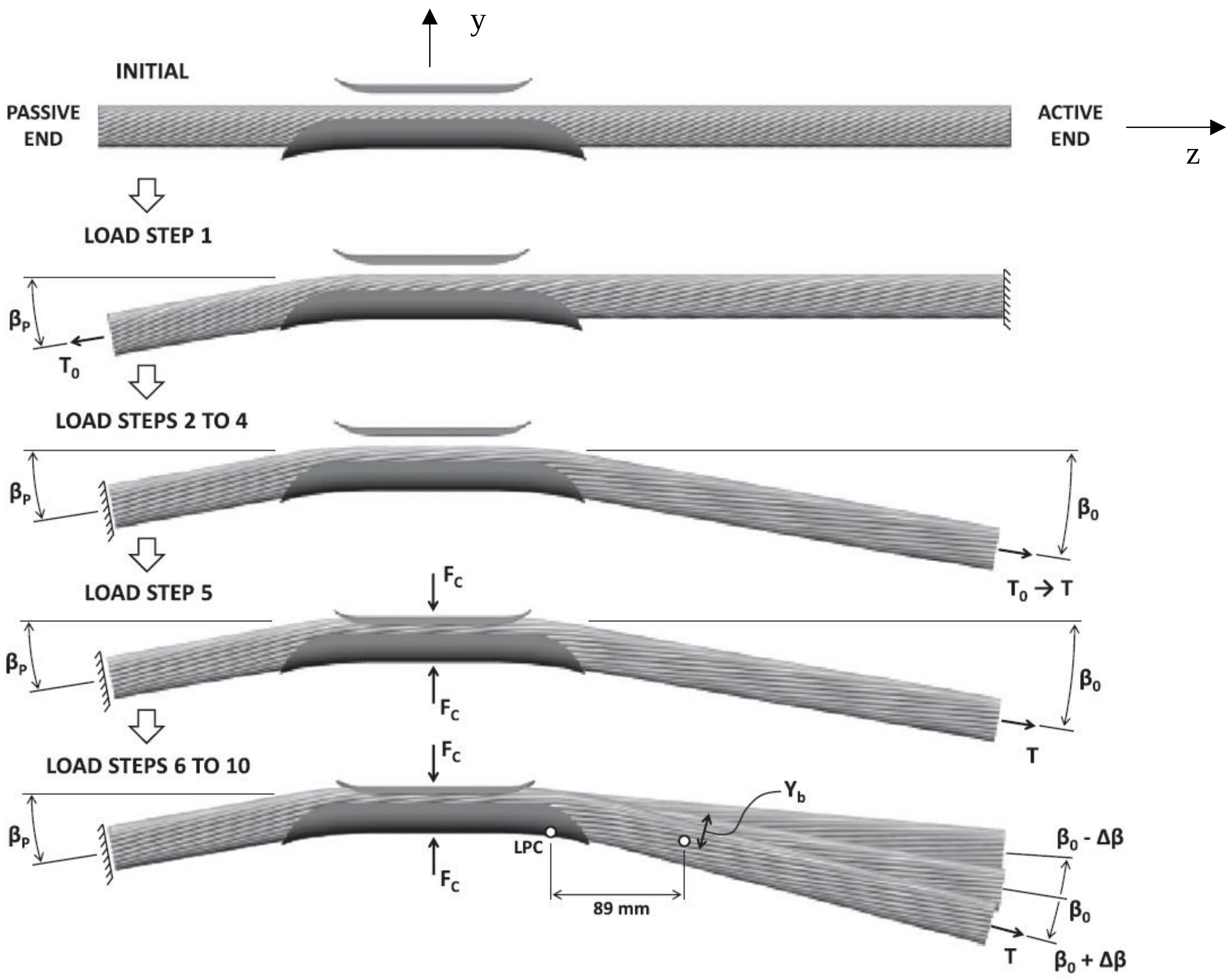

Figure 5: Loading sequence of Bersfort conductor-clamp assembly (Adapted from Lalonde et al (2018))

except for the displacement in the y-direction.

The first step of the loading protocol is to incrementally apply an initial tension T_0 at the passive end of the conductor at an angle β_p relative to the horizontal while the active end of the conductor is restrained for all 6 DOFs (Figure 5.5). At the end of step 1, the passive end is fixed at its current position and the z-direction and y-direction displacement DOF at the active end is released, this is followed by the application of the conductor tension T_0 at the master node of the active end at an angle β_0 (step 2 in Figure 5.5). During the loading steps 3 and 4, the conductor tension at the active end is increased from T_0 to T. The effect of the clamping force is simulated by introducing a force F_c in the y-direction on the keeper master node in loading step 5. Once the clamping force is completely applied, it is replaced by the displacement induced by F_c. The loading steps 6 to 10 consist in cycling the angle of the active end of the conductor with tension T by $\pm\Delta\beta$ to induce a displacement Y_b. The value of $\pm\Delta\beta$ is specified to match the target bending amplitude Y_b . The loads and angles corresponding to the experimental setup are provided in Table 5.2. Additional details can be found in Lalonde et al. (2018) and Levesque (2005).

Table 5.2: Applied Boundary conditions in Finite Element Model

$\boldsymbol{T_0}$ (kN)	T (kN)	$\boldsymbol{F_c}$ (kN)	$\boldsymbol{\beta_p}$ (°)	$\boldsymbol{\beta_0}$ (°)
1.85	45	74.8	4.3	6.2

5.4 CONDUCTOR FATIGUE MODEL

5.4.1 Model Formulation

Fretting fatigue analysis for a single contact can be performed by specifying displacement and force boundary conditions on the two bodies in contact, a plain fatigue model, and a procedure to define an equivalent stress state that is related to the fretting fatigue potential. This approach that has been followed by (Redford et al., 2019; Rocha et al., 2019) in the assessment of fretting fatigue failure for two wires in contact at a single point. However, for a multiple contacts system such as a conductor, it has been shown that contacts are subjected to at least three different fretting regimes – sticking regime, mixed fretting regime and gross slip regime (Zhou and Vincent, 1995) and that the analysis must first determine if a contact is in a fretting regime that leads to crack initiation and propagation. This state introduces an additional criterion for the analysis of conductor fatigue in comparison to single contact fretting fatigue.

In the proposed methodology, a criterion is proposed that considers both the tangential force *Q(t)* and sliding distance $u(t)$. This criterion is based on the energy dissipated E at the contact and is given by:

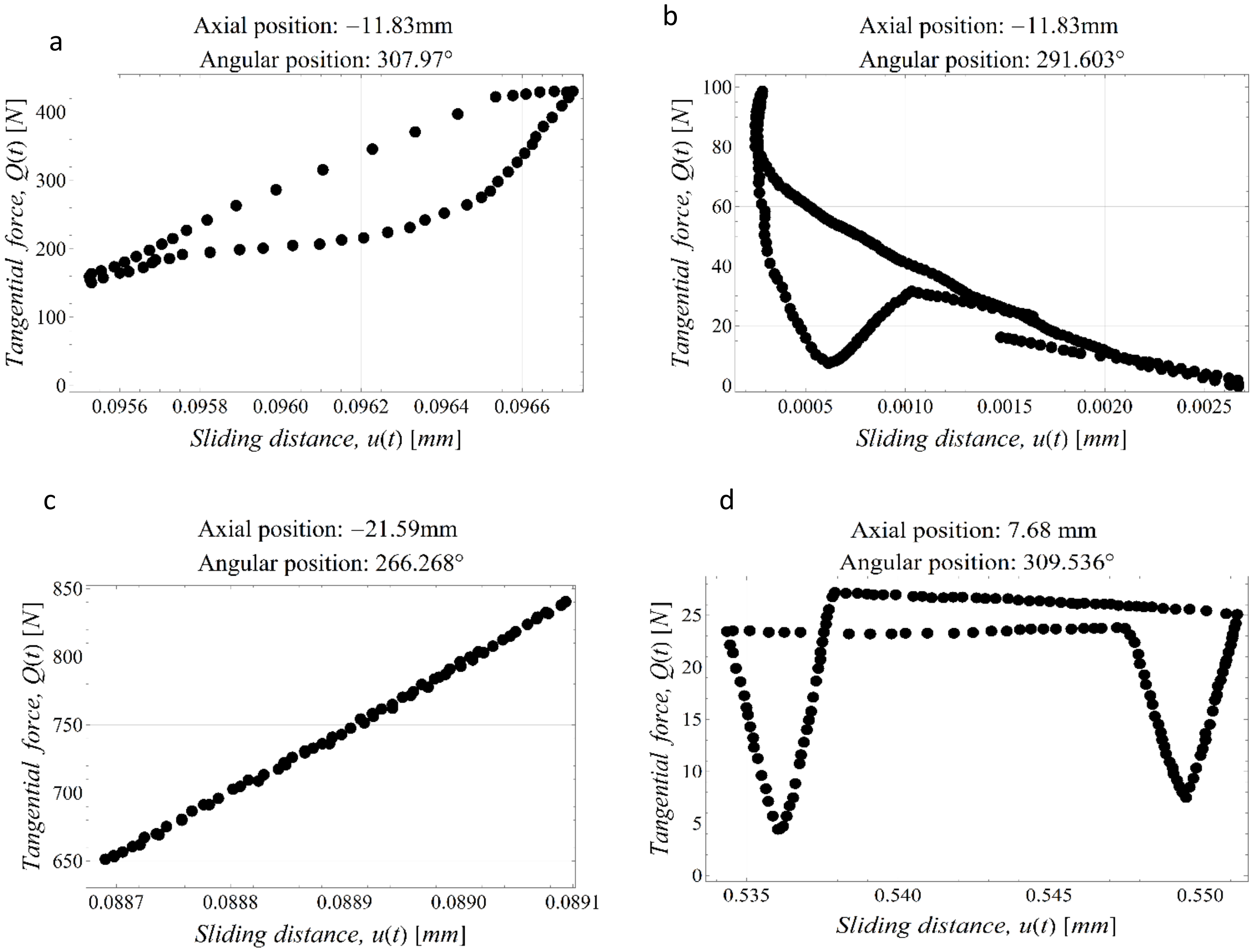

Figure 6: Examples of fretting regimes indicated by the plot of Q(t) against u(t) when the conductor goes through $\beta_0 \pm\Delta\beta$ for bending amplitude of 0.75mm. (a). Miixed fretting regime on a Layer 4 to 3 Contact. (b). Mixed fretting regime on a Layer 4 to Clamp Contact. (c). Sticking contact on a layer 4 to 3 contact . (d). Gross slip contact on a layer 4 to contact

$$E = \oint Q(t)u(t)\,dt \tag{5.3}$$

Where t is a time tracking parameter. A plot of $Q(t)$ against *u(t)* illustrates the various fretting regimes (Figure 5.6). In these Figures the axial position of contacts is:

$$\text{Axial position} = \text{z coordinate} - LPC_{exp} \tag{5.4}$$

where $LPC_{exp} = 685mm$ and is the Last point of contact determined by Levesque (2005). A negative value of the axial position indicates that the contact is within the clamp while a positive value indicates that the contact is outside the clamp.

The three fretting regimes: sticking, mixed fretting, and gross slip, as defined by Zhou and Vincent (1995) are shown in Figure 6. The fretting regimes are defined by the energy dissipation curves for contacts between wire-to-wire and wire-to-clamp in conductor-clamp assemblies. Characteristic behavior of the energy dissipation curves of these fretting regimes are given in Degat et al. (1997) and summarized as follows: The mixed fretting regime has a closed energy dissipation curve of elliptical shape, small or large tangential force, and short sliding distance (Figure 5.6 (a)). The sticking regime is characterized by a closed loop energy dissipation curve in the shape of a line and large tangential force (Figure 5.6 (c)). The gross slip is characterized by an open energy dissipation curve (often rectangular), small tangential force and large sliding distance (Figure 5.6 (d)).

The fretting regime is combined with the stress-based Smith-Watson-Topper (SWT) criteria to formulate the conductor fatigue criteria as:

$$G(E)\ (SWT_L \mid Y_b = y) \geq (SWT_R \mid N = N_i) \tag{5.5}$$

where $SWT_L \mid y_b$ represents the Smith-Watson-Topper criteria of the wire contact at a given bending amplitude, the SWT is defined in Rocha et al.(2019) as:

$$SWT = \sqrt{\frac{\Delta\sigma}{2}\langle\sigma_{max}\rangle} \tag{5.6}$$

where $\frac{\Delta\sigma}{2}$ is the stress amplitude and σ_{max} is the maximum stress in a loading cycle. The *SWT* is a tension-based fatigue criterion. From the 3D beam model, the stress range $\Delta\sigma$ and maximum stress σ_{max} are obtained as:

$$\Delta\sigma = |\sigma_1(\beta_0 + \Delta\beta) - \sigma_1(\beta_0 - \Delta\beta)| \tag{5.7}$$

$$\sigma_{max} = \max(\sigma_1(\beta_0 + \Delta\beta), \sigma_1(\beta_0 - \Delta\beta)) \tag{5.8}$$

where σ_1 is the maximum principal stress at the beam nodes.

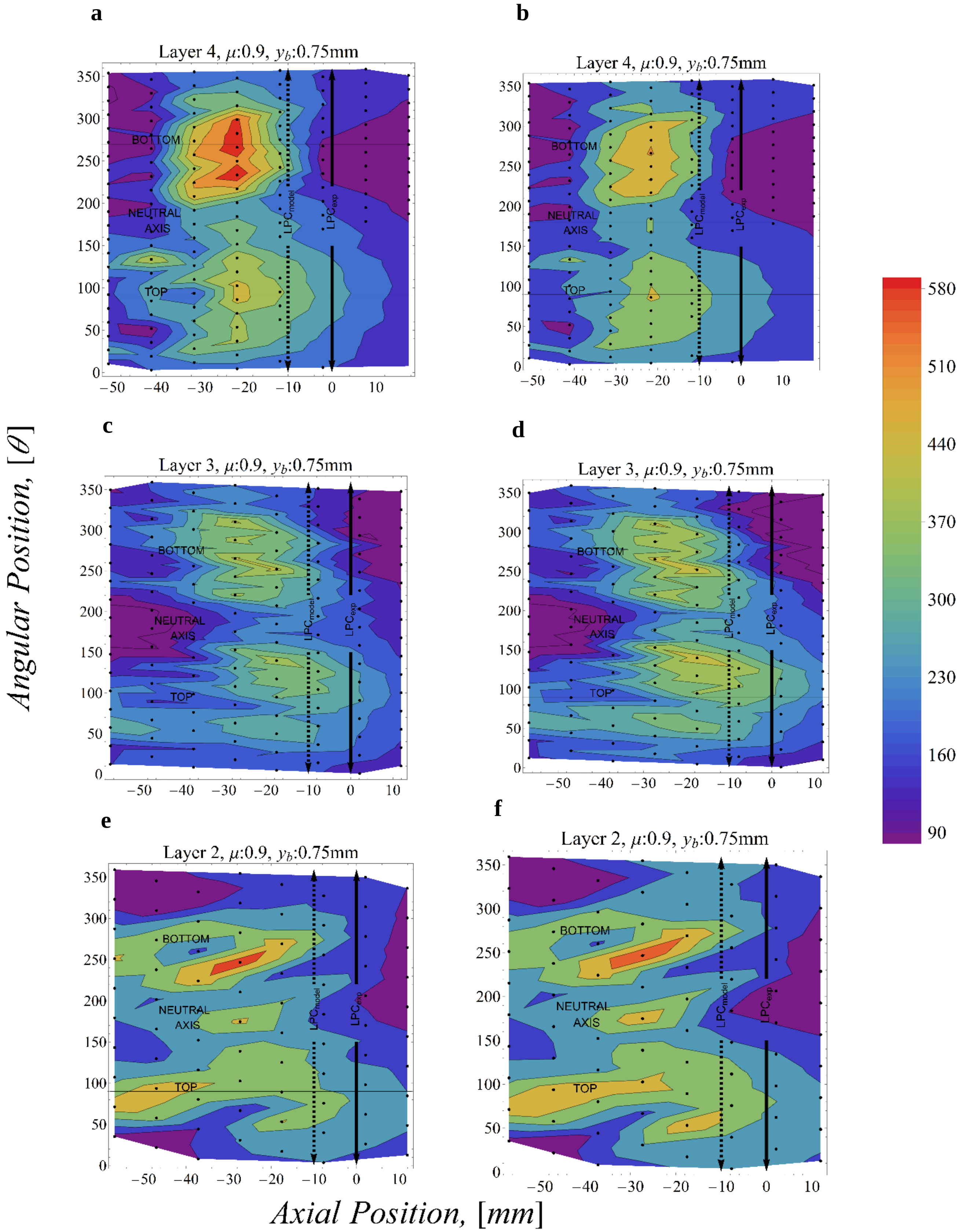

Figure 7: Distribution of maximum principal stresses (in MPa) for a bending amplitude of 0.75mm. (a,c,e) $\beta_0 + \Delta\beta$ and (b,d,f) $\beta_0 - \Delta\beta$

The values of $\sigma_1(\beta_0 + \Delta\beta)\ and\ \sigma_1(\beta_0 + \Delta\beta)$ obtained from the FE analysis are shown in Figure 5.7 for a bending amplitude of 0.75mm for different wires (layers) in the Bersfort conductor-clamp assembly.

In the following section, the fatigue resistance of a wire to plain fatigue for a given number of cycles N_i is defined through the Smith-Watson-Topper criteria $(SWT_R \mid N = N_i)$ and is estimated from rotating bending data provided in Kaufman (2008) for aluminium wires. A Basquin type stress–life relationship is used to describe $SWT_R \mid N = N_i$ and it is assumed that $f_{SWT_R}(SWT_R \mid N = N_i)$ follows a lognormal distribution with mean $\mu(SWT)$ and standard deviation $\sigma(SWT)$ which are defined as (Babuška et al. 2016; Pascual and Meeker, 1997):

$$\mu(SWT_R) = A_1 + A_2\, log(SWT_R\ -\ A_3) \tag{5.9}$$

$$\sigma(SWT_R) = exp(B_1\ +\ B_2\ log(SWT_R\ )) \tag{5.10}$$

where $f_{SWT_R}(.)$ is the probability distribution function. The parameter vector of the model $\boldsymbol{\theta} = (A_1, A_2, A_3, B_1\ , B_2\ )$ is estimated by the method of maximizing likelihood $(A_1 = 48.04, A_2 = -7.37, A_3 = 2.23, B_1 = 5.46\ , B_2 = -1.29\ )$ (Figure 5.8). The function G(E) defines the type of fretting regime as:

$$G(E) = \begin{cases} 0 & sticking\ regime \\ 1 & mixed\ fretting\ regime \\ 0 & gross\ slip\ regime \\ 0 & no\ contact \end{cases} \tag{5.11}$$

This indicator function follows from experimental observations that the mixed fretting regime is the most critical for fretting fatigue in conductors (Zhou and Vincent, 1995). This function excludes other contacts that are not in this regime from the analysis. The value of E for which a contact transitions from one regime to another is difficult to define precisely and relies on heuristics, such as the shape of hysteresis curve to assign values to $G(E)$ (Figure 5.6). Ideally, all types fretting regimes should be considered. Both the sticking and gross slip regimes can lead to crack initiation as shown in Zhou and Vincent (1995); however, the cracks do not propagate in the gross slip regime and do not lead to fatigue failure. In the case of the sticking regime, cracks can propagate to failure but typically this occurs for a number of cycles much larger than for the mixed fretting regime and can be ignored for a failure criteria based on a small number (< 4) of wire failures.

In the following, only contacts between wires of different layers or between wires and the suspension clamp are considered for fretting fatigue. Contacts between wires on the same layer have much lower normal and tangential forces and are much less likely to be locations for the initiation and propagation of fretting fatigue failure. Considering the two contacts at the top and bottom of a wire segment discretized with a beam element m, the probability of failure of the wire segment for N_i cycles at an amplitude y_b is:

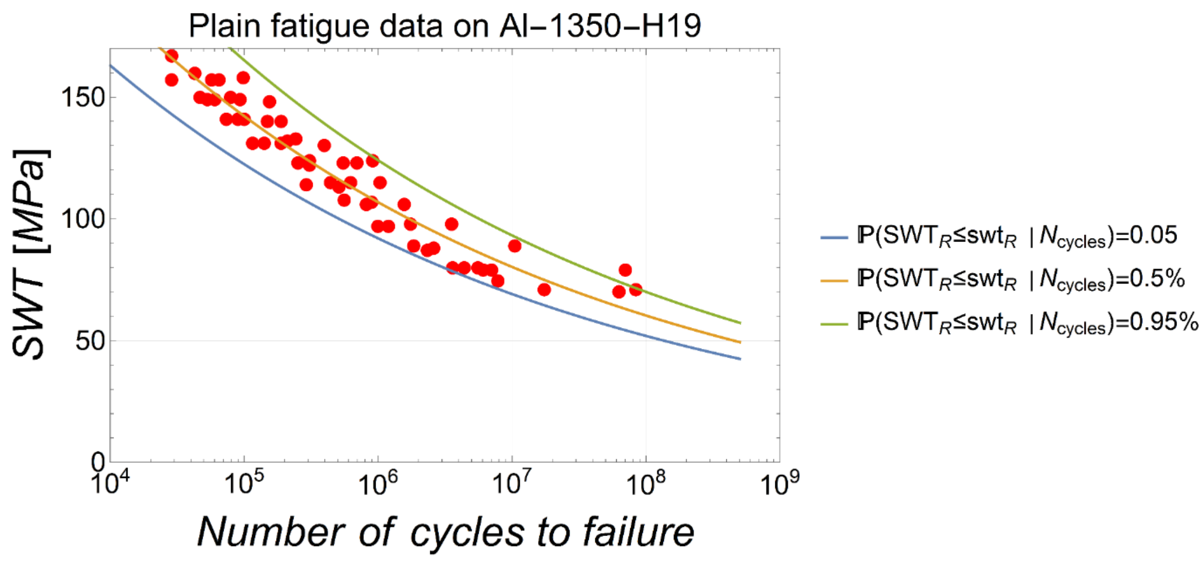

Figure 8: Fatigue Data obtained from (Kaufman, 2008) and the fitted fatigue model.

$$\mathbb{P}_m(N = N_i) = \mathbb{P}\left(G(E_m)\left(SWT_{L_m} \mid y_b\right) \geq (SWT_R \mid N = N_i)\right) \tag{5.12}$$

The probability of failure of k wires within the conductor-clamp assembly can then be expressed as:

$$\mathbb{P}(k|N = N_i) = \sum_{A \in \mathcal{G}_k} \prod_{t \in A} \mathbb{P}_m(N = N_i) \prod_{j \in A^c}\left(1 - \mathbb{P}_m(N = N_i)\right) \tag{5.13}$$

where $\mathcal{G}_k$ is the set of size $\binom{n}{k}$ of all combinations of *k* failed wires that can be formed from the set of *n* contact points within the conductor/clamp assembly, *A* is the set of contact points where fretting fatigue failure occurs, *t* are members of A, A^{C} is the set of contacts points that do not fail in fretting fatigue, and *j* are members of A^{C} . This equation is the Poisson binomial distribution described in Wang (1993) and provides the probability of obtaining exactly *k* wire failures at a given number of cycles. The failure of a conductor can then be defined as the first wire failure or by specifying the number of multiple wire failures. Assuming that failure of a conductor is defined when *k* (or more) wires have failed, the probability of failure of the conductor is evaluated as,

$$\mathbb{P}(K \geq k|N = N_i) = 1 - \mathbb{P}(K < k|N = N_i) \tag{5.14}$$

The Equation (5.14) considers both the top and bottom contacts acting on a wire segment. For 3D beam finite elements, the maximum principal stress σ_1 occurs at either the top or bottom contact since bending stresses predominate as shown by Lalonde et. al (2018). In consequence, only the contact with the maximal principal stress is considered in Equations (5.13) and (5.14).

Since the finite element model is formulated for a specific position of the cable in contact with the clamp, contact points are spaced at 10mm intervals in the axial direction and the angular position at 16° intervals as shown by the black dots in Figure 5.7. The results from experimental tests can correspond to locations of contacts that vary within this range. Since analyses cannot be performed to reproduce the exact conductor-clamp configuration of each experiment, a procedure based on interpolating the $SWT_L \mid y_b$ is used instead. The interpolation procedure averages stresses locally as a function of axial position d and angular position θ through a Gaussian kernel function with parameters σ_d, σ_θ as:

$$\overbrace{SWT_L \mid y_b(d,\theta)}^{smoothened} = \sum_{j=1}^{n_{nodes}} k(\sigma_d, \sigma_\theta) \cdot SWT_L \mid y_b(d_j, \theta_j) \tag{5.15}$$

$$k(\sigma_d, \sigma_\theta) = \frac{1}{\sigma_d \sqrt{2\,\pi}} e^{-\left(\frac{d-d_j}{\sigma_d}\right)^2} \cdot \frac{1}{\sigma_\theta \sqrt{2\,\pi}} e^{-\left(\frac{\theta-\theta_j}{\sigma_\theta}\right)^2} \tag{5.16}$$

where n_{nodes} is the number of nodes from which the maximum principal stresses are extracted from the finite element model; d_j and θ_j are the axial and angular positions of the node j.

The estimates of σ_d and σ_θ are obtained by maximizing the likelihood of the observed failures given the number of cycles and location of failure:

$$l(\sigma_d, \sigma_\theta) = \prod_{j=1}^{n_{failed\,wires}} f_{SWT_R|Y_b,\sigma_d,\sigma_\theta,d_j,\theta_j}\left(SWT_L\left(Y_b, \sigma_d, \sigma_\theta, d_j, \theta_j\right)\middle|N_j\right) \tag{5.17}$$

where $l(\sigma_d, \sigma_\theta)$ is the likelihood function, $SWT\left(Y_b, \sigma_d, \sigma_\theta, d_j, \theta_j\right)$ is obtained from Eq. 6, $n_{failed\,wires}$ is the set of observed first wire failures given Y_b (0.75mm and 0.6mm), (d_j, θ_j) is the position of the failure wire, N_j the number of cycles at failure, and f_{SWT_R} is the probability distribution of SWT from plain fatigue wire data given failure occurs at N cycles (Equations 5.9 and 5.10).

5.4.2 Procedure for the Derivation of Fragility Curves

This section summarizes the steps in the procedure for deriving fragility curves (Figure 5.9). First, the finite element model of the conductor-clamp assembly is formulated in ANSYS finite element program. In step 2, the maximum principal stress at the top or bottom contact of each wire element is obtained. In step 3, the tangential force and sliding distance at the contact with the maximum principal stress are obtained from the FE model to define the fretting regime (Figure 5.6). This is followed by step 4, where $SWT_L \mid y_b$ is evaluated using Eq. (6). Step 5 involves averaging the $SWT_L \mid y_b$values using Eq. (15) to obtain $\overbrace{SWT_L \mid y_b(d,\theta)}^{smoothened}$. The

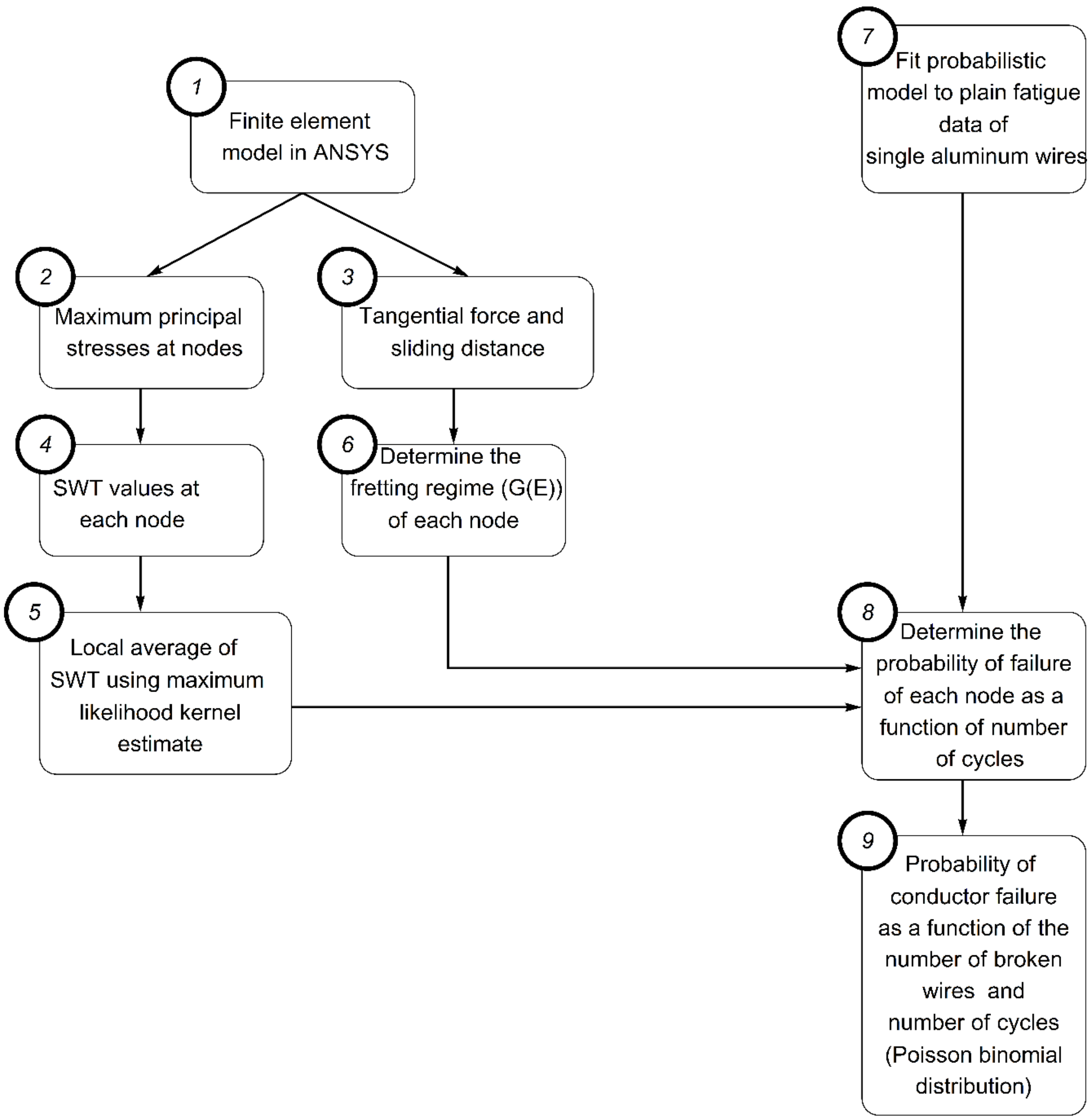

Figure 9: Flow chart for developing conductor-clamp assembly fragility curve

indicator function G(E) (Eq. (11)) is assigned to each node as a function of the corresponding fretting regime in step 6. Step 7 consists in fitting the fatigue model (Eq. 9 and 10) to the plain fatigue data (Figure 5.8) to obtain $f_{SWT_R}(SWT_R \mid N = N_i)$. In step 8, the indicator function

G(E) and the $\overbrace{SWT_L \mid y_b(d,\theta)}^{smoothened}$ used to obtain the probability of failure for each beam element (Eq. 12). Finally, in step 9, the probability of *k* wire failures in the conductor is computed using the Poisson binomial distribution given by Equations (5.13) and (5.14).

The procedure from step 8 to step 9 is repeated to evaluate the probability of failure for the desired range of number of cycles (10^4 to 10^7).

5.4.3 Model Validation and Discussion

Validation of the framework is done by first comparing the predicted $\overbrace{SWT_L \mid y_b(d,\theta)}^{smoothened}$ and indicator function G(E) from the FE model to observed failure locations reported in Levesque (2005). Next, the empirical cumulative distribution function (ECDF) of the fatigue life for a given number of wire failure is compared against the predicted cumulative distribution function (CDF) generated by the Poisson binomial distribution given in Equation (5.14).

For bending amplitudes of 0.75mm, only 13 of the experiments report the location, order of wire failure and number of cycles to failure (39 events for 1^{st} to 3^{rd} wire failures), while 15 experiments report the same for an amplitude 0.60mm. Two additional experiments providing the first wire failure for bending amplitudes of 0.4mm and 0.5mm are also available.

In application of the framework, the number of potential failure points are limited to the region within the clamp. Thus, checking for failure is restricted to the region between the last point of contact (LPC) and the keeper edge (KE). It has been shown that this is the critical region for failure in conductor-clamp assemblies by Levesque (2005) and Zhou et al. (1994).

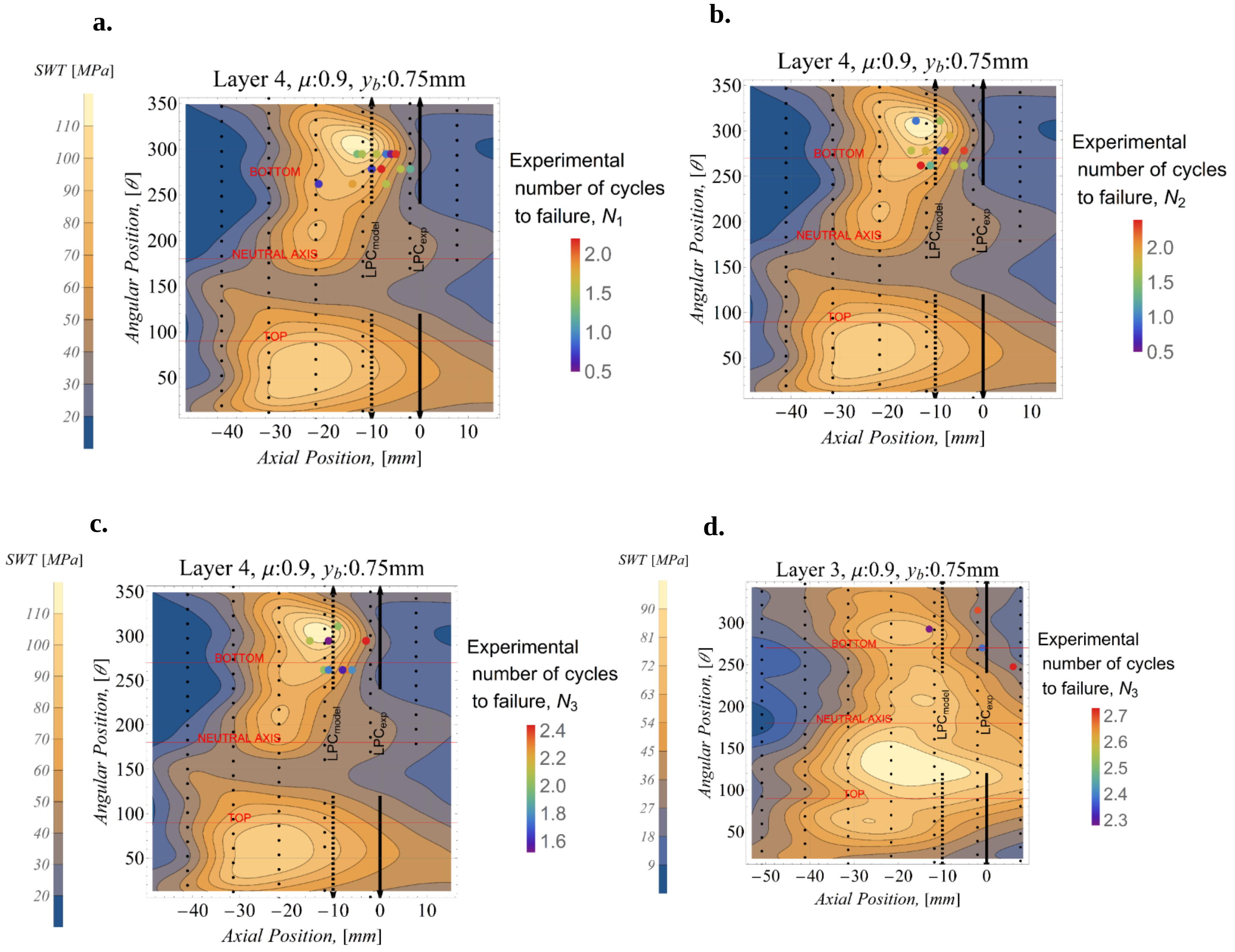

Figure 10: Location and number of cycles of Experimental Observation of Levesque[19] : (a) first wire failure (b) second wire failure (c) third wire failure on layer 4 (d) third wire failure on layer 3; All for bending amplitude of 0.75mm. Indicated number of cycles are in Millions (10^6).

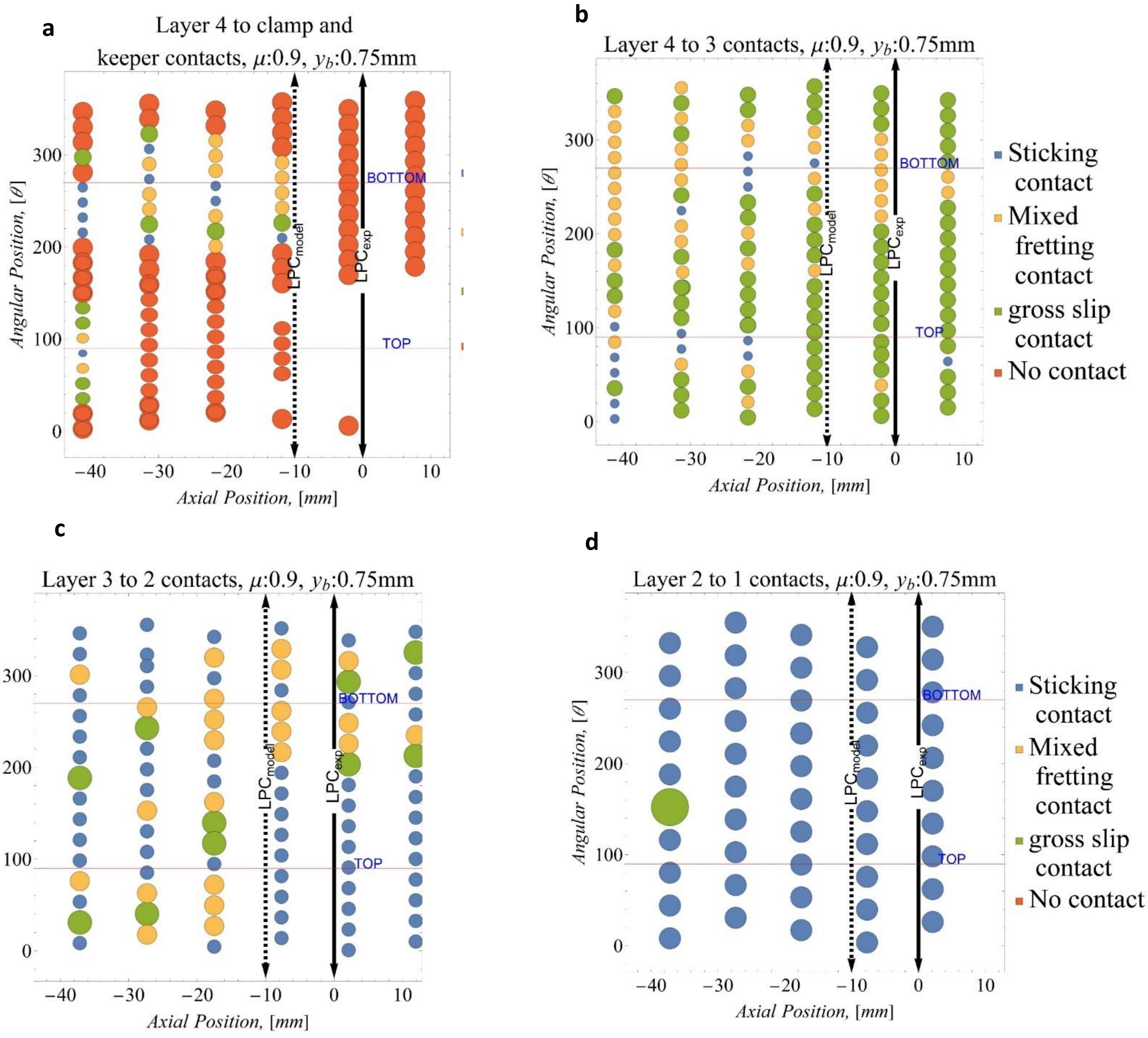

Figure 11: Indicator function G(E) for : (a). Layer 4 to clamp contacts (b). Layer 4 to 3 contacts. (c). Layer 3 to layer 2 contacts. (d). Layer 2 to layer 1 contacts.

A comparison of the spatial variation of $\overbrace{SWT_L \mid y_b(d,\theta)}^{smoothened}$ for a bending amplitude of 0.75mm (Figure 5.10(a-c)) against the locations of observed wire failures in the experiments by Levesque (2005) show good agreemnt and demosntrates that the FE model can correctly identify regions susceptible to wire fatigue failure in the conductor-clamp assembly. For the 3rd wire failures in layer 3 (Figure 5.10 (d)), high values of SWT are not as well correlated with wire failure locations; however, this can be explained by the observation the mixed fretting regime occurs at contacts in the lower part of the conductor where wire failures are most likely to occur (Figure 5.11 (b) and (c)). This observation highlights the importance of considering

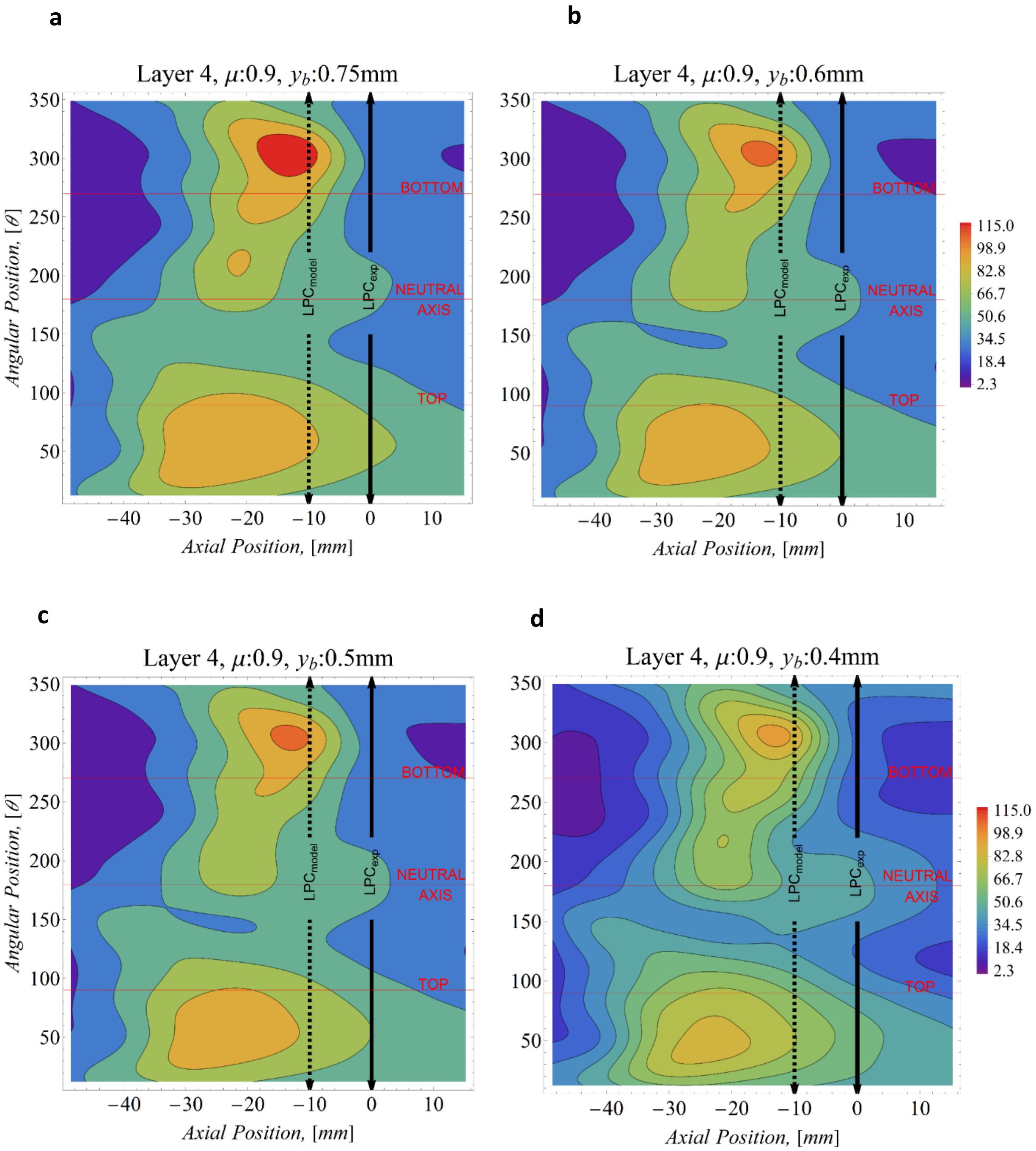

Figure 12: Maximum SWT distribution on the wires of layer 4 of the Bersfort conductor. Units of the SWT are in MPa.

both the $\overbrace{SWT_L \mid y_b(d,\theta)}^{smoothened}$ fatigue parameter and the fretting regime to predict fatigue failure in conductor-clamp assemblies and distinguishes the proposed approach from the current practice that only considers the fatigue parameter.

Furthermore, the LPC from the experiment of Levesque (2005) and that from the numerical model shown as black double head arrow and broken double head arrow in Figures 5.10 and 5.11 show some difference. This difference in the location of the LPC between the model and experimental setup has been attributed by Lalonde et al. (2018) to plasticity effects that are not included in the numerical model. Indeed, it has been noted that the Timoshenko beam theory exhibits a stiffer response when in contact with a surface as compared with a full elasticity solution (Essenburg, 1975; Gasmi et al., 2012; Naghdi and Rubin, 1989). Nonetheless, the analysis provides estimates of the spatial variation of stresses that are sufficiently precise for the purpose of the fatigue analysis of multi-body systems such as conductors (Lalonde et al. 2018; Omrani et al., 2021).

Figure 5.12 shows the SWT distribution for other bending amplitudes. The $\overbrace{SWT_L \mid y_b(d,\theta)}^{smoothened}$ of Figure 5.12 and the wire fatigue resistance $f_{SWT_R}(SWT_R \mid N = N_i)$ are substituted in Equation (12) to obtain the probability of failure for each contact point. The results are shown as probability contour plots for the wires of layer 4 at bending amplitudes of 0.75mm, 0.6mm, 0.5mm and 0.4mm respectively in Figures 5.13 and 5.14. For the case where the bending amplitude is 0.75mm and 0.6mm, the probabilities of failures are governed by the wires at the bottom in layer 4 for number of cycles $10^5 - 10^6$. However, as the number of cycles increases to 10^7 the probabilities of failures at the top of the conductor increases. In the case of lower bending amplitudes of 0.5mm and 0.4mm, the increment in size of the region of failure is less with the

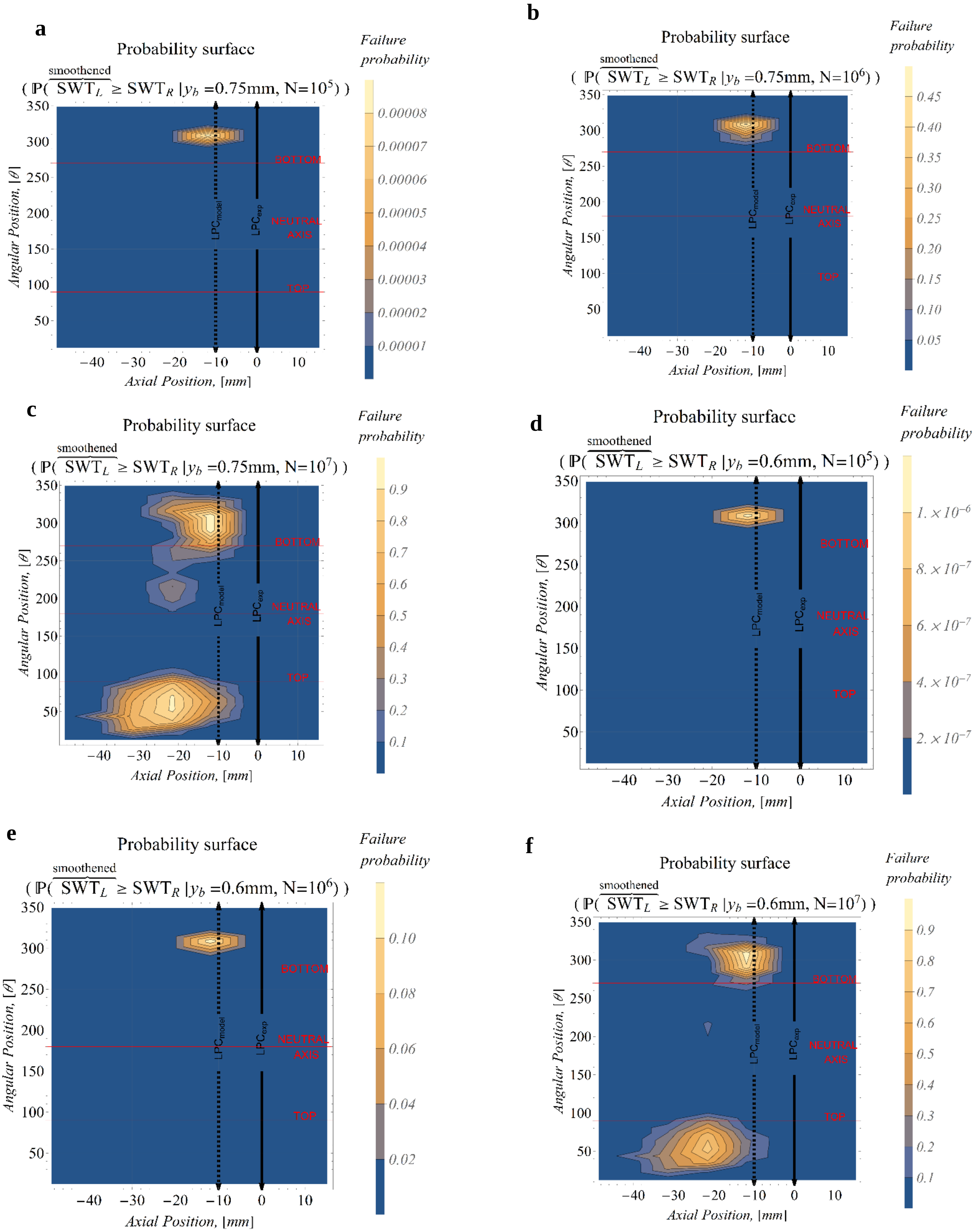

Figure 13: Probability of failure for the wires in layer 4 of the Bersfort conductor at a bending amplitude of 0.75mm (a to c) and 0.6mm (d to f)

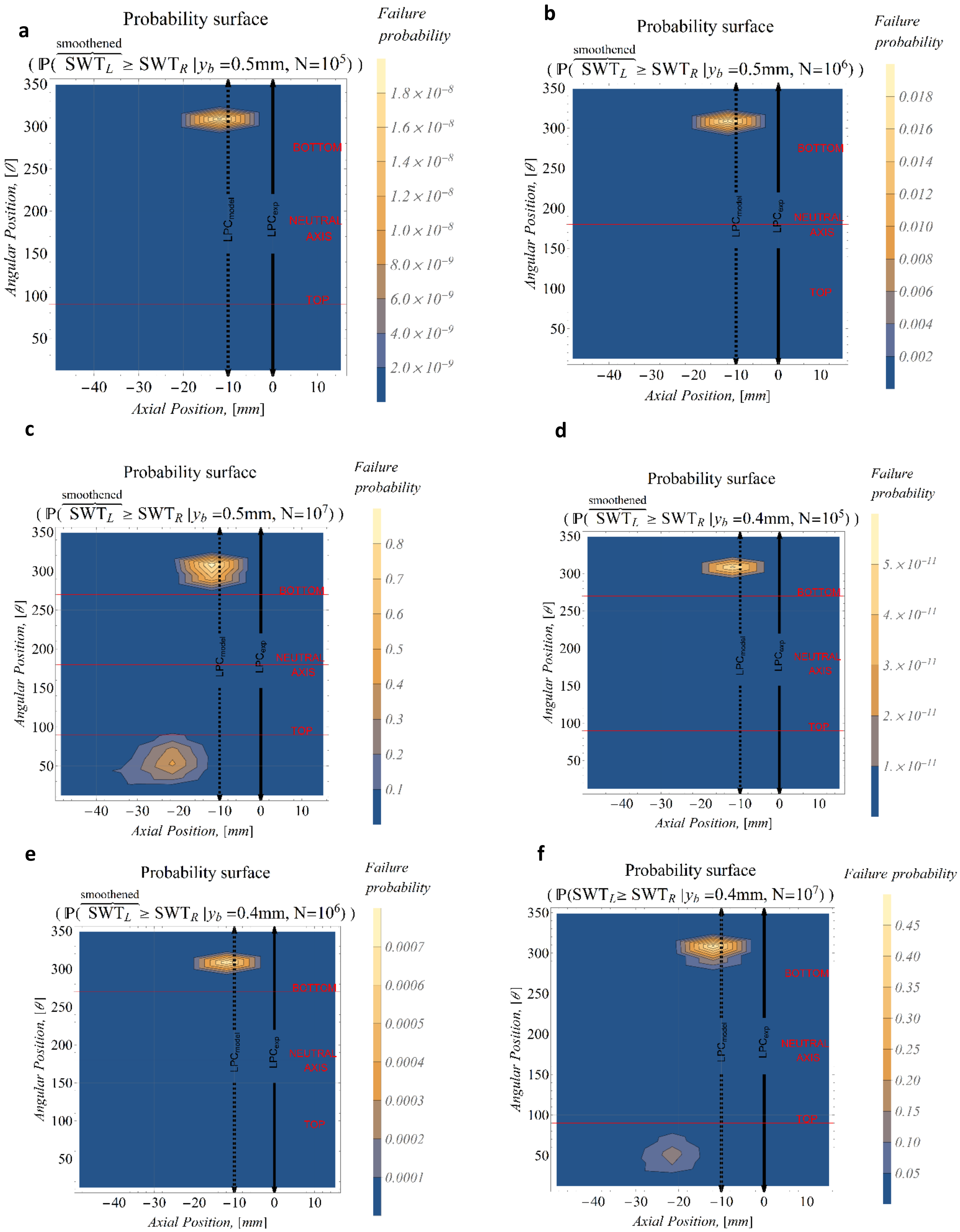

Figure 14: Probability of failure for the wires in layer 4 of the Bersfort conductor at a bending amplitude of 0.5mm (a to c) and 0.4mm (d to f)

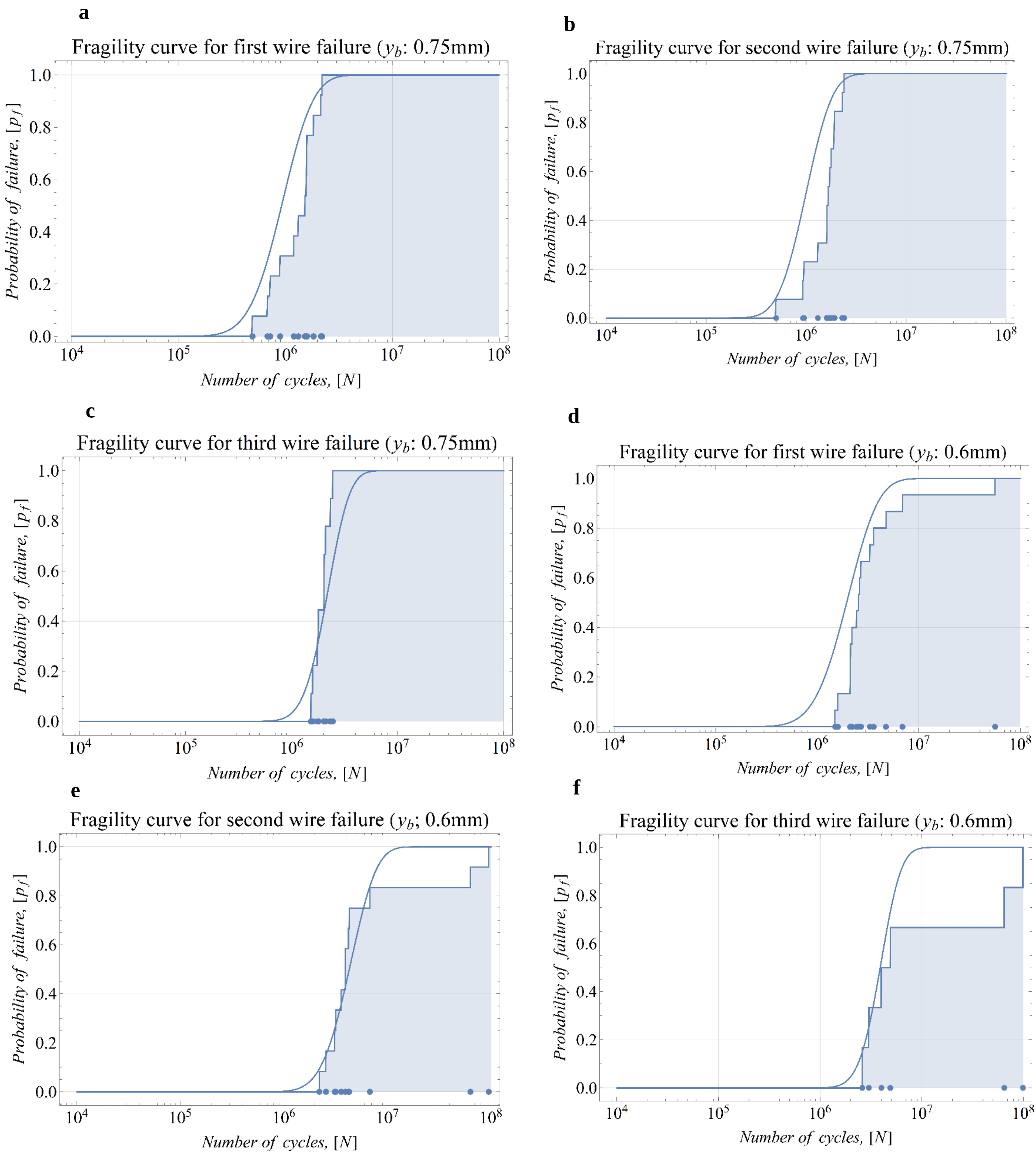

Figure 15: Fragility curves for Bersfort conductor clamp assembly. (a,b,c). Bending amplitude of 0.75mm. (d,e,f). Bending amplitude of 0.6mm.

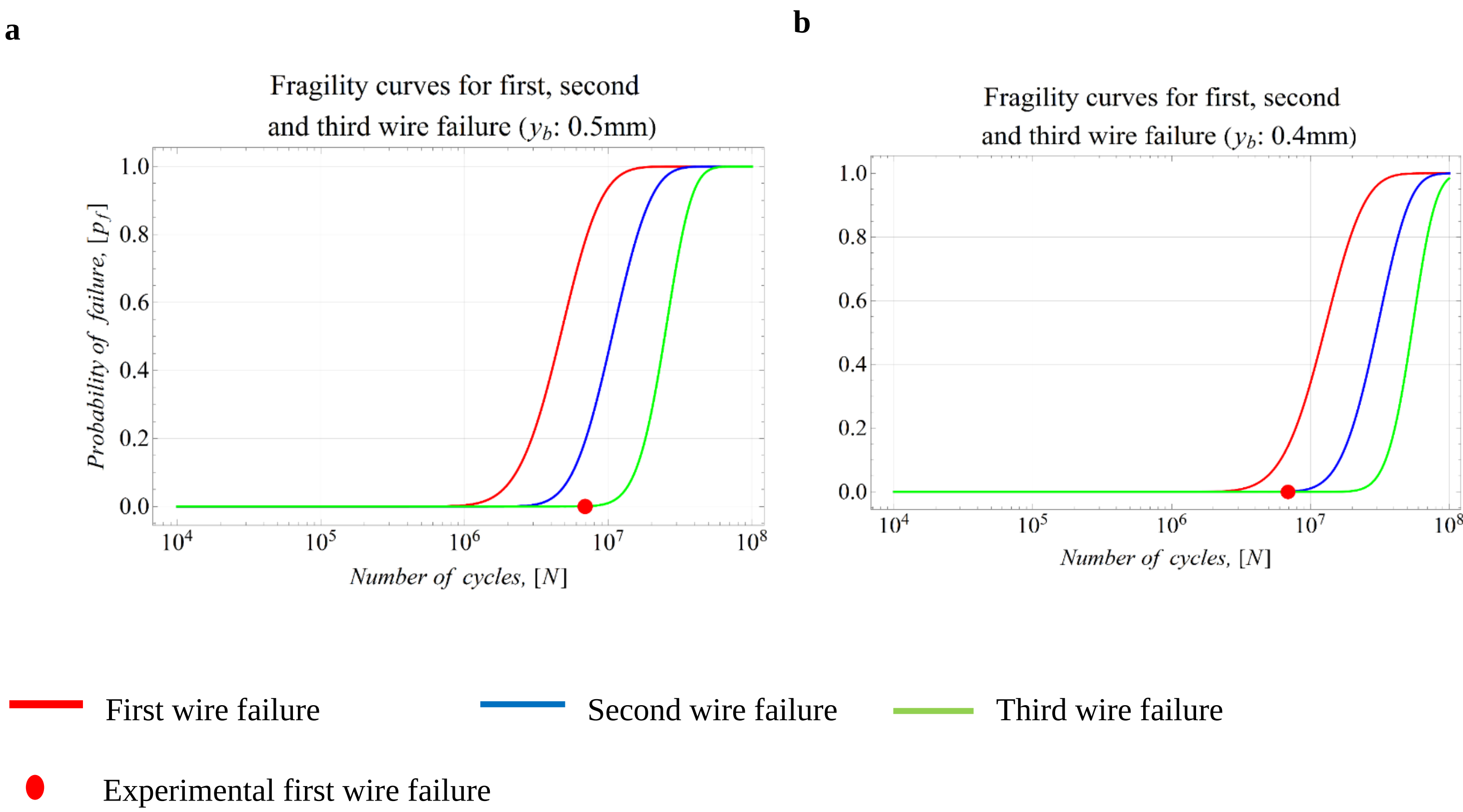

Figure 16: Fragility curves for the Bersfort conductor at a bending amplitude of : (a). 0.5mm. (b). 0.4mm.

increasing number of cycles as compared to higher amplitudes. This shows that for lower amplitudes, the number of wires at risk of failure is smaller.

Given the probabilities of failure for each contact point $\mathbb{P}\left(\overbrace{SWT_L \mid y_b(d,\theta)}^{smoothened} \geq (SWT_R \mid N = N_i)\right)$ and the fretting indicator function G(E), the probability of failure of the conductor can be obtained by using Equation (14). The results of these computations are fragility curves shown in terms of the cumulative distribution function (CDF) of $N \mid y_b$ in Figures 5.15 and5. 16 for bending amplitudes 0.75mm, 0.6mm, 0.5mm and 0.4mm respectively. The plots are shown for the first, second and third wire failures.

To validate the predicted fragility CDF, the empirical cumulative distribution functions (ECDF) for the experimental data in Levesque (2005) on the same Bersfort conductor are also presented. For the bending amplitudes 0.75mm and 0.6mm for which a reasonable amount of experimental data is available, the CDF compares well with the ECDF for the first, second and third wire failures.

For a bending amplitude of 0.6mm, the fragility curves given in Figure 5.15 (a-c) shows that there are outliers in the experimental data presented in Levesque (2005). The cause of these outliers is not known and may possibly be due to different experimental conditions.

Different models, exclusively derived from experimental data, such as the CIGRE Safe Boarder Line (CSBL) (CIGRE, 1979), the EPRI dataset (Cloutier et al., 2006), the safe limit of Hardy and Leblond (2001) and the confidence interval of Thomas et al.(2020), have been proposed for the fatigue resistance of overhead conductor-clamp systems for first wire failure. The stress-life predictions derived from the numerical model are compared to these empirical models in Figure 5.17. The SN curve for the numerical model is obtained by computing the quantile of the Poisson Binomial distribution for the first wire failure as:

$$\mathbb{P}\left(N_p \leq N | k \geq k\right) = p \tag{5.18}$$

where the values of the probability p are {0.05, 0.5, 0.95} which represents the 5th, 50th and 95th fractiles of the SN curve and *k=1*. SN curves for second and third wire failures can also be generated by using *k=2 and k=3.*

For large amplitudes (0.75mm), the median predicted life from the proposed model is close to the median curve proposed by (Thomas et al., 2020). It also noted that the CIGRE-CSBL is not a safe boarder line since it is above the 5% probability of failure predicted by the new model. Such a limitation of the CIGRE-CSBL has also been noted by Hardy and Leblond (2001). The results of the new model also show that the safe limit of Hardy and Leblond (2001) is also above the 5% probability of failure predicted by the new model and the model of Thomas et al., (2020).

It is also noted that the 95% confidence interval for the new model is narrower than the interval proposed in Thomas et al. (2020). This can be explained by the fact that conductor fatigue data in Cloutier et al. (2006) used by Thomas et al. (2020) includes data using different experimental conditions and conductor-clamp types and configurations on the basis of idealized stress model.

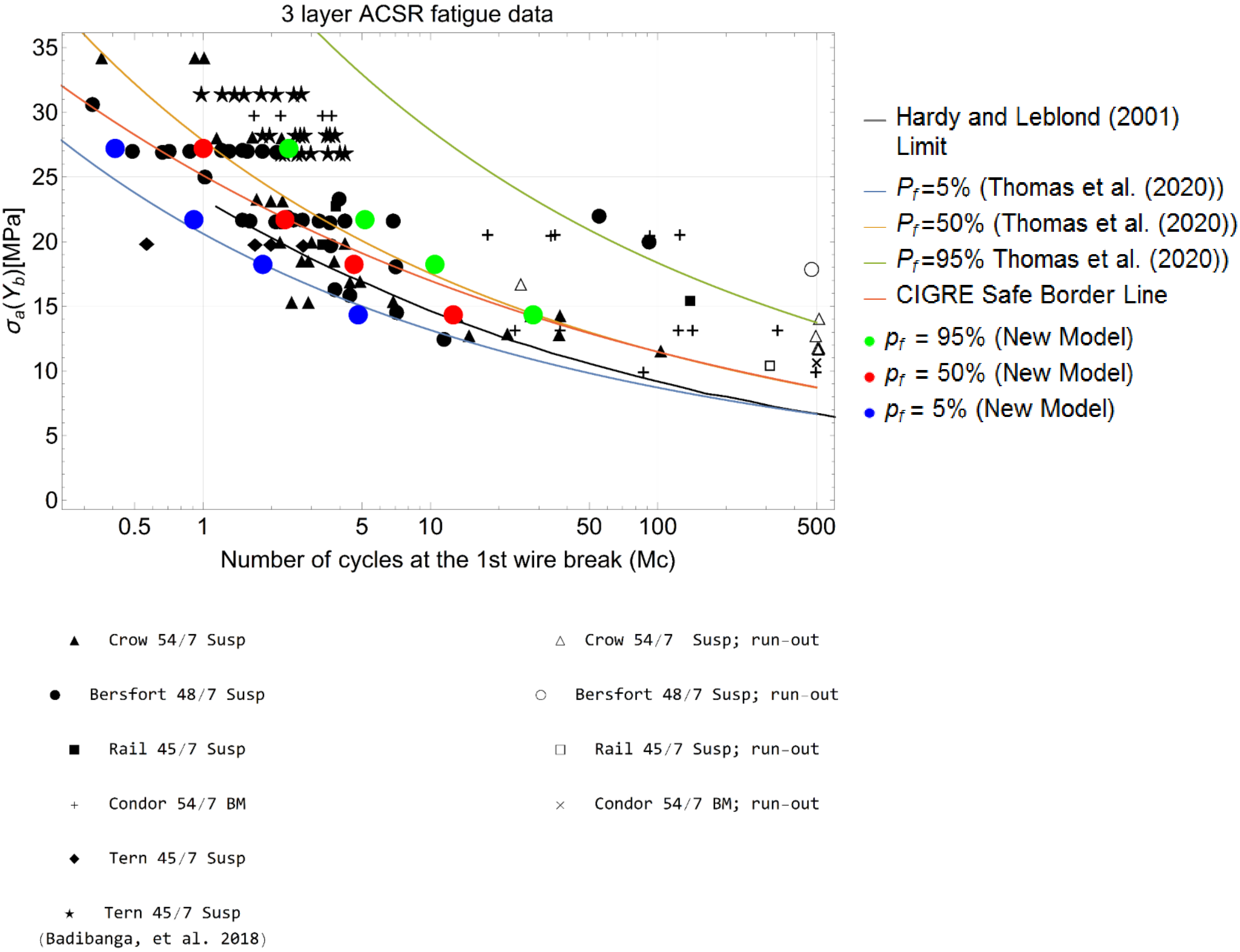

Figure 17: A comparison of the stress-life curves derived from the proposed framework for first wire failure with previous models. All black data points are from (Cloutier, Goudrea, & Cardou, 2006) except otherwise stated.

In addition to the fragility curves and SN curves, the expected value and variance of the number of failed wires $\mathfrak{B}$ as a function of number of cycles can be obtained (Wang, 1993):

$$\mathbb{E}(\mathfrak{B}|N = N_i) = \mathbb{E}\left(\sum_{m=1}^{n} \mathbb{P}_m(N = N_i)\right) \tag{5.19}$$

$$\mathbb{V}\mathrm{ar}(\mathfrak{B}|N = N_i) = \sum_{m=1}^{n} \mathbb{P}_m(N = N_i)\big(1 - \mathbb{P}_m(N = N_i)\big) \tag{5.20}$$

The conditional mean and variance of Equations (5.19) and (5.20) are compared to observed values in Table 3.

Table 3: Comparison of predicted number of wire failures against experimental observation

Bending amplitude y_b (mm)	Number of cycles to failure N_i	Predicted expectation of number of wire failures $\mathbb{E}(\mathfrak{B}\|N = N_i)$	Predicted variance of number of wire failures $\mathbb{V}\mathrm{ar}(\mathfrak{B}\|N = N_i)$	Experimental expectation of number of wire failures $\overbrace{\mathbb{E}(\mathfrak{B}\|N = N_i)}^{sample\ estimate}$	Experimental variance of number of wire failures $\overbrace{\mathbb{V}\mathrm{ar}(\mathfrak{B}\|N = N_i)}^{sample\ estimate}$
0.75	10^5	-	-	0	0
	10^6	0.6	0.34	1.75	0.21
	10^7	3.95	1.32	4.33	0.32
0.60	10^5	-	-	0	0
	10^6	0.07	0.06	0	0
	10^7	2.24	0.48	2.29	1.14
0.5	10^5	-	-	No Data	
	10^6	0.0036	0.0036		
	10^7	1.4	0.38		
0.4	10^5	-	-		
	10^6	-	-		
	10^7	0.35	0.25		

The information in Table 5.3, can be used to supplement the fragility curves by considering both a target probability of failure for a conductor and an allowable number of wire failures for the conductor-clamp system . However, more data is needed to validate Equations (5.19) and (5.20) for lower amplitudes.

5.5 CONCLUSIONS

A methodology for the derivation of fragility curves for electric overhead conductor-clamp systems has been presented. First a finite element model of the conductor-clamp assembly is used to evaluate the contact stresses and fretting regime at all contact points between wires and between wires and clamp for a given amplitude of displacement. The state of stress at each contact is used to evaluate a fretting fatigue criterion based on the SWT and the potential for a mixed fretting fatigue regime that is most conducive to failure. For contacts that are characterized with a mixed fretting regime, the probability of failure as a function of number of cycles is evaluated as a function SWT by considering the distribution of SWT at failure as a function of number of cycles for fatigue data obtained from single aluminum wires. The probability of failure of the conductor as a function of number of cycles is then evaluated by considering a single, two or three wires as the failure criterion. The model is validated by a comparison of the predicted location of failed wires as well as the number of cycles to failure with experimental data available in the literature. The presented methodology offers the following advantages and innovations:

- The conductor is not idealized as a single entity but models the conductor fatigue failure as a system of wires;
- The model accounts for the configuration of a conductor-clamp assembly, clamp radius, clamping torque etc.;

- It provides predictions of single and multiple wire failures and avoids or reduces the number of tests that are performed in practice to derive SN curves for each type of conductor-clamp assembly;
- Fragility curves for a Bersfort conductor are presented for up to three wire failures for any amplitude of vibration;
- The SN model derived from the proposed method has much smaller variance than current models that combine experimental results from different conductor-clamp assemblies on the basis of the simple flexion model and improves significantly the accuracy of fatigue life predictions.

The next steps for future developments of the approach are to apply the procedure to the other conductor/clamp configurations, extend the analysis to damage accumulation rules that considers a combination of cycles of vibrations of different amplitude, and to investigate procedures to extend the applicability of the model for conductor failures based on larger numbers of conductor wires. However, it is unlikely that the industry would adopt such a criteria considering the current practice in addition to the significant increase in the complexity of the analysis of stress redistribution needs to be considered.

Data Availability

The experimental data sets used in the article can be found in the cited references.

Author Contributions

OOT carried out the numerical modeling and probabilistic analysis, analyzed the result and prepared the manuscript. LC supervised all phases of the research project, provided guidance on the probabilistic aspects of the project and edited the manuscript. SL conceived the research project, supervised all phases of the research project and edited the manuscript. All authors approved the submitted version of the article.

5.6 References

Badibanga, R., Miranda, T., Rocha, P., Ferreira, J., da Silva, C., and Araújo, J. (2018). The effect of mean stress on the fatigue behaviour of overhead conductor function of the H/w parameter. *MATEC Web of Conferences, 165*. doi:10.1051/matecconf/201816511001

Baumann, R., and Novak, P. (2017). Efficient Computation and Experimental validation of ACSR Overhead Line Conductors Under Tension and Bending. *CIGRE Science and Engineering, 9*, 5-16.

Cardou, A., and Cloutier, L. (1990). Fatigue Strength Characterization of ACSR Electrical Conductors at Suspension Clamps. *Electric Power Systems Research, 19*, 61-71.

CIGRE-WG-B2.30. (2010). *Engineering Guidelines Relating To Fatigue Endurance Capability of Conductor/Clamp Systems*.

CIGRE. (1979). *Recommendation for the Evaluation of the Lifetime of Transmission Line Conductors* (Electra n 63).

Cloutier, L., Goudrea, S., and Cardou, A. (2006). Fatigue of Overhead Conductors. In J. K. Chan, D. G. Havard, C. B. Rawlins, & J. Weisel (Eds.), *EPRI Transmission Line Reference Book: Wind-induced Conductor Motion* (2nd ed.). Palo Alto, CA: EPRI.

Degat, P. R., Zhou, Z. R., and Vincent, L. (1997). Fretting cracking behaviour on pre-stressed aluminium alloy specimens. *Tribology International*, *30*(3), 215-223. doi:https://doi.org/10.1016/S0301-679X(96)00046-1

Essenburg, F. (1975). On the Significance of the Inclusion of the Effect of Transverse Normal Strain in Problems Involving Beams With Surface Constraints. *Journal of Applied Mechanics, 42*(1), 127-132. doi:10.1115/1.3423502 %J Journal of Applied Mechanics

Gasmi, A., Joseph, P. F., Rhyne, T. B., and Cron, S. M. (2012). The effect of transverse normal strain in contact of an orthotropic beam pressed against a circular surface. *International Journal of Solids and Structures*, *49*(18), 2604-2616. doi:https://doi.org/10.1016/j.ijsolstr.2012.05.022

Goudreau, S., Levesque, F., Cardou, A., and Cloutier, L. (2010). Strain Measurements on ACSR Conductors During Fatigue Tests III—Strains Related to Support Geometry. *IEEE Transactions on Power Delivery, 25*(4), 3007-3016. doi:10.1109/TPWRD.2010.2045399

Hardy, C., and Leblond, A. (2001). *Statistical Analysis of Stranded Conductor fatigue Endurance Data* Paper presented at the Proceeding of the Fouth International Symposium on Cable Dynamics, Montreal, Canada

Hills, D. A., and Nowell, D. (1994). *Mechanics of Fretting Fatigue* Springer-Science.

Jang, Y. H., and Barber, J. R. (2011). Effect of phase on the frictional dissipation in systems subjected to harmonically varying loads. *European Journal of Mechanics - A/Solids, 30*(3), 269-274. doi:https://doi.org/10.1016/j.euromechsol.2011.01.008

Kaufman, J. G. (2008). *Properties of Aluminum Alloys: Fatigue Data and Effects of Temperature, Product Form, and Processing* . Ohio, USA:

Lalonde, S., Guilbault, R., and Langlois, S. (2017). Modeling multilayered wire strands, a strategy based on 3D finite element beam-to-beam contacts - Part II: Application to wind-induced vibration and fatigue analysis of overhead conductors. *International Journal of Mechanical Sciences, 126,* 297-307. doi:http://dx.doi.org/10.1016/j.ijmecsci.2016.12.015

Lalonde, S., Guilbault, R., and Langlois, S. (2018). Numerical Analysis of ACSR Conductor–Clamp Systems Undergoing Wind-Induced Cyclic Loads. *IEEE Transactions on Power Delivery, 33*(4), 1518-1526. doi:10.1109/TPWRD.2017.2704934

Levesque, F. (2005). *Etude de l'applicabilite de la regle de Palmgren-Miner aux conducteurs electriques sous chargements de flexion cyclique par blocs.* (MSc), Universite Laval,

Naghdi, P. M., and Rubin, M. B. (1989). On the significance of normal cross-sectional extension in beam theory with application to contact problems. *International Journal of Solids and Structures, 25*(3), 249-265. doi:https://doi.org/10.1016/0020-7683(89)90047-4

Omrani, A., Langlois, S., Van Dyke, P., Lalonde, S., Karganroudi, S. S., and Dieng, L. (2021). Fretting fatigue life assessment of overhead conductors using a clamp/conductor numerical model and biaxial fretting fatigue tests on individual wires. *Fatigue & Fracture of Engineering Materials & Structures, 44*(6), 1498-1514. doi:10.1111/ffe.13444

Poffenberger, J. C., and Swart, R. L. (1965). Differential Displacement and Dynamic Conductor Strain. *IEEE Transactions on Power Apparatus and Systems, 84*(4), 281-289. doi:10.1109/TPAS.1965.4766192

Pouliot, N., Rousseau, G., Gagnon, D., Valiquette, D., Leblond, A., Montambault, S., and komljenovic, D. (2020). *An Integrated Asset Management Strategy for Trasmission Line Conductors, Based on Robotics, Sensors, and Aging Modelling*. Paper presented at the Engineering Assets and Public Infrastructures in the Age of Digitalization Confrence, Norway.

Rawlins, C. B. (1979). Fatigue of overhead conductors. In *EPRI Transmission Line Reference Book: Wind-induced Conductor Motion*. Palo Alto, CA: EPRI.

Redford, J. A., Gueguin, M., Nguyen, M. C., Lieurade, H. P., Yang, C., Hafid, F., and Ghidaglia, J. M. (2019). Calibration of a numerical prediction methodology for fretting-fatigue crack initiation in overhead power lines. *International Journal of Fatigue, 124*, 400-410. doi:https://doi.org/10.1016/j.ijfatigue.2019.03.009

Rocha, P. H. C., Díaz, J. I. M., Silva, C. R. M., Araújo, J. A., and Castro, F. C. (2019). Fatigue of two contacting wires of the ACSR Ibis 397.5 MCM conductor: Experiments and life prediction. *International Journal of Fatigue, 127*, 25-35. doi:https://doi.org/10.1016/j.ijfatigue.2019.05.033

Said, J., Garcin, S., Fouvry, S., Cailletaud, G., Yang, C., and Hafid, F. (2020). A multi-scale strategy to predict fretting-fatigue endurance of overhead conductors. *Tribology International, 143*, 106053. doi:https://doi.org/10.1016/j.triboint.2019.106053

Thomas, O. O., Chouinard, L., and Langlois, S. (2020). *A Probabilistic Stress-Life Model for Fretting Fatigue of Aluminum Conductor Steel Reinforced Cable-Clamp Systems. Engineering Assets and Public Infrastructures in the Age of Digitalization. Lecture Notes in Mechanical Engineering*: Springer.

Wang, Y. H. (1993). On the Number of Successes in Independent Trials. *Statistica Sinica, 3*(295-312).

Zhou, Z. R., Cardou, A., Goudreau, S., and Fiset, M. (1994).Fretting Patterns in a Conductor-Clamp Contact Zone. *17*(6), 661-669. doi:10.1111/j.1460-2695.1994.tb00264.x

Zhou, Z. R., and Vincent, L. (1995). Mixed fretting regime. *Wear, 181-183*, 531-536. doi:https://doi.org/10.1016/0043-1648(95)90168-X

6 CONCLUSIONS

6.1 SUMMARY OF RESEARCH FINDINGS

The main goal of this thesis was to develop a framework for which fragility curves and SN curves for multiple wire failures in overhead conductor-clamp assemblies under conditions of fretting fatigue could be generated using the finite element method and methods of structural reliability. This approach should reduce the number of experimental tests required for overhead conductor fatigue testing.

The research activities carried out in this work and the corresponding observations are as follows

- In Chapter 3 an improved SN curve with nonconstant variance for overhead conductor-clamp fatigue was developed in terms of the idealized bending stress amplitude of Poffenburger-Swart. This study illustrated that in fitting SN curves to overhead conductor fatigue data, accounting for the effect of nonconstant variance and use of the Weibull distribution led to tighter confidence interval and better prediction around the median and left tail. However, on the right tail of the distribution of the number of cycles for a given stress level, the prediction is less accurate due to the presence of run-out and errors in tail probability estimation due to small sample size. Based on the method
- In chapter 4, the difference between the 3D Timoshenko beam FE and 3D solid FE are compared for their accuracy in fatigue life evaluation. It was observed that while the Timosheko beam model can predict the fatigue life of wire to clamp contacts in over head conductor-clamp assemblies, its predictions are biased and should be corrected.
- In chapter 5, the prediction of the 3D Timoshenko beam theory are corrected by a maximum likelihood approach, the finite element method is combined with the Poisson

binomial distribution to generate fatigue fragility curves for overhead-conductor clamp systems. SN curves for the multiple wire failures (i.e. 1^{st} to 3^{rd} in the case study) for overhead conductor-clamp systems are also generated. The distribution of the number of wire failures in a overhead conductor-clamp system after undergoing a given number of cycles is also presented. The SN curves generated in this study is compared with that generated in chapter 3 using the idealized stress criterion. It was observed that the variance appearing in the SN curved generated using the idealized stress approach is larger than that due to the new model. This is as expected given that the new approach accounts for a variety of factors such as the clamping toque, clamp radius etc that have been considered that variability in the classical approach using the idealized stress.

The framework proposed in this thesis will allow for the generation of fragility and SN curves for specific conductor-clamp assemblies and reduce the number of tests required to characterize the fatigue resistance of conductor-clamp assemblies.

6.2 SUGGESTIONS FOR FUTURE WORKS

The research reported in this thesis involved the development of a probabilistic method for the fatigue strength analysis of overhead conductor-clamp assemblies. There are several areas that improvements can be made. These areas are classified as follows:

6.2.1 Computational Mechanics in Overhead-Conductor Clamp Assemblies

- It was observed that a lot of time was spent in processing the wire to clamp and wire to keeper contact. The detection and computation of the contact integrals for these elements dominated the solution even with the rigid clamp and keeper assumption. It is thus apparent that a methodology that enhances the detection and computation of the wire to clamp/wire to keeper contact will speed up the solution and enhance the computation of reliability measures for overhead conductor-clamp assemblies.

- The second time consuming element of the computation analysis was in determining the stick-slip/contact-separation transition in time. This is a function of the constraint algorithm and numerical integration algorithm. Since commercial finite element codes such as ANSYS used in this work do not implement special routines for solving PDEs with discontinuous right-hand sides, it will be interesting to see if implementations of such routines can lead to efficient solution times.
- Although this work has demonstrated that the Timoshenko beam theory can be used for fatigue analysis of overhead conductors, it was observed that this beam theory is stiffer than the full 3D solution. It has a larger error in the prediction of the failure location and gives a wrong distribution for the contact pressure. Given that it is still difficult to model an appreciable length of a conductor using full 3D theory, the suggested alternative here is the development of higher-order beam theories with appropriate displacement kinematics that can match the results of the full 3D theory in prediction of stress distribution and contact length prediction.

6.2.2 Conductor Fatigue

- The methodology presented for the constructing conductor SN curves should be extended to variable amplitude loading
- The methodology developed in this thesis should be extended to account for the influence of wire failure on the distribution of stress in region of KE and LPC
- Development of loading models for transmission line conductors that could be combined with the fatigue resistance models developed herein will be useful for the residual life estimation of overhead conductors under conditions of fretting fatigue.

- The conductors that have been studied in this work are in ideal situations in a laboratory. Conductors in the field are subjected to conditions of corrosion, electrical energy and thermal fatigue. These phenomena can have an influence on the fatigue resistance of conductors. A study is thus required to extend the methods presented herein to these situations.
- The contact behavior in overhead conductor has mostly been described to go through a sticking phase. However, in this work it was observed that some contacts also under a separation phase (i.e. stick-slip-separation). Most of these contacts also had very low contact normal force and a varying normal force. It will be important to study the difference between these kinds of contact and those of the sticking contact in fatigue.

6.2.3 Structural Reliability of Overhead Conductor-Clamp Assemblies

- The probability that a conductor fails in fretting fatigue is composed of two parts – the probability that the contacts are in the fretting zone and the probability for fatigue to occur. In this thesis, the probability that the contact is in the fretting zone has been approximated by a Boolean indicator function due to lack of information on this probability distribution. Although, this Boolean approach has been shown to be sufficient, a more theoretical approach to determining the probability of a contact is required.
- In the reliability method presented in this thesis, it has been assumed that the probability of failure of a contact point is not affected by that of another contact point i.e. they are independent. This statement holds true for the first wire failure. The case studies in this thesis also show that it holds true for the second wire failure. However, it appears that the dependence between the probability of failures should be considered for higher number of failure.

- During this work, it was noticed that the conductor reliability problem could be posed as a network reliability problem with the network topology specified by the finite element mesh on which the computation was made. In this way, the contacts and wires of the conductors are simply edges and vertices of a graph whose probability of failure is to be computed. Also, since very efficient algorithms are already available for computations on graphs, the computations of fragility for overhead conductor fatigue can become easier using such an approach. Also, this network approach allows the extension of the method presented in this thesis to large scale network of transmission lines when appropriate loading models become available.
- Given that it now possible to generate fragility and SN curves computationally for overhead conductors, the time has come to build a knowledge base of available overhead conductor fatigue data that will include important variables such as the clamp dimension, the clamping force and loading protocol to serve as validation tool for developed fragility and SN curves. The method developed herein can then be used to study the effect of these parameters This knowledge base can also serve as a backend library to an overhead conductor fatigue residual life estimation program.
- The methodology presented in this work can be extended to the robust optimization of conductor-clamp design to reduce the probability of failure. In other words, what is the best combination of conductor and clamp that present the minimum probability of failure after *N* years in service.
- The methodology developed in this thesis for defining the probability of failure for conductors does not account for the effect of the sequence of failure. Further studies are required to account for this effect on the conductor fatigue resistance distribution.

References

ASCE (2021). A Comprehensive Assessment of America's Infrastructure: 2021 Report Card for America's Infrastructure.

Andresen, H., Hills, D. A., and Vázquez, J. (2019). Closed-form solutions for tilted three-part piecewise-quadratic half-plane contacts. *International Journal of Mechanical Sciences, 150*, 127-134. doi:https://doi.org/10.1016/j.ijmecsci.2018.09.024

Andresen, H., Hills, D. A., and Moore, M. R. (2020). The steady state partial slip problem for half plane contacts subject to a constant normal load using glide dislocations. *European Journal of Mechanics - A/Solids, 79*, 103868. doi:https://doi.org/10.1016/j.euromechsol.2019.103868

ANSYS (2018a). ANSYS Mechanical APDL Contact Technology Guide (Version R19.0). Canonsburg, USA: ANSYS.

ANSYS (2018b). ANSYS Mechanical APDL Element Reference (Version R19.0). Canonsburg, USA: ANSYS

Arnold, B. C., Castillo, E., and Sarabia, J. M. (1999). *Conditional Specification of Statistical Models* (1st ed.): Springer

Azevedo, C. R. F., Henriques, A. M. D., and Pulino filho, A. R. (2009). Fretting fatigue in overhead conductors: Rig design and failure analysis of a Grosbeak aluminum cable steel reinforced conductor *Engineering Failure Analysis, 16*, 136-151.

Bannantine, J., Comer, J., and Handrock, J. (1989). *Fundamentals of metal fatigue analysis* New Jersey Prentice Hall.

Barber, J. R. (2010). *Elasticity* (3rd ed. Vol. 172): Springer.

Barber, J. R. (2011). Frictional systems subjected to oscillating loads. *Annals of Solid and Structural Mechanics, 2*(2), 45-55. doi:10.1007/s12356-011-0017-5

Barber, J. R. (2012). Frictional systems under periodic loads — History-dependence, non-uniqueness and energy dissipation. *Journal of Physics: Conference Series, 382*, 012002. doi:10.1088/1742-6596/382/1/012002

Barber, J. R. (2018). *Contact Mechanics* (Vol. 250): Springer.

Barber, J. R., Davies, M., and Hills, D. A. (2011). Frictional elastic contact with periodic loading. *International Journal of Solids and Structures, 48*(13), 2041-2047. doi:https://doi.org/10.1016/j.ijsolstr.2011.03.008

Baumann, R., and Novak, P. (2017). Efficient Computation and Experimental validation of ACSR Overhead Line Conductors Under Tension and Bending *CIGRE Science and Engineering, 9*, 5-16.

Beisheim, J. R., and Sinclair, G. B. (2008). Three-Dimensional Finite Element Analysis of Dovetail Attachments With and Without Crowning. *Journal of Turbomachinery, 130*(2). doi:10.1115/1.2751486

Belytschko, T., Kam Liu, W., Moran, B., and Elkhodary, K. (2014). *Nonlinear Finite Elements for Continua and Structures*: John Wiley & Sons, Ltd.

Besag, J. (1974). Spatial Interaction and the Statistical Analysis of Lattice Systems. *Journal of the Royal Statistical Society. Series B (Methodological), 36*(2), 192-236
.

Bhattacharyya, A. (1943). On Some Sets of Sufficient Conditions Leading to the Normal Bivariate Distribution. *Sankhyā: The Indian Journal of Statistics (1933-1960), 6*(4), 399-406.

Brunair, R. M., Ramey, G. E., and Duncan, R. R. (1988). An Experimental Evaluation of S-N curves and validity of Miner's Cumulative Damage Hypothesis for an ACSR Conductor *IEEE Transactions on Power Delivery, 3*.

Cãmara, E. C. s. B., Kalombo, R. B., Ferreira, J. L. A., Araújo, J. A., and Freire Júnior, R. C. S. (2021). Estimating fatigue behavior of a family of aluminum overhead conductors using ANNs. *Fatigue & Fracture of Engineering Materials & Structures, 44*(4), 983-996. doi:10.1111/ffe.13408

Câmara, E. C. B., Kalombo, R. B., Ferreira, J. L. A., Araújo, J. A., and Freire Júnior, R. C. S. (2022). Estimating the fatigue behavior of a family of aluminum conductor cables using ANNs applying the Poffenberger-Swart formula. *International Journal of Fatigue, 159*. doi:10.1016/j.ijfatigue.2022.106766

Cardou, A., and Cloutier, L. (1990). Fatigue Strength Characterization of ACSR Electrical Conductors at Suspension Clamps *Electric Power Systems Research, 19*, 61-71.

Cardou, A., and Jolicoeur, C. (1997). *Mechanical Models of Helical Strands* (Vol. 50).

Cardou, A., Leblond, A., and Cloutier, L. (1993). Suspension Clamp and ACSR Electrical Conductor Contact Conditions. *Journal of Energy Engineering, 119*(1), 19-31. doi:10.1061/(ASCE)0733-9402(1993)119:1(19)

Castillo, E. (1988). *Extreme value Theory in Engineering*. Carlifornia, USA. : Academic Press Inc. .

Castillo, E. and Fernandez-Canteli, A. (2009). *A Unified Statistical Methodology for Modeling Fatigue Damage*: Springer.

Castillo, E. and Galambos, J. (1987). LIFETIME REGRESSION MODELS BASED ON A FUNCTIONAL EQUATION OF PHYSICAL NATURE. *Journal of Applied Probability, 24*(1), 160-169.

Cattaneo, C. (1938). Sul contatto di due corpi elastici. *Atti Accad. Naz. Lincei Rc, 27*, 342-348, 434-436, 474-478.

Chen, J.-S. (2011). On the contact behavior of a buckled Timoshenko beam constrained laterally by a plane wall. *Acta Mechanica*, *222*(3), 225-232. doi:10.1007/s00707-011-0529-4

Ciavarella, M., Hills, D. A., and Monno, G. (1998). The influence of rounded edges on indentation by a flat punch. *212*(4), 319-327. doi:10.1243/0954406981521259

Ciavarella, M. (1998a). The generalized Cattaneo partial slip plane contact problem. I—Theory. *International Journal of Solids and Structures, 35*(18), 2349-2362. doi:https://doi.org/10.1016/S0020-7683(97)00154-6

Ciavarella, M. (1998b). The generalized Cattaneo partial slip plane contact problem. II—Examples. *International Journal of Solids and Structures, 35*(18), 2363-2378. doi:https://doi.org/10.1016/S0020-7683(97)00155-8

CIGRE-WG-B2.30. (2010). *Engineering Guidelines Relating To Fatigue Endurance Capability of Conductor/Clamp Systems*

CIGRÉ (1979). *Recommendations for the Evaluation of the Lifetime of Transmission Line Conductors* (Electra n 63).

CIGRÉ WG B 2.47(2017). *Guide on Repair of Conductors and Conductor-Fittings.*

Cloutier, L., Goudrea, S., and Cardou, A. (2006). Fatigue of Overhead Conductors. In J. K. Chan, D. G. Havard, C. B. Rawlins, & J. Weisel (Eds.), *EPRI Transmission Line Reference Book: Wind-induced Conductor Motion* (2nd ed.). Palo Alto, CA: EPRI.

Cormier, N. G., Smallwood, B. S., Sinclair, G. B., and Meda, G. (1999). Aggressive submodelling of stress concentrations. *46*(6), 889-909. doi:10.1002/(sici)1097-0207(19991030)46:6<889::Aid-nme699>3.0.Co;2-f

Costello, G. A. (1997). *Theory of Wire Ropes* (2nd ed.). New York Springer Science + Business

Cousineau, D. (2009). Fitting the three-parameter weibull distribution: review and evaluation of existing and new methods. *IEEE Transactions on Dielectrics and Electrical Insulation, 16*(1), 281-288. doi:10.1109/TDEI.2009.4784578

Crowder, M. J., kimber, A. C., Smith, R. L., and Sweeting, T. J. (1991). *Statistical Analysis of Reliability Data* Springer Science + Business Median, B.V. .

D'Agostino, R. B., and Stephens, M. A. (1986). *Goodnss of Fit Techniques* New York Marcel Dekker, Inc.

Ditlevsen, O., and Madsen, H. O. (2007). *Structural Reliability Methods* (2nd Edition ed.). Denmark, Technical University of Denmark.

Duvaut, G., & Lions, J. L. (1976). *Inequalities in Mechanics and Physics* (J. Charlotte, Trans.): Springer.

Elke, W. J., III, and Sracic, M. W. (2019). *Effects of Cut Boundary Location on Finite Element Submodels With Contacts.* Paper presented at the ASME 2019 International Design Engineering Technical Conferences and Computers and Information in Engineering Conference.

England, A. H. (2003). *Complex Variable Methods in Elasticity* Dover.

EPRI. (1979). *Transmission Line Reference Book*. Retrieved from Palo Alto, CA.

Essenburg, F. (1975). On the Significance of the Inclusion of the Effect of Transverse Normal Strain in Problems Involving Beams With Surface Constraints. *Journal of Applied Mechanics, 42*(1), 127-132. doi:10.1115/1.3423502 %J Journal of Applied Mechanics

Fadel, A. A., Rosa, D., Murça, L. B., Fereira, J. L. A., and Araújo, J. A. (2012). Effect of high mean tensile stress on the fretting fatigue life of an Ibis steel reinforced aluminium conductor. *International Journal of Fatigue, 42*, 24-34. doi:https://doi.org/10.1016/j.ijfatigue.2011.03.007

Feyrer, K. (2015). *Wire Ropes (Tension, Endurance, Reliability)* (2nd ed.): Springer

Foggi, J. H. (2020). *Degradation Mechanisms of AA 1350 Aluminium Alloy Conductor Strands in Air and Chloride Solutions* (Ph.D), Norwegian University of Science and Technology Trondheim.

Frigerio, M., Buehlmann, P. B., Buchheim, J., Holdsworth, S. R., Dinser, S., Franck, C. M., . . . Mazza, E. (2016). Analysis of the tensile response of a stranded conductor using a 3D finite element model. *International Journal of Mechanical Sciences, 106*, 176-183. doi:https://doi.org/10.1016/j.ijmecsci.2015.12.015

Gang, Qi. (2013). *Computational Modeling for Stress Analysis of Overhead Transmission Line Stranded Conductors Under Design and Fretting Fatigue Conditions* (PhD), McGill University Montreal, Quebec

Gasmi, A., Joseph, P. F., Rhyne, T. B., and Cron, S. M. (2012). The effect of transverse normal strain in contact of an orthotropic beam pressed against a circular surface. *International Journal of Solids and Structures, 49*(18), 2604-2616. doi:https://doi.org/10.1016/j.ijsolstr.2012.05.022

Goudreau, S., Levesque, F., Cardou, A., and Cloutier, L. (2010). Strain Measurements on ACSR Conductors During Fatigue Tests III—Strains Related to Support Geometry. *IEEE Transactions on Power Delivery, 25*(4), 3007-3016. doi:10.1109/TPWRD.2010.2045399

Goudreau, S., Lévesque, F., Cardou, A., and Cloutier, L. (2010). Strain measurements on ACSR conductors during fatigue tests II - Stress fatigue indicators. *IEEE Transactions on Power Delivery, 25*(4), 2997-3006. doi:10.1109/TPWRD.2010.2042083

Goudrea, S., Charette, F., Hardy, C., & Louis., C. (1998). Bending Energy Dissipation of Simplified Single-Layer Stranded Conductor *ASCE Journal of Engineering Mechanics, 124*(8), 811-817.

Gray, A., Abbena, E., and Salamon, S. (2006). *Modern Differential Geometry of Curves and Surfaces with Mathematica*: Chapman & Hall/CRC.

Green, A. E., and Zerna, W. (1992). *Theoretical Elasticity* Dover.

Haldar, A. (2012). *Past, Present and Future of Engineering under Uncertainty: Safety Assessment and Management* Paper presented at the International Symposium on Engineering Under Uncertainty (Safet Assessment and Management).

Hanaki, S., Yamashita, M., Uchida, H., and Zako, M. (2010). On stochastic evaluation of S–N data based on fatigue strength distribution. *International Journal of Fatigue, 32*(3), 605-609. doi:https://doi.org/10.1016/j.ijfatigue.2009.06.001

Hardy, C., and Leblond, A. (2001). *Statistical Analysis of Stranded Conductor fatigue Endurance Data* Paper presented at the Proceeding of the Fouth International Symposium on Cable Dynamics, Montreal, Canada

Hardy, C. (1990). *Analysis of self-damping characteristics of stranded cables in transverse vibrations* Paper presented at the Proceedings of the CSME Mechanical Engineering Forum Toronto.

Hardy, C., and Leblond, A. (2003). *On the Dynamic Flexural Rigidity of Taut Stranded Cables* Paper presented at the 5th International Symposium on Cable Dynamics Italy.

Hardy, C., Leblond, A., Goudreau, S., and Cloutier, L. (1999). *Application of Contact Mechanics to Cable Self-Damping* Paper presented at the 3rd International Conference on Cable Dynamics

Hathout, I. (2016). *Fuzzy probabilistic expert system for overhead conductor assessment and replacement* Paper presented at the Best practices for EHV line design and asset management San Diego, USA.

Hathout, I., Callery-Broomfield, K., and Tang, T. T. T. (2015). *Fuzzy probabilistic expert system for overhead conductor assessment and replacement.* Paper presented at the IEEE Power and Energy Society General Meeting.

Hetenyi, M. (1946). *Beams on Elastic Foundations (Theory With Applications In The Fileds of Civil and Mechanical Engineering)*. Ann Arbor: The University of Michigan Press

Hertz, H. (1881). Uber die Beruhrung fester elastischer Korper. *J Reine Angew Math, 92*, 156-171.

Hills, D. A., and Andresen, H. (2021). *Mechanics of Fretting and Fretting Fatigue* (Vol. 266): Springer.

Hills, D. A., and Nowell, D. (1994). *Mechanics of Fretting Fatigue* Springer-Science.

Hills, D. A., Nowell, D., and Sackfield, A. (1993). *Mechanics of Elastic Contacts* Butterworth Heinemann.

Hills, D. A., Ramesh, R., Barber, J. R., and Moore, M. R. (2018). Methods to solve half-plane partial slip contact problems. *International Journal of Solids and Structures, 155*, 155-159. doi:https://doi.org/10.1016/j.ijsolstr.2018.07.019

Hills, D. A., Nowell, D., & Sackfield, A. (1993). *Mechanics of Elastic Contacts* Butterworth Heinemann.

Hills, D. A., Ramesh, R., Barber, J. R., & Moore, M. R. (2018). Methods to solve half-plane partial slip contact problems. *International Journal of Solids and Structures, 155*, 155-159. doi:https://doi.org/10.1016/j.ijsolstr.2018.07.019

Jang, Y. H., and Barber, J. R. (2011). Effect of phase on the frictional dissipation in systems subjected to harmonically varying loads. *European Journal of Mechanics - A/Solids, 30*(3), 269-274. doi:https://doi.org/10.1016/j.euromechsol.2011.01.008

Ja¨ger, J. (1998). A New Principle in Contact Mechanics. *Journal of Tribology, 120*(4), 677-684. doi:10.1115/1.2833765 %J Journal of Tribology

Jeong, S. H., and Lee, Y. Z. (2006). *Determination of the Fretting Regimes Under Stick-Slip Condition Using the Phase Difference Between Friction and Relative Displacement*. Paper presented at the ASME 2006 International Joint Tribology Conference, San Antonio, USA.

Johnson, K. L. (1985). *Contact Mechanics*. Cambridge, UK: Cambridge University Press.

Klarbring, A., and Björkman, G. (1988). A mathematical programming approach to contact problems with friction and varying contact surface. *Computers & Structures, 30*(5), 1185-1198. doi:https://doi.org/10.1016/0045-7949(88)90162-9

Kalombo, R. B., Martínez, J. M. G., Ferreira, J. L. A., da Silva, C. R. M., and Araújo, J. A. (2015). Comparative Fatigue Resistance of Overhead Conductors Made of Aluminium and Aluminium Alloy: Tests and Analysis. *Procedia Engineering, 133*(Supplement C), 223-232. doi:https://doi.org/10.1016/j.proeng.2015.12.662

Kalombo, R. B., Pestana, M. S., Freire Júnior, R. C. S., Ferreira, J. L. A., Silva, C. R. M., Veloso, L. A. C. M., . . . Araújo, J. A. (2020). Fatigue life estimation of an all aluminium alloy 1055 MCM conductor for different mean stresses using an artificial neural network. *International Journal of Fatigue, 140*. doi:10.1016/j.ijfatigue.2020.105814

Kalker, J. J. (1972). On Elastic Line Contact. *Journal of Applied Mechanics, 39*(4), 1125-1132. doi:10.1115/1.3422841 %J Journal of Applied Mechanics

Kaufman, J. G. (2008). *Properties of Aluminum Alloys: Fatigue Data and Effects of Temperature, Product Form, and Processing* Retrieved from Ohio, USA:

Kim, J. H., Ahn, Y. J., Jang, Y. H., and Barber, J. R. (2014). Contact problems involving beams. *International Journal of Solids and Structures, 51*(25), 4435-4439. doi:https://doi.org/10.1016/j.ijsolstr.2014.09.013

Kikuchi, N., and Oden, J. T. (1988). Contact Problems in Elasticity (A Study of variational Inequalities and Finite Element Methods): Society for Industrial and Applied Mathematics (SIAM).

Knopp, K. (1945). *Theory of Functions (Elements of the General Theory of Analytic Functions)*: Dover

Kohlas, J., and Monney, P.-A. (1994). Theory of Evidence - A Survey of its Mathematical Foundations, Applications and Computational Aspects *Mathematical Methods of Operations Research, 39*, 35-68.

Konyukhuv, A., and Izi, R. (2015). *Introduction to Computational Contact Mechanics (A Geometrical Approach)* (1st ed.): Wiley.

konyukhuv, A., and Schweizerhof, K. (2012). *Computational Contact Mechanics (Geometrically Exact Theory for Arbitrary Shaped Bodies)* (Vol. 67): Springer.

Kotz, S., and Nadarajah, S. (2000). *Extreme Value Distributions: Theory and Applications* London, UK: Imperial Collge Press.

Lalonde, S. (2017). *Strategie de Modelisation 3D Des Solides Toronnes Appliquee a L'etude de La Fatigue Des Conducteurs de Lignes de Transport D'Energie Electrique* (Ph.D), Universite de Sherbrooke Serbrooke.

Lalonde, S., Guilbault, R., and Langlois, S. (2017). Modeling multilayered wire strands, a strategy based on 3D finite element beam-to-beam contacts - Part II: Application to wind-induced vibration and fatigue analysis of overhead conductors. *International Journal of Mechanical Sciences, 126*, 297-307.doi:http://dx.doi.org/10.1016/j.ijmecsci.2016.12.015

Lalonde, S., Guilbault, R., and Langlois, S. (2018). Numerical Analysis of ACSR Conductor–Clamp Systems Undergoing Wind-Induced Cyclic Loads. *IEEE Transactions on Power Delivery, 33*(4), 1518-1526. doi:10.1109/TPWRD.2017.2704934

Laursen, T. A. (2002). Computational Contact and Impact Mechanics (1st ed.): Springer

Levesque, F. (2005). *Etude de l'applicabilite de la regle de Palmgren-Miner aux conducteurs electriques sous chargements de flexion cyclique par blocs.* (MSc), Universite Laval,

Levesque, F. (2009). *Analyse de la Fatigue par Petits Debattements (Fretting Fatigue) de Fils D'un Conductor Electrique* (PhD), Universite Laval, Laval, Quebec.

Levesque, F., Goudrea, S., and Cloutier, L. (2011). Elastic-Plastic Microcontact Model for Elliptical Contact Areas and Its Application to a Treillis Point in Overhead Electric Conductors *ASME Journal of Tribology, 133*.

Levesque, F., Goudreau, S., Cardou, A., and Cloutier, L. (2010). Strain Measurements on ACSR Conductors During Fatigue Tests I—Experimental Method and Data. *IEEE Transactions on Power Delivery, 25*(4), 2825-2834. doi:10.1109/TPWRD.2010.2060370

Lévesque, F., Goudreau, S., Cloutier, L., and Cardou, A. (2011). Finite element model of the contact between a vibrating conductor and a suspension clamp. *Tribology International, 44*(9), 1014-1023. doi:https://doi.org/10.1016/j.triboint.2011.04.006

Levesque, F., and Legeron, F. (2012). *Effect of mean tension on interwire contacts in overhead conductors*

Levesque, F., and Legron, F. (2010). *Contact mechanics based fatigue indicators for overhead conductors*

Litewka, P. (2010). *Finite Element Analysis of Beam-to-Beam Contact* (Vol. 53): Springer

Marshall, A. W., & Olkin, I. (2007). *Life Distributions* New York: Springer

McConnel, K. G., and Zemke, W. P. (1982). A Model to Predict the Coupled Axial Torsion Properties of ACSR Electrical Conductors *Experimental Mechanics, 22*(7), 237-244.

McGill, P. B., and Ramey, G. E. (1986). EFFECT OF SUSPENSION CLAMP GEOMETRY ON TRANSMISSION-LINE FATIGUE. *Journal of Energy Engineering-Asce, 112*(3), 168-184.

Mechatrofice (2020, May, 03). Overhead vs Underground Lines-Advantages and Disadvantages. Mechatrofice.com. https://mechatrofice.com/electrical/overhead-vs-underground

Melchers, R. E. (2002). *Structural Reliability Analysis and Prediction* (2nd Edition ed.). Chichester, England John Wiley & Sons.

Milella, P. P. (2013). *Fatigue and Corrosion in Metals* Springer.

Mindlin, R. D. (1949). Compliance of Elastic Bodies in Contact *ASME Journal of Applied Mechanics, 71*, 259-268.

Montgomery, D. C., and Runger, G. C. (2003). *Applied Statistics and Probability for Engineers* (3rd ed.). New York, USA: John Wiley & Sons, Inc. .

Muskhelishvili, N. I. (1954). *Some Basic Problems of the Mathematical Theory of Elasticity* (J. R. M. Radok, Trans.): Springer.

Naghdi, P. M., and Rubin, M. B. (1989). On the significance of normal cross-sectional extension in beam theory with application to contact problems. *International Journal of Solids and Structures, 25*(3), 249-265. doi:https://doi.org/10.1016/0020-7683(89)90047-4

Noiseux, D. U., Hardy, C., and Houle, S. (1986). Statistical Methods Applied to Aeolian Vibrations of Overhead Conductors. *Journal of Sound and Vibrations, 113*(2), 245-255.

Olsson, K.-G., & Dahlblom, O. (2016). *Structural Mechanics (Modelling and Analysis of Frames and Trusses)*. Sussex: John Wiley & Sons.

Omrani, A. (2021). *Evaluation De La Resistance En fatigue Des Conducteurs Aeriens Par Le Couplage D'Une Approache Numerique Et Experimentale.* (Ph.D), Universite de Sherbrooke Quebec.

Omrani, A., Langlois, S., Van Dyke, P., Lalonde, S., Karganroudi, S. S., and Dieng, L. (2021). Fretting fatigue life assessment of overhead conductors using a clamp/conductor numerical model and biaxial fretting fatigue tests on individual wires. *Fatigue & Fracture of Engineering Materials & Structures, 44*(6), 1498-1514. doi:10.1111/ffe.13444

Omrani, A., Dieng, L., Langlois, S., and Van Dyke, P. (2022). Friction Properties at the Contact Interfaces of Overhead Line Aluminium Conductors. *IEEE Transactions on Power Delivery, 37*(1). doi:10.1109/TPWRD.2021.3062704

Papadrakakis, M. (1981). A method for the automatic evaluation of the dynamic relaxation parameters. *Computer Methods in Applied Mechanics and Engineering, 25*(1), 35-48. doi:https://doi.org/10.1016/0045-7825(81)90066-9

Papailiou, K. O. (1997). On the bending stiffness of transmission line conductors. *IEEE Transactions on Power Delivery, 12*(4), 1576-1583. doi:10.1109/61.634178

Pereira, K., Bordas, S., Tomar, S., Trobec, R., Depolli, M., Kosec, G., and Abdel Wahab, M. (2016). On the Convergence of Stresses in Fretting Fatigue *Materials, 9*(639), 1-15.

Pereira, R., Diaz, J., Ferreira, J. L. A., Da Silva, C. R. M., and Araújo, J. A. (2020). Numerical and Experimental Analysis of Fretting Fatigue Performance of the 1350-H19 Aluminum Alloy. *Journal of the Brazilian Society of Mechanical Sciences and Engineering, 42*(419), 1-13.

Poffenberger, J. C., and Swart, R. L. (1965). Differential Displacement and Dynamic Conductor Strain. *IEEE Transactions on Power Apparatus and Systems, 84*(4), 281-289. doi:10.1109/TPAS.1965.4766192

Popov, V. L., and Heb, M. (2015). *Method of Dimensionality Reduction in Contact Mechanics and Friction* (J. A. T. Gray, Trans.): Springer.

Rajasekaran, R., and Nowell, D. (2005). On the finite element analysis of contacting bodies using submodelling. *40*(2), 95-106. doi:10.1243/030932405x7836

Rawlins, C. B. (1979). Fatigue of overhead conductors. In *EPRI Transmission Line Reference Book: Wind-induced Conductor Motion*. Palo Alto, CA: EPRI.

Redford, J. A., Gueguin, M., Nguyen, M. C., Lieurade, H. P., Yang, C., Hafid, F., and Ghidaglia, J. M. (2019). Calibration of a numerical prediction methodology for fretting-fatigue crack initiation in overhead power lines. *International Journal of Fatigue, 124*, 400-410. doi:https://doi.org/10.1016/j.ijfatigue.2019.03.009

Redford, J. A., Lieurade, H. P., Gueguin, M., Hafid, F., Yang, C., and Ghidaglia, J. M. (2018). Numerical Modeling of the Phenomenon of Fretting-Fatigue involved in the Aging of Overhead Line Conductors. *Materials & Techniques, 106*(3).

Rocha, P. H. C., Díaz, J. I. M., Silva, C. R. M., Araújo, J. A., and Castro, F. C. (2019). Fatigue of two contacting wires of the ACSR Ibis 397.5 MCM conductor: Experiments and life prediction. *International Journal of Fatigue, 127*, 25-35. doi:https://doi.org/10.1016/j.ijfatigue.2019.05.033

Roshan Fekr, M., McClure, G., & Farzaneh, M. (1999). Application of ADINA to stress analysis of an optical ground wire. *Computers & Structures, 72*(1), 301-316. doi:https://doi.org/10.1016/S0045-7949(99)00037-1

Said, J., Fouvry, S., Cailletaud, G., Yang, C., and Hafid, F. (2020). Shear driven crack arrest investigation under compressive state: Prediction of fretting fatigue failure of aluminium strands. *International Journal of Fatigue, 136*, 105589. doi:https://doi.org/10.1016/j.ijfatigue.2020.105589

Said, J., Garcin, S., Fouvry, S., Cailletaud, G., Yang, C., and Hafid, F. (2020). A multi-scale strategy to predict fretting-fatigue endurance of overhead conductors. *Tribology International, 143*, 106053. doi:https://doi.org/10.1016/j.triboint.2019.106053

Stephens, R. I., Fatemi, A., Stephens, R. R., and Fuchs, H. O. (2001). *Metal fatigue in engineering.* Wiley-Interscience

Strohmeyer, C. E. (1914). *The determination of fatigue limits under alternating stress conditions* Paper presented at the Proceedings of the Royal Society of London

Suresh, S. (1998). *Fatigue of Materials* (2nd ed.). Cambridge, UK: Cambridge University Press

Taylor, D. (2007). *The Theory of Critical Distances : A New Perspective in Fracture Mechanics* Oxford, UK: Elsevier

Thi-lien, D. (2015). *Analyse des essais a amplitudes variables realises sur le conducteur Aster 570.*

Timoshenko, S. (1941). *Strength of Materails II: Advanced Theory and Problems* (2nd ed.): D. Van Nostrand Company

Timoshenko, S., and Goodier, J. N. (1951). *Theory of Elasticity* (2nd ed.). New York McGraw-Hill.

Vapnik, V. N. (1998). *Statistical Learning Theory* New York: John Wiley & Sons, Inc

Varney, T. (1926). Notes on the Vibration of Transmission-Line Conductors. *Transactions of the American Institute of Electrical Engineers, XLV*, 791-795. doi:10.1109/T-AIEE.1926.5061272

Varney, T. (1928). The Vibration of Transmission-Line Conductors. *Transactions of the American Institute of Electrical Engineers, 47*(3), 799-807. doi:10.1109/T-AIEE.1928.5055059

Vázquez, J., Sackfield, A., Hills, D., and Domínguez, J. (2010). The mechanical behaviour of a symmetrical punch with compound curvature. *45*(4), 209-222. doi:10.1243/03093247jsa633

Wang, Y. H. (1993). On the Number of Successes in Independent Trials *Statistica Sinica, 3*(295-312).

Wang, J. J.-A., Lara-Curzio, E., King, T., Graziano, J., & Chan, J. (2008). The Integrity of ACSR Full Tension Splice Connector at Higher Operation Temperature. *IEEE Transactions on Power Delivery, 23*(2), 1158-1165. doi:10.1109/TPWRD.2008.917661

Washizu, K. (1975). *Variational Methods in Elasticity and Plasticity* (2nd ed.): Pergamon press.

Washizu, K. (1982). *Variational Methods in Elasticity and Plasticity* (3rd ed.): Pergamon press.

Waterhouse, R. B. (1992). Fretting fatigue. *International Materials Reviews, 37*(1), 77-98. doi:10.1179/imr.1992.37.1.77

Wriggers, P. (2006). Computational Contact Mechanics (2nd ed.). Netherlands Springer

Yastrebov, V. (2013). *Numerical Methods in Contact Mechanics*. Great Britain: ISTE Wiley.

Zavarise, G., and Wriggers, P. (2000). Contact with friction between beams in 3-D space. *49*(8), 977-1006. doi:10.1002/1097-0207(20001120)49:8<977::Aid-nme986>3.0.Co;2-c

Zhong, Z.-H. (1993). Finite Element Element Procedures for Contact-Impact Problems: Oxford University Press.

Zhou, Z. R., Cardou, A., Fiset, M., and Goudreau, S. (1994a). Fretting fatigue in electrical transmission lines. *Wear, 173*(1), 179-188. doi:http://dx.doi.org/10.1016/0043-1648(94)90271-2

Zhou, Z. R., Cardou, A., Goudreau, S., and Fiset, M. (1994b). FRETTING PATTERNS IN A CONDUCTOR–CLAMP CONTACT ZONE. *17*(6), 661-669. doi:10.1111/j.1460-2695.1994.tb00264.x

Zhou, Z. R., Cardou, A., Goudreau, S., and Fiset, M. (1996). Fundamental investigations of electrical conductor fretting fatigue. *Tribology International, 29*(3), 221-232. doi:http://dx.doi.org/10.1016/0301-679X(95)00074-E

Zhou, Z. R., Goudreau, S., Fiset, M., and Cardou, A. (1995). Single wire fretting fatigue tests for electrical conductor bending fatigue evaluation. *Wear, 181-183,* 537-543. doi:https://doi.org/10.1016/0043-1648(95)90169-8

Zhou, Z. R., and Vincent, L. (1995). Mixed fretting regime. *Wear*, *181-183,* 531-536. doi:https://doi.org/10.1016/0043-1648(95)90168-X

Appendix A: Some Methods for Analysis of Contact Problems

Method	Types of loading	Assumptions	Applications on conductor	References
Glide dislocations	Constant normal load Monotonic shear Monotonic bulk tension Cyclic shear load Cyclic bulk tension Cyclic bending	Half-plane Partial slip Elastic material behaviour Holds for any contact profile Uncoupled contact		(Hills et al. 2018) (Andresen et al. 2020)
Ciavarella-Jäger principle	Constant normal load Monotonic shear Monotonic bulk tension Constant moment Cyclic shear load Cyclic bulk tension Cyclic moment	Half – plane Partial slip Elastic material behaviour Holds for any contact profile Uncoupled contact		(Ciavarella, 1998a, 1998b) (Ja¨ger, 1998)
Green’s function method	Any loading	No assumptions		(Barber, 2018)
Cattaneo and Mindlin Methodology	Constant normal load	Half-plane / space	(Goudrea, Charette,	(Cattaneo, 1938) (Mindlin, 1949)

	Monotonic shear load Monotonic moment	Quadratic contact profile Uncoupled contact	Hardy, & Louis., 1998) (Hardy, 1990) (Frederic. Levesque & Legron, 2010) (Leblond & Hardy, 2005) (Hardy & Leblond, 2003) (F. Levesque, 2009)	(Hills et al.1993)
Hertz Methodology	Constant normal loading	Half space Body with quadratic profiles Frictionless contact	(Frederic. Levesque & Legron, 2010) (Pereira, Díaz, Ferreira, da Silva, & Araújo, 2020) (Hardy, Leblond, Goudreau, & Cloutier, 1999) (F. Levesque, 2009) (Frederic. Levesque & Legeron, 2012)	(Hertz, 1881) (Johnson, 1985)
Kalker's Line contact theory	Any loading	Half-space		(Kalker, 1972)
Mossakovskii-Barber Procedure	Any loading	Half-plane		Hills and Andresen (2021)
Displacement functions	Any loading	No assumptions		(Barber, 2018)

				(Johnson, 1985)
Stress functions	Any loading	No assumptions		(England, 2003) (Barber, 2018) (Green & Zerna, 1992) (Muskhelishvili, 1977) (Johnson, 1985) (Timoshenko & Goodier, 1951)
Finite element method	Any loading	No assumptions	(Roshan Fekr, McClure, & Farzaneh, 1999) (Gang, 2013) (Lalonde, 2017) Lalonde et al. (2018) (Baumann & Novak, 2017) (J. Said et al., 2020) (Said, Fouvry, Cailletaud, Yang, & Hafid, 2020) (Pereira et al., 2020) (Omrani, 2021) (Rocha, Díaz, Silva, Araújo, & Castro, 2019) (Frigerio et al., 2016)	Kikuchi and Oden (1988). Zhong (1993) Laursen (2002) Wriggers (2006) Litewka (2010) Konyukhuv and Schweizerhof, (2012) Yastrebov (2013) Konyukhuv and Izi, (2015)

			(F. Levesque, 2009) (Wang, Lara-Curzio, King, Graziano, & Chan, 2008) (Frederic. Levesque & Legeron, 2012)	
Analytical Beam Theory	Any loading	No assumptions		(Johnson, 1985) (Barber, 2018) (Castillo and Barber, 1997) (Kim, Ahn, Jang, and Barber, 2014) (Naghdi and Rubin, 1989) (Essenburg, 1975) (Gasmi, Joseph, Rhyne, and Cron, 2012) (Timoshenko and Goodier, 1951)
Method of Dimensionally Reduction	Any loading	Approximate contact profile by equivalent 2D profile		(Popov and Heb, 2015)
Boundary element method	Any loading	No assumption		(Washizu, 1982)
Variational Inequalities and Optimization Techniques	Any loading	No assumption		(Duvaut and Lions, 1976) (Klarbring and Björkman, 1988)

APPENDIX B: EQUILIBRIUM EQUATIONS FOR OVERHEAD CONDUCTORS

The Case of a Wire to Clamp Contact

Details of the equilibrium equation of the wire to clamp contact presented in chapter 2 (Equation (2.4)) are presented herein.

The detailed formed form of the equilibrium Equation is:

$$\int (\nabla_i \dot{\sigma}^{ij}) \delta \dot{u}_{j,B} \, d\Omega_B + \int (\nabla_i \dot{\sigma}^{ij}) \delta \dot{u}_{j,W} \, d\Omega_W + \int (\nabla_i \dot{\sigma}^{ij}) \delta \dot{u}_{j,C} \, d\Omega_C$$

$$= -\underbrace{\left(\int (\nabla_i \delta \dot{u}_{j,B}) \dot{\sigma}^{ij} \, d\Omega_B + \int (\nabla_i \delta \dot{u}_{j,W}) \dot{\sigma}^{ij} \, d\Omega_W + \int (\nabla_i \delta \dot{u}_{j,C}) \dot{\sigma}^{ij} \, d\Omega_C \right)}_{internal\ virtual\ work}$$

$$+ \underbrace{\int \dot{t}^{j}_{(n)} \ \delta \dot{u}_{j,W} \, \Gamma_{W_R} + \int \dot{p}^{j}_{(n)} \ \delta \dot{u}_{j,B} \, \Gamma_{B_T}}_{force\ boundary\ terms\ (external\ virtual\ work)}$$

$$+ \left(\underbrace{\int \dot{\sigma}^{j}_{(n)} \delta \dot{u}_{j,B} \, d\Gamma_{B_B} + \int \dot{\sigma}^{j}_{(n)} \delta \dot{u}_{j,W} \, d\Gamma_{W_T} + \int \dot{\sigma}^{j}_{(n)} \delta \dot{u}_{j,W} \, d\Gamma_{W_B} + \int \dot{\sigma}^{j}_{(n)} \delta \dot{u}_{j,C} \, d\Gamma_{C_T}}_{contact\ terms\ (external\ vitual\ \ work)} \right)$$

$$= \mathbf{0} \, ;$$

$$i, j = 1,2,3, \qquad (B.1)$$

where $\nabla_i(.) = \frac{\partial(.)}{\partial x^i}$ and $\nabla_i \dot{\sigma}^{ij} = \sum_{i=1}^{3} \nabla_i \dot{\sigma}^{ij} = \nabla_1 \dot{\sigma}^{1j} + \nabla_2 \dot{\sigma}^{2j} + \nabla_3 \dot{\sigma}^{3j}$

Using the condition of equilibrium at each point of contact between the wire to bearing contact and wire to clamp contact given in Equation (2.2) and (2.3), we have :

$$\int \left(\nabla_i \dot{\sigma}^{ij}\right)\delta\dot{u}_{j,B}\, d\Omega_B + \int \left(\nabla_i \dot{\sigma}^{ij}\right)\delta\dot{u}_{j,W}\, d\Omega_W + \int \left(\nabla_i \dot{\sigma}^{ij}\right)\delta\dot{u}_{j,C}\, d\Omega_C$$

$$= -\left(\int \left(\nabla_i \delta\dot{u}_{j,B}\right)\dot{\sigma}^{ij}\, d\Omega_B + \int \left(\nabla_i \delta\dot{u}_{j,W}\right)\dot{\sigma}^{ij}\, d\Omega_W + \int \left(\nabla_i \delta\dot{u}_{j,C}\right)\dot{\sigma}^{ij}\, d\Omega_C\right)$$

$$+ \int \dot{t}^{j}_{(n)}\ \delta\dot{u}_{j,W}\, \Gamma_{W_R} + \int \dot{p}^{j}_{(n)}\ \delta\dot{u}_{j,B}\, \Gamma_B$$

$$+\left(-\int \dot{\sigma}^{j}_{(n)}\delta\dot{u}_{j,B}\, \frac{d\Gamma_{W_T}}{d\Gamma_{B_B}} d\Gamma_{B_B} + \int \dot{\sigma}^{j}_{(n)}\delta\dot{u}_{j,W}\, d\Gamma_{W_T} + \int \dot{\sigma}^{j}_{(n)}\delta\dot{u}_{j,W}\, d\Gamma_{W_B}\right.$$

$$\left. + \int -\dot{\sigma}^{j}_{(n)}\delta\dot{u}_{j,C}\, \frac{d\Gamma_{W_B}}{d\Gamma_{C_T}}\, d\Gamma_{C_T}\right) = \mathbf{0};$$

$$i, j = 1,2,3, \qquad (B.2)$$

Collecting like terms in the above gives:

$$\int \left(\nabla_i \dot{\sigma}^{ij}\right)\delta\dot{u}_{j,B}\, d\Omega_B + \int \left(\nabla_i \dot{\sigma}^{ij}\right)\delta\dot{u}_{j,W}\, d\Omega_W + \int \left(\nabla_i \dot{\sigma}^{ij}\right)\delta\dot{u}_{j,C}\, d\Omega_C$$

$$= -\left(\int \underbrace{\left(\nabla_i \delta\dot{u}_{j,B}\right)\dot{\sigma}^{ij}\, d\Omega_B}_{bearing\ internal\ energy} + \int \underbrace{\left(\nabla_i \delta\dot{u}_{j,W}\right)\dot{\sigma}^{ij}\, d\Omega_W}_{wire\ internal\ energy}\right.$$

$$\left. + \int \underbrace{\left(\nabla_i \delta\dot{u}_{j,C}\right)\dot{\sigma}^{ij}\, d\Omega_C}_{clamp\ intenal\ energy}\right) + \underbrace{\int \dot{t}^{j}_{(n)}\ \delta\dot{u}_{j,W}\, \Gamma_{W_R} + \int \dot{p}^{j}_{(n)}\ \delta\dot{u}_{j,B}\, \Gamma_B}_{boundary\ conditions}$$

$$-\int \dot{\sigma}^{j}_{(n)} \underbrace{\left(\delta\dot{u}_{j,W} - \delta\dot{u}_{j,B}\right)}_{penetration\ and\ slip\ rate} d\Gamma_{W_T}$$

$$-\int \underbrace{\dot{\sigma}^{j}_{(n)}}_{contact\ stresses} \left(\delta\dot{u}_{j,W} - \delta\dot{u}_{j,C}\right) d\Gamma_{W_B} = \mathbf{0};$$

$$(B.3)$$

Subject to:

$$on\ the\ boudaries: \begin{cases} \left\| \int \dot{t}^{j}_{(n)}\ d\Gamma_{W_R} \right\| = \dot{\boldsymbol{t}} \quad and \quad \left\| \int \dot{p}^{j}_{(n)}\ d\Gamma_{B_T} \right\| = \dot{\boldsymbol{p}} \\ \| \dot{u}_{j,W_L} \| = \dot{\boldsymbol{u}}\ and\ \| \dot{u}_{j,C_B} \| = 0 \end{cases} \tag{B.4}$$

$$\begin{cases} \underbrace{\begin{matrix} \dot{\sigma}^{1}_{(n)} = \dot{\sigma}^{1}_{(n)} \left[H\left(-\left(\dot{u}_{1,W} - \dot{u}_{1,B} \right) \right) \right]\ :\ \dot{u}_{1,W} - \dot{u}_{1,B} \le 0\ , \quad on\ \Gamma_{W_B} \cap \Gamma_{C_T} \\ \dot{\sigma}^{1}_{(n)} = \dot{\sigma}^{1}_{(n)} \left[H\left(-\left(\dot{u}_{1,W} - \dot{u}_{1,C} \right) \right) \right]\ :\ \dot{u}_{1,W} - \dot{u}_{1,C} \le 0, \quad on\ \Gamma_{W_T} \cap \Gamma_{B_B} \end{matrix}}_{contact\ conditions} \end{cases} \tag{B.5}$$

$$\begin{cases} \underbrace{\begin{matrix} \dot{\sigma}^{1}_{(n)} = \dot{\sigma}^{1}_{(n)} \left[H\left(-\left(\dot{u}_{1,W} - \dot{u}_{1,B} \right) \right) \right]\ :\ \dot{u}_{1,W} - \dot{u}_{1,B} > 0\ , \quad on\ \Gamma_{W_B} \cap \Gamma_{C_T} \\ \dot{\sigma}^{1}_{(n)} = \dot{\sigma}^{1}_{(n)} \left[H\left(-\left(\dot{u}_{1,W} - \dot{u}_{1,C} \right) \right) \right]\ :\ \dot{u}_{1,W} - \dot{u}_{1,C} > 0, \quad on\ \Gamma_{W_T} \cap \Gamma_{B_B} \end{matrix}}_{separation\ \ conditions} \end{cases} \tag{B.6}$$

$$\begin{cases} \underbrace{\begin{matrix} \dot{\sigma}^{1}_{(n)} \left(\dot{u}_{1,W} - \dot{u}_{1,B} \right) = 0\ , \quad on\ \Gamma_{W_B} \cap \Gamma_{C_T} \\ \dot{\sigma}^{1}_{(n)} \left(\dot{u}_{1,W} - \dot{u}_{1,C} \right) = 0, \quad on\ \Gamma_{W_T} \cap \Gamma_{B_B} \end{matrix}}_{normal\ complementary\ condition} \end{cases} \tag{B.7}$$

$$\begin{cases} \left\| \dot{\sigma}^{j}_{(n)} \right\| < \mu \left| \dot{\sigma}^{1}_{(n)} \right|, \quad on\ \ \Gamma_{W_T} \cap \Gamma_{B_B}\ and\ \ \Gamma_{W_B} \cap \Gamma_{C_T} \\ \left[Sgn\left(\dot{u}_{j,W} - \dot{u}_{j,B} \right) \right] = 0, \quad on\ \ \Gamma_{W_T} \cap \Gamma_{B_B} \\ \underbrace{\left[Sgn\left(\dot{u}_{j,W} - \dot{u}_{j,C} \right) \right] = 0, \quad on\ \Gamma_{W_B} \cap \Gamma_{C_T}}_{sticking\ condition}; \quad j = 2{,}3 \end{cases} \tag{B.8}$$

$$\begin{cases} \underbrace{\begin{matrix} \left\| \dot{\sigma}^{j}_{(n)} \right\| = \mu \left| \dot{\sigma}^{1}_{(n)} \right| \left[Sgn\left(\dot{u}_{j,W} - \dot{u}_{j,B} \right) \right], \quad on\ \ \Gamma_{W_T} \cap \Gamma_{B_B} \\ \left\| \dot{\sigma}^{j}_{(n)} \right\| = \ \mu \left| \dot{\sigma}^{1}_{(n)} \right| \left[Sgn\left(\dot{u}_{j,W} - \dot{u}_{j,C} \right) \right], \quad on\ \Gamma_{W_B} \cap \Gamma_{C_T} \end{matrix}}_{sliding\ condition} \end{cases} ; \quad j = 2{,}3 \tag{B.9}$$

$$\begin{cases} \underbrace{\begin{matrix} \left\| \dot{u}_{j,W} - \dot{u}_{j,B} \right\| \left(\mu \left| \dot{\sigma}^{1}_{(n)} \right| - \left\| \dot{\sigma}^{j}_{(n)} \right\| \right) = 0, \quad on\ \ \Gamma_{W_T} \cap \Gamma_{B_B} \\ \left\| \dot{u}_{j,W} - \dot{u}_{j,C} \right\| \left(\mu \left| \dot{\sigma}^{1}_{(n)} \right| - \left\| \dot{\sigma}^{j}_{(n)} \right\| \right) \ = 0, \quad on\ \Gamma_{W_B} \cap \Gamma_{C_T} \end{matrix}}_{tangential\ complementary\ condition} \end{cases} ; \quad j = 2{,}3 \tag{B.10}$$

where $[H(.)]$ is the Heaviside function, $[Sgn(.)]$ is the sign function and μ is the isotropic friction coefficient.

The Case of a Conductor-Clamp Assembly

As given in Equation (2.5) of Chapter 2, the equilibrium equation for a conductor-clamp assembly can be written using the principle of virtual work as:

$$\sum_{k=1}^{n+2}\left(\int \underbrace{(\nabla_i \delta \dot{u}_{j,k})\dot{\sigma}^{ij}}_{internal\ energy\ terms} d\Omega_k\right) + \sum_{k=1}^{2n+2} \underbrace{bc_k}_{boundary\ terms} + \underbrace{\sum_{k=1}^{n_{contact}}\left(\int \dot{\sigma}^{j}_{(n)} \underbrace{(\delta\dot{u}_{j,k} - \delta\dot{u}_{j,k+1})}_{contact\ terms} d\Gamma_k\right)}_{cross-contacts}$$

$$+\underbrace{\sum_{k=1}^{n}\left(\int \dot{\sigma}^{j}_{(n)} \underbrace{(\delta\dot{u}_{j,k} - \delta\dot{u}_{j,k+1})}_{contact\ terms} d\Gamma_k\right)}_{line\ contacts} + \underbrace{\sum_{k=1}^{n_{keeper/camp}}\left(\int \dot{\sigma}^{j}_{(n)} \underbrace{(\delta\dot{u}_{j,k} - \delta\dot{u}_{j,k+1})}_{contact\ terms} d\Gamma_k\right)}_{keeper\ and\ clamp\ contacts} = \mathbf{0}; \qquad (B.11)$$

where n is the number of wires in the conductor, and as such, there are *n*+2 terms that contribute to the internal virtual work (i.e. all *n* wires, the keeper and suspension clamp), $2n + 2$ boundary conditions that contribute to the external virtual work, $n_{contact}$ is the number of cross contacts in the conductor. The number of cross contact point between all wire in layer *i* and all wires in layer *i+1 over a lay length h* can be determined from Cardou (2013):

$$n_{cw,i} = \left[1 + n_{i+1}\left(1 + \frac{tan\ \alpha_{i+1}}{tan\ \alpha_i}\right)\right] \times n_i \qquad (B.12)$$

where n_{i+1} is the number of wires in layer i+1, n_i is the number of wires in layer i and α is the lay angle. For the length of the conductor, the number of contacts between layer *i* and *i+1over a length L* is then:

$$n_{cw,i,L} \approx \left[1 + n_{i+1}\left(1 + \frac{tan\ \alpha_{i+1}}{tan\ \alpha_i}\right)\right] \times n_i \times \frac{L}{h} \qquad (B.13)$$

From which the $n_{contact}$, the total number of cross contact in the conductor can be estimated as :

$$n_{contact} = \sum_{i=1}^{n_{layer}} n_{cw,i,L} \qquad (B.14)$$

where $n_{layer}$is the number of layers in the conductor.

For the line contacts, the number of line-to-line contacts in a layer is the same as the number of wires in that layer, so the number of line-to-line contacts in a conductor is equivalent to the number of wires in the conductor.

The number of contact points between the keeper/clamp and the conductor $n_{keeper/camp}$ depends on the geometry of the keeper/clamp and the number of wires in the external layer of the conductor.

The boundary conditions bc_k represents the boundary conditions applied to each end of all wires *(i.e. 2n)* and the keeper and clamp, giving *2n+2* boundary conditions. However, in the conductor the force/displacement is applied to the conductor as a single entity thus requiring a constraint between wire displacement/forces and the force/displacement of the conductor.

The exact mathematical form of this constraint will depend on how the load is applied to the conductor boundaries in the experimental set-up. For example, in the experiment of Papailou (1995), a rigid block was used to apply forces to the boundaries of the conductor. Herein, only a general formulation is given. Using the principle of virtual work, a constraint between the rigid block and wires in the conductor at one end of the conductor can be written as (Olsson and Dahlblom, 2016):

$$\underbrace{\delta\, c(\boldsymbol{u}_{RB}, \boldsymbol{u}_{wires}) = \delta(\boldsymbol{u}_{RB} - \boldsymbol{C}\, \boldsymbol{u}_{wires}) = 0}_{displacement/rotation\ compatibility} \qquad (B.15)$$

where $\boldsymbol{u}_{RB}$ is the displacement vector of the rigid block, $\boldsymbol{u}_{wires}$ is the set of displacement vectors of all wires in the conductor at the point of connection between the rigid block and the conductor, $\boldsymbol{C}$ is a coefficient matrix that ensures that the displacement of the wires is compatible to that of the rigid block. Equation (B.15) is a statement of the compatibility of displacement and rotation between the wires and the rigid block.

In addition to the compatibility of displacement and rotation, the force at the connection between the rigid bar and the wires in the conductor should be equvalent. This equilibrium condition is given by:

$$\delta \boldsymbol{u}_{RB}^{T} \boldsymbol{F}_{RB} + \delta \boldsymbol{u}_{wires}^{T} \boldsymbol{F}_{wires} = 0 \qquad (B.16)$$

where $\boldsymbol{u}_{RB}^{T}$ is the transpose of the displacement vector $\boldsymbol{u}_{RB}$ and $\boldsymbol{u}_{wires}^{T}$ is the transpose of the displacement vector $\boldsymbol{u}_{wires}$, $\boldsymbol{F}_{RB}$ is the force vector applied to the conductor through the rigid block and $\boldsymbol{F}_{wires}$ is the force vector of the individual wire forces. One may think of $\boldsymbol{F}_{wires}$ as a vector that contains each set of wire forces.

Using (B.15) in (B.16), the equilibrium equation is transformed to

$$\delta(\, \boldsymbol{C}\, \boldsymbol{u}_{wires})^{T} \boldsymbol{F}_{RB} + \delta \boldsymbol{u}_{wires}^{T} \boldsymbol{F}_{wires} = 0$$

$$\boldsymbol{C}^{\boldsymbol{T}} \delta(\, \boldsymbol{u}_{wires})^{T} \boldsymbol{F}_{RB} + \delta \boldsymbol{u}_{wires}^{T} \boldsymbol{F}_{wires} = 0 \qquad (B.17)$$

since the virtual displacement are arbitrary, the equilibrium condition yields:

$$\underbrace{\boldsymbol{F}_{wires} = -\boldsymbol{C}^{\boldsymbol{T}} \boldsymbol{F}_{RB}}_{\text{force/moment equilibrium}} \qquad (B.18)$$

From (B.18) it is clear that the set of forces in the wires $\boldsymbol{F}_{wires}$ is obtained by redistributing the applied conductor force $\boldsymbol{F}_{RB}$ by the coefficient matrix.

Hence, in addition to the constraint (B.5) to (B. 10), for each contact, multipoint constraint (B.15) and (B.18) are added for the conductor-clamp assembly case (B.11) due to boundary conditions.